

AperTO - Archivio Istituzionale Open Access dell'Università di Torino

**Design and development of a benchtop X-Ray based instrument and its heritage science applications**

**This is the author's manuscript**

*Original Citation:*

*Availability:*

This version is available <http://hdl.handle.net/2318/1920850> since 2023-07-19T07:18:21Z

*Terms of use:*

Open Access

Anyone can freely access the full text of works made available as "Open Access". Works made available under a Creative Commons license can be used according to the terms and conditions of said license. Use of all other works requires consent of the right holder (author or publisher) if not exempted from copyright protection by the applicable law.

(Article begins on next page)



*Alla mamma*

# Contents

<b>Abstract</b>	<b>3</b>
<b>Preface</b>	<b>4</b>
<b>List of included articles</b>	<b>5</b>
<b>Introduction</b>	<b>6</b>
<b>1 Theoretical background</b>	<b>7</b>
1.1 The role of conservation processes in cultural heritage: from the poli- cies to the techniques . . . . .	7
1.2 Material analysis and heritage science applications . . . . .	8
1.3 An overview on the transportable X-ray based instruments . . . . .	10
1.4 The INFN-CHNet collaboration . . . . .	11
<b>2 Available experimental techniques</b>	<b>13</b>
2.1 The X-ray source . . . . .	13
2.2 X-ray fluorescence: theory, experimental set-up, examples . . . . .	14
2.2.1 Principles of XRF analysis . . . . .	14
2.2.2 Experimental set-up and examples . . . . .	17
2.3 X-ray induced luminescence: theory, experimental set-up, examples .	21
2.3.1 Principles of XRIL analysis . . . . .	21
2.3.2 Experimental set-up and examples . . . . .	22
2.4 Digital radiography: theory, experimental set-up, examples . . . . .	28
2.4.1 Principles of DR analysis . . . . .	28
2.4.2 Experimental set-up and examples . . . . .	30
<b>3 Design, development, and test of the instrument</b>	<b>33</b>
3.1 Design of the instrument . . . . .	33
3.2 X-ray detector set-up . . . . .	36
3.3 Electronics and acquisition system . . . . .	39
3.4 Software for MA-XRF . . . . .	47
3.5 Test of the instrument . . . . .	49
3.6 Radiation safety measurements . . . . .	54

<b>4 Preliminary measurements with MODESTA: test applications for heritage science</b>	<b>56</b>
4.1 Applications of MODESTA on paintings . . . . .	56
4.1.1 Painting on canvas . . . . .	56
4.1.2 Painting on copper foil . . . . .	60
4.2 Applications of MODESTA on ceramics . . . . .	63
4.3 Applications of MODESTA on stones . . . . .	65
4.4 Applications of MODESTA on an inkstick . . . . .	68
4.5 Preliminary CT with MODESTA . . . . .	69
<b>Conclusion and Outlook</b>	<b>71</b>
<b>Bibliography</b>	<b>73</b>

# Abstract

The role of scientific analyses during conservation processes and studies is more and more important in heritage science. In particular, portable and transportable instruments are demanded for in-situ analysis since it is not often possible to move works of art out of their place.

During the research project, a transportable device capable of performing both spectroscopic and structural analyses was developed. At the moment, the operating techniques, all using the same X-ray source, are X-ray Fluorescence (XRF), X-ray Induced Luminescence (XRIL), and Digital Radiography (DR).

The work presented in this thesis describes the design and the development of the instrument, named MODESTA, as well as some preliminary test of its performances and several applications on objects, as paintings, stones, and ceramics. Moreover, some upgrades of the techniques have been exploited, as the macro-XRF (MA-XRF) analysis, for mapping an extended area, and the computed tomography (CT) technique, that provides 3D images of the internal structure of a sample.

# Preface

The work presented in this thesis was conducted at the Department of Physics, University of Turin, and at the INFN of Turin in the period between November 2019 and October 2022. Further, a training period was spent at the INFN of Florence.

I wish to thank the former and the present members of the solid state physics group at the University of Turin, in particular the group of the Phd students that shared with me this period. Further, I have to thank the other members of the INFN-CHNet collaboration, that have made possible to realise this project, and the Radiation Protection staff at the University of Turin. Special acknowledgement to the technicians that strictly have followed me in this project: Silvano Gallian, INFN of Turin, and Marco Manetti and Lorenzo Sodi, INFN of Florence. In addition, I would like to thank Dr. Piero Mazzinghi and Dr. Anna Mazzinghi for their suggestions in data analysis.

The research presented has been supported by the INFN-CHNet project. Moreover, this project has received funding from the European Union's Horizon 2020 research and innovation programme under the Marie Skłodowska-Curie grant agreement No 754511 (PhD Technologies Driven Sciences: Technologies for Cultural Heritage—T4C).

Borgo San Lorenzo, April 2023

Leandro Sottili

# List of included articles

The author of this thesis did the data analysis in article PI, PII, PIII, PV, and part of the data analysis in PIV. The author wrote the manuscripts of all the papers.

**PI** Sottili L.; Guidorzi L.; Mazzinghi A.; Ruberto C.; Castelli L.; Czelusniak C.; Giuntini L.; Massi M.; Taccetti F.; Nervo M.; Re A.; Lo Giudice A. INFN-CHNet meets CCR La Venaria Reale: First results. 2020 IMEKO TC-4 International Conference on Metrology for Archaeology and Cultural Heritage. 2020, 507-511

**PII** Sottili, L.; Guidorzi, L.; Mazzinghi, A.; Ruberto, C.; Castelli, L.; Czelusniak, C.; Giuntini, L.; Massi, M.; Taccetti, F.; Nervo, M.; De Blasi, S.; Torres, R.; Arneodo, F.; Re, A.; Lo Giudice, A. The Importance of Being Versatile: INFN-CHNet MA-XRF Scanner on Furniture at the CCR “La Venaria Reale”. Appl. Sci. 2021, 11, 1197. <https://doi.org/10.3390/app11031197>

**PIII** Sottili, L.; Guidorzi, L.; Lo Giudice, A.; Mazzinghi, A.; Ruberto, C.; Castelli, L.; Czelusniak, C.; Giuntini, L.; Massi, M.; Taccetti, F.; et al. Macro X-ray fluorescence analysis of XVI-XVII century Italian paintings and preliminary test for developing a combined fluorescence apparatus with digital radiography. Acta Imeko 2022, 11, 8

**PIV** Sottili, L.; Giuntini, L.; Mazzinghi, A.; Massi, M.; Carraresi, L.; Castelli, L.; Czelusniak, C.; Giambi, F.; Mandò, P.A.; Manetti, M.; Ruberto, C.; Guidorzi, L.; Re, A.; Lo Giudice, A.; Torres, R.; Arneodo, F.; Mangani, S.M.E.; Calusi, S.; Taccetti, F. The Role of PIXE and XRF in Heritage Science: The INFN-CHNet LABEC Experience. Appl. Sci. 2022, 12, 6585. <https://doi.org/10.3390/app12136585>

**PV** Sottili, L.; Guidorzi, L.; Mazzinghi, A.; Ruberto, C.; Castelli, L.; Czelusniak, C.; Giuntini, L.; Massi, M.; Taccetti F.; Nervo M.; Ferrero, M.; Torres, R.; Arneodo F.; Re, A.; Lo Giudice, A. INFN-CHNet at work: X-ray fluorescence analyses on works of art at the CCR “La Venaria Reale”. Nuovo Cimento C, 2022, 6



# Introduction

The presence of scientific analyses during conservation processes and studies is more and more required in heritage science. As reported in literature [1, 2, 3, 4, 5, 6], the information achievable with the available techniques on dating, producing processes, composition and structure of artefacts has been largely exploited in the last decades. Since a full list of the different methodologies in use in heritage science is beyond the scope of this work, only few examples are cited in section 1.2.

One of the difficulties in dealing with works of art is the impossibility - for their weight, fragility, preciousness, or the authorisations required - of being transported out of their place. This inconvenience, common in heritage science, has been overcome developing portable and transportable instrumentation for supporting the activities of restorers, conservation scientists, and teams working in this field in general. Many laboratories and companies have developed instrumentation for this purpose, and a continuous crosstalk between the development of methods and analytical techniques and the open queries in heritage science is more than ever active [7, 8, 9, 10].

At the moment a large number of such kind of devices is available on the market and many of them are employed in research projects. Some examples are presented in section 1.3. The research project conducted during this thesis work aimed to add the possibility of a multi-technique analysis, usually available in large-scale facilities as the accelerator laboratories, to the transportability of the instrumentation, for increasing the possible information achievable in a single measurement session.

The techniques combined, two spectroscopic techniques (X-ray fluorescence and X-ray induced luminescence) and an imaging technique (digital radiography), are all based on the interaction of an X-ray beam with artefacts. A brief background on the state of the art of the transportable instrumentation using X-ray beams as well as the application of the scientific analyses in heritage science is presented in chapter 1. In chapter 2 the three techniques are introduced and the relative instrumentation is discussed through few applications. The third chapter describes the design and assembling of the device starting from its components and first tests of the performances are given. In the last chapter some applications on ornaments (small decorative items as paintings and dishes) are presented for showing the possibilities of the instrument on real objects.

# Chapter 1

## Theoretical background

### 1.1 The role of conservation processes in cultural heritage: from the policies to the techniques

The importance of the conservation of works of art, and preservation of cultural heritage in general, is underlined in the policies of many organisations worldwide, both national (e.g. the Italian Ministry for Cultural Heritage) and international, such as the European Union (EU) and the United Nations (UN).

The fundamental role of cultural heritage was established when, during the 1972 World Heritage convention of UNESCO<sup>1</sup>, it was declared that “Each State Party to this Convention recognizes that the duty of ensuring the identification, protection, conservation, presentation and transmission to future generations of the cultural and natural heritage referred to in Articles 1 and 2 (as monuments, groups of buildings and sites for the cultural side, Ed.) and situated on its territory, belongs primarily to that State.” [12]. Moreover, in 2002, on occasion of the 30<sup>th</sup> Anniversary of the Convention, the Conservation was declared as one of the four strategic objectives, known as the “4 Cs”: Credibility, Conservation, Capacity-building, and Communication.

Narrowing to the EU, even though the responsibility of their cultural heritage is primarily of each member state, regional and local authorities, Europe’s cultural heritage is self-guarded and enhanced by a number of policies and programmes. As reported on the EU website [13], in EU’s policy, cultural heritage comprises:

- tangible (castles, museums, works of art, etc.),
- intangible (songs, traditions, etc.),
- digital (born-digital and digitised),

---

<sup>1</sup>UNESCO is the United Nations Educational, Scientific and Cultural Organization created in 1945 as the specialised agency of the UN with the mission of “promoting world peace and security through international cooperation in education, arts, sciences, and culture” [11].

including monuments, sites, landscapes, skills, practices, knowledge and expressions of human creativity. Moreover, it is reported that "Research and innovation nurture smart and technologically advanced solutions to help Europe protect and promote its cultural heritage."

In this context, analytical techniques are involved in the tangible cultural heritage. For instance, in Italy there is a number of infrastructures and institutions involved in those activities related to conservation, preservation and understanding of cultural heritage, in particular E-RIHS.it is the Italian node of the European research infrastructure on heritage science [14]. Among the others, a valuable service is offered by its mobile laboratories that provide in-situ investigation in this field [15]. Some examples of these analyses, conducted either by the researchers of E-RIHS.it or not, are reported in section 1.2, while little information on INFN-CHNet collaboration, part of E-RIHS.it, is given in section 1.4.

## 1.2 Material analysis and heritage science applications

The scientific analyses of works of art are more and more used to support their conservation processes, study of production techniques, dating, and in general a deeper knowledge of the artefacts. Moreover, it is important to underline that the multidisciplinary approach of material science has allowed a more and more complete understanding of objects of interest in heritage science, and is nowadays an expanding field.

Among the different analytical methods, non-invasive techniques have the advantage of avoiding sampling and damaging the artefacts, therefore are commonly preferred in cultural heritage. Some examples are applications of Raman spectroscopy (RM), digital radiography (DR), X-ray spectroscopy, X-ray diffraction (XRD), Fiber Optics Reflectance spectroscopy (FORS), Multispectral Imaging (MSI) and Hyperspectral imaging technology (HSI). Few case studies are reported in the following. Moreover, it is worth noting that the complementarity of those analyses has been exploited since the limit of one is overcome by the advantages of the others, and, if available, are applied in synergy.

As reported in [16], FORS was used for studying many Medieval and Renaissance manuscripts held by different Italian institutions, providing information on mixtures of colourants and identifying paint binders. One important result reported in this study is the use of a 'yellow pigment painted as a glaze on the blue sky made with lapis lazuli' on the Graduale of San Domenico at the San Marco Museum of Florence by Guido di Pietro <sup>2</sup>. It is worth noting that the authors underlined the benefits of

---

<sup>2</sup>Guido di Pietro is one of the most important artists of the XV century, excelling at wall-painting, panel painting and at manuscript illumination, also known as Beato Angelico or Fra

extending the spectral range of analysis into the short-wave infrared, typically not detected with FORS.

Two examples of application of RM on illuminated manuscripts from Western Europe [17] and Iran [18] are explicative of the potentiality of this technique. In the first, it is reported the presence of calomel ( $\text{Hg}_2\text{Cl}_2$ ) as white pigment on a decorative motif of an English manuscript that is, at the moment, the first evidence of use of this pigment, predating its documented use in South America as previously believed. In the second, RM is used for studying the painting palette of four Persian manuscripts of the 16<sup>th</sup> and 17<sup>th</sup> centuries. Besides establishing the pigment mixtures of the illuminations, RM identified an intermediate phase between realgar and pararealgar and the use of carmine in two different manuscripts.

An example of in-situ application of DR is reported in [19]. The instrument is a scanner designed for paintings large until 1.5 m  $\times$  2.5 m. The system comprises a Varian M-147 X-ray tube with a maximum voltage of 49 kV and an Hamamatsu CCD flat panel detector of 176 mm  $\times$  220.8 mm with a pixel dimension of 50  $\mu\text{m}$ . A study of the portrait of Giacomo Masino, XVI century, oil on canvas, 62  $\times$  80 cm<sup>2</sup> is reported. The DR reveals an underneath painting of a clergyman, not visible with naked eyes.

A recent application of XRF on painting on canvas is [20], carried out at the conservation centre Opificio delle Pietre Dure, in which the Raffaello<sup>3</sup>'s Portrait of Leo X was studied. As reported, thanks to the scientific analysis, the possible use of iron-gall ink in the underdrawing was hypothesised by the Zn elemental map. Other applications of XRF analyses are reported in [21],[22].

The XRD technique has been long in use for studying the properties of crystal lattices and it is nowadays in use in heritage science. An example is reported in [23]. In this study, the XVII century oil painting Girl with a Pearl Earring (c. 1665) by Johannes Vermeer<sup>4</sup> was analysed with a combination of transmission and reflection mode macro X-ray powder diffraction. A number of original pigments were identified as well as the degradation occurring on its surface. Some results, such as the identification of secondary alteration products in a non-invasive manner, made it a relevant technique for attesting the chemical composition of works of art.

As an example of MSI technique, it was used for studying illuminated manuscripts, as the leaf Christ in Majesty with Twelve Apostles (workshop of Pacino di Buonaguida, c. 1320), reported in [24]. Thanks to the technique, primary pigments were mapped and identified (e.g., azurite, lead-tin yellow, red lead, a red organic compound likely insect-derived, a copper-containing green, brown iron oxide, and lead

---

Giovanni da Fiesole.

<sup>3</sup> Raffaello Sanzio da Urbino, better known as Raffaello, was an Italian painter and architect of the Renaissance. Together with Leonardo da Vinci and Michelangelo, he forms the traditional trinity of old masters of that period.

<sup>4</sup> Johannes Vermeer was a Dutch Baroque Period painter who specialised in domestic interior scenes of middle-class life.

white). In this article are underlined the potentiality of a multitechnique approach, and a semi-automatic procedure for identifying pigments through spectral maps as a technological advance. A full list of the different methodologies in use is beyond the scope of this work, therefore many of them are not cited here. A comprehensive review on them is [25].

### 1.3 An overview on the transportable X-ray based instruments

Due to the indubitable advantage of in-situ analyses in heritage science, and the large variety of information achievable by X-ray analysis, a number of benchtop devices, both commercial and home-made, have been developed and are in use. The majority of this kind of instrumentation offers one technique, of which the most diffuses are XRF, DR and XRD.

Limiting the list to the XRF instruments developed within a research project, some of the most popular are:

- a punctual micro-XRF instrument with the beam size of  $126\ \mu\text{m}$  [26];
- the device developed by Alfeld et al.[27], capable of imaging the distribution of an area up to  $80 \times 60\ \text{cm}^2$  detecting the main constituents with a lateral resolution of  $100\ \mu\text{m}$ ;
- a combined XRF and Raman spectrometer for in-situ analyses [28];
- the 2D-XRF set-up developed at the C2RMF laboratory at Louvre (FR) [29], where the size of the images acquired were  $140 \times 140\ \text{mm}^2$  with a step size of  $1\ \text{mm}$ ;
- the first version of the INFN-CHNet scanner, developed in 2015 at the INFN-LABEC laboratory in Florence, performing analysis on areas up to  $20 \times 20\ \text{cm}^2$ , with spatial resolution related to the dimension of the collimator in use (smaller  $0.3\ \text{mm}$ )[30];
- the CRONO scanner developed by the XGLab, that allows the scanning of areas up to  $450 \times 600\ \text{mm}^2$ , with spatial resolution related to the dimension of the collimator in use (smaller  $0.5\ \text{mm}$ )[31];
- an XRF scanner developed by P. Romano et al. [32], capable of scanning a  $110 \times 70\ \text{cm}^2$  large area focusing down to  $25\ \mu\text{m}$  its beam size by means of a polycapillary lens;
- a portable 2D XRF scanner capable to scan  $35 \times 35\ \text{cm}^2$  areas, with a map resolution of  $1.4\ \text{mm}$  [33];

- an XRF scanner covering an area of  $80 \times 80 \text{ cm}^2$ , with a spatial resolution of about  $100 \mu\text{m}$  [34];
- FUXYA2020, a punctual XRF spectrometer recently developed at the Universities of Milan and Milano Bicocca [35].

An historical development of XRF equipment is clearly and extensively presented in [36]. In addition, in the last years, the combination of more than one X-ray-based technique has started to be exploited, as reported in [37],[38].

## 1.4 The INFN-CHNet collaboration



**Figure 1.1.** Maps of the departments and the institutions involved in the INFN-CHNet collaboration from [39].

The National Institute for Nuclear Physics (INFN) is the Italian research agency dedicated to the study of the fundamental constituents of matter and the laws that govern them [40]. The main fields of research are nuclear, particle, theoretical and astroparticle physics. However, it conducts technological research and promotes the use of fundamental physics instruments, methods and technologies in other sectors. One of the fields of application of nuclear techniques is heritage science and, in 2017, the network of the INFN for cultural heritage, INFN-CHNet [39], was founded, with the mission to harmonise and to enhance the expertise of the Institute in the field towards its structures spread over the Italian territory. To date, the INFN-CHNet collaboration gathers 16 local divisions, five Italian partners among which the conservation centres CCR “La Venaria Reale” nearby Turin and the Opificio delle Pietre Dure in Florence, that are second level nodes in the network, and international partners (see Fig.1.1). The synergy of the members of the network has led to achieve noticeable results as the development of transportable instruments for in-situ analyses, methodologies for compositional studies in heritage science, and technological advances for the dating of artefacts.

Three examples are:

- the INFN-CHNet MA-XRF<sup>5</sup> scanner (see section 3.1 and [41]);
- a different method for accurate online measurements of low fluences dose for calibrating thermoluminescence response of materials of interest for heritage science applications [42];
- the development of a high resolution time of flight at the Atomic Mass Spectroscopy beam line at the INFN-LABEC laboratory in Florence [43].

In addition, the INFN-CHNet group, in collaboration with the Conseil Européen pour la Recherche Nucléaire (CERN) and the Opificio delle Pietre Dure, has started the construction of MACHINA [44], an accelerator of about 600 kg weight, with a footprint of about  $2.5 \times 1.6 \text{ m}^2$ , services included, and a power of a few kW. It produces 2 MeV proton beams thanks to a radio frequency source and a radio-frequency quadrupole accelerating part.

---

<sup>5</sup>MA-XRF technique allows the elemental mapping of large, mostly flat, surfaces.

# Chapter 2

## Available experimental techniques

Three techniques have been studied for being combined in a single instrument: X-Ray Fluorescence (XRF), X-Ray Induced Luminescence (XRIL), and Digital Radiography (DR). This chapter describes the X-ray source (section 2.1) and the techniques. For each one, the description of the experimental set-up follows a brief overview of the theory. Some examples are also presented. XRF is presented in section 2.2, XRIL in section 2.3, and DR in section 2.4.

### 2.1 The X-ray source

The X-ray source selected for the device is the model MAGPRO by Moxtek. It is a vacuum tube producing X-rays by heating a metal filament, in turn produced by an electric current (indicated as tube current). The electrons produced by Thermionic effect are accelerated by an electrostatic potential (indicated as tube voltage) between the cathode and the anode.

This model is an end-window tube, in which the anode of rhodium is hit by electrons that generates X-rays emitted in the same direction as the electrons are moving<sup>1</sup>.

The tube voltage can be set in a range between 4 and 60 kV, while the tube current between 20  $\mu\text{A}$  and 1 mA. The specifications of this X-ray source are reported in Tab.2.1 and a picture of it is shown correspondingly.

The dimensions of its case are  $70 \times 112 \times 47 \text{ mm}^3$ , with a cylindrical brass tube 52 mm long ending with the tube window. Its weight is about 700 g in total, therefore lightweight and compact for being used in a portable or transportable instrument.

---

<sup>1</sup>In sources with this configuration, the cathode is around the anode and the window is orthogonal to the tube axis, avoiding the electrons to reach the window and therefore reducing the anode-window distance. Moreover, since the take-off angle of the electron beam is large, the self-absorption of the X-rays by the anode is reduced, and therefore end-window sources are particularly suitable for low-energy measurements.



**Table 2.1.** Specification (left) of the MAGPRO source (right).

<b>Target material</b>	<b>Rh</b>
<b>Cathode material</b>	<b>W</b>
<b>Window</b>	<b>Be (250 <math>\mu\text{m}</math>)</b>
<b>Operating temperature</b>	<b>-10° to 65° C</b>
<b>Cooling</b>	<b>Forced air (vent)</b>
<b>Weight</b>	<b>~ 700g</b>
<b>HV potential</b>	<b>4 to 60 kV</b>
<b>Beam current</b>	<b>5 to 1000 <math>\mu\text{A}</math></b>
<b>Maximum power</b>	<b>12 W</b>
<b>Focal spot size</b>	<b>400 <math>\mu\text{m}</math></b>
<b>Input power</b>	<b>12 VDC</b>



The shape of the emission spectrum is a continuous spectrum between zero keV and an end-point at the energy corresponding to the tube voltage set. It is characterised by the energy lines of the anode (for this model Rh, therefore at 2.70 keV, 2.83 keV, 20.22 keV, 22.72 keV, and 23.27 keV), and the Bremsstrahlung radiation [45]. An example from [46] is presented in Fig.2.1. Further information on this type of source can be found in [47], while further details on this model can be found in the data-sheet available here [48].

## 2.2 X-ray fluorescence: theory, experimental set-up, examples

### 2.2.1 Principles of XRF analysis

The XRF technique is an analytical method providing information on elemental composition of a sample. In a typical experiment, an X-ray beam impinges on a target and, due to the radiation-matter interactions of the beam with the inner-shell bound electrons of the target, its characteristic X-rays may be emitted and detected. Since they are related to the energy levels of the atoms, the elemental composition of the target can be deduced.

As for any X-ray emission spectrometry, the created vacancy is filled by an outer-shell electron, and the atom can de-excite by emitting a characteristic X-ray with energy equal to the difference of energies of the two levels interested in the transition.

According to the electron shell nomenclature, the emitted X-ray is indicated with the shell of the electron emitted (K,L,M,...). For example, if the electron has been ejected from the shell corresponding to  $n=1$ , the corresponding X-ray transition is

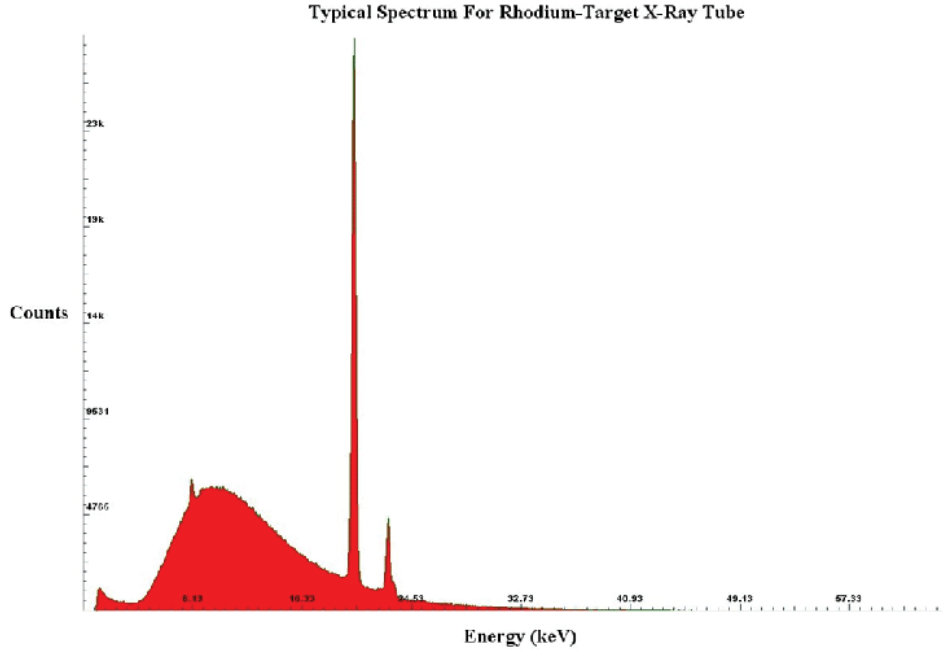


**Figure 2.1.** The spectrum is gathered by pointing a Rhodium-target Oxford Instruments X-Ray Technology’s tube directly at a Si-PIN photodiode detector system [46].

called K-line in the spectrum, if  $n=2$ , the transition is called L-line, and so on. Moreover, if the transition involves two adjacent shells, the transition is indicated with the Greek letter  $\alpha$ , if the  $\Delta n = 2$  with  $\beta$ , and so on. A schematic view of the interaction of the X-ray beam with the target atom is shown in Fig.2.2. The X-ray energy range for the shells  $K_\alpha$ ,  $K_\beta$ ,  $L_\alpha$ ,  $L_\beta$  as a function of the atomic number is reported in Fig.2.3. The values of the corresponding transitions are tabulated for each element in the table of the energies of the X-ray emission lines [50].

The typical set-up for an XRF measurement is made by an X-ray source, and a detector for energy measurements. The X-ray source may vary from a synchrotron light beam to an hand-held X-ray tube. The kind of detectors are high purity solid state semiconductors, silicon drift detectors (SDD) or scintillator detectors.

The lines of the anode of the source and a continuous background radiation due to the Bremsstrahlung radiation emitted by secondary electrons are present in each XRF spectrum, in addition to the characteristic energy lines of each element. Moreover, other contributions to the spectrum are due to the Compton scattering and the Rayleigh scattering. The Compton scattering occurs when the incident radiation loses part of its energy in the interaction with the target atom, and scatters with the residual energy. In the scattering Rayleigh process the incident X-ray scatters with an energy equal to its initial energy, and the target atom is not excited or ionised. The Compton scattering is more probable when the incident radiation energy is higher than the binding energy of the atom, while its probability is lower

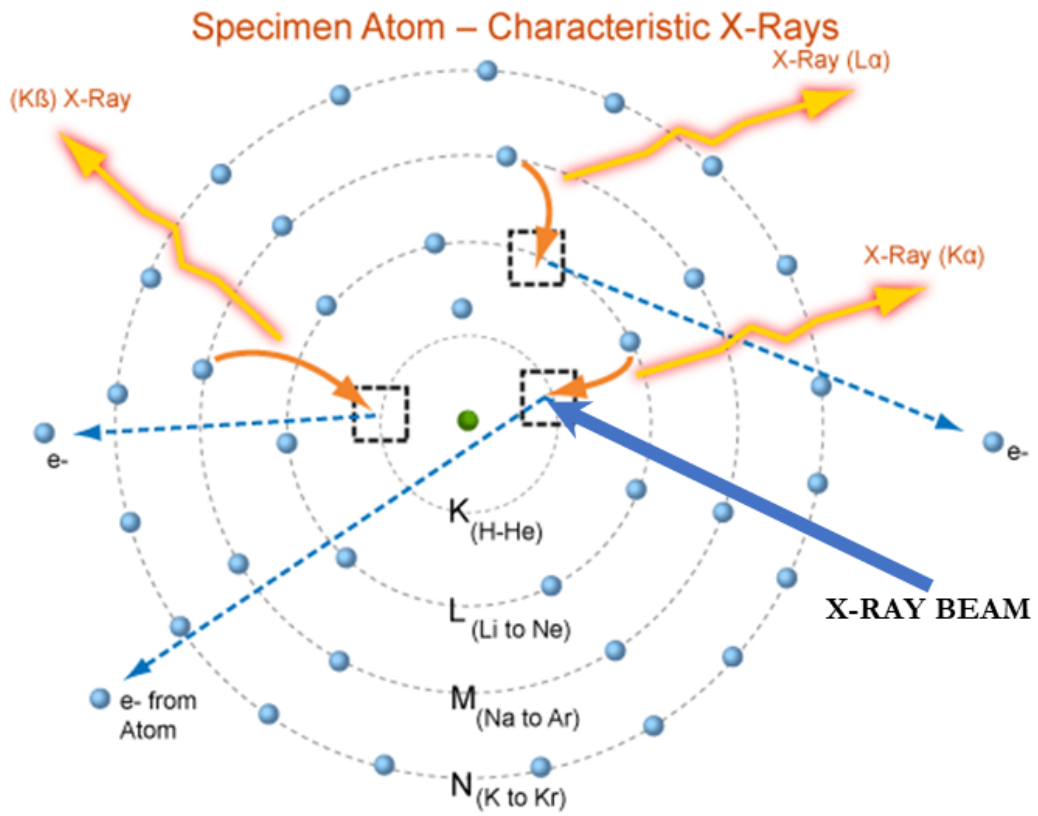


Figure 2.2. Schematic view of the beam-target interaction modified from [49].

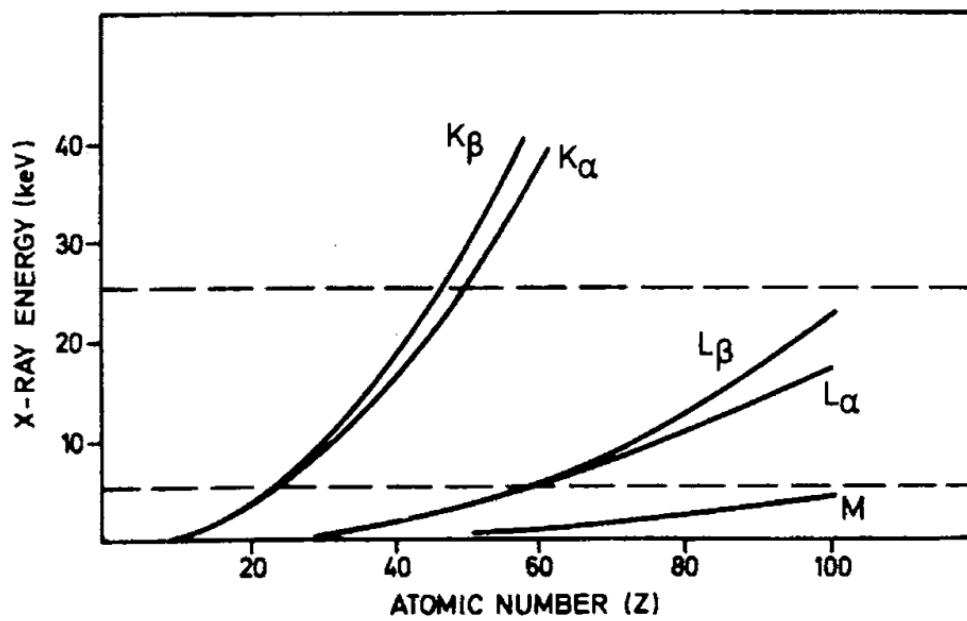


Figure 2.3. X-rays energies as a function of the atomic number  $Z$  from [51].

then the photoelectric process at the energies typically used for XRF analysis. At these energies, the effect due to the Rayleigh scattering is comparable or higher than the Compton scattering. For more details see for example [52].

### 2.2.2 Experimental set-up and examples

The detector used for this project is the XR-100 FAST SDD by Amptek [53]. Its working principle is based on the depletion of all free charge carriers for generating electron-hole pairs while an ionising radiation impinges. As in a reverse biased p-n junction, the depletion is achieved by a reverse biasing of the electrode n+ respect to the sideways electrodes p+ on the surfaces. The two arrays of p+ electrodes on both sides of the wafer generate an additional electric field parallel to the surface of the wafer so that the drifting electrons can be forced to move towards the n+ electrode, where are collected. This electrode, indicated as the anode, is connected to a preamplifier. On the opposite, the holes are collected by the p+ junctions.



**Figure 2.4.** Picture of the XR-100 FAST SDD by Amptek.

The detector has an active area of  $25 \text{ mm}^2$  and a thickness  $500 \text{ }\mu\text{m}$ . The entrance window is made of Beryllium  $12.5 \text{ }\mu\text{m}$  thick. The case of the detector, containing the bias electronics and the preamplifier, weights about 125 g, and its size is  $7.6 \times 4.4 \times 2.9 \text{ cm}^3$ . A picture is presented in Fig. 2.4. Due to the detectable X-ray energy range (typically 1 - 30 keV), XRF is sensitive to a wide range of elements: medium

atomic number ( $10 < Z < 50$ ) and high atomic number ( $Z > 50$ ) species can be detected by K and L lines respectively, as can be seen in Fig.2.3. However, light elements ( $Z \leq 10$ ) can not be detected because of X-ray attenuation inside the target and in the all path between the target and the detector active volume.

The SDD detector was tested using a number of known metallic samples. It was placed at  $45^\circ$  respect to the source-sample axis, at a distance from the sample of about 3 cm (see Fig.2.5). Data were collected connecting the case with the Amptek PX5 module that operates as a digital pulse processor and provides both low and high voltage power supplies.

The Full Width Half Maximum (FWHM) and the threshold energy for a characteristic X-ray emission were measured. Different thick samples of a pure ( $> 90\%$ )



**Figure 2.5.** Picture of the XRF set-up described in the text.

single metal of iron, copper, tungsten, lead, and tin were irradiated for a minute. The tube voltage was set to 30 kV and the tube current to  $5 \mu\text{A}$ . Results for the FWHM are presented in Fig.2.7 . As can be seen from the graph, the trend is in agreement with literature [53].

The threshold energies were measured varying the tube voltage in steps of 1 kV around the X-ray absorption edges reported on the website of the University of Washington [54]. The spectra for the measured values around the threshold for iron and copper are presented in Fig.2.8 and Fig.2.9.

Results for different elements are presented in Tab.2.2. The first column shows the

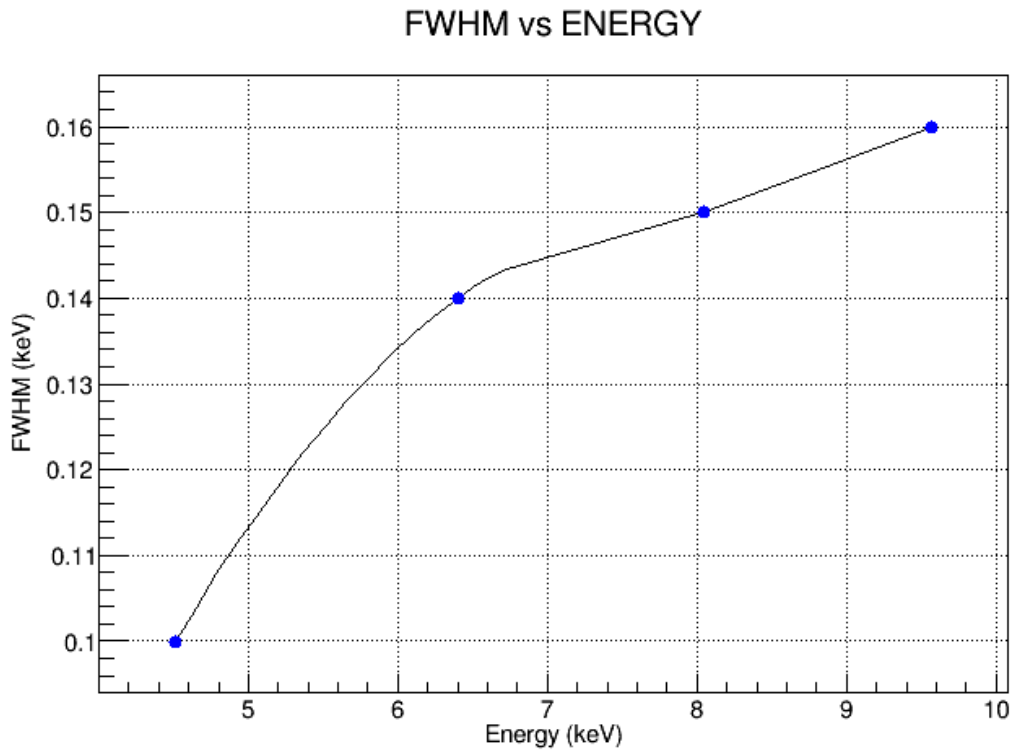


**Figure 2.6.** Trend of the FWHM with the emission energy. The acquisition was made with the PX5 module.

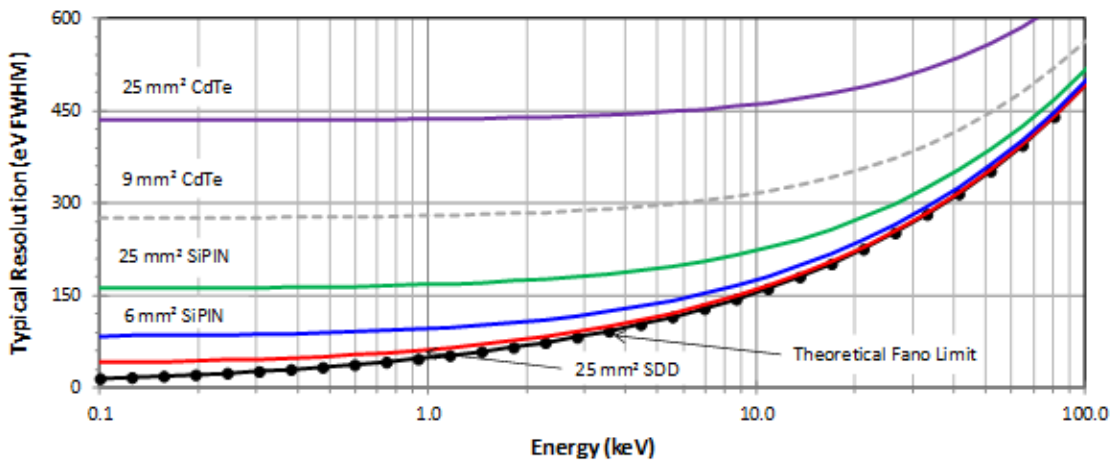


**Figure 2.7.** Trend of the FWHM with the emission energy provided by the manufacturer [53].

transition lines of the element under study, the second the corresponding energy line, the third the absorption edge from the table, and the last the minimum tube voltage for exciting the energy line.

**Table 2.2.** Values of the tube voltages for detecting the characteristic transitions of same elements.

ELEMENT AND TRANSITION	ENERGY LINE (keV)	ABSORPTION EDGE (keV)	TUBE VOLTAGE (kV)
Fe $K\alpha_1$	6.40	7.11	8
Cu $K\alpha_1$	8.04	8.98	10
W $L\alpha_1$	8.39	10.21	12
Pb $L\alpha_1$	10.55	13.04	16
Sn $K\alpha_1$	25.27	29.20	30

As can be seen the results are in agreement with the literature, however, the experimental values are higher of the data of the table due to the continuous shape of the spectrum, of which the majority of the X-rays are lower energy than the end point, as can be seen in Fig.2.1.

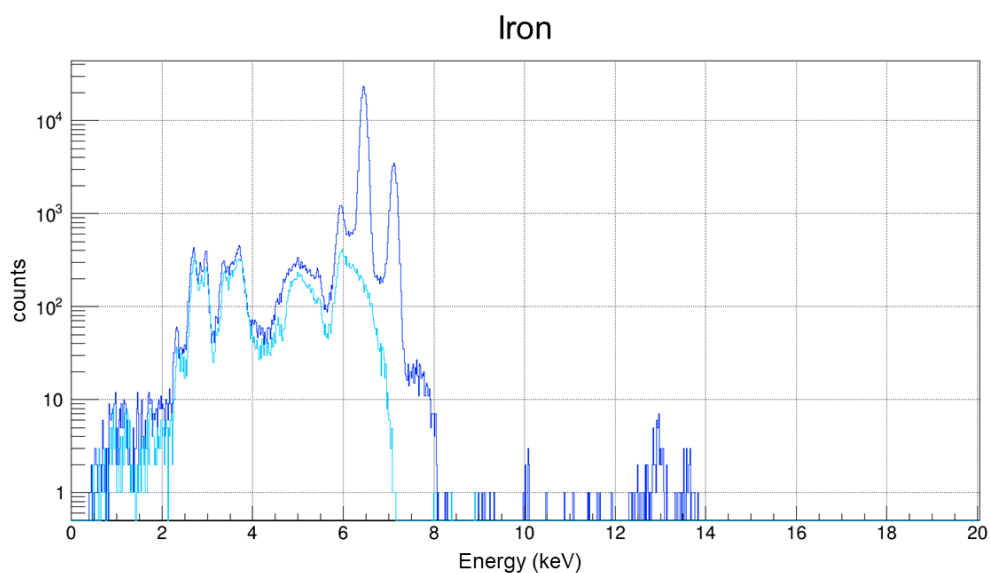


**Figure 2.8.** Spectra of iron irradiated with tube voltage of 7 kV (azure) and of 8 kV (blue). The peak visible around 13 keV is due to the pile-up.

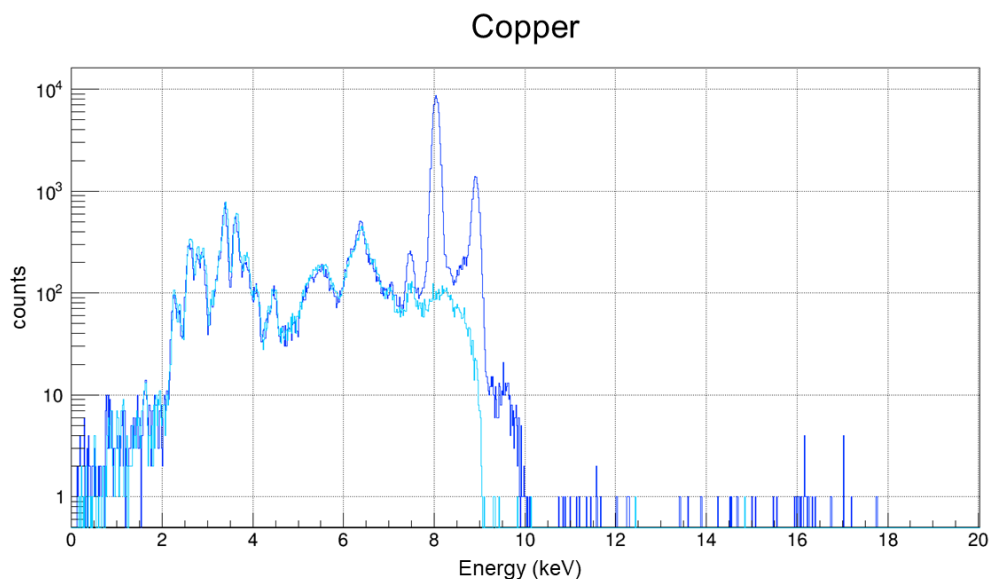


**Figure 2.9.** Spectra of copper irradiated with tube voltage of 9 kV (azure) and of 10 kV (blue).

## 2.3 X-ray induced luminescence: theory, experimental set-up, examples

### 2.3.1 Principles of XRIL analysis

The term luminescence includes the emission of light resulting from all processes except incandescence, that is the process of producing a black-body emission while heating. This phenomenon is typically studied for minerals [55]. According to the Energy Band Theory of solids, a crystal consists of a lattice of atoms. Referring to the energy levels structure of insulators and semiconductors, of which minerals are part, some intermediate energy levels may be present within the forbidden gap, for example due to impurity atoms. The luminescence phenomenon results from the transition of electrons between the energy levels, and the luminescent emission occurs when the excited electron returns to a lower energy level releasing a photon. Luminescent minerals can be classified according to the relationship between the luminescent atom and the host crystal structure.

In some minerals, the fluorescent atom is an essential chemical component and the fluorescent element is included in the chemical formula. Some examples are uranium minerals, as reported in [56]. In other cases, the luminescent atom is not an essential chemical component, but does form a part of the crystal lattice. Such atoms are known as activators and are commonly present in extremely small quantities (of the order of one part in a million or less). Nevertheless these activators have a



considerable effect on the properties of many minerals, and they often determine the characteristic colours of subvarieties. An example is the blue and pink-orange luminescence in calcite reported in [57].

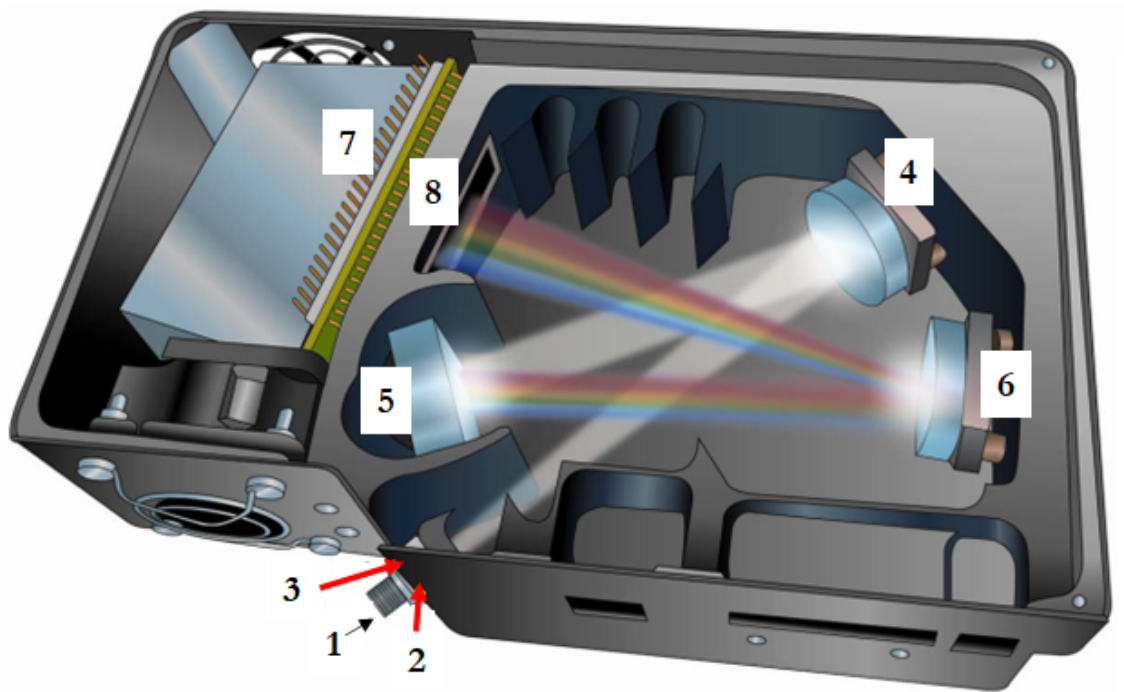
The luminescence process in minerals may be induced by a number of probes. Among them, the luminescence induced by ionising radiation is nowadays in use for provenance and material studies in heritage science, for example by means of ion beams (Ion Beam Induced Luminescence, IBIL) [58] and electron beams (cathodoluminescence, CL) [59, 60]. Despite their sensitivity, those techniques have the disadvantage of non-transportability of the instrumentation, therefore limiting their application. One possibility to overcome this limit is to use X-rays as exciting radiation. At the moment, at least three types of instrumentation have been used for this scope [61, 62, 63, 64], however, the main limit of those is the weight and the size of the source. Conversely, thanks to the portability of the X-ray source as the one described in section 2.1, it has been possible to develop a portable XRIL system.

### 2.3.2 Experimental set-up and examples

The detector used is a QEPro spectrometer by OceanOptics [65]. The components inside the detector are presented in Fig. 2.10

The optical fibre is connected via an SMA connector (1). Behind it, a removable rectangular aperture (slit, 2) is mounted for regulating the amount of light that enters inside the spectrometer controlling the spectral resolution. Moreover, a bandpass filter is present to transmit only a selected wavelength range (3). The first mirror (4) collimates the incoming light towards the grating (5), that diffracts the light according to its wavelength onto the focusing mirror (6). This one focuses the light onto the CCD detector (7). In addition, a variable long-pass order-sorting filter (8) is present for blocking second- and third - order light from reaching specific detector elements and thus from the overlap of different wavelengths. The CCD detector is a Hamamatsu S7031-1006S FTT-CCD detector with a 2-D arrangement of pixels (1044 horizontal  $\times$  64 vertical) cooled down to  $-15^{\circ}$  C for the noise reduction, which enables low intensity signals and integration time up to 60 minutes. The region of detectable wavelengths is between 250 nm and 1100 nm. Other specifications are reported in Tab.2.3

A set-up for XRIL measurements was prepared for testing the capabilities of the instrumentation. For the purpose, a ZnS(Ag) scintillator deposited on a thick support of light plastic with an area of few  $\text{cm}^2$  was used as reference sample. This material has a broadband emission band at 450 nm, as reported in [67]. A thick lead collimator with a diameter of 3 mm was placed in front of the X-ray source for reducing its beam size. The UV-74 collecting lens was placed at about  $45^{\circ}$  at its focal distance from the sample. The OCEAN Optics spectrometer was connected via the 1 mm diameter optical fibre, 2 metres long (model QP1000-2-UV-VIS). The



**QE Pro spectrometer with components**

**Figure 2.10.** Scheme of the components of the QEPro spectrometer. See the text for the description of the components indicated by numbers.

slit mounted allows an aperture-slit assembly sizes of  $200 \mu\text{m}^2$ . Measurements were carried out darkening the environment around the measuring point. The XRIL set-up is presented in Fig.2.11.

For maximising the intensity of the XRIL signal, the ZnS(Ag) crystal was aligned with the set-up. A number of measurements were conducted with a camera controlled remotely and the position of the scintillator was stored on the screen of the acquisition station. The position corresponding to the maximum intensity of the XRIL signal was marked for establishing the source-lens mutual position and therefore was used for placing the samples in the same position afterwards. For studying the technique, the XRIL signals were recorded with different setting of the source, and two results are presented. First, the tube voltage was set to 40 kV and the tube current was varied. In the second set of measurements, both the voltage and the current of the source were changed maintaining the same power of 8 W for each measurement. A background subtraction routine was applied for the following analysis. Results are presented in Fig.2.12 and Fig.2.13 respectively.

As can be seen from Fig.2.12, the trend of the XRIL signal increases linearly with the

<sup>2</sup>An intense and methodical study of the effects of the different slits and fibre optics was previously conducted and is reported in the Master's thesis [66].

**Table 2.3.** Specification of the QEPro spectrophotometer from [65] and [66].

PARAMETER	DESCRIPTION/VALUE
Dimensions	7.16 x 4.33 x 1.85 in. (182 x 110 x 47 mm)
Weight (QE Pro + power supply)	(1.15 + 0.45) kg
Temperature	TE cooler can only cool 40°C below ambient temperature
Operation	-40 °C to + 50°C
Humidity	≤ 90% noncondensing
Detector	Hamamatsu S7031-1006, low etaloning
Supply voltage	4.5 – 5.5 V
Detector range (*)	185-1100 nm.
Pixels	1024 active
Sensitivity	22 electrons/count all $\lambda$ ; 26 photons/count @ 250 nm
Quantum efficiency	90 % peak; 65% at 250 nm
Entrance aperture	field replaceable 5, 10, 25, 50, 100 or 200 $\mu$ m wide slits
Grating options (**)	14 gratings available (H1-H14), HC1 grating.
OFLV filter options (***) (8 in fig. 2)	OFLV-QE (200-950 nm); OFLV-QE-250 (250-1000 nm); OFLV-QE-300 (300-1050 nm); OFLV-QE-350 (350-1100 nm); OFLV-QE-400 (400-1150 nm).
Fibre optic connector	SMA 905 to 0.22 NA single strand optical fibre
Wavelength range	grating dependent
Optical resolution	depends on grating and size of entrance aperture
Signal-to-noise ratio	1000:1 (single acquisition)
A/D resolution	18 bit
Dynamic range	85000:1 circa
Integration time	8 ms ÷ 60 minutes



\* The spectrometer in use has a wavelength range from 250 to 633 nm.

\*\* The spectrometer in use has an H2 grating blazed at 400nm.

\*\*\* The H2 grating of the spectrometer in use do not support an OFLV filter.

tube current. On the contrary, the different combinations of tube voltage and current do not show the same intensity. According to Fig.2.13, the maximum intensity is recorded for 20 kV and 400  $\mu$ A, then decreases with the tube current, with the exception of the setting 10 kV and 800  $\mu$ A, that presents the lower intensity. This result can be explained with the characteristic spectrum of the source, that is a continuous spectrum till the end point (see section 2.1). However, since the XRIL technique is still not a common technique in heritage science, a more deep study of the intensity of the output signal with the tube parameters should be conducted.

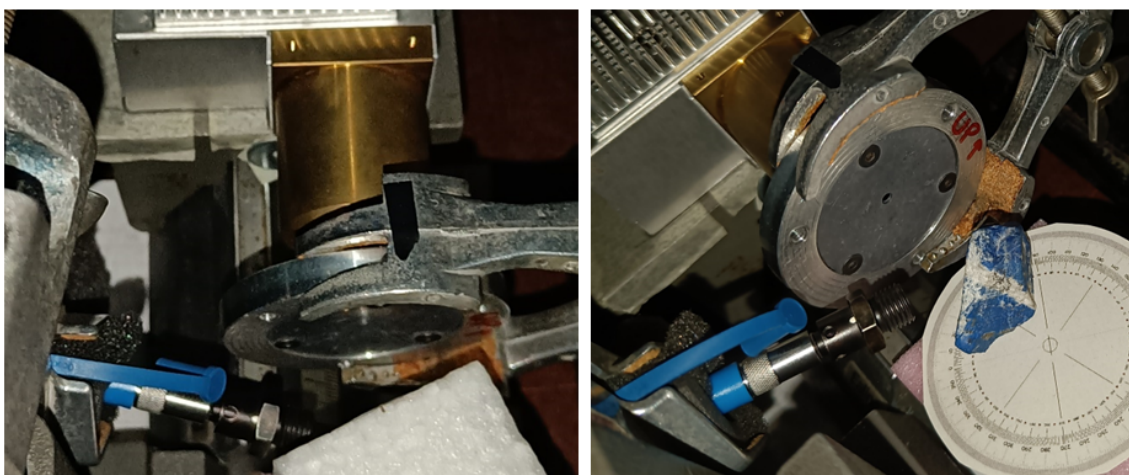


**Figure 2.11.** Picture of the set-up while measuring the ZnS(Ag) (left), and a lapis lazuli (right).

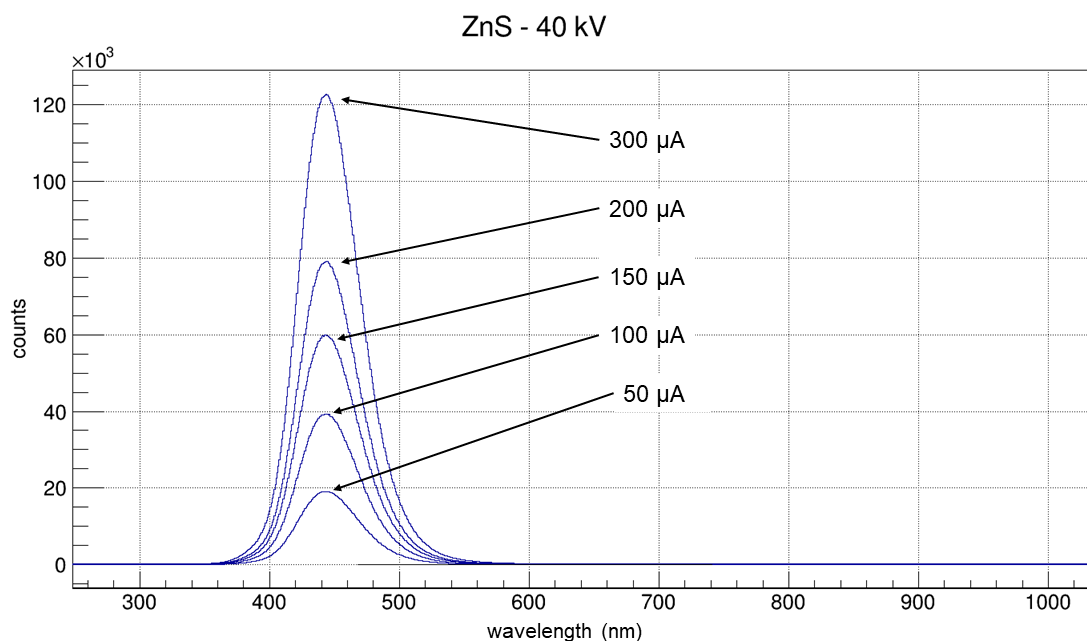


**Figure 2.12.** Spectra of ZnS(Ag) irradiated at 40 kV with different currents.

Afterwards, XRIL signals from two samples of lapis lazuli and a fluorite stone were collected. The lapis lazuli stones are one from Chile (sample Chile6) and one from Afghanistan (sample Afg9), and are part of a set of reference samples in use for the ongoing study of a protocol for establish their provenances [68]. The spectra are presented in Fig.2.14 and Fig.2.15 respectively.

As can be seen, the signals collected show the double band at 560 nm and 620 nm in Fig.2.14, and the band at 585 nm in Fig.2.15. The results are in agreement with the presence of wollastonite ( $CaSiO_3$ ) in Chilean samples and diopside ( $CaMgSi_2O_6$ )

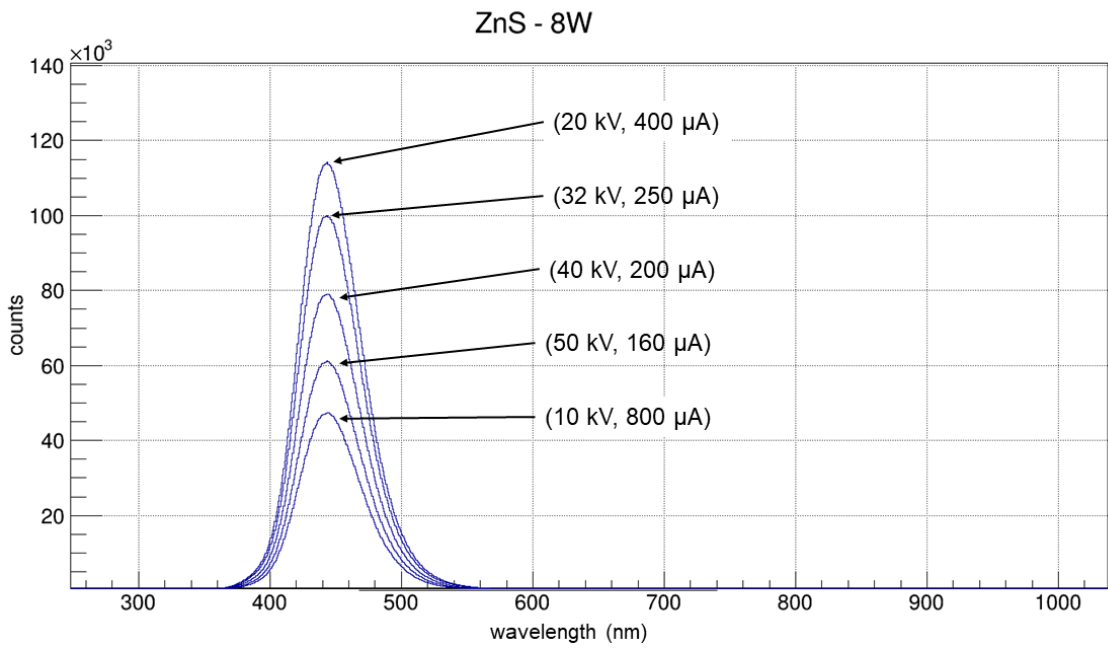


**Figure 2.13.** Spectra of ZnS(Ag) irradiated with 8 W power.

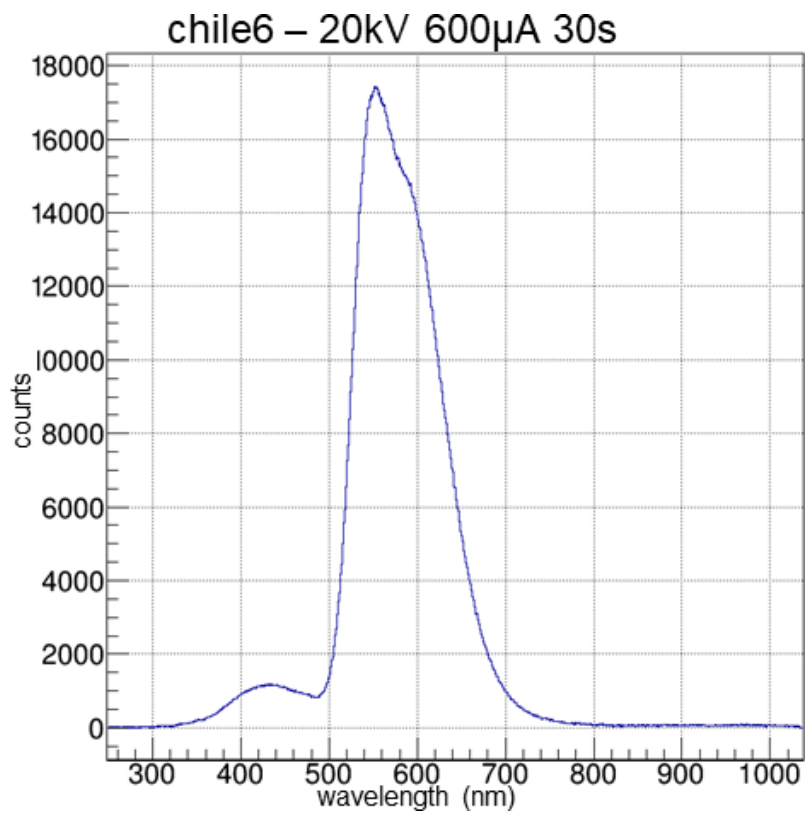


**Figure 2.14.** Spectra of Chile6 sample (20 kV, 600 μA, 30 seconds).

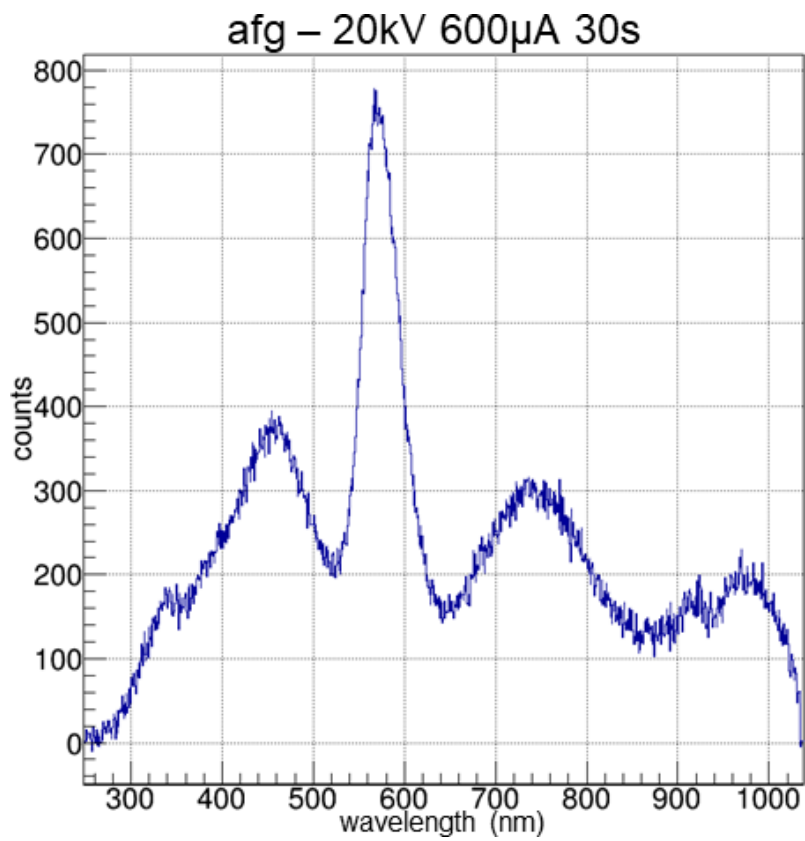


Figure 2.15. Spectra of Afg9 sample (20 kV, 600  $\mu$ A, 30 seconds).

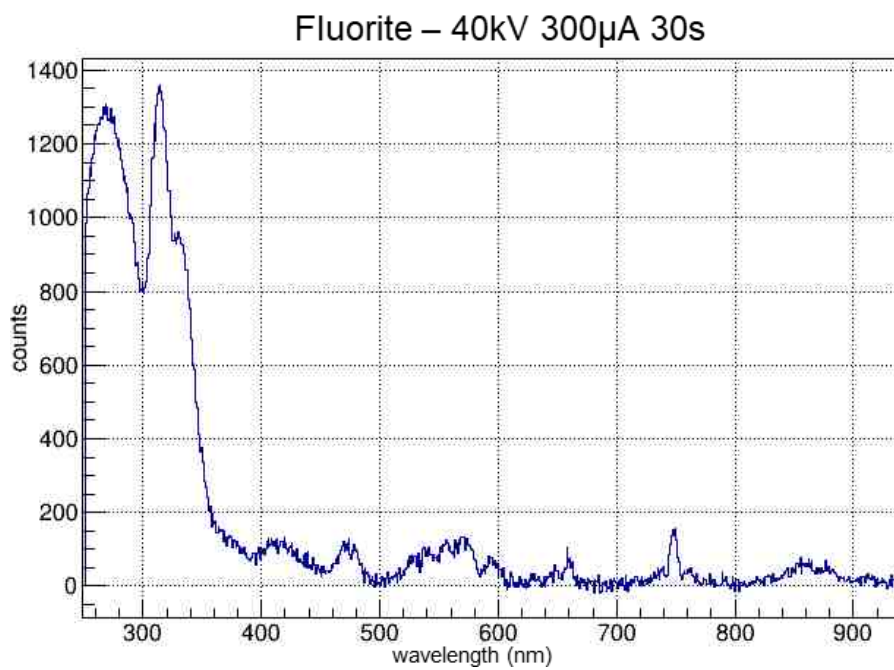


Figure 2.16. XRIL spectrum of a sample of fluorite.

in Afghanistan samples obtained by IBIL technique [69].

In the XRIL spectrum of fluorite the bands at 320 nm, 340 nm, 420 nm, 480 nm, 575 nm, 660 nm, and 750 nm are present. According to the literature [70],[71], comparing the spectrum in Fig.2.16 with the ones obtained by laser induced luminescence and cathodoluminescence measurements, they can be related with the presence - respectively - of Cesium (320 and 340 nm), Europium (420 nm), and Dysprosium (480, 575, 660 and 750 nm) as activators. In these three cases, small quantities of atomic species responsible of the luminescence of the samples are detected with the XRIL technique.

The advantage of the set-up presented in this section respect to the others found in literature - e.g. synchrotron radiation or the one reported in [61, 62] - is its portability in terms of lightweight and the size of the detector and the source. However, the integration time for XRIL signals is longer compared with the other techniques (IBIL,CL).

## 2.4 Digital radiography: theory, experimental set-up, examples

### 2.4.1 Principles of DR analysis

The term radiography includes all the techniques using radiation to view the internal structure of a 3D object in two dimensions. When the ionising radiation used are X-rays, the technique is called X-ray radiography. The resulting image is due to the X-rays from the source transmitted over the sample and collected by a material sensitive to this radiation, typically a radiographic plate or a detector for ionising radiation connected with a computer. In this last case, the technique is called digital radiography (DR).

According to the Lambert-Beer law, the intensity  $I$  of the transmitted beam is related with the primary beam  $I_0$  by the equation:

$$I = I_0 \cdot e^{-\mu x}, \quad (2.1)$$

where  $\mu$  is the coefficient of attenuation of the material and  $x$  is the thickness of the sample. If the thickness and the composition of the object are not constant, the equation 2.4.1 modifies as follow:

$$I = I_0 \cdot e^{-\int_{x_1}^{x_2} \mu(x) dx}, \quad (2.2)$$

where the dependence of  $\mu$  by the position is made explicit. Furthermore, if the X-ray beam is polychromatic, such as for the Moxtek source, the dependence of the

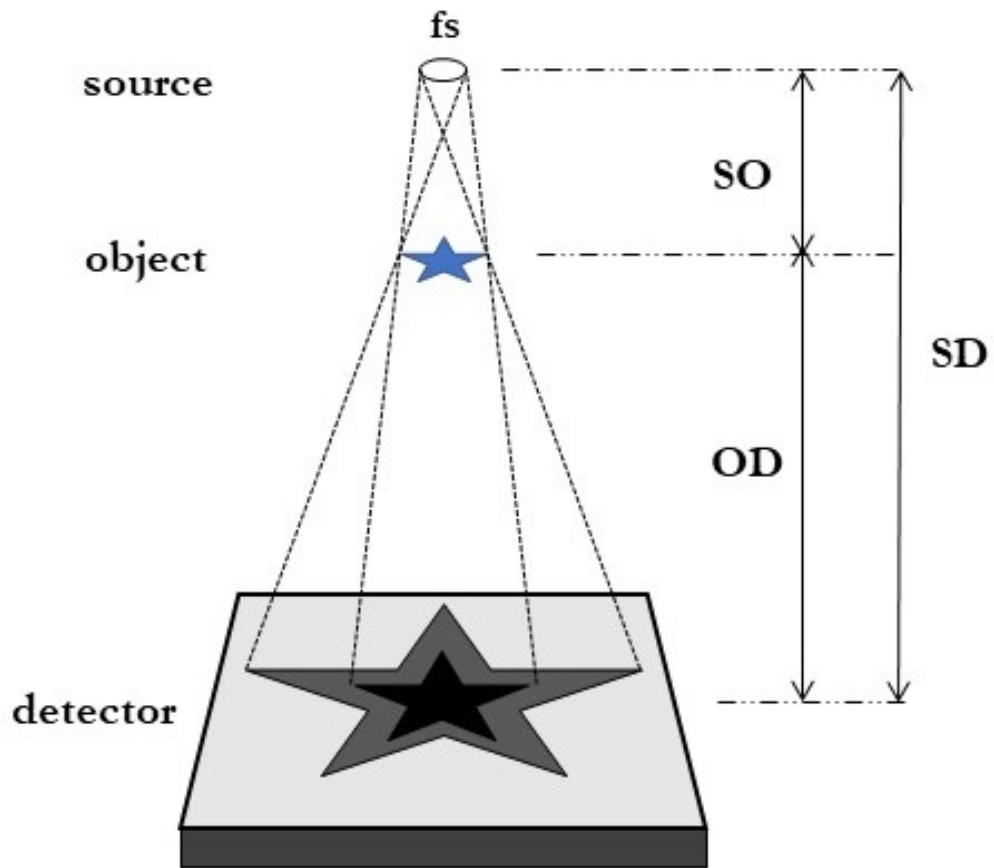


**Figure 2.17.** Sketch of a radiographic set-up.

intensity by the energy has to be considered, and the equation 2.4.1 assumes the form

$$I = \int_E I_0(E) \cdot e^{-\int_{x_1}^{x_2} \mu(x) dx} dE, \quad (2.3)$$

where  $E$  is the energy of the impinging beam.

The intensity  $I$  is related to the anode current and the voltage of the source. Another parameter of the source involved in a radiography is the focal spot  $fs$ , that is the area projected on the anode of the source by the primary electrons from the cathode that produce the X-ray beam.

In addition to them, there are two parameters related to the mutual distances of the components, the magnification and the penumbra. The magnification in radiography is the ratio between the image size and the object size, while the penumbra is the blurring at the edges of the image. Referring to Fig.2.17, the magnification  $M$  is measured as

$$M = \frac{SD}{SO}, \quad (2.4)$$



and it is greater than one. The penumbra  $P$  is given by the equation:

$$P = fs \cdot \frac{OD}{SO}, \quad (2.5)$$

and it worsen the quality of the image. Both of them increase with the distance between the object and the detector  $OD$ , therefore it is not possible to minimise the penumbra and maximise the magnification simultaneously. For this reason, the position of the sample in a radiography has to be planned according to the possibilities of the system and the queries.

## 2.4.2 Experimental set-up and examples



**Figure 2.18.** Picture of the Shad-o-Box HS detector by Teledyne [72].

A Shad-o-Box HS detector by Teledyne, model 6K (Fig. 2.18), is used for collecting the X-rays. The detector contains an active area of  $11.4 \text{ cm} \times 14.6 \text{ cm}$  with a pixel size of  $49.5 \mu\text{m}$  and it weights 2.5 kg. The range of the integration time is between 13 ms and 65 s. The video signal is digitised to 14 bits, reassembled within the camera's FPGA, and then transferred to a computer via a high-speed Gigabit Ethernet interface. The CMOS sensor inside the detector contains a direct-contact CsI scintillator, that converts X-ray photons into visible light that is sensed by

the CMOS photodiodes. A thin graphite cover protects the sensor from accidental damage as well as from ambient light. The Shad-o-Box HS camera also contains lead and steel shielding to protect its electronics from radiation. The cameras are sensitive to X-ray energies as low as 15 keV, and may be used with generators up to 225 kVp. The active area of the detector is fully covered by the X-ray beam of the source described in section 2.1 at 25 cm of distance.

According to Fig.2.19(a), the range of the energy detected is related to the thickness of the CsI scintillator. For maintaining an high spatial resolution ( $49.5 \mu m$ ) and sensitivity, the light emitted by the impinging radiation is confined to a narrow vertical channel (Fig.2.19(b)), which prevents it from scattering or spreading sideways. The

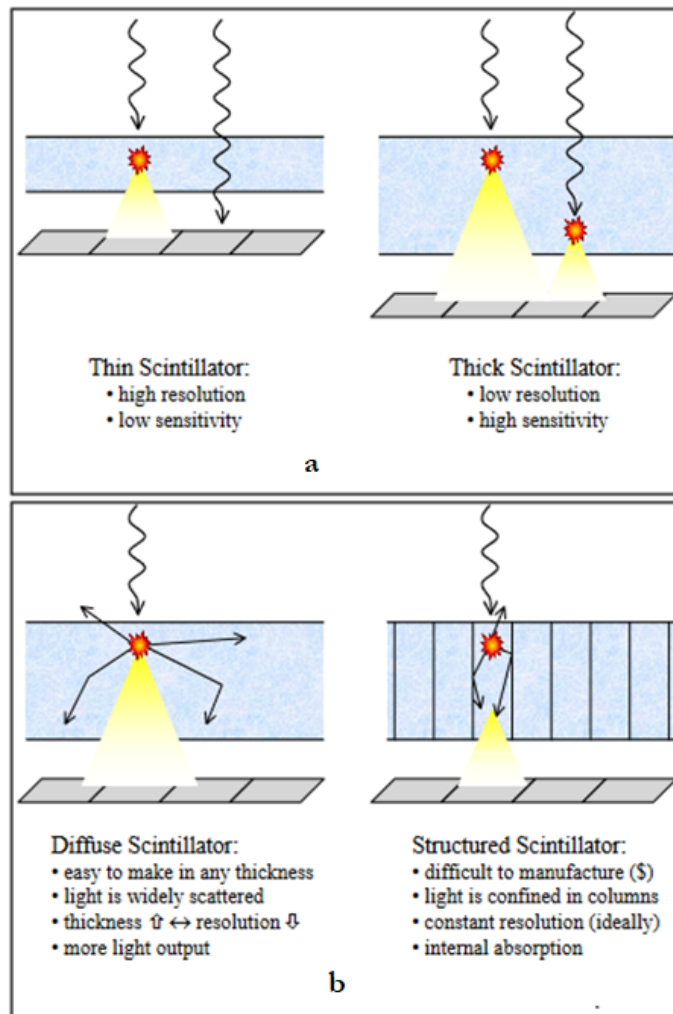


**Figure 2.19.** Sketch of the scintillating mechanism of the detector from [72].  
a) Thick vs thin scintillator; b) diffuse vs structured scintillator.

CamExpert software for acquiring images is provided by the manufacturer.

For improving the quality of the digital image, the flat-field correction is carried out. It reduces the effects of artefacts due to differences sensitivity among the pixels

(e.g. dark currents and gains of the CMOS sensors) and by the different distance of each pixel from the source. For each acquisition, both the dark and white images are acquired. The white image  $W$  is recorded irradiating the detector with the same parameters without the sample, while the dark image  $D$  is the acquisition of the image in the same exposure time with the source switched off. The corrected image  $C$  is obtained by the raw image  $R$  operating as:

$$C = \frac{R - D}{W - D}. \quad (2.6)$$

This processing is made pixel by pixel by means of dedicated software. ImageJ software was used in this work. As an example, a radiography of a starfish is presented in Fig.2.20. As can be seen the radial canals and the foot-ampulla system are clearly visible in the DR.

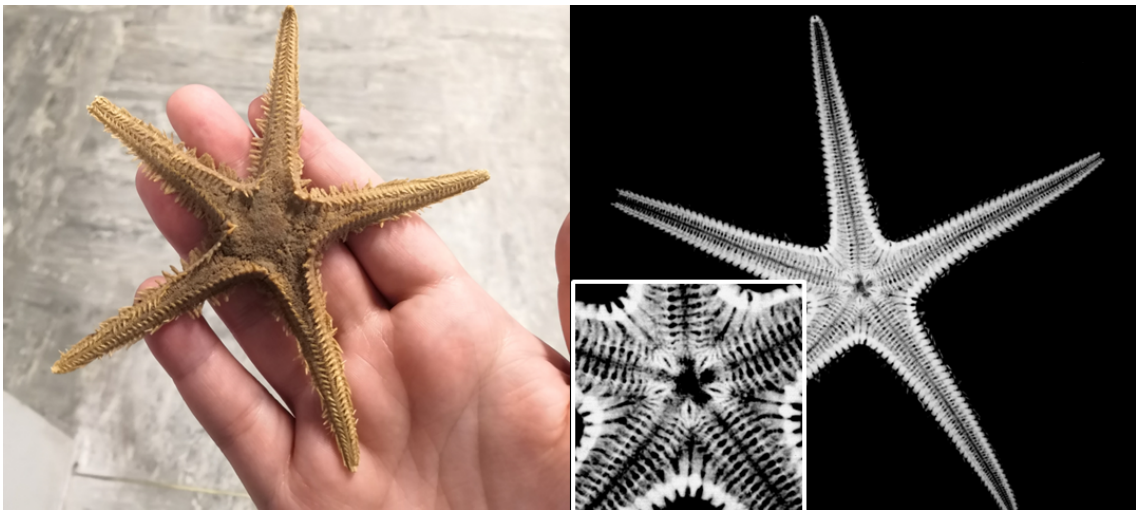


**Figure 2.20.** Radiography a starfish and the magnification of the central part. Source parameters were 20 kV and 600  $\mu$ A. Acquisition time 7 seconds.

# Chapter 3

## Design, development, and test of the instrument

The device has been developed using the detectors and the source described in chapter 2. In the following, its assembling is described starting from the design both of the case containing the electronics and the motorised system moving the measuring head (section 3.1). Afterwards, it is reported the mounting of the measuring point (section 3.2) as well as of the components inside the case (section 3.3). In section 3.4 the software for the scanning macro X-Ray Fluorescence (MA-XRF) technique is illustrated. The chapter ends with some tests of the device.

### 3.1 Design of the instrument

The device has been conceptualised as an upgrade of the MA-XRF scanner developed by the researchers of the INFN-CHNet group. As reported in [73], the latter is a lightweight (about 10 kg) and compact ( $60 \times 50 \times 50 \text{ cm}^3$ ) instrument completely designed and built within the INFN-CHNet collaboration. The main parts are the measuring head, composed by an X-ray tube (Moxtek© MAGNUM, 40 kV maximum voltage, 0.1 mA maximum anode current, Mo anode) with a collimator (changeable, typical diameter between  $400 \mu\text{m}$  and 2 mm), a silicon drift detector (Amptek© XR100 SDD,  $50 \text{ mm}^2$  effective active surface, 140 eV FWHM at 5.9 keV), a telemeter (Keyence, model IA-100), three linear motors, and a case containing all the electronics for acquisition and control. The motor stages (Physik Instrumente©, travel ranges 30 cm horizontally, x axis; 15 cm vertically, y axis; and 5 cm towards the specimen, z axis) holding the measuring head are screwed onto the carbon-fibre case containing the electronic components and the power supplies.

The operating voltage can be set in a range between 4 and 40 kV. Signals are collected with a multichannel analyser (model CAEN DT5780, also inside the carbon-fibre case), and the whole system is controlled by a laptop. The control–acquisition–analysis

software is developed within the collaboration and allows both on-line and off-line analysis. The instrument is presented in Fig.3.1.

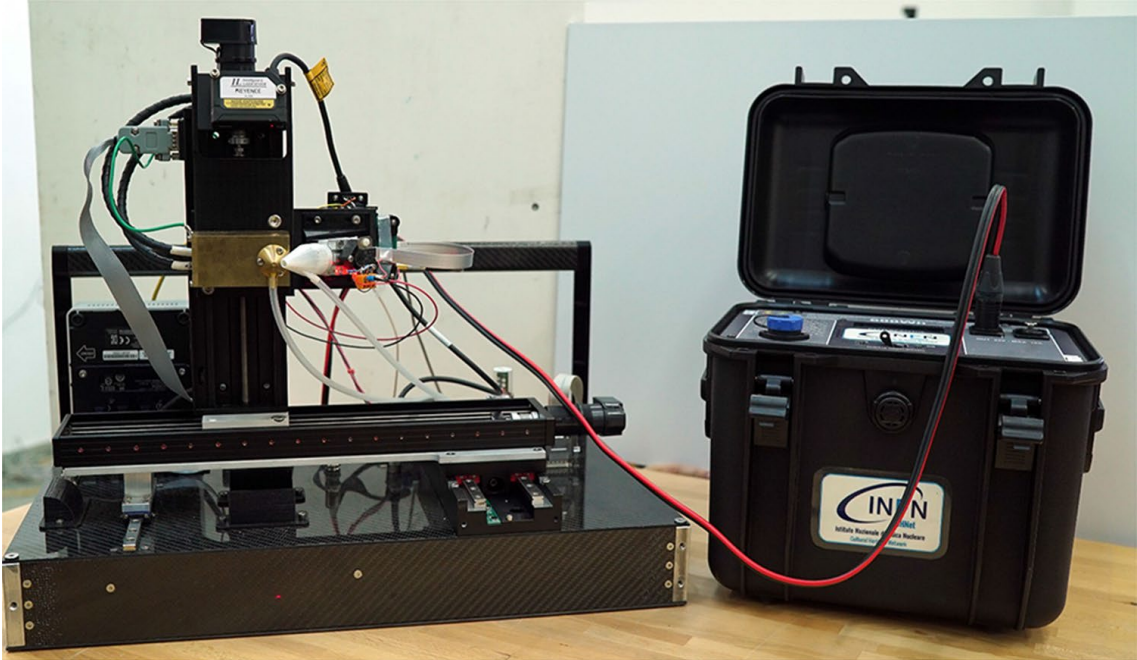


**Figure 3.1.** Picture of the INFN-CHNet scanner from [73].

In the present work, a further device was developed aimed to maintain the lightweight and compactness of the previous, but capable to perform all the three techniques XRF, XRIL, and DR, already described in sections 2.2, 2.3, 2.4.

For these reasons, the choice of the carbon-fibre material for the case is maintained: the carbon fibre has an high stiffness, high tensile strength, high strength to weight ratio, high-temperature tolerance, low thermal expansion, and low weight. Moreover, the case is covered with resins for insulating it on its flat surfaces, however, maintaining its conductivity and therefore grounding all the components while plugged.

For making the device transportable, the dimension of the case has to be minimised for reducing its size, however, it has to contain a number of electronic components inside (see section 3.3) as well as to support the motors. Starting from the case developed for the INFN-CHNet scanner, some modifications were done with the software Autodesk Inventor 2018 [74]. It is worth noting that only with a computer-aided design software it was possible to design the different parts of the device simulating their assemble, and building it only as a conclusive step. After its design, the optimal size was established to be  $50 \times 30 \times 6 \text{ cm}^3$ . A number of holes were created on the different panels for screwing the components inside and outside the case.

For connecting the motorised system to the case, a linear guide rail (9 mm width,

395 mm length) was screwed onto the top panel. A miniature linear carriage is free of sliding on the rail, and it is connected on its top to the horizontal motor (VT-80, see below) through a connector designed on purpose by means of Autodesk Inventor and printed using Polylactic acid (PLA)<sup>1</sup>. For clarify, three pictures of the top panel during the mounting process are presented in Fig.3.2. As can be seen, the linear carriage with the connector (blue PLA) slide from the edge to the central part bordering the power inlet. Several rectangular holes were done for the cables that control the motors.



**Figure 3.2.** Pictures of the top panel of the instrument during its construction. Different positions of the stage of the M404.8PD motor (top left and down), and its connection with a ribbon cable (top right).

The motors used are a M404.8PD, and two VT-80 linear stages by the Physik Instrumente. The first has a travel range of 200 mm and a maximum load of  $\sim 20$  kg, whereas the VT-80 have a travel range of 300 mm and a maximum load of  $\sim 5$  kg each. The first was screwed on the fibre case and the others over it perpendicularly

<sup>1</sup>The different pieces in PLA were realised using the Creator Pro Flashforge 3D printer.

forming a motorised system capable to scan a vertical planar surface - with the two VT-80 - and the M404.8PD motor is used for changing the distance between the measuring head and the sample. The three motors can be controlled separately or a dedicated software for matching their movements can be developed, such as the one described in section 3.4. Moreover, a power inlet with one pole red neon switch for supplying the different components was fixed on the top panel.

Last, thanks to the possibilities of the Autodesk Inventor software, in particular to a wide database of mechanical pieces and to a flexible user-friendly interface, it was used to design the different pieces as the X-Ray source and the detector holders, the controllers of the manipulator holders, the cover for the suppliers, and all the other pieces needed to connect the different components inside the carbon fibre case.

## 3.2 X-ray detector set-up

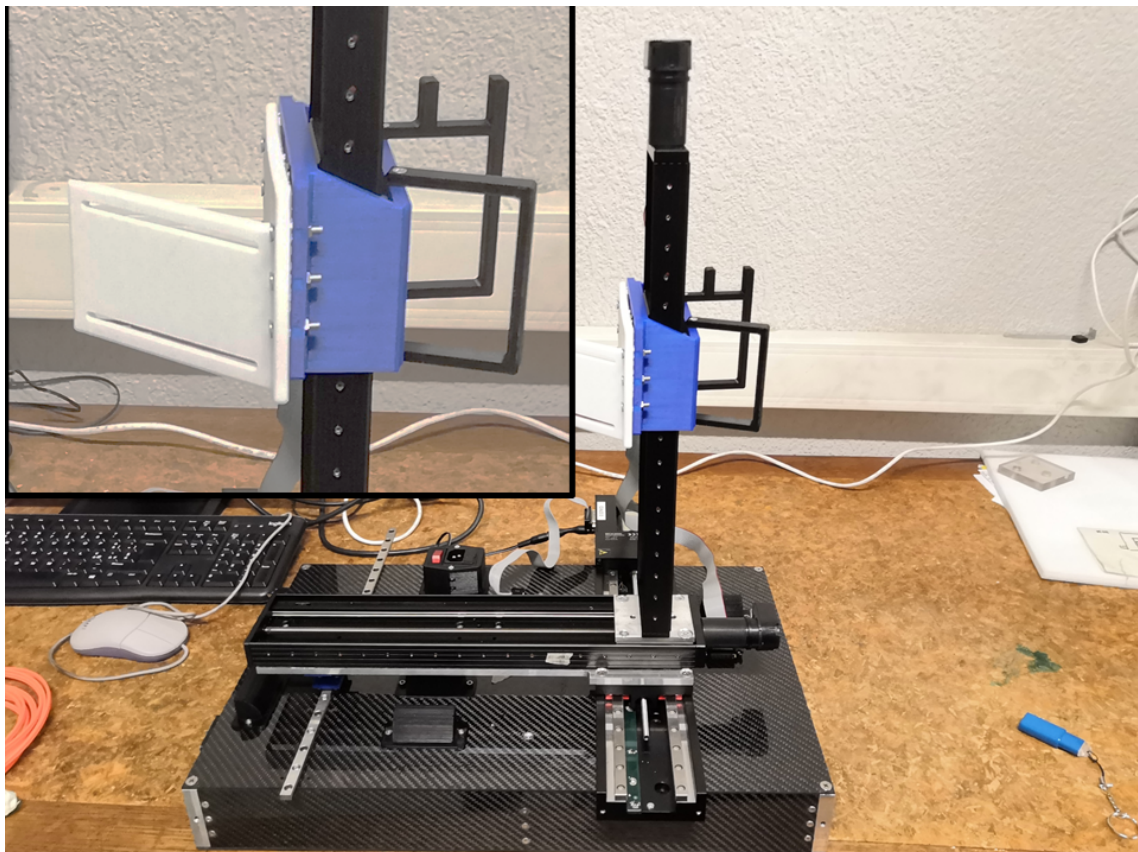


**Figure 3.3.** Picture of the instrument while mounting the measuring head, and a magnification of the area where the junctions are mounted on the sliding stage of the vertical axis on the top left.

As anticipated in section 3.1, the measuring head of the device is installed on the sliding stage of the VT-80 motor used as vertical axis. For adding the set-up, some

junctions were designed and printed in PLA and used for connecting the source on a side and the SDD detector on the other side of the stage. Thanks to the Autodesk Inventor 2018 software, the length and the mutual angles have been studied for pointing both the source and the SDD detector to the same area. Referring to Fig.3.3, two C-shaped pieces (in black) are used for connecting the X-ray source, and a single V-shaped piece forming an angle of  $55^\circ$  (in white) for connecting the detector. Both of them are screwed on the piece in blue, fixed on the sliding stage of the motor and moving solidly with it.

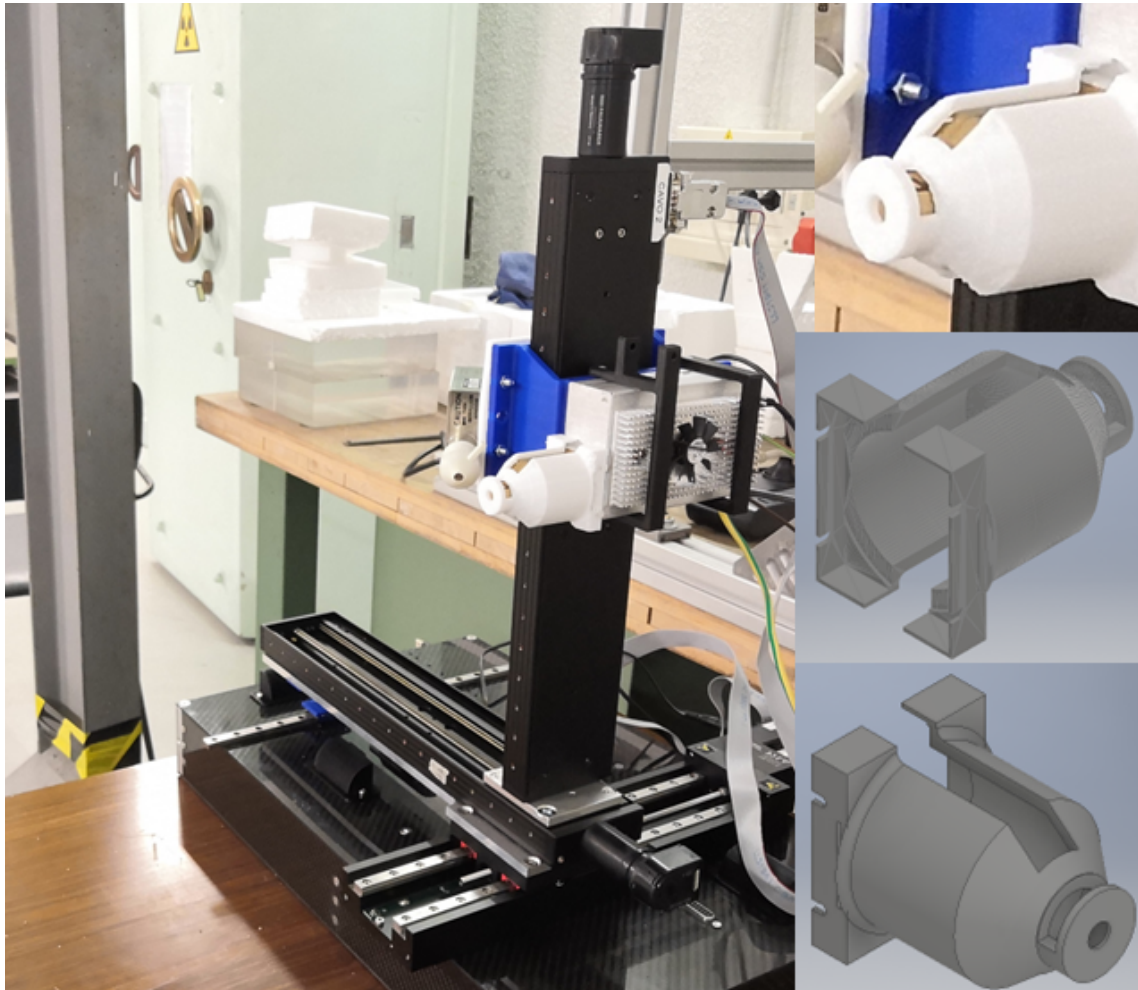


**Figure 3.4.** Picture of the instrument with the collimator mounted, and a magnification of it and of the CAD of the collimator holder for two different perspectives (right).

As stated in section 2.2, for XRF measurements is necessary to define a size of the beam spot of the same dimension of the area that has to be irradiated. For this purpose, a set of eight brass collimators of different diameter size has been designed and realised. Based on the experience of the researchers of the INFN-CHNet collaboration about MA-XRF measurements, the sizes of the diameters realised are between 0.3 mm and 1 mm in step of 0.1 mm, and their thickness is 5 mm.



For holding the collimator, another piece was designed and printed: it can be joint to the X-ray tube with four screws (type 2'56" UCF), and the collimator selected for the measurement can be inserted and hold in front of the source. It is worth noting that this choice allows to switch between an XRF and a DR measurement just unscrewing and removing the collimator holder. A picture of the collimator holder mounted is presented in Fig.3.4.

For adding the UV-74 lens, necessary for the XRIL measurements, other two versions of the collimator holder have been realised (see Fig.3.5). The main difference between the two is the mutual angle between the source and the XRIL detection system, allowing different geometries while measuring, according to the shape and the dimension of the object. In fact, the set-up presented in Fig.3.5 allows XRIL on small samples (about a centimetre), whereas if the specimen is larger, the collimator holder to be used is sketch on the top left.

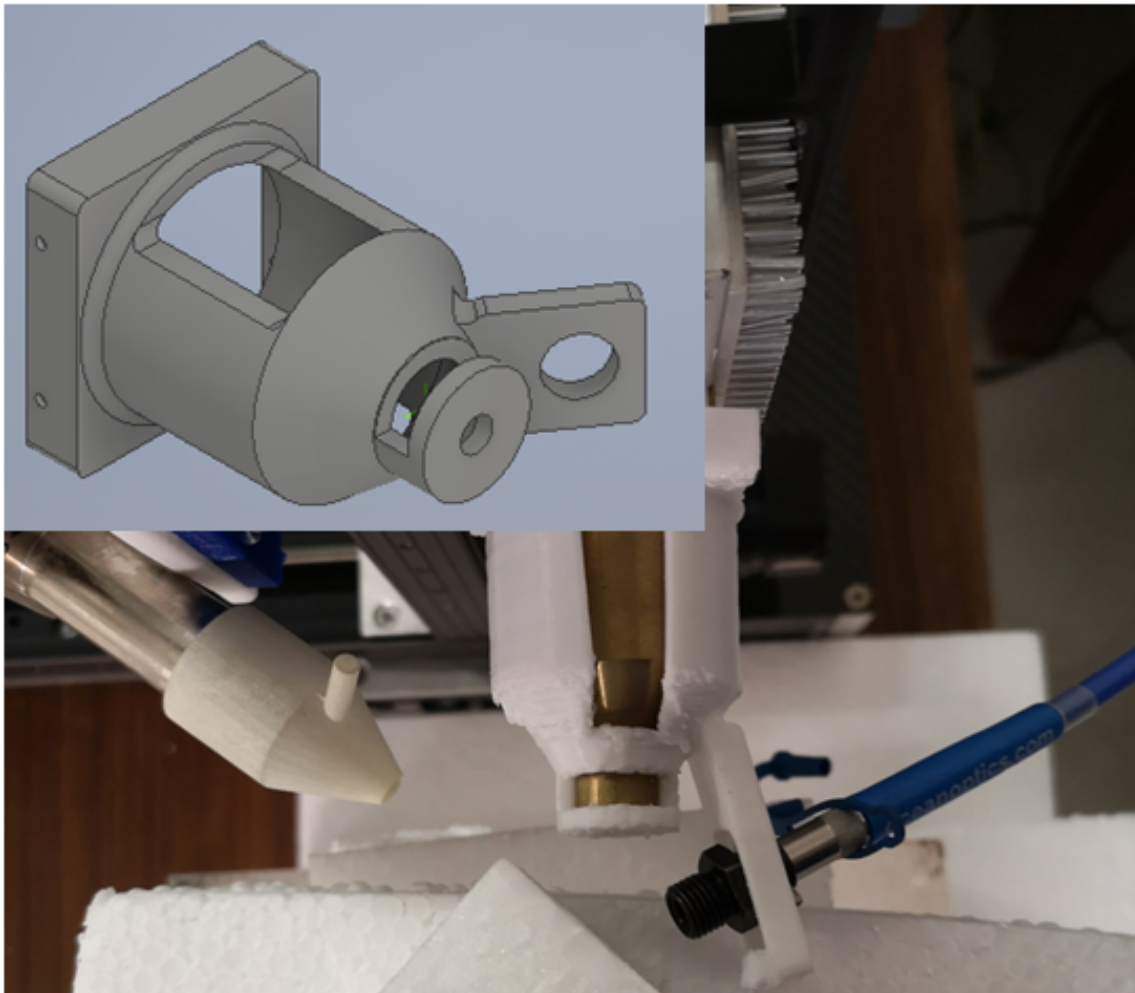


**Figure 3.5.** Picture of measuring head for XRIL measurements, and a CAD of another version of the collimator holder (top left).

### 3.3 Electronics and acquisition system

A sketch of the electronics inside the case is presented in Fig.3.6. The hardware placed in it consists of two AC/DC power supplies, models Meanwell RSP-100-12 and LRS-350-24 (see Fig.3.7), three controller board by Physik Instrumente, model C-863, one for each motor, and the benchtop multichannel analyser (MCA) model DT5780M by CAEN. For supplying the electronic components, the power inlet was cabled inside the case. Spade connectors were used for connecting the high voltage wires from the poles to the LRS-350-24 supplier, whose the input terminals are in turn connected in parallel to the input terminals of the RS-100-12 power supply.

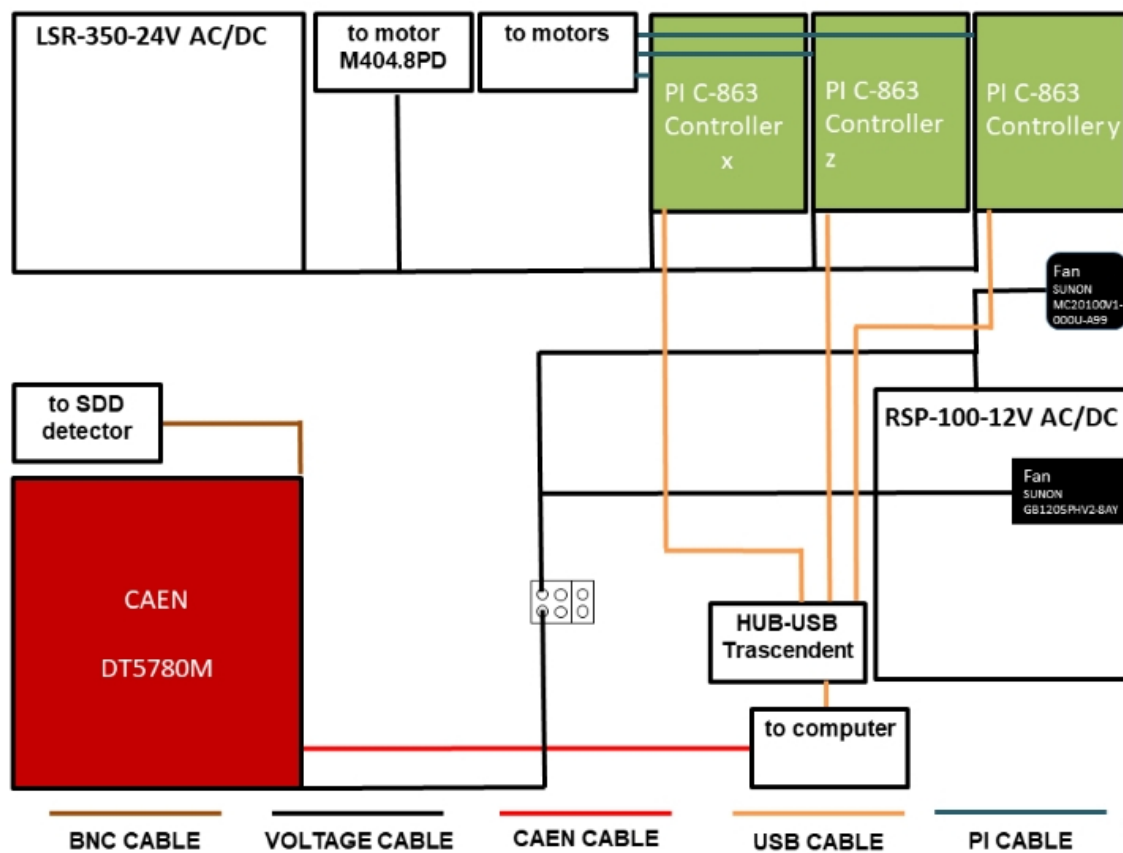


**Figure 3.6.** Sketch of the electronic components inside the case and their connections. The links to the parts placed outside are also reported.

The AC/DC power supplies are single output enclosure type. They operate for 85-264 VAC input voltage, the input frequency is in the range 47-63 Hz and the input AC current is 0.8 A (RSP-100-12) and 3.4 A (LRS-350-24) at 230 VAC. Their output specifications are reported in table 3.1. Each model is cooled by a vent for working with a temperature up to 70°C. The cabling was done through eyelet or spade connectors, and the wires were attached to these terminals through soldering.

According to Fig.3.6, the M404.8PD motor and the three PI boards were connected

to the LRS-350-24 power supply, while the fans and the MCA were connected to the model RSP-100-12.



**Figure 3.7.** Pictures of the RSP-100-12 (left) and LRS-350-24 (right) power supplies. Their sizes are  $179 \times 119 \times 30 \text{ mm}^3$  and  $215 \times 115 \times 30 \text{ mm}^3$  respectively.

**Table 3.1.** Output specifications of the RSP-100-12 and LRS-350-24 power supplies.

MODEL NAME	DC VOLTAGE	CURRENT RANGE	RATED POWER	RIPPLE & NOISE	VOLTAGE ADJ. RANGE
RSP-100-12	12 V	0 - 8.5 A	102 W	100 mVp-p	11.4 - 13.2 V
LRS-350-24	24 V	0 - 14.6 A	350.4 W	150 mVp-p	21.6 - 28.8 V

The C-863 Mercury DC motor controller is designed by the PI company for flexible motion control applications where a precision positioner has to be controlled by a PC or PLC (programmable logic controller). Its operating voltage is between 12 to 48 VDC, with a maximum power consumption of 80 mA without load at 24 V and a current limitation of 2.5 A. The PIMikroMove user software is provided by the manufacturer, however, software support for C++ and other programming languages is available for custom coding, as the one in use for the MA-XRF and briefly described in section 3.4. The available communication interfaces are the RS-232 and the USB, and the latter was used in this application for all the three controllers.

The CAEN DT5780M MCA (Fig.3.8) is a compact desktop system integrating two independent signal inputs with a 14 bits ADC and featuring HV and preamplifiers capabilities for nuclear spectroscopy applications. Moreover, the MCA allows a sampling rate of 100 Msamples/s. As reported in [75], it was designed for high energy resolution detectors, such as High Purity Germanium detectors and scintillator

detectors coupled with photomultiplier tubes. For using this MCA for X-ray spectroscopy, an integrator circuit was built as presented in Fig.3.9 by the researchers of the INFN-CHNet group.

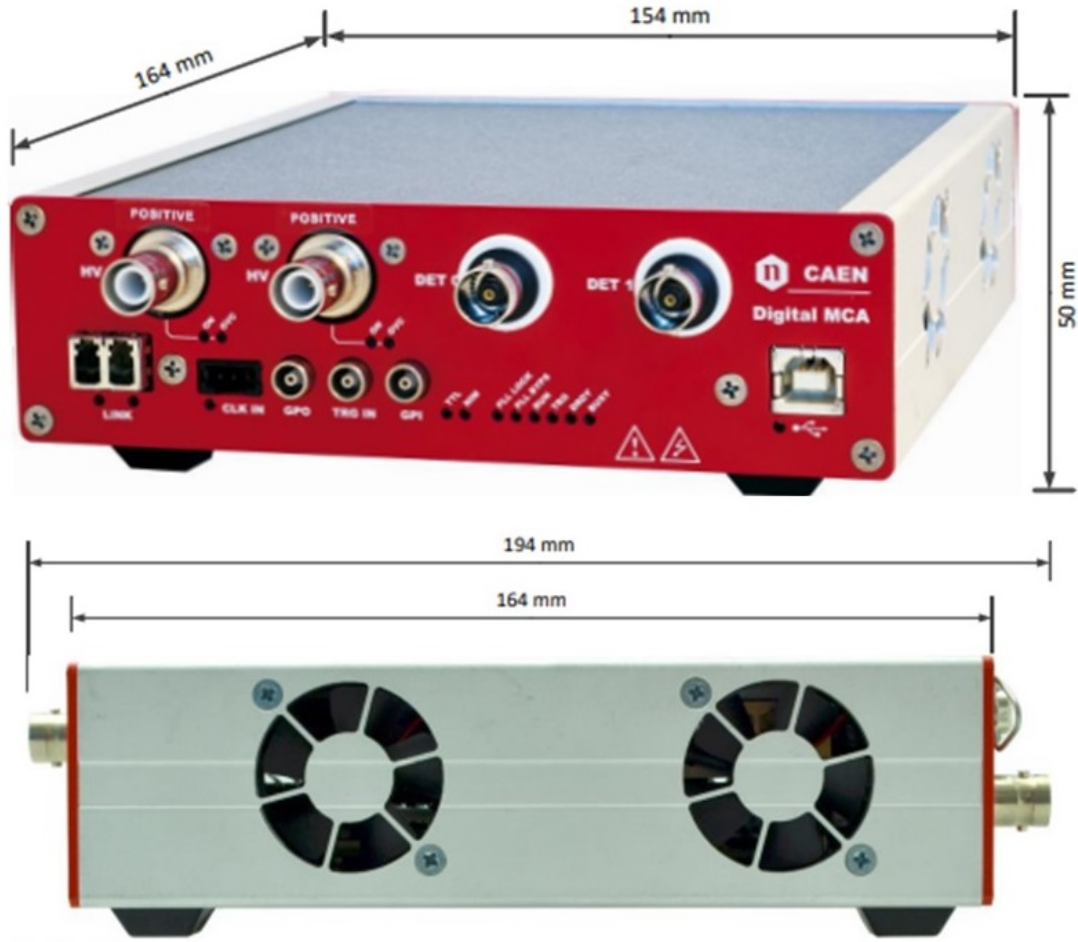


**Figure 3.8.** Front (up) and lateral (bottom) view of the CAEN DT5780M module from [75].

The dimension of this module is  $154 \times 194 \times 50 \text{ mm}^3$  including connectors, and its weight about 1 kg. The operating voltage supply is 12 V with a consumption of about 45 W. The manufacturer provides dedicated software for acquisition and data analysis both on Microsoft and Linux based operating systems. In addition, CAEN provides drivers for the different types of physical communication channels and a set of C and LabView libraries that can be used for developing a custom software. The MCA houses both USB and Optical links interfaces, and it allows a high-rate data transfer via optical link up to 80 MB/s. The analog signals can be collected via a BNC cable.

According to Fig.3.10, the digitiser executes all the functions of an analog electronic chain from the shaping amplifier to the PC. The input signals are sampled by the flash-ADC, and its output is analysed by the Field Programmable Gate

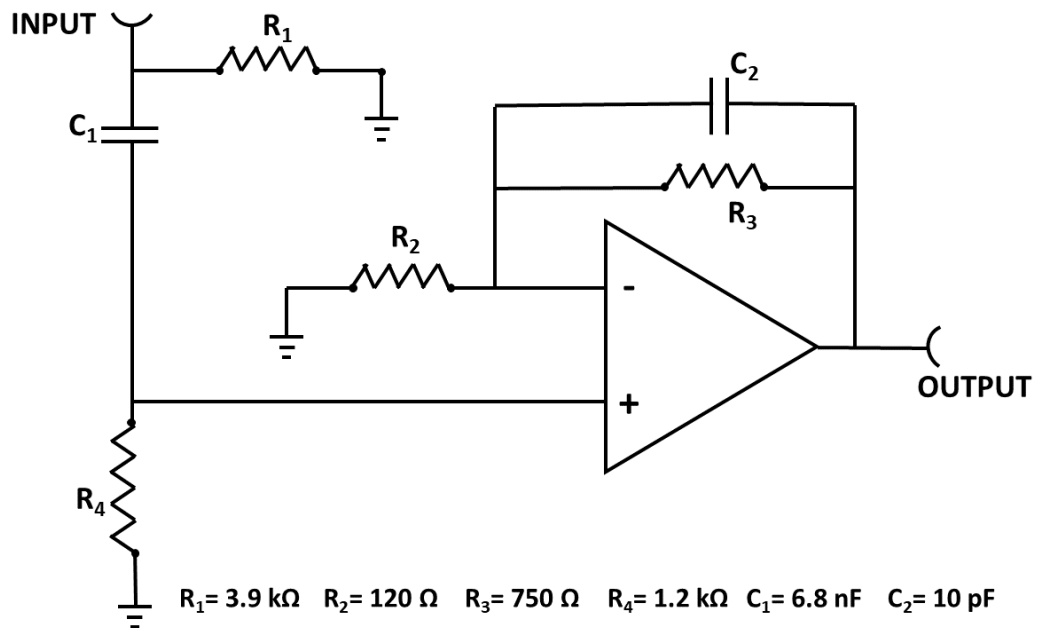


**Figure 3.9.** Sketch of the analog circuit modified for adapting the MCA to the XRF measurements.

Array (FPGA) board with the Digital Pulse Processing for Pulse Height Analysis (DPP-PHA) algorithm. Further details can be found in [75].

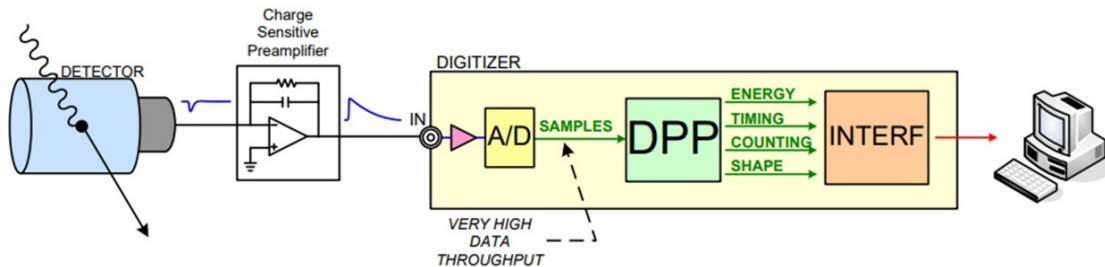


**Figure 3.10.** Block diagram of a digitiser-based spectroscopic system from [75].

The DPP-PHA algorithm is based on the Jordanov trapezoidal filter [76]. It is able to transform an exponential decay signal into a digital signal with the shape of a trapezoid whose flat top height is proportional to the amplitude of the input pulse, in turn proportional to the energy released by the ionising radiation in the detector (see Fig.3.11).

A number of input parameters have to be set in the algorithm for the signal processing, of which the principals are:

- the decay time of the input pulse;
- the trapezoid rise time for reaching the flat top after the input signal is detected;

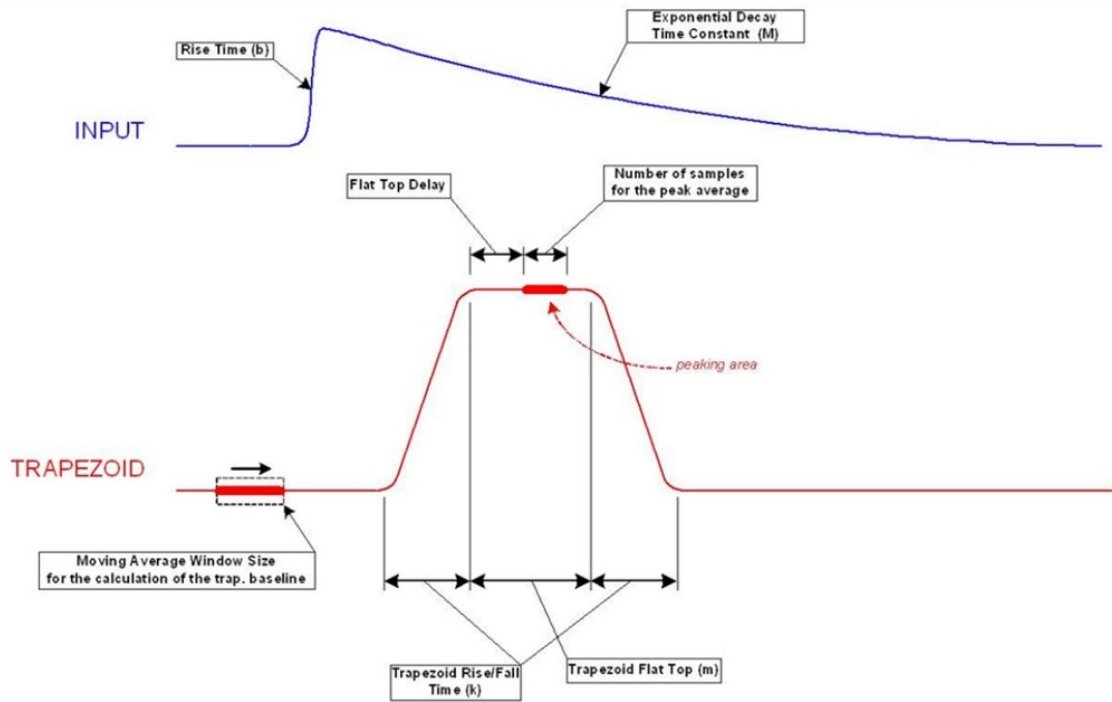


**Figure 3.11.** Illustration of the input signal (top) and the trapezoidal filter (bottom) and related parameters from [75].

- the flat top time on which the maximum value is maintained;
- the baseline mean, that is the number of samples for averaging the baseline before the starts of the trapezoid;
- the trapezoid gain, that allows to rescale the signal charge;
- the peaking delay between the rising of the input signal and the beginning of the flat top of the trapezoid;
- the peak mean, that is the number of samples of the flat top for measuring the input energy;
- the baseline and the peaking hold-off, that are the times in which the baseline and the energy peak value are maintained constant.

Other specifications of the CAEN DT5780M are reported in [75]. Fig.3.12 shows the input signals and the trapezoidal filters of two signals detected with the digital oscilloscope.

A number of tests were carried out for establishing the best parameter setting for XRF analysis. For this scope different samples were irradiated and the FWHM for different elements was measured. Results are presented in Tab.3.2 and the trend of the FWHM with the energy is presented in Fig.3.13.

Moreover, for comparing the detection efficiencies of this acquisition system with

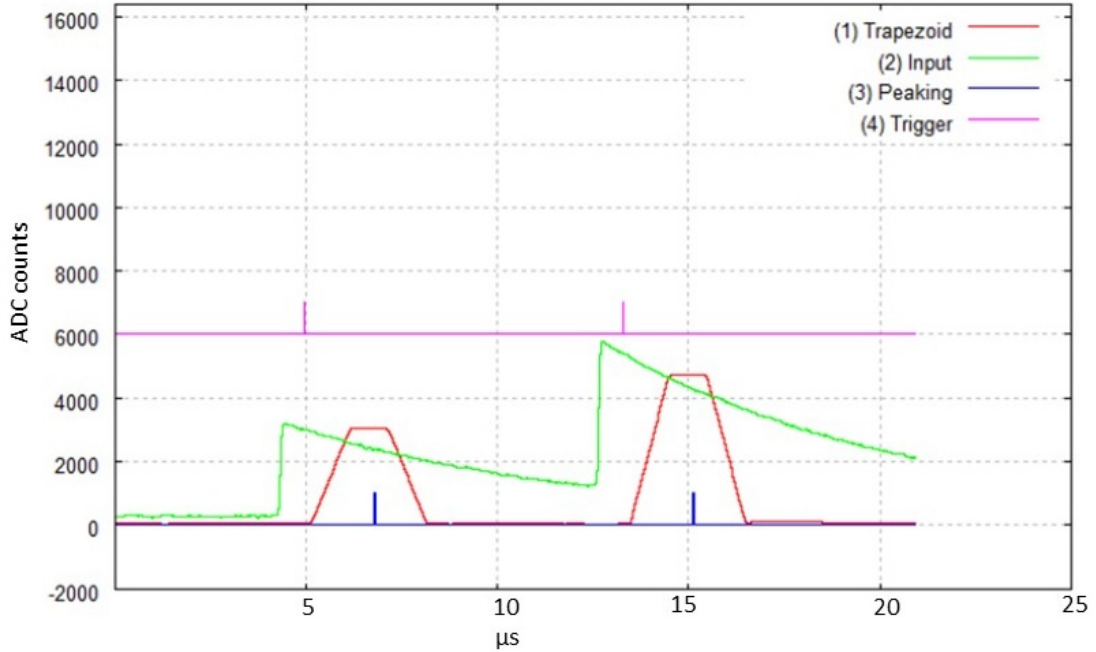


**Figure 3.12.** Screenshot of the digital oscilloscope tool while performing XRF.

**Table 3.2.** Setting of the parameters of the CAEN DT5780M for XRF measurements.

PARAMETER	VALUE
Decay time	$7.5 \mu s$
Rise time	$1 \mu s$
Flat top	$2 \mu s$
Baseline mean	1024
Trapezoid gain	1
Peaking delay	$1.2 \mu s$
Peak mean	4
Baseline hold-off	$5 \mu s$
Peak hold-off	$1.1 \mu s$

the PX5, a thick sample made of copper, lead, and tin was irradiated with the two different electronics, the one described in section 2.2, and the second connecting the output signal of the preamplifier to the DT5780M with the parameters described above. The tube voltage was set to 50 kV, the tube current to 50  $\mu A$ , and the acquisitions lasted 120 seconds in both cases.

As can be seen from the comparison between the two graphs presented in Fig.3.14, the detection efficiency rises more than ten times for each energy peak using the

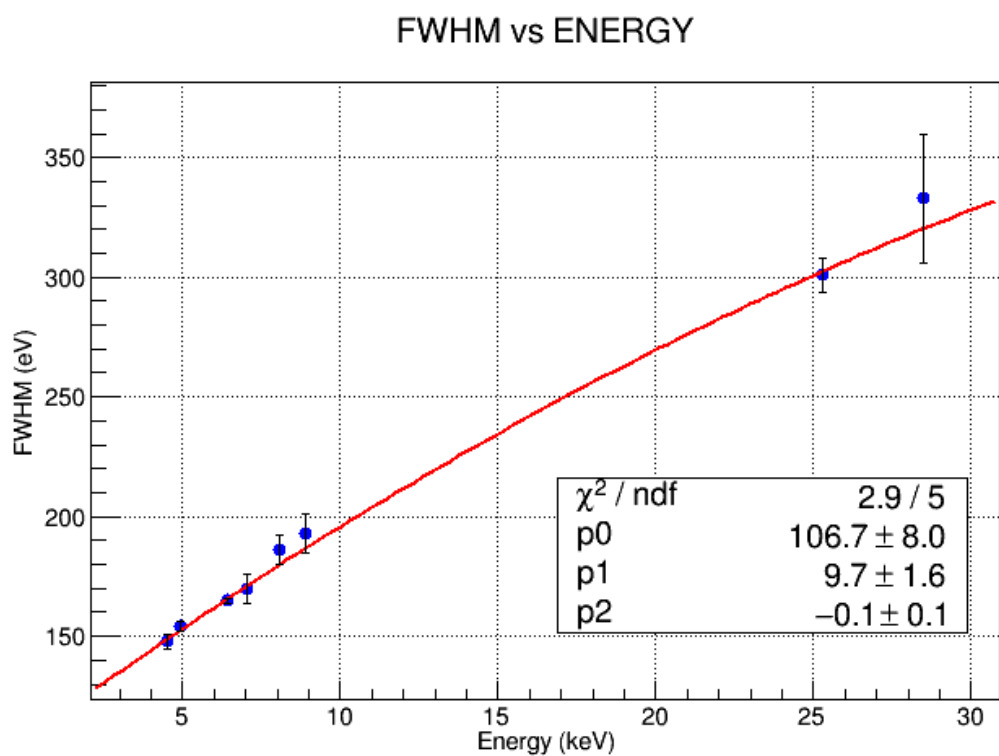


**Figure 3.13.** Trend of the FWHM with the emission energy. Samples were irradiated with the tube setting of 50 kV and 50  $\mu\text{A}$ .

CAEN module. This result is significant for MA-XRF measurements, when a macroscopic area is irradiated, and the irradiation time spent for each point is reduced compared with the acquisition time of a punctual XRF measurements.

A picture of the electronics inside the case in the present configuration is shown in Fig.3.15.



Spectra of CuPbSn sample with two acquisition systems

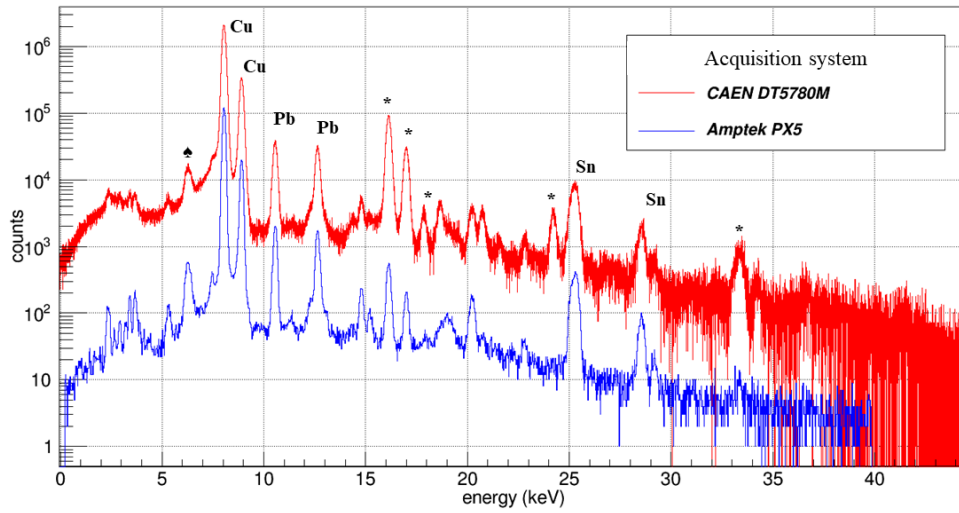


**Figure 3.14.** Comparison between the acquisition systems (PX5 by Amptek in blue, DT5780M by CAEN in red). The sample irradiated is made of copper, lead, and tin. Diffractions peaks are indicated with stars, while spades indicates the escape peak of Copper.

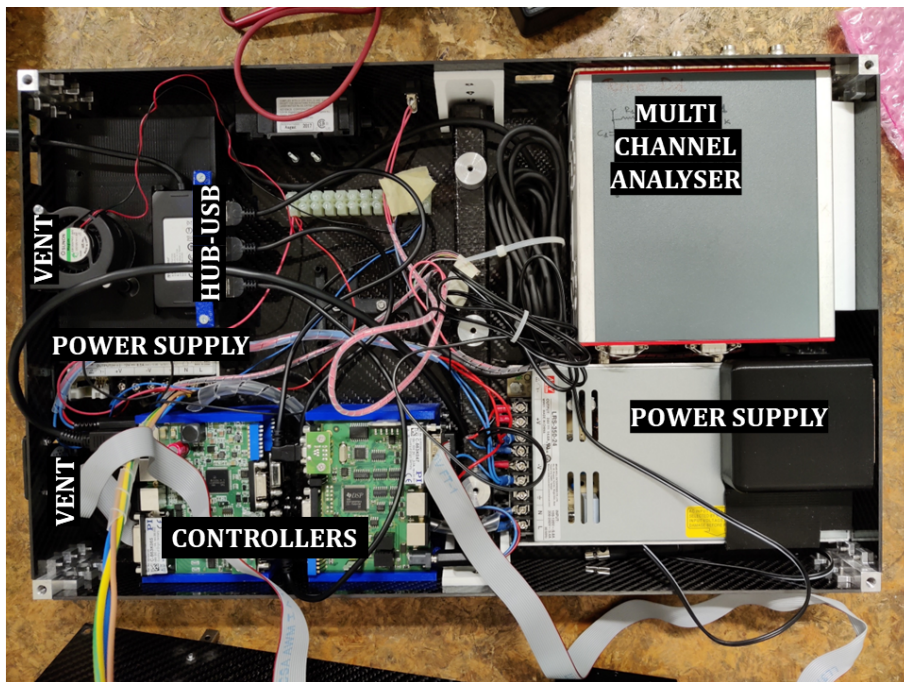


**Figure 3.15.** Picture of the electronics illustrated in Fig.3.6. The different components are indicated with labels.

## 3.4 Software for MA-XRF

In MA-XRF measurements, collected spectra are linked to the position of the irradiated area. Contrary to the others, for this technique an home-made software was developed by the researchers of the INFN-CHNet group. The software, written in C++, uses the QT's framework [77] for the graphical user interface and the CERN-Root's framework [78] can be used for the data analysis. The software has an user-friendly interface through which it is possible both to set the acquisition parameters of the digitiser and to control the motors. The main page is presented in Fig.3.16. For scanning, some parameters are defined, that are:

- the initial and final positions of the two scanning axis;
- the speed of the motor scanning continuously;
- the step size.

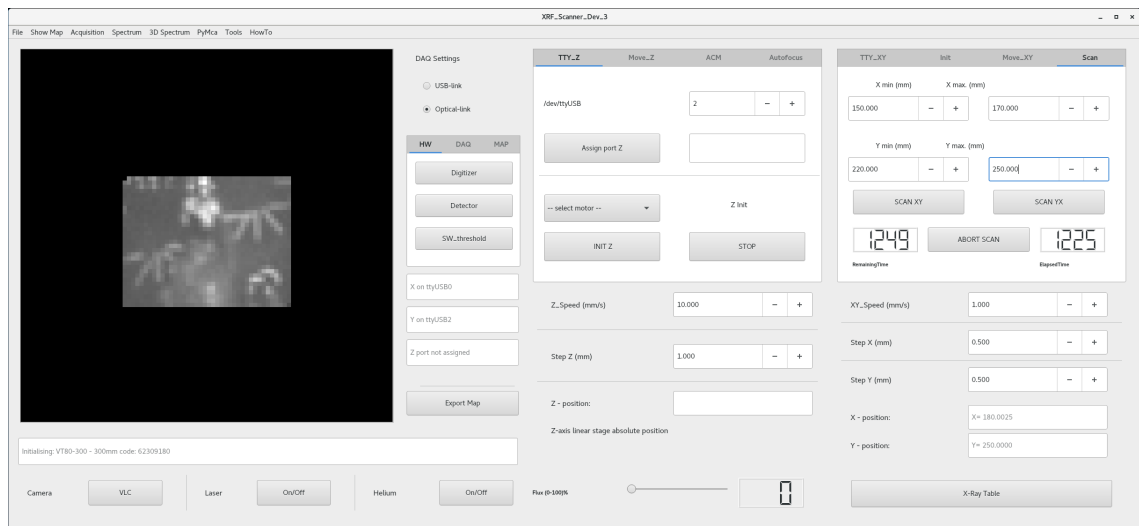


**Figure 3.16.** Screenshot of the main page of the software developed by the researchers of the INFN-CHNet collaboration.

For starting a MA-XRF measurement, the travel range of the VT-80 motors is set to determine the size of the area. The scan is made moving continuously one axis over the selected range and, at the end of each line, the second axis makes a step before the first one moves again in the opposite towards. The scan ends when both motors cover their scanning range.

The other parameters that have to be set for a scan are the motor speed and the step size of each motor. The speed is set for the first motor that continuously scans each line. Typical values are around few and ten millimetres per second. The step size is defined as the scanned length for which data are recorded in a single position, and it corresponds to the step of the second motor. Usually, the two step sizes are

set to the same value for both motors. A simple sketch of the scanning process is presented in Fig.3.17.

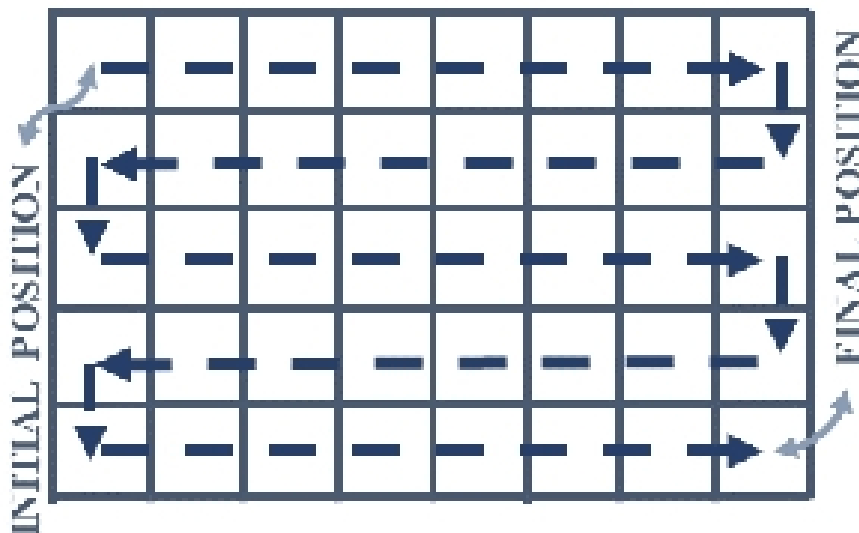


**Figure 3.17.** Sketch of the acquisition path of the scanner.

The output of a MA-XRF acquisition is a file containing the scanning coordinates and, for each position, the spectrum acquired. As a result, the counts are recorded for each position. For each scanned area, or a part of it, a single element can be selected by its energy transition value and shown as an elemental 2D map. For each peak, the energy range is manually selected around the centroid according to its FWHM. The relative intensity of each element in a map is shown in grey scale, in which the maximum intensity is in white and the minimum in black. Furthermore, multi-elemental maps can be created. In those maps, different elements are displayed in different colours (red, green, blue). This option permits the association of one or more pigments, by means of their chemical elements, to the visible features, allowing an immediate spatial distribution of the pigments [21].

Some output parameters (X and Y positions, remaining time) are displayed on-line while measuring. Other windows are present in the software: one for displaying the spectrum of a punctual measurement or of a selected area of a map; one for an on-line measure of the data rate acquisition; and one for setting the acquisition parameters of the CAEN DT5780M digitiser.

Other tools are available, such as the control of a profilometer for maintaining constant the distance between the specimen and the X-ray source are available, however, they are not in use for this device. Further information on the software can be found in [41].

### 3.5 Test of the instrument

The device, of which the different parts have been previously described, was assembled during the Summer 2022. Being a prototype of a MOvable DEvice for in-SiTU Analyses, it has been named MODESTA. A picture of it is presented in Fig.3.18. Some preliminary tests, here presented, are the measurement of the relative detection efficiency for XRF analysis, of the spot size of the beam, and the feasibility of XRIL technique. Some applications on objects, instead, are presented in chapter 4.

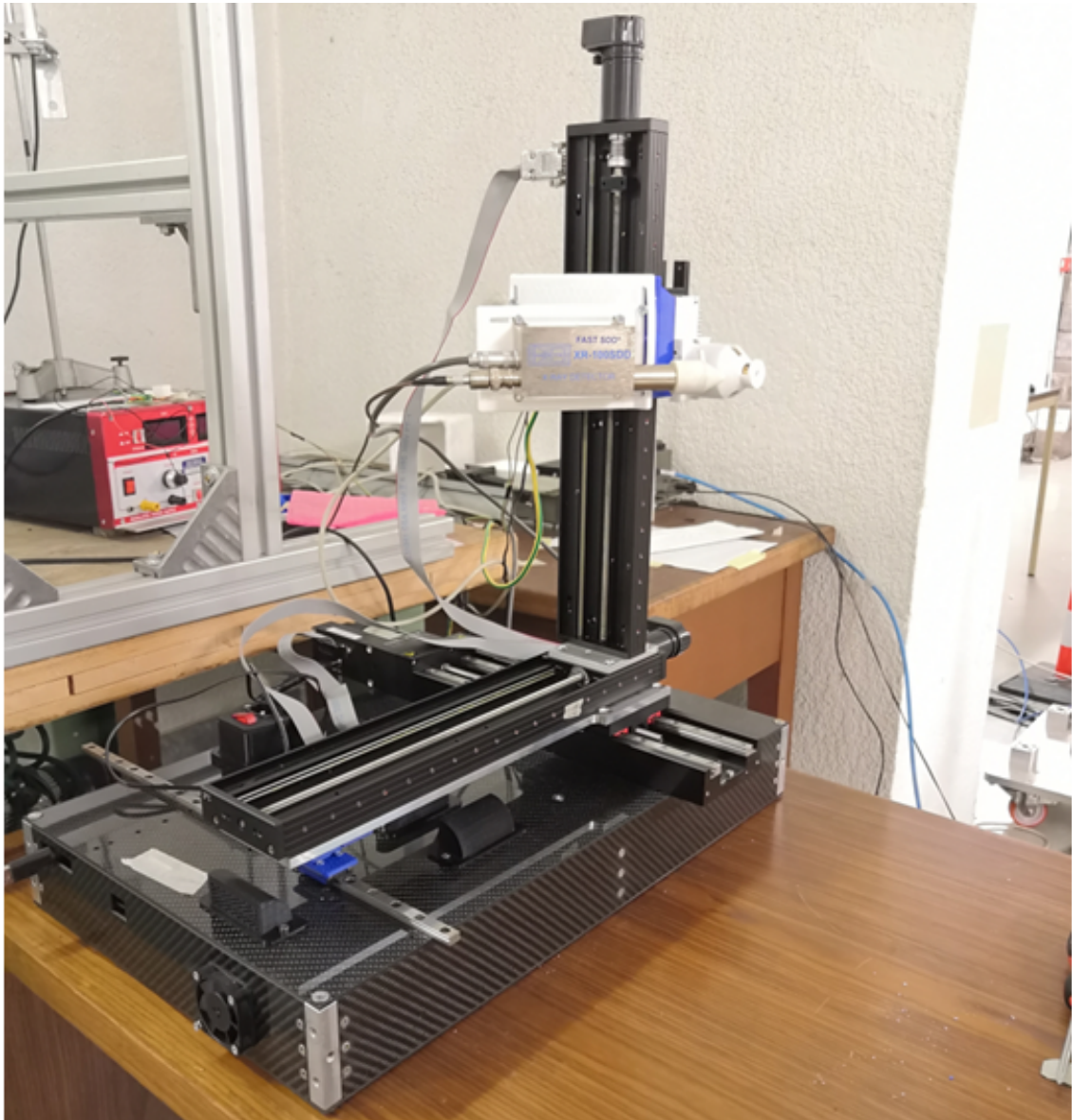


**Figure 3.18.** Picture of MODESTA.

For characterising the set-up for XRF measurements, the relative detection efficiency  $\epsilon$  of some elements was measured at the tube voltages of 20 kV, 30 kV, 40 kV, and

50 kV. It is defined as

$$\epsilon = \frac{A}{i \cdot t \cdot d} \left[ \frac{cm^2}{C \cdot \mu g} \right], \quad (3.1)$$

where  $A$  is the area of the corresponding energy peak given by the fit of Pymca software [79],  $i$  is the tube current,  $t$  is the irradiation time, and  $d$  is the areal density in  $\frac{\mu g}{cm^2}$  given by the manufacturer. For its measurement, some MicroMatter standards of mono or bi-elemental composition were used. The results are presented in Fig.3.19 for the energies of the  $K_{\alpha}$  lines of Ti (4.51 keV), Mn (5.90 keV), Cu (8.04 keV), Sn (25.27 keV), I (28.61 keV), and Ba (32.19 keV), as well as for the 10.55 keV and 12.61 keV L lines of Pb <sup>2</sup>.

According to the results presented in Tab.2.2, not all of the elements can be detected by XRF technique below a certain threshold (e.g 30 keV for Sn). As can be seen, the set-up is most efficient for Mn respect to the other elements in each condition. For Cu and Zn the relative efficiency is practically constant at 30 kV, 40 kV and 50 kV, while it increases with the tube voltage for higher Z elements. The trend of the curve decreases with the energy of the transitions, however, a higher number of data in the range between 15 keV and 25 keV would be necessary for confirming this result.

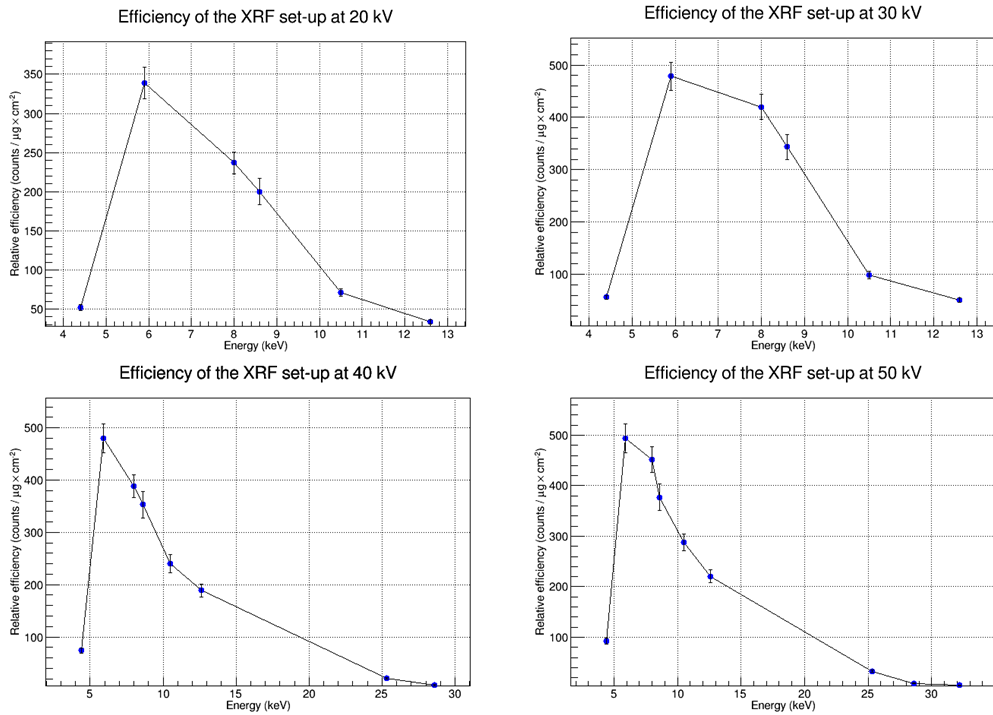


**Figure 3.19.** Graphs of the relative detection efficiencies for XRF analysis at 20 kV, 30 kV, 40 kV, and 50 kV.

<sup>2</sup>Since the tube current and the acquisition time were the same for all the measurements, they are not used in the calculation presented in Fig.3.19.

The dimension of the irradiating spot of the source was measured either without and with the collimator of one millimetre of diameter. Those two measurements aim to provide a first estimation of the angle of the X-ray beam when used for DR - without the collimator - or for XRF and XRIL - using a collimator - techniques. For the purpose, the flat panel detector was used. It was placed in front of the instrument, and the mutual distances between it and the measuring head were set using the M404.8PD motor. The software ImageJ was used for the analyses.

Even though the focal spot of the source is not a circle, for estimating the order of magnitude of the area irradiated by MODESTA, the shape of the spots on the flat panel detector was supposed to be circular in the analysis, and the tools for measuring its area, its diameter, and its perimeter were used in this hypotheses giving three values independently. The diameter of the equivalent circle of the spot, indicated in the following as the equivalent diameter  $d_{eq}$ , was calculated as their average and its standard deviation was used as its error. Accordingly, the equivalent radius  $r_{eq}$  is defined as its half. Results are reported in Tab.3.3. The source parameters are 30 kV and 5  $\mu$ A, while the acquisition time is set to 13 ms.

**Table 3.3.** Equivalent diameter of the irradiating area by the source at three different distances and corresponding half-opening angle (without collimator).

DISTANCE (mm)	DIAMETER (mm)	ANGLE (degree)
9 $\pm$ 1	12.08 $\pm$ 0.07	34 $\pm$ 3
14 $\pm$ 1	16.08 $\pm$ 0.02	31 $\pm$ 2
24 $\pm$ 1	29.5 $\pm$ 0.6	32 $\pm$ 2

The corresponding half-opening angle  $\alpha_{eq}$  was measured as

$$\alpha_{eq} = atan\left(\frac{r_{eq}}{d}\right), \quad (3.2)$$

where d is the mutual distance between the tube and the detector. As can be seen from the table, the results are in good agreement each others, and the angle is about 32°.

**Table 3.4.** Diameter of the irradiating area by the source at nine different distances and corresponding half-opening angle (with collimator).

DISTANCE (mm)	DIAMETER (mm)	ANGLE (degree)
10 $\pm$ 1	3.0 $\pm$ 0.1	5.7 $\pm$ 0.6
12 $\pm$ 1	3.3 $\pm$ 0.1	5.5 $\pm$ 0.5
13 $\pm$ 1	3.5 $\pm$ 0.1	5.4 $\pm$ 0.4
14 $\pm$ 1	3.6 $\pm$ 0.2	5.4 $\pm$ 0.4
16 $\pm$ 1	3.9 $\pm$ 0.2	5.2 $\pm$ 0.3
29 $\pm$ 1	5.30 $\pm$ 0.09	4.2 $\pm$ 0.1
34 $\pm$ 1	5.8 $\pm$ 0.1	4.1 $\pm$ 0.1
39 $\pm$ 1	6.9 $\pm$ 0.5	4.3 $\pm$ 0.1
44 $\pm$ 1	7.35 $\pm$ 0.08	4.2 $\pm$ 0.1

The same procedure was carried out collimating the source with the collimator with the diameter of 1 millimetre. Results are presented in Tab.3.4, and the angle is extrapolated from the graph presented in Fig.3.20.

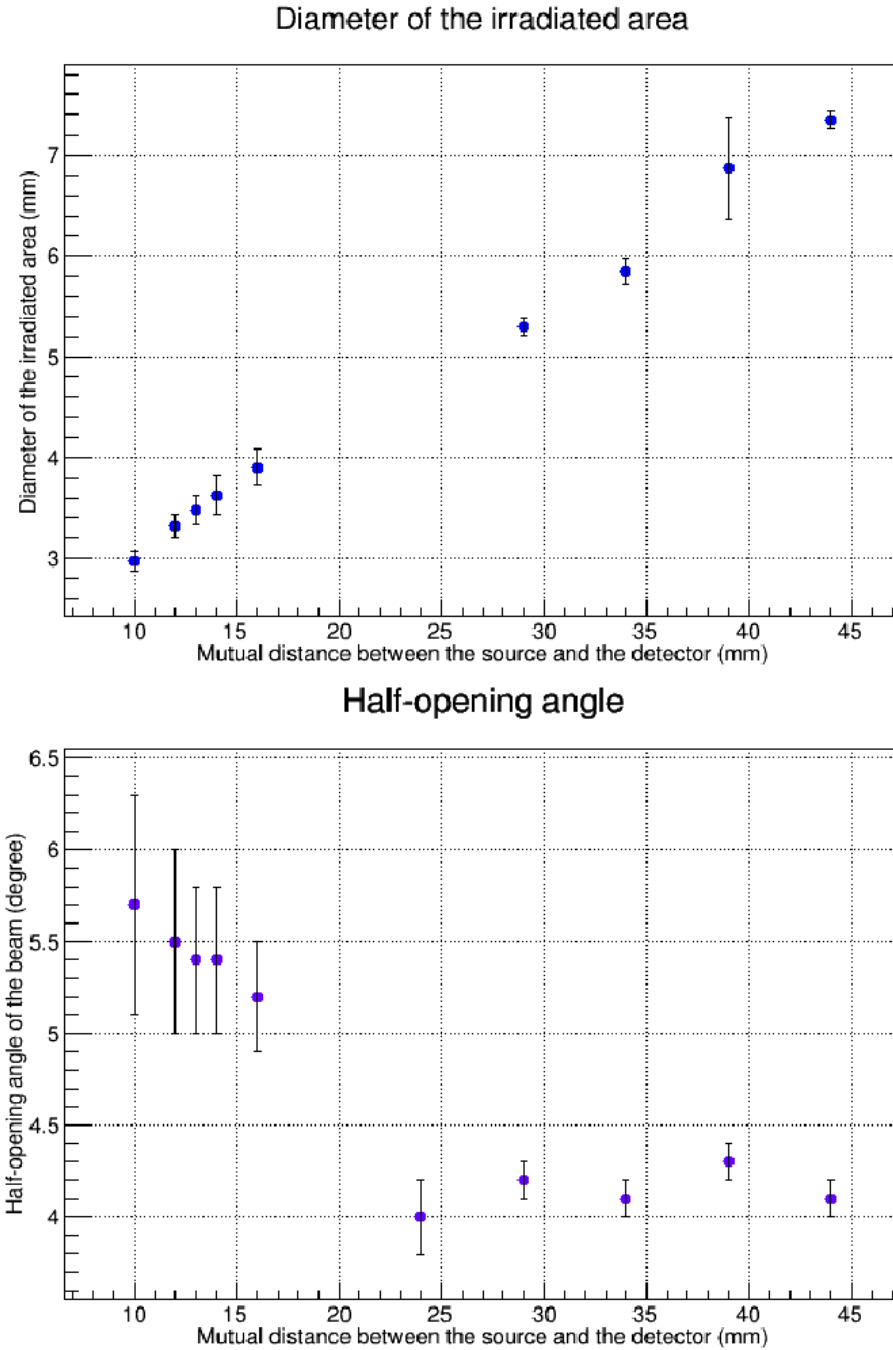


**Figure 3.20.** Diameter of the irradiated area (top) and corresponding half-opening angle with the mutual distance between the source and the detector for the collimated beam. The source parameters were 40 kV and 50  $\mu$ A.

The angle in the proximity of the source has a decreasing trend, whereas, above 25

mm, it is constant. By fitting the graph in Fig.3.20 in two parts, below and above 20 mm, the angle at the entrance window is  $(6.5 \pm 1.3)^\circ$ , whereas, when it is steady it measures  $(4.1 \pm 0.3)^\circ$ . This result can be explained by the absorption of the low energy (below keV) X-rays by the source from their path in the air. Moreover, it is worth noting that all those results are an overestimation, since a later straggling in the detector due to the crosstalk between the scintillators can be present during the irradiation. Those results can be used for determining the irradiated area with those configurations, furthermore, such kind of measurements could be repeated for the whole set of collimators.

For studying the feasibility of the XRIL technique, the collimator holder illustrated in Fig.3.5 was used. The same ZnS(Ag) scintillator was used for testing the feasibility of this technique with MODESTA. The same procedure presented in section 2.3 was used, however, the diameter of the collimator is 1 millimetre, and the geometry of the measuring head is fixed. The spectrum of ZnS(Ag) is presented in Fig.3.21, in which the tube setting is 20 kV and 600  $\mu$ A and the acquisition time was 60 seconds. Even though the intensity is lower compared with the ones presented in section 2.3, the advantages are a fixed geometry of the measurements, and the possibility of combining XRF and XRIL measurements together, guaranteeing the same experimental conditions for different samples measured subsequently.

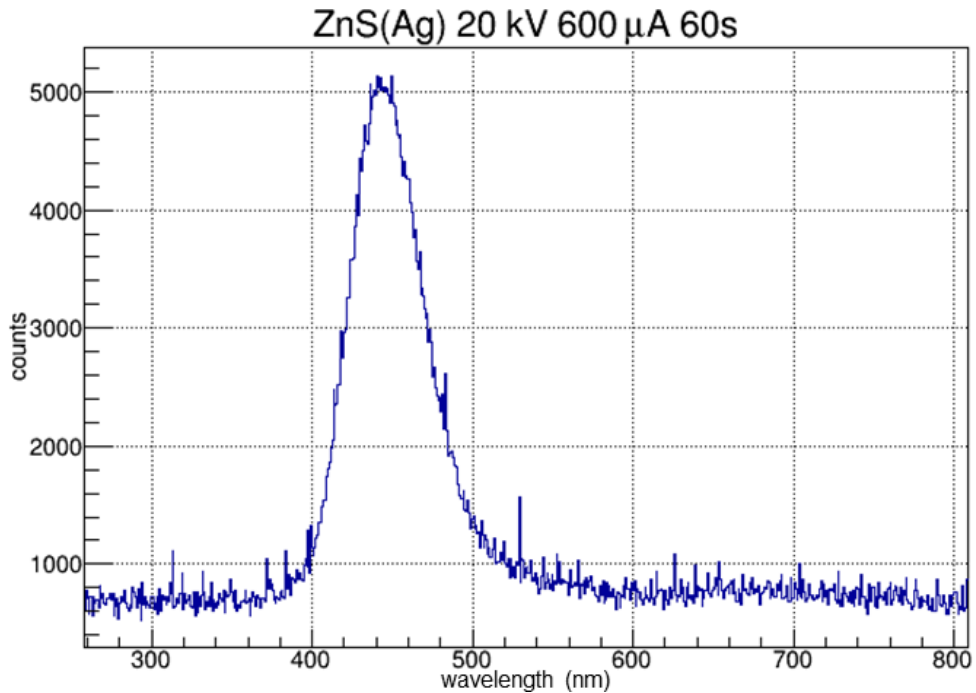


**Figure 3.21.** Spectrum of ZnS(Ag) acquired with the set-up presented in Fig.3.5 .



### 3.6 Radiation safety measurements

A number of measurements were carried out for radiation safety, both with and without collimators. Three different specimens have been used: a piece of cherry tree (circa ten centimetres thick), a painting on canvas (few millimetres thick), and a bronze thick sample (few centimetres thick). The results are used for evaluating the radiation risk of the device according to the Italian Legislative Decree 101/2020 [80].

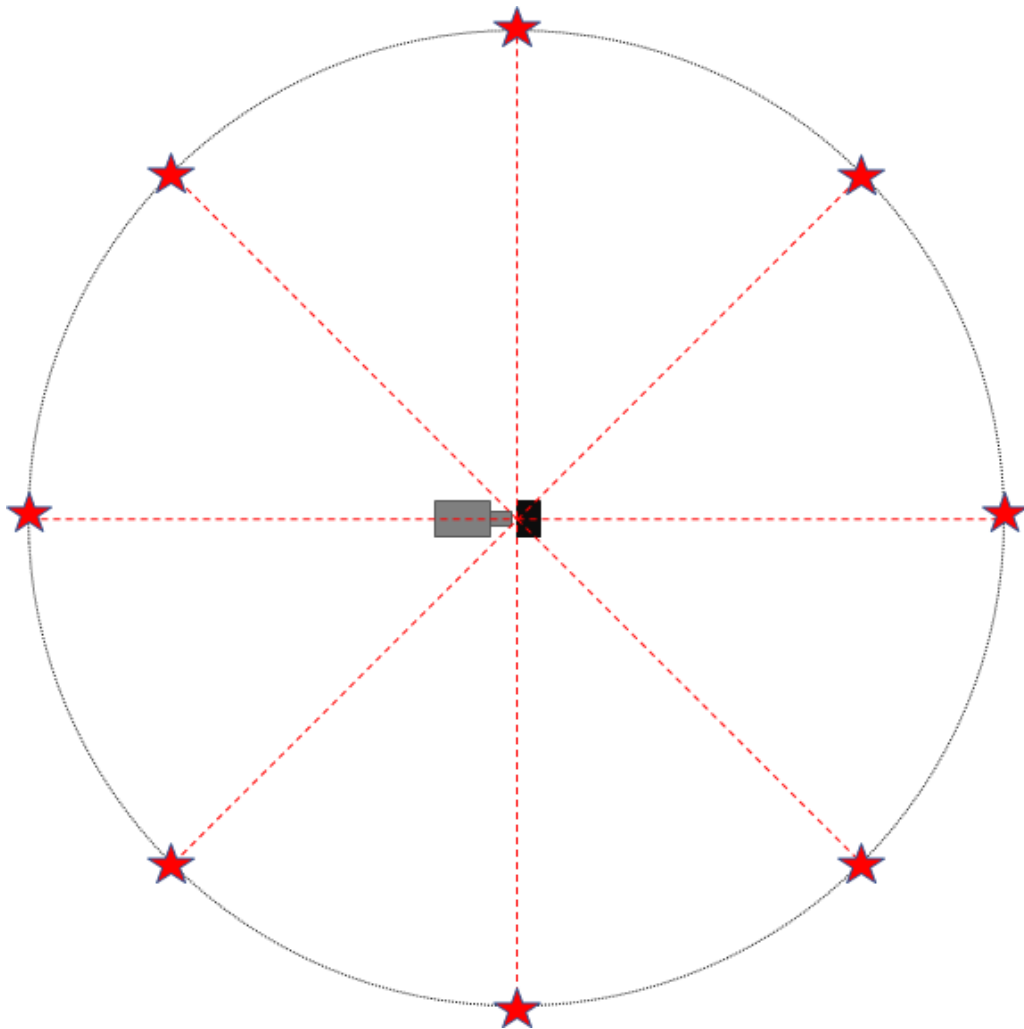


**Figure 3.22.** Sketch of the different positions (red stars) of the detector for the radiation safety measurements. The samples used in front of the source (in grey) are sketched as a black box.

The source, with the 1-millimetre collimator in front of it, was set to the maximum power with 60 kV and 200  $\mu\text{A}$ . The Berthold UMO LB 1230 multimeter with the LB 1236 proportional counter detector was placed at a distance of one metre in eight different positions, every 45°, as presented in Fig.3.22. The minimum dose of

scattered radiation was measured backward, while the maximum dose measured among the different positions was  $13.8 \mu\text{Sv/h}$  irradiating the cherry tree<sup>3</sup>. The dose of the direct radiation (without collimating the beam of the source and without any sample) was  $800 \mu\text{Sv/min}$ . It was measured straightforward with the Fluke 451B-DE-SI-RYR proportional chamber detector.

Moreover, for radiation protection and safety, four photoelectric sensors (model GL10 by SICK [81]) were used for defining a perimeter around the device and switching off the X-ray source in case someone accidentally cross the delimited area. The electric circuit connecting the sensors to MODESTA, developed by the members of the INFN-CHNet collaboration, allows the irradiation after a safety button is pressed and a green light shines. In addition, two others safety procedures are present:

- a red button, blocking the radiation if pressed;
- a button in the software controlling the source, that allows the emission of the X-rays only if is flagged.

---

<sup>3</sup>The cherry tree has the highest probability of scattering of the X-rays in comparison with the canvas and the bronze thick samples.

## Chapter 4

# Preliminary measurements with MODESTA: test applications for heritage science

In this chapter some preliminary measurements with MODESTA are presented. The aim of the following sections is to present the potentialities of the device through its application on objects of unknown composition having their structure typical of samples part of the cultural heritage (paintings, stones, ceramics).

### 4.1 Applications of MODESTA on paintings

Two kinds of paintings were investigated with the device, a painting on canvas and a painting on copper foil. In each of them, both DR and MA-XRF techniques have been used for a preliminary characterisation of the materials used.

#### 4.1.1 Painting on canvas

The first example is a painting on canvas of unknown composition representing three boats going through the horizon at the sunset (Fig.4.1). For XRF measurements, the distance between the measuring head and the sample was set to 10 mm, and the 1-mm collimator was mounted. The source was set to 50 kV and 200  $\mu\text{A}$ . The central area ( $100\times 100\text{ mm}^2$ ) was scanned with a speed of 5 mm/s and step sizes of 500  $\mu\text{m}$ . After data collection, the elemental maps were created selecting the corresponding energy lines with the software presented in section 3.4.

As can be seen from Fig.4.2, the two sides present a different composition. In particular, the left part is characterised by the presence of different elements, whereas on the right side no metal has been detected, most probably due to the use of organic



**Figure 4.1.** Painting on canvas representing three boat at the sunset.

compounds as pigments. On the left, the maps of selenium and cadmium led to the likely hypothesis of use of cadmium sulphide ( $\text{CdS}$ ) for the yellow, cadmium selenide ( $\text{CdSe}$ ) for the red/orange part of the sky, and burned cadmium selenide for the hull and keel [82]. The cobalt and chromium in the sea may be explained with the use of chromium oxides for the green colour and a cobalt-based compounds for the darkening hues [83]. In the same area, the map of the zinc reveals its use corresponding to the white colour, explicable with the use of zinc white ( $\text{ZnO}$ ) [82]. According to the literature [84], all these pigments were used during and after the XIX century, attesting, as expected, the recent production of the painting.

An area of  $30 \times 30 \text{ mm}^2$  around the keel of the small boat on the left has been scanned four times with the same setting of the source (50 kV,  $200 \mu\text{A}$ ), but different step sizes, once 0.5 mm and the other 1 mm, and speeds (5 mm/s and 10 mm/s). As can be seen from Fig.4.3, the spatial resolution between the measurements is improved when the step size is smaller. For this reason, when the details of a sample need a better spatial resolution, this parameter can be set to a smaller value for defining the spatial distribution of the elemental maps. Conversely, no significant differences are visible in spatial resolution if a different speed is used. On the other side, smaller step sizes require longer measurement times.

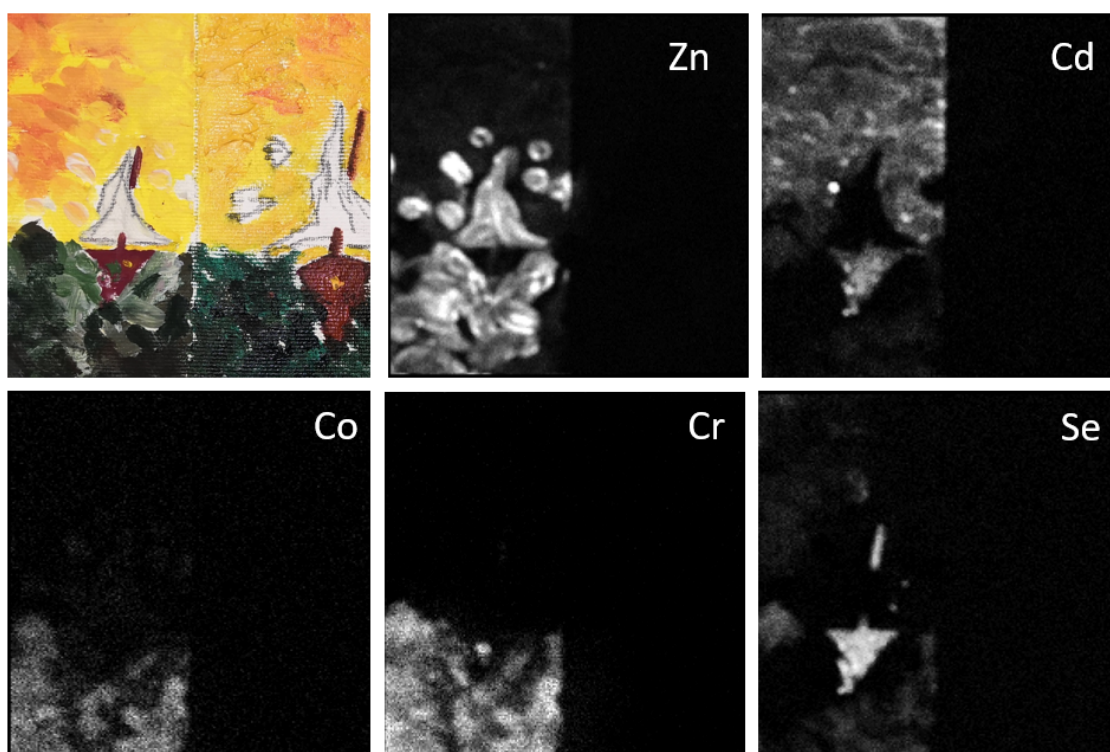


**Figure 4.2.** Visible image and elemental maps of the central area of the painting presented in Fig.4.1.

The central part of the same painting presented in Fig. 4.1 was irradiated without the collimator for performing DR. The measuring parameters of the source were 40 kV and  $100 \mu\text{A}$ , and the acquisition time for the radiography, presented in Fig.4.4, was 1 second. The mutual distance between the X-ray source and the flat panel detector was 185 mm, while the painting was placed 10 mm distant from the detector. In this configuration, the magnification is about 1 and the penumbra about  $25 \mu\text{m}$ .

As can be seen, the painting presents a different radiopacity of the two sides respect to the central vertical axis. This result is explicable both with the different composition detected with the MA-XRF technique, and also with the different thickness of the painting layer on the canvas.

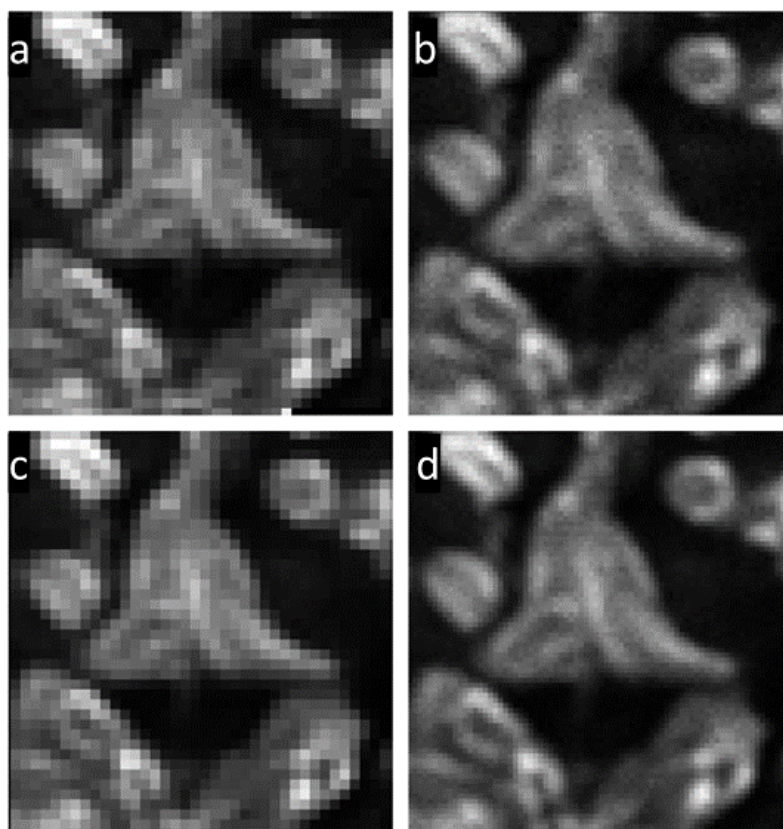


**Figure 4.3.** Elemental maps of Zn acquired with different step size and scanning speed: a) 1 mm, 10 mm/s; b) 0.5 mm, 10 mm/s; c) 1 mm, 5 mm/s d) 0.5 mm, 5 mm/s.

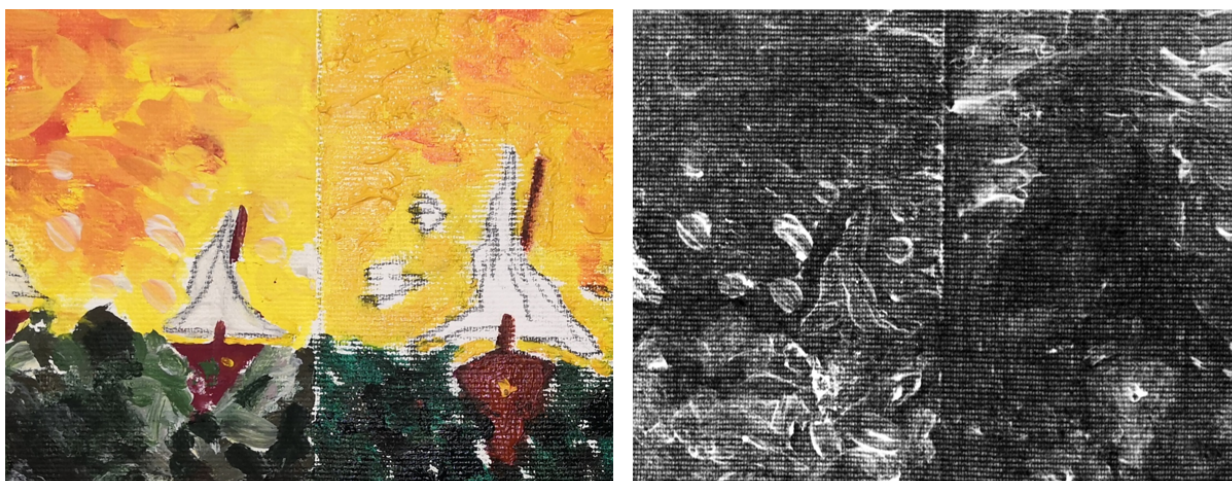


**Figure 4.4.** Visible image of the part of the painting irradiated (left) and its radiography (right).

## 4.1.2 Painting on copper foil

The painting on copper has an octagonal shape (maximum dimensions: 80 mm  $\times$  140 mm) and is in a wooden frame. A house in a countryside landscape is depicted in this painting (Fig.4.5). A water mirror is present on the front, probably representing a lake, and on the background there are mountains with white hues on the top probably for the snow. Vegetation is around the house as well as on the border of the lake, in particular there are trees of different colours around the house.



**Figure 4.5.** Picture of the central part of the painting on copper foil (see the text for further details).

Such as in the previous case, both scanning MA-XRF and DR were used. For the DR analysis, the painting was placed 38 cm far from the source, and the mutual distance between the object and the detector has been set to 2 cm. The tube setting was 60 kV and 200  $\mu$ A, while the acquisition time was 2.5 s. The radiography of the central part is presented in Fig.4.6. As can be seen, some elements of the landscape (e.g. the white top of the mountains) are clearly visible since they present a higher radiopacity,

probably due to a different composition respect to the rest of the painting layer. For the same reason, both the house and trees present a higher signal, explicable with heavier materials used for the painting layer. In addition, a more radiopaque area is present along the left side, that does not have a corresponding depicted visible area, and therefore it is not explicable with only this technique.

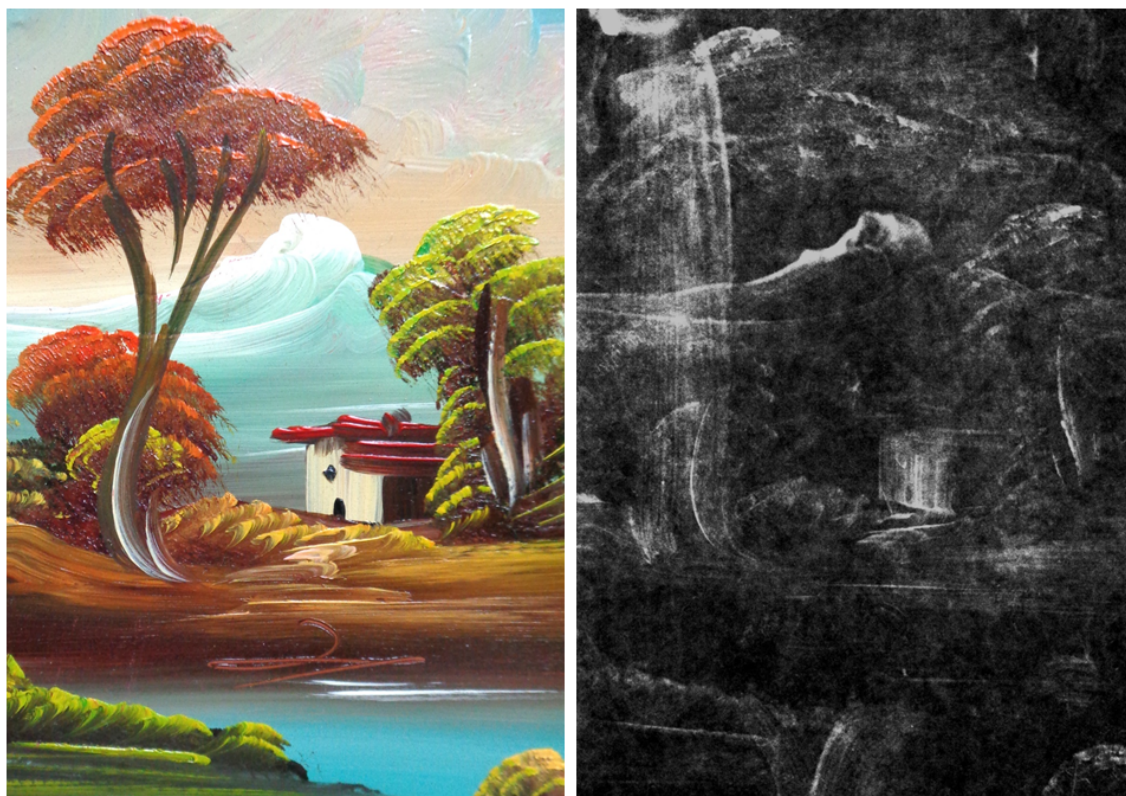


**Figure 4.6.** Visible area of the painting irradiated (left) and its DR (right).

The MA-XRF technique was carried out on an area of  $40 \times 130 \text{ mm}^2$  in the central part of the painting. The mutual distance between the source and the sample was set to 8 mm, the 1-mm collimator was used and the source was set to 50 kV and  $200 \mu\text{A}$ .

The elemental maps are presented in Fig.4.7. As expected, copper, the material of the support, is detected in all the scanned area and shows the typical absorption effects due to the pictorial layers on. The match between the visible colours and the maps reveals that the white house as well as the white in the brush strokes of the tree trunk were realised with a zinc-compound (e.g. ZnO). However, also barium and strontium are detected in conjunction with it in the house, explicable with the use of lithopone (mixture of ZnS and BaSO<sub>4</sub>)[82]. On the contrary, only Ba and Sr are present on the white of the top of the mountains, probably due to the use of barium sulphate (BaSO<sub>4</sub>). Lead was detected in the colour of the crowns of the trees and in the clearing, attesting its presence in the palette in different pigments (e.g. litharge or massicot for the yellow, minium for red/orange [85]). It is



worth remembering that with only this technique a conclusive identification of the materials is not possible.

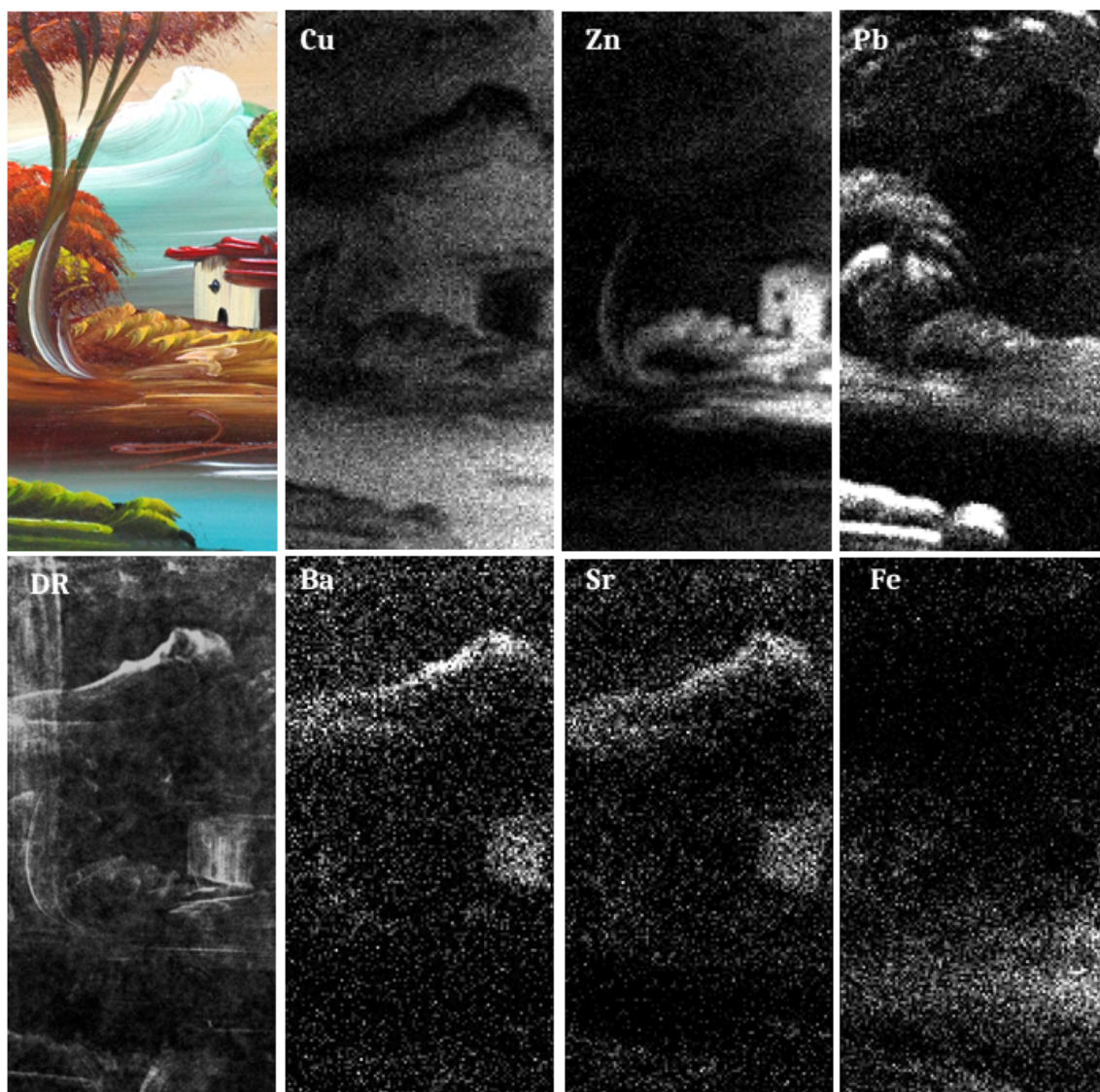


**Figure 4.7.** DR and elemental maps of the central area of the painting presented in Fig.4.5.

Last, no information is found on the radiopaque area on the left side of the painting identified with DR. For this reason, it is most likely related with some structure beneath the painting layer. This fact was attested by the presence of a wooden panel behind the copper foil found opening the painting from the back side.

## 4.2 Applications of MODESTA on ceramics

Two ceramic dishes were irradiated and, as in the cases of the paintings, both DR and MA-XRF techniques were employed. They are most likely European modern porcelains whose the production process achieved a considerable success and diffusion in Europe, especially after the discovery of the kaolin deposit in Limoges in 1767.

According to Colomban [86], decorations, which are glazes with the addition of chromophores or complex compounds such as spinels, can be broadly divided into overglaze and underglaze depending on which layer of the object they are present, over the glaze or over the ceramic body (and thus under a colourless glaze).

Two industrial techniques were used for overglaze decorations: transfer printing and chromolithography. Transfer printing gives a monochrome decoration, which can be filled with other colours afterwards [87]. Chromolithography, instead, gives a polychrome decoration which can be promptly reproduced on several objects [88]. The pieces are then made permanent by a further fire. In the case of underglaze decorations, instead, the coloured glass is fixed to the ceramic body during a single firing carried out at higher temperature. This reduces notably the palette as compounds suitable for high-temperature are required, but for a more durable result [89].

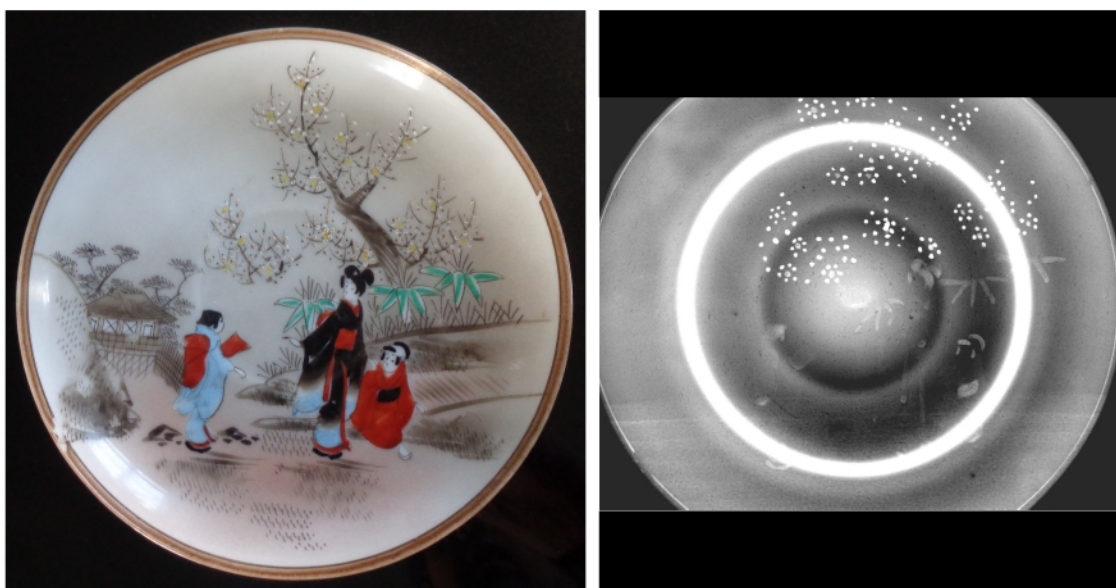


**Figure 4.8.** Visible image of the dish (left) and its radiography (right). The most radiopaque circle corresponds to the maximum thickness.

One of the two samples shows likely a mixed technique of underglaze and overglaze decoration (Fig.4.8), whereas the other presents an underglaze decoration. <sup>1</sup>. In the first, three people are depicted in a countryside of an Asian building. The colours

<sup>1</sup>This distinction is visible by raking light.

of their dresses are black, light blue and red. The landscape in the background is painted in brown colour, representing the grass, a trunk and a building. Three plants have green leaves and the tree has white and yellow flowers painted as dots.

The DR was conducted with the source parameters of 60 kV and 200  $\mu\text{A}$  and a magnification of 1 was achieved with the geometry of the set-up. The DR is presented in Fig.4.8. As can be seen, the leaves and the flowers show a higher radiopacity compared with the trunks of the trees and the other brown features. Similarly, the black and red dresses are more radiopaque than the light blue one. This can be explained either with a different thickness of the decorating layer, or with the use of a heavier elements in their composition.

A more detailed information on the latter aspect arises from the result of the MA-XRF analysis, presented in Fig.4.9. Data were collected using the tube setting 50 kV and 200  $\mu\text{A}$ . The mutual distance was set to 8 mm and the collimator had a diameter of 700  $\mu\text{m}$ . The irradiated area was 50 mm  $\times$  50 mm, the acquisition speed was set to 5 mm/s and the step sizes to 500  $\mu\text{m}$ .

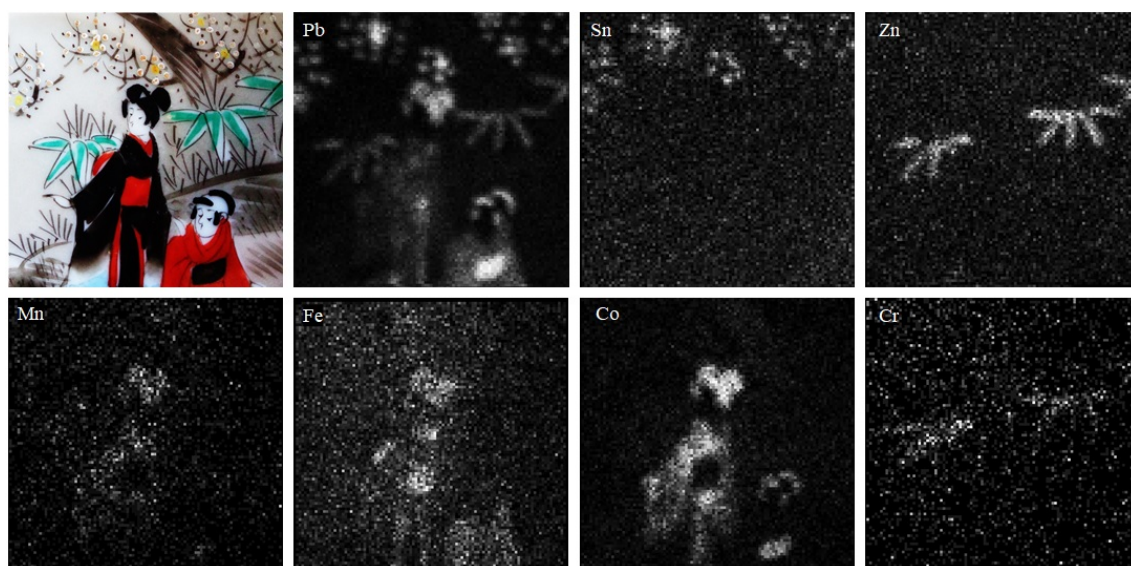


**Figure 4.9.** Elemental maps of the part of the dish presented in Fig.4.8 in the visible image.

As can be seen from the maps, the brown features in the background are not visible in any of the maps. Since organic pigments can not be used for ceramics due to the heating process, their absence in the maps is probably due to the fact that were painted underglaze. Conversely, the map of lead matches with all the other colours, probably due to the use of lead for their glazing. Tin is detected in the areas of yellow flowers, probably due to the use of lead tin yellow [82]. Cobalt and manganese are detected in the black colours, suggesting a mixture of metal based pigments for those decorations [86]. Iron is detected in the red areas, attesting the presence of an iron-based pigment. However, according to literature, it is most probable the

use of haematite. Zinc and chromium are detected in the green colours as visible in Fig.4.9. The presence of these two metals can be explained with the use of zinc green, however, as in the other cases, it is not possible to determine conclusively the composition of this material.

Conversely, the second dish is decorated entirely with an overglaze technique. Lead is largely present in the whole sample, attesting the use of a lead-containing glaze. The map of Lead indeed presents an homogeneous distribution. The other two elements detected are cobalt and iron. The corresponding maps reveal their presence in the red (Iron) and blue (Cobalt) areas, as presented in Fig.4.10, probably due to the use of haematite and a Cobalt-based pigment (e.g., smalt) [90].

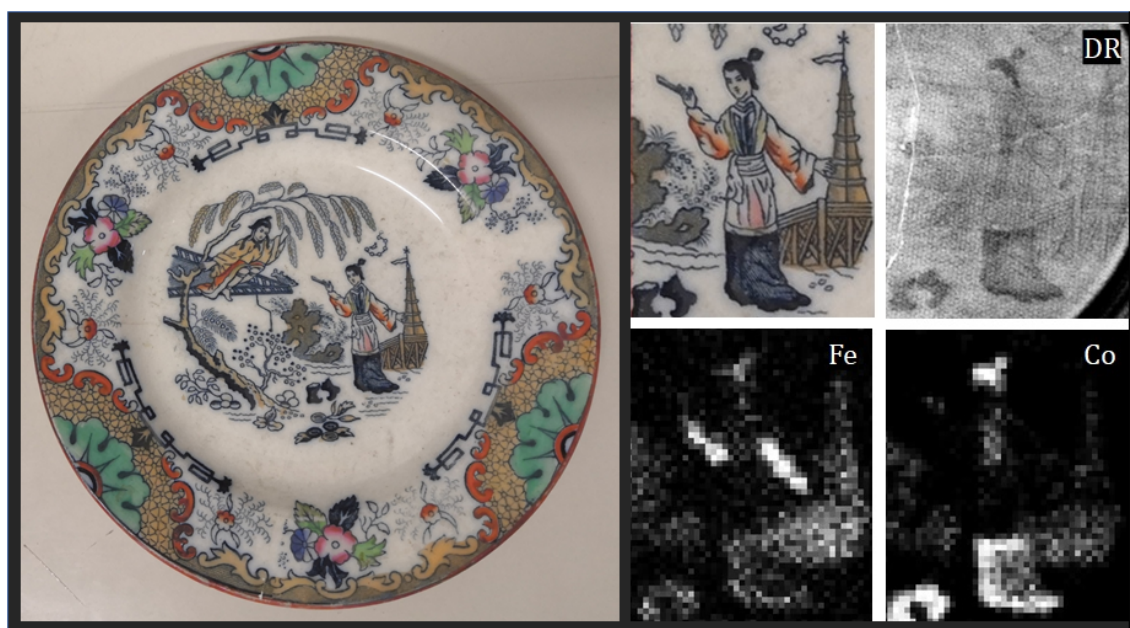


**Figure 4.10.** Picture of the overglaze dish (left) and magnification of the visible area irradiated, DR, and elemental maps of cobalt and iron (right).

### 4.3 Applications of MODESTA on stones

As presented in sections 2.3 and 3.5, the XRIL measurements can be used for studying the luminescence of minerals for provenance studies, and MODESTA can be used for this purpose for in-situ analysis. Here are presented the first two measurements on the same Chilean sample presented in section 2.3, and on a Iceland spar stone. For the first, the collimator holder used is the one presented in Fig.3.5, while for the latter, since the sample is a cube of  $1 \text{ cm}^3$  with flat surfaces, the other collimator holder was used. The set-up is presented in Fig.4.11 and the luminescence spectra of the lapis lazuli in Fig.4.12.



**Figure 4.11.** Picture of the set-up for the XRIL measurement of the Chilean sample presented in section 2.4.

As can be seen, the bands at 455 nm and at 560 nm in the Chilean sample are detected, respectively due to structural defects and Mn activators in wollastonite. In the second measurement, presented in Fig.4.13, a band between 580 nm and 620 nm is detected. Since Iceland spar is a type of calcite, it can be identified by the band due to the activator Mn, as reported in literature. Even if the intensities are not comparable with the ones presented in section 2.3, the device is capable of performing XRIL technique since the intensities are enough for being detected, and the acquisition time (60 seconds) is still comparable with the ones for XRF measurements. It is worth mentioning that the two cases presented are just examples, and they cannot be considered as general cases, but rather feasibility studies for in-situ XRIL measurements.

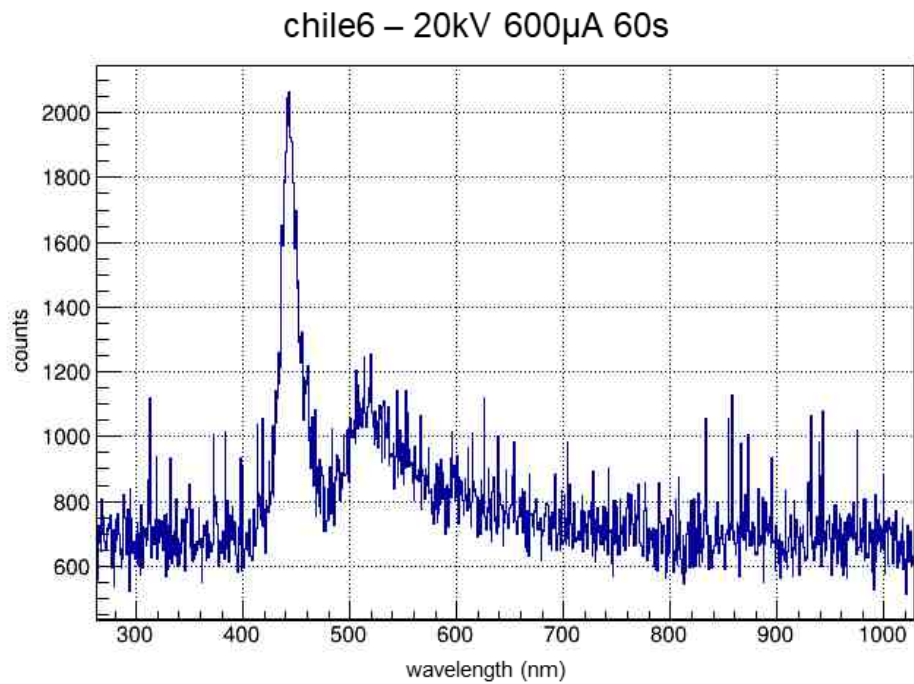


**Figure 4.12.** XRIL signal of the Chilean sample presented in section 2.4. Source parameters are 20 kV, 600  $\mu$ A; and 60 seconds of acquisition time.

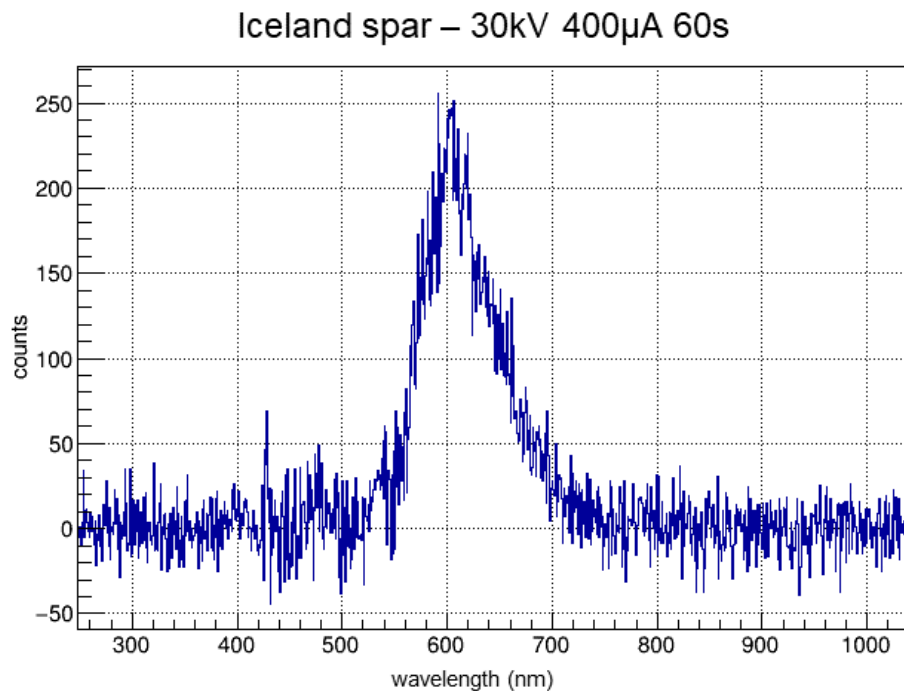


**Figure 4.13.** XRIL signal of a sample of Iceland spar (calcite). Source parameters are 30 kV, 400  $\mu$ A; acquisition time was set to 60 seconds.

## 4.4 Applications of MODESTA on an inkstick

As a third type of application, both DR and MA-XRF techniques were used for study a Chinese inkstick, a solid ink, traditionally used in Chinese and East Asian art forms such as calligraphy and brush painting [91]. The object is shown in Fig.4.14, and its dimensions are about  $3 \times 9 \times 2 \text{ cm}^3$ . On a side is represented the landscape of a mountain with a valley, with rivers and trees, while on the other side there is a writing text that means “ancient ink from Huangshan mountain”.

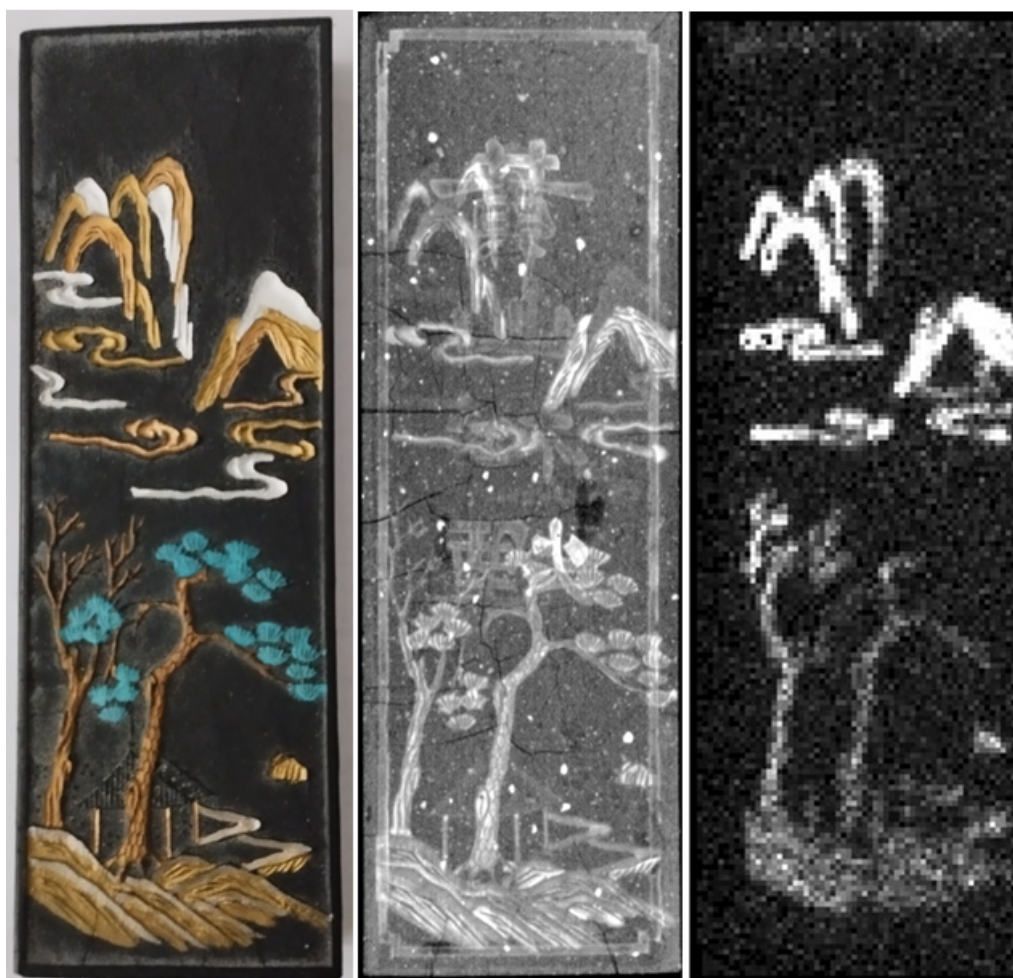


**Figure 4.14.** Picture of the inkstick (left), DR (centre) and copper map (right).

The Huangshan (Yellow Mountain) Pine Soot ink stick bears its name since it is made of pine soot, which produces a matte black finish of the ground ink. Many black ink sticks are made from oil soot, which provides a glossy finish, and are usually used for painting the main subjects of an artwork.

For the MA-XRF measurement the setting of the X-ray source was 50 kV, 200  $\mu\text{A}$ . The speed of the scan was set to 5 mm/s with a step size of 500  $\mu\text{m}$ . The collimator

used has a diameter of  $700\ \mu\text{m}$ . The entire object was scanned. The setting for the DR were  $60\ \text{kV}$  and  $200\ \mu\text{A}$  (source) and acquisition time was set to 3.5 seconds. The distance between the source and the detector was set to 47 cm, while the stick was placed at 34 cm from the source. The resulting magnification is  $\sim 1.4$  and the penumbra  $153\ \mu\text{m}$ . As can be seen by the radiography, the visible features are more radiopaque compared with the bulk. Moreover, both the writing on the back and some inclusions (white dots) can be seen as well as some cracks not clearly visible at naked eye, compatible with the light elements in the composition.

The MA-XRF analysis reveals the presence of copper in the trees and in the mountain as visible in Fig.4.14, whereas no other elements were present in the spectrum. No elements were detected in correspondence of the white and blue colours, probably due to the use of organic compounds or minute quantities of material.

The results confirm the use of a metal for the figures and a bulk composed by organic materials, deduced from the lower radiopacity and the absence of XRF signals. For determining the depth of the inclusions, a second radiography from a side was done (Fig.4.15). A more detailed study of the structure could be done by means of a CT analyses, such as the one performed in section 4.5.

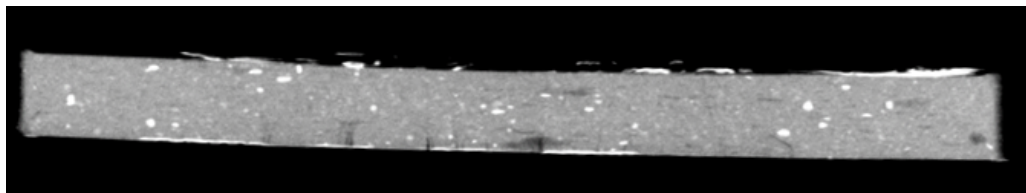


**Figure 4.15.** DR of the inkstick from the lateral side.

## 4.5 Preliminary CT with MODESTA

As a feasibility study of CT with the X-ray source and the flat panel, a first set-up was mounted using the rotating stage URS150.BPP by NewPort [92]. For this preliminary measurement a seashell of about  $12 \times 16 \times 30\ \text{mm}^3$  and a wisdom tooth of the author was irradiated. The source parameters were  $60\ \text{kV}$  and  $200\ \mu\text{A}$ , the exposure time of the detector 3.5 seconds for each projection, and the angular step between two following projections was 0.25 degree. The acquisition software has been developed by the researchers of the collaboration in LabView, while the projections for the CT has been created using the software Dragonfly [93], a software for scientific image processing. The distance between the source and the detector was 47 cm, while the object was placed 13 cm far from the detector. The resulting magnification is  $\sim 1.4$ , the penumbra  $153\ \mu\text{m}$ , and the voxel size, calculated as the ratio between the pixel and the magnification, is  $\sim 36\ \mu\text{m}^2$ . A picture of the

---

<sup>2</sup>The voxel is the 3D smallest unitary element of the reconstruction matrix of a CT.



set-up is presented in Fig.4.16. A preliminary result is presented in Fig.4.17. As

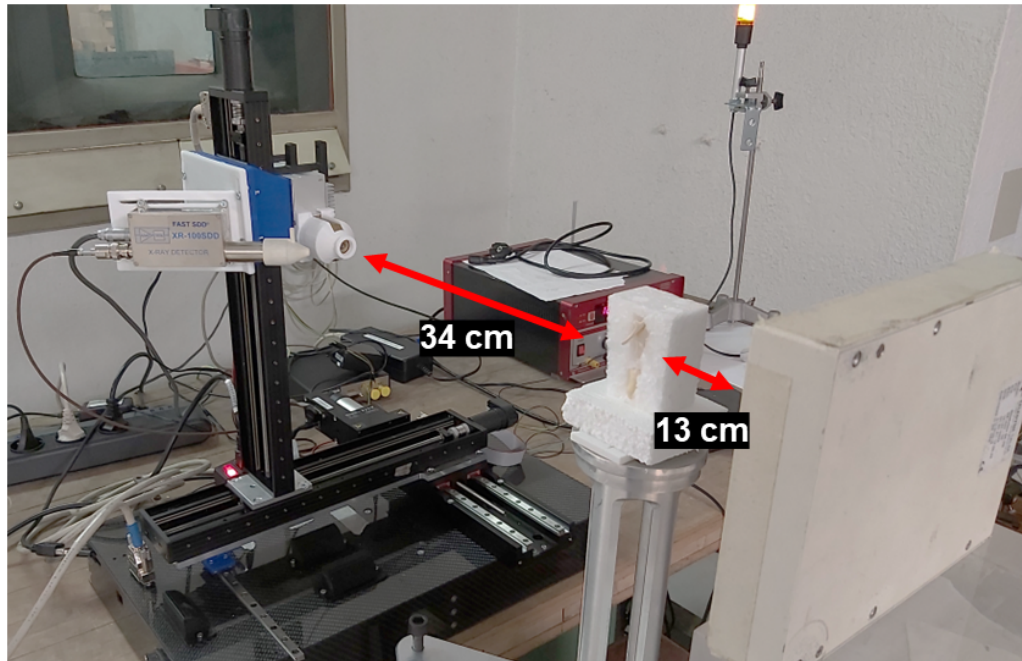


**Figure 4.16.** Picture of the set-up for the CT.

can be seen the CT of the seashell and the tooth has been realized with this set-up, expanding the possible application of the device.

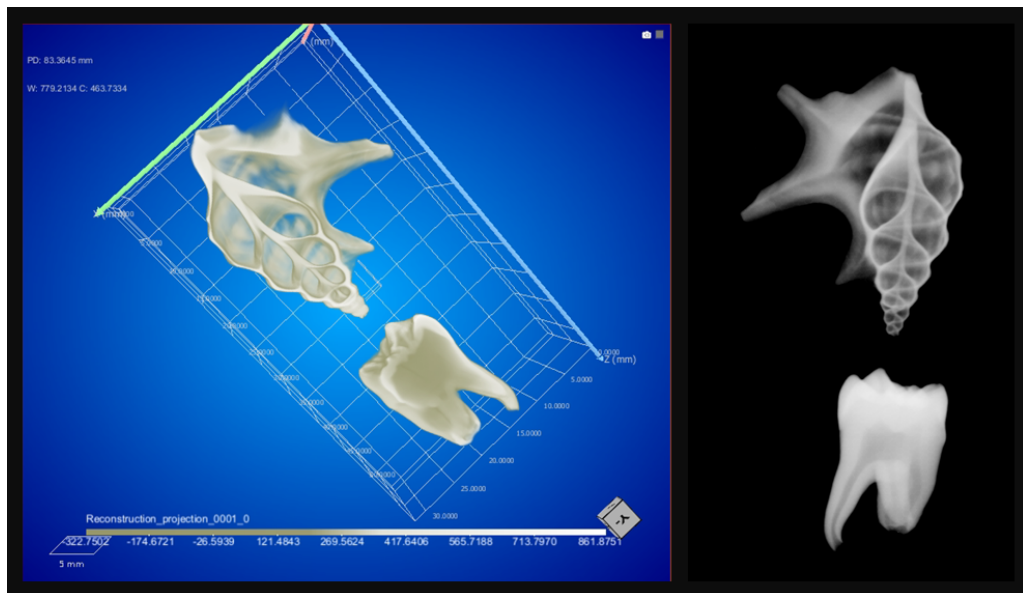


**Figure 4.17.** Three dimensional reconstruction (left) and a DR (right) of the sample. They were acquired with the same set-up.

# Conclusion and Outlook

The aim of the research project was to develop a device performing in-situ analysis. It had to be transportable, combining different non-invasive and non-destructive techniques for offering a number of information on objects of interest for the cultural heritage, without the need of any preparation of the sample. The analyses available at the moment, all using an X-ray beam as a probe, are XRF, XRIL, and DR.

The XRF technique provides information on elemental composition, detecting the X-rays emitted by the sample. In an XRIL measurement, the luminescence of a material is collected once an X-ray beam impinges on it. The DR technique allows to study the inner structure of an object through two dimensional images.

The different components (source, detectors, motors) were tested, and both the mechanical and the electronic parts have been developed in the project. The performances of the device, named MODESTA, have been described in section 3.5, while its capabilities have been presented through same examples (paintings, stones, ceramics) in chapter 4.

One of the strength of MODESTA, in comparison with other portable and transportable instruments, is the variety of information provided thanks to the combination of the three analytical methods. Moreover, both MA-XRF and CT have been exploited as further analyses, expanding the achievable information obtainable.

Moreover, being part of a research project, MODESTA can be improved and upgraded in the near future. For example, the software for MA-XRF and CT, developed by the researchers of the INFN-CHNet collaboration, could be integrated as a single software controlling the acquisition of all the techniques. In addition, thanks to the expertise within the research group, a further version of MODESTA can be realised with longer axes, enlarging the size of scanned and imaged areas. It is worth noting that, thanks to the database of the drawings of the different parts designed with Autodesk Inventor, they can be easily modified and printed according to future needs.

A further improvement, that is at the moment under study, is the construction of another motorised system for placing the flat panel detector on it, and translate it in parallel with the measuring head, and therefore imaging a larger area in the same measuring session without moving neither the detector nor the object. The case has

been already designed and is under realisation.

# Bibliography

- [1] S. Dupré, S. Kusukawa, K. Leonhard, N. Forshaw, K. Comer, H. Seccaroni, E. Stege, Basso, and B. Berrie, “Mining for color: New blues, yellows, and translucent paint,” *Early Science and Medicine*, vol. 20, pp. 308–334, 12 2015.
- [2] P. Urbanova, E. Boaretto, and G. Artioli, “The state-of-the-art of dating techniques applied to ancient mortars and binders: A review,” *Radiocarbon*, vol. 62, pp. 1–23, 06 2020.
- [3] M. Chiari, S. Barone, A. Bombini, G. Calzolari, L. Carraresi, L. Castelli, C. Czelusniak, M. Fedi, N. Gelli, F. Giambi, F. Giardi, L. Giuntini, S. Lagomarsino, L. Liccioli, F. Lucarelli, M. Manetti, M. Massi, A. Mazzinghi, S. Nava, and P. Mandò, “Labec, the infn ion beam laboratory of nuclear techniques for environment and cultural heritage,” *The European Physical Journal Plus*, vol. 136, p. 472, 04 2021.
- [4] M. Vermeulen, E. Muller, and M. Leona, “Non-invasive study of the evolution of pigments and colourants use in 19th-century ukiyo-e,” *Arts of Asia*, vol. 50, p. 103, 03 2020.
- [5] [www.c2rmf.fr](http://www.c2rmf.fr), Retrieved 09 April 2023.
- [6] F. Zanini and F. Bernardini, “Echo: The elettra cultural heritage office,” in *Handbook of Cultural Heritage Analysis*, pp. 315–353, Springer, 01 2022.
- [7] <https://www.ucl.ac.uk/bartlett/heritage/research-1>, Retrieved 07 July 2023.
- [8] <https://www.heritageresearch-hub.eu/member/institute-of-heritage-science-cnr-ispc/>, Retrieved 07 July 2023.
- [9] <https://www.rijksmuseum.nl/en/research/our-research/conservation-science>, Retrieved 07 July 2023.
- [10] <https://www.bruker.com/en/applications/academia-materials-science/art-conservation-archaeology.html>, Retrieved 07 July 2023.
- [11] <https://www.unesco.org/en/legal-affairs/constitution> , Retrieved 24 January 2023.

- [12] <https://whc.unesco.org/en/conventiontext/> ,article 4. Retrieved 24 January 2023.
- [13] <https://culture.ec.europa.eu/cultural-heritage/eu-policy-for-cultural-heritage>. Retrieved 24 January 2023.
- [14] <https://www.e-rihs.it/en/>. Retrieved 24 January 2023.
- [15] <https://www.e-rihs.it/en/laboratori-mobili/>. Retrieved 24 January 2023.
- [16] M. Aceto, A. Agostino, G. Fenoglio, A. Idone, M. Gulmini, P. Marcello, P. Ricciardi, and J. Delaney, “Characterisation of colourants on illuminated manuscripts by portable fibre optic uv-visible-nir reflectance spectrophotometry,” *Anal. Methods*, vol. 6, pp. –, 03 2014.
- [17] M. Crippa, S. Legnaioli, C. Kimbriel, and P. Ricciardi, “New evidence for the intentional use of calomel as a white pigment,” *Journal of Raman Spectroscopy*, vol. 52, no. 1, pp. 15–22, 2021.
- [18] S. Muralha, L. Burgio, and R. Clark, “Raman spectroscopy analysis of pigments on 16–17th c. persian manuscripts,” *Spectrochimica acta. Part A, Molecular and biomolecular spectroscopy*, vol. 92, pp. 21–8, 02 2012.
- [19] A. Impallaria, F. Evangelisti, F. Petrucci, F. Tisato, L. Castelli, and F. Taccetti, “A new scanner for in situ digital radiography of paintings,” *Applied Physics A*, vol. 122, 11 2016.
- [20] A. Mazzinghi, C. Ruberto, L. Giuntini, P. Mandò, F. Taccetti, and L. Castelli, “Mapping with macro x-ray fluorescence scanning of Raffaello’s portrait of Leo X,” *Heritage*, vol. 5, pp. 3993–4005, 12 2022.
- [21] L. Sottili, L. Guidorzi, A. Mazzinghi, C. Ruberto, L. Castelli, C. Czelusniak, L. Giuntini, M. Massi, F. Taccetti, M. Nervo, S. Blasi, R. Torres, F. Arneodo, A. Re, and A. Giudice, “The Importance of Being Versatile: INFN-CHNet MAXRF Scanner on Furniture at the CCR “La Venaria Reale”,” *Applied Sciences*, vol. 11, p. 1197, 01 2021.
- [22] L. Sottili, L. Guidorzi, A. Giudice, A. Mazzinghi, C. Ruberto, L. Castelli, C. Czelusniak, L. Giuntini, M. Massi, F. Taccetti, M. Nervo, R. Torres, F. Arneodo, and A. Re, “Macro X-ray fluorescence analysis of XVI-XVII century Italian paintings and preliminary test for developing a combined fluorescence apparatus with digital radiography,” *ACTA IMEKO*, vol. 11, p. 8, 03 2022.
- [23] S. De Meyer, F. Vanmeert, R. Vertongen, A. van Loon, V. Gonzalez, G. Van der Snickt, A. Vandivere, and K. Janssens, “Imaging secondary reaction products at the surface of vermeer’s girl with the pearl earring by means of macroscopic x-ray powder diffraction scanning,” *Heritage Science*, vol. 7, 09 2019.
- [24] J. Delaney, P. Ricciardi, L. Glinsman, M. Facini, M. Thoury, M. Palmer, and R. de la Rie, “Use of imaging spectroscopy, fiber optic reflectance spec-

- troscopy and x-ray fluorescence to map and identify pigments in illuminated manuscripts,” *Studies in Conservation*, vol. 59, 01 2013.
- [25] D. Pinna, M. Galeotti, and M. Rocco, *Scientific Examination for the Investigation of Paintings: A Handbook for Conservators-restorers*. 09 2009.
- [26] D. Papadopoulou, G. Zachariadis, A. Anthemidis, N. Tsirliganis, and J. Stratis, “Development and optimisation of a portable micro-xrf method for in situ multi-element analysis of ancient ceramics,” *Talanta*, vol. 68, pp. 1692–9, 03 2006.
- [27] M. Alfeld, J. Pedroso, M. van Eikema Hommes, G. Van der Snickt, G. Tauber, J. Blaas, M. Haschke, K. Erler, J. Dik, and K. Janssens, “A mobile instrument for in situ scanning macro-xrf investigation of historical paintings,” *Journal of Analytical Atomic Spectrometry*, vol. 28, pp. 760–767, 03 2013.
- [28] M. Guerra, S. Longelin, S. Pessanha, M. Manso, and M. Carvalho, “Development of a combined portable x-ray fluorescence and raman spectrometer for in situ analysis,” *Review of Scientific Instruments*, vol. 85, pp. 063113–063113, 06 2014.
- [29] M. Eveno, E. Ravaud, T. Calligaro, L. Pichon, and E. Laval, “The louvre crucifix by giotto – unveiling the original decoration by 2d-xrf, x-ray radiography, emissigraphy and sem-edx analysis,” *Heritage Science*, vol. 2, p. 17, 08 2014.
- [30] C. Ruberto, A. Mazzinghi, M. Massi, L. Castelli, C. Czelusniak, L. Palla, N. Gelli, M. Betuzzi, A. Impallaria, R. Brancaccio, E. Peccenini, and M. Raffaelli, “Imaging study of Raffaello’s “la muta” by a portable xrf spectrometer,” *Microchemical Journal*, vol. 126, 11 2015.
- [31] R. Alberti, T. Frizzi, L. Bombelli, M. Gironda, N. Aresi, F. Rosi, C. Miliani, G. Tranquilli, F. Talarico, and L. Cartechini, “Crono: a fast and reconfigurable macro x-ray fluorescence scanner for in-situ investigations of polychrome surfaces,” *X-Ray Spectrometry*, vol. 46, 02 2017.
- [32] F. P. Romano, C. Caliri, P. Nicotra, S. Dimartino, L. Pappalardo, F. Rizzo, and H. Santos, “Real-time elemental imaging of large dimension paintings with a novel mobile macro x-ray fluorescence (ma-xrf) scanning technique,” *J. Anal. At. Spectrom.*, vol. 32, 02 2017.
- [33] P. De Campos, C. Appoloni, M. Rizzutto, A. Leite, R. Assis, H. Santos, T. Silva, C. L. Rodrigues, M. Tabacniks, and N. Added, “A low-cost portable system for elemental mapping by xrf aiming in situ analyses,” *Applied Radiation and Isotopes*, vol. 152, 06 2019.
- [34] E. Pouyet, N. Barbi, H. Chopp, O. Healy, A. Katsaggelos, S. Moak, R. Mott, M. Vermeulen, and M. Walton, “Development of a highly mobile and versatile large ma-xrf scanner for in situ analyses of painted work of arts,” *X-Ray Spectrometry*, 07 2020.

- [35] L. Bonizzoni, J. Orsilli, and A. Galli, “Fuxya2020: A low-cost homemade portable edxrf spectrometer for cultural heritage applications,” *Applied Sciences*, vol. 12, 01 2022.
- [36] S. A. Barcellos Lins, *Development of a 2D-XRF scanner for cultural heritage applications*. PhD thesis, Sapienza University of Rome, 2022.
- [37] M. Eveno, B. Moignard, and J. Castaing, “Portable apparatus for in situ x-ray diffraction and fluorescence analyses of artworks,” *Microscopy and microanalysis : the official journal of Microscopy Society of America, Microbeam Analysis Society, Microscopical Society of Canada*, vol. 17, pp. 667–73, 05 2011.
- [38] <https://www.quantanalitica.com/en/i-nuovi-modelli-di-xrf-e-xrd-xrf-di-olympus/>, Retrieved 09 April 2023.
- [39] <https://chnet.infn.it/en/home-3/> Retrieved 05 February 2023.
- [40] <https://home.infn.it/it/>, Retrieved 09 April 2023.
- [41] F. Taccetti, L. Castelli, C. Czelusniak, N. Gelli, A. Mazzinghi, L. Palla, C. Ruberto, C. Corsori, A. Lo Giudice, A. Re, D. Zafropulos, F. Arneodo, V. Conicella, A. Di Giovanni, R. Torres, F. Castellá, N. Mastrangelo, D. Gallegos, M. Tascon, and L. Giuntini, “A multipurpose x-ray fluorescence scanner developed for in situ analysis,” *Rendiconti Lincei. Scienze Fisiche e Naturali*, vol. 30, 01 2019.
- [42] L. Palla, C. Czelusniak, F. Taccetti, L. Carraresi, L. Castelli, M. Fedi, L. Giuntini, P. Maurenzig, L. Sottili, and N. Taccetti, “Accurate on line measurements of low fluences of charged particles,” *The European Physical Journal Plus*, vol. 130, 03 2015.
- [43] L. Palla, L. Castelli, C. Czelusniak, M. Fedi, L. Giuntini, L. Liccioli, P. Mandò, M. Martini, A. Mazzinghi, C. Ruberto, L. Schiavulli, E. Sibilia, and F. Taccetti, “Preliminary measurements on the new tof system installed at the ams beamline of infn-labec,” *Nuclear Instruments and Methods in Physics Research Section B: Beam Interactions with Materials and Atoms*, vol. 361, 04 2015.
- [44] M. Serge, G. Anelli, S. Atieh, A. Bilton, B. Bulat, T. Callamand, S. Calvo, G. Favre, J.-M. Geisser, A. Gerardin, A. Grudiev, A. Lombardi, E. Montesinos, F. Motschmann, H. Pommerenke, P. Richerot, K. Scibor, M. Timmins, M. Vretenar, and L. Giuntini, “The cern pixe-rfq, a transportable proton accelerator for the machina project,” *Nuclear Instruments and Methods in Physics Research Section B: Beam Interactions with Materials and Atoms*, vol. 459, pp. 153–157, 11 2019.
- [45] Anonymous, “On x-ray wave-lengths,” *Phys. Rev.*, vol. 6, pp. 166–172, Aug 1915.
- [46] <https://xray.oxinst.com/learning/view/article/typical-x-ray-spectra-by-anode-material>, Retrieved 24 March 2023.

- [47] W. D. Coolidge, “X-ray tube,” 1917.
- [48] <https://www.moxtek.com/wp-content/uploads/pdfs/TUB-DATA-1013-MAGPRO.pdf> , Retrieved 24 March 2023.
- [49] C. Zheng, *Metallic oxide nano-clusters synthesis by ion implantation in high purity Fe10Cr alloy*. PhD thesis, 11 2015.
- [50] <https://xdb.lbl.gov/Section1/>, Retrieved 09 April 2023.
- [51] S. Johansson and J. Campbell, *PIXE: A Novel Technique for Elemental Analysis*. JOHN WILEY and SONS, 1988.
- [52] R. Van Grieken and A. Markowicz, *Handbook of X-ray Spectrometry*. CRC Press, 11 2001.
- [53] <https://www.amptek.com/internal-products/xr-100-xray-detector-and-preamplifier>, Retrieved 24 March 2023.
- [54] <https://skuld.bmsc.washington.edu>, Retrieved 09 April 2023.
- [55] A. S. Marfunin *et al.*, *Spectroscopy, Luminescence and Radiation Centers in Minerals [electronic resource]*. Berlin, Heidelberg: Springer Berlin Heidelberg,.
- [56] G. Geipel, G. Bernhard, M. Rutsch, V. Brendler, and H. Nitsche, “Spectroscopic properties of uranium(vi) minerals studied by time-resolved laser-induced fluorescence spectroscopy (trlfs),” *Radiochimica Acta - RADIOCHIM ACTA*, vol. 88, 09 2000.
- [57] M. Gaft, L. Nagli, G. Panczer, G. Waychunas, and N. Porat, “The nature of unusual luminescence in natural calcite, caco<sub>3</sub>,” *American Mineralogist - AMER MINERAL*, vol. 93, pp. 158–167, 01 2008.
- [58] A. Quaranta, J. C. Dran, J. Salomon, J. C. Pivin, A. Vomiero, M. Tonezzer, G. Maggioni, S. Carturan, and G. D. Mea, “Analysis of art objects by means of ion beam induced luminescence,” *Journal of Physics: Conference Series*, vol. 41, p. 543, may 2006.
- [59] E. Palamara, P. P. Das, S. Nicolopoulos, L. Tormo Cifuentes, E. Kouloumpi, A. Terlix, and N. Zacharias, “owards building a cathodoluminescence (cl) database for pigments: characterization of white pigments,” *Heritage*, vol. 9, pp. 7–19, 03 2021.
- [60] M. Emami, R. Chapoulie, and K. Abdi, “Cathodoluminescence microscopy for interpreting the fabric and heating process of ancient pottery; preliminary study on the technological features of pottery from the kur river basin,” *Archaeometry*, vol. 64, 09 2021.
- [61] Y. Tariwong, N. Chanthima, R. R. H. Kim, and J. Kaewkhao, “X-ray induced luminescence, optical, compositional and structural investigations of natural



- and imitation rubies: Identification technique,” *Radiation Physics and Chemistry*, vol. 177, p. 109089, 08 2020.
- [62] Y. Tariwong, N. Chanthima, N. Kiwsakunkran, H. Kim, R. R, S. Kothan, and J. Kaewkhao, “Radiance properties of corundum and feldspar minerals under x-ray induced luminescence,” *Radiation Physics and Chemistry*, vol. 199, p. 110391, 07 2022.
- [63] A. Re, M. Zangirolami, D. Angelici, A. Borghi, E. Costa, R. Giustetto, L. Gallo, L. Castelli, A. Mazzinghi, C. Ruberto, F. Taccetti, and A. Giudice, “Towards a portable x-ray luminescence instrument for applications in the cultural heritage field,” *The European Physical Journal Plus*, vol. 133, 09 2018.
- [64] M. Saleh, L. Bonizzoni, J. Orsilli, S. Samela, M. Gargano, S. Gallo, and A. Galli, “Application of statistical analyses for lapis lazuli stone provenance determination by xrl and xrf,” *Microchemical Journal*, vol. 154, p. 104655, 05 2020.
- [65] <https://www.oceaninsight.com/products/spectrometers/high-sensitivity/qepro-uv-vis/?qty=1>, Retrieved 09 April 2023.
- [66] M. Zangirolami, *Development of non-invasive and portable X-Ray Luminescence apparatus and its application for the provenance study of lapis lazuli in combination with X-Ray Fluorescence*. PhD thesis, University of Turin, 2015.
- [67] V. Mikhailik, S. Henry, M. Horn, H. Kraus, A. Lynch, and M. Pipe, “Investigation of luminescence and scintillation properties of a zns-ag/(lif)-li-6 scintillator in the 7-295 k temperature range,” *Journal of Luminescence*, vol. 134, p. 63–66, 02 2013.
- [68] L. Guidorzi, A. Re, M. Magalini, D. Angelici, A. Borghi, G. Vaggelli, F. Fantino, V. Rigato, L. Torre, Q. Lemasson, C. Pacheco, L. Pichon, B. Moignard, and A. Lo Giudice, “Micro-pixe and micro-ibil characterization of lapis lazuli samples from myanmar mines and implications for provenance study,” *The European Physical Journal Plus*, vol. 138, 02 2023.
- [69] A. Lo Giudice, D. Angelici, A. Re, G. Gariani, A. Borghi, S. Calusi, L. Giuntini, M. Massi, L. Castelli, F. Taccetti, T. Calligaro, C. Pacheco, Q. Lemasson, L. Pichon, B. Moignard, G. Pratesi, and M. Guidotti, “Protocol for lapis lazuli provenance determination: evidence for an afghan origin of the stones used for ancient carved artefacts kept at the egyptian museum of florence (italy),” *Archaeological and Anthropological Sciences*, vol. 9, 06 2017.
- [70] Gaft, Reisfeld, and Panczer, *Luminescence spectroscopy of Minerald and Materials*. 2005.
- [71] C. M. MacRae and N. C. Wilson, “Luminescence database i—minerals and materials,” *Microscopy and Microanalysis*, vol. 14, no. 2, p. 184–204, 2008.
- [72] <https://www.teledynedalsa.com/en/products/imaging/industrial-x-ray/shad-o-box-hs/>.

- [73] F. Taccetti, L. Castelli, C. Czelusniak, N. Gelli, A. Mazzinghi, L. Palla, C. Ruberto, C. Corsori, A. Lo Giudice, A. Re, *et al.*, “A multipurpose x-ray fluorescence scanner developed for in situ analysis,” *Rendiconti Lincei. Scienze Fisiche e Naturali*, vol. 30, pp. 307–322, 2019.
- [74] <https://knowledge.autodesk.com/support/inventor-products/learn-explore/caas/CloudHelp/cloudhelp/2018/ENU/Inventor-WhatsNew/files/GUID-917AEB83-27BB-44BA-A809-44E0748A41AE-htm.html>, Retrieved 28 February 2023.
- [75] <https://www.caen.it/products/dt5780/> Retrieved 30 March 2023.
- [76] A. Georgiev, W. Gast, and R. Lieder, “Analog-to-digital conversion based on a moving window deconvolution,” *Nuclear Science, IEEE Transactions on*, vol. 41, pp. 1116 – 1124, 09 1994.
- [77] M. Blanchette, Jasmin; Summerfield, *C++ GUI Programming with Qt 4*. Prentice Hall, February 2008.
- [78] R. Brun and F. Rademakers, “Root — an object oriented data analysis framework,” *Nuclear Instruments and Methods in Physics Research Section A: Accelerators, Spectrometers, Detectors and Associated Equipment*, vol. 389, no. 1, pp. 81 – 86, 1997. New Computing Techniques in Physics Research V.
- [79] <http://www.silx.org/doc/PyMca/dev/index.html>.
- [80] <https://www.gazzettaufficiale.it/eli/id/2020/08/12/20G00121/sg>.
- [81] <https://www.farnell.com/datasheets/2339962.pdf>.
- [82] C. Seccaroni and P. Moioli, *Prontuario per l’analisi XRF portatile applicata a superfici policrome*. Firenze, IT: Nardini Editore, 2002.
- [83] N. Eastaugh, V. Walsh, T. Chaplin, and R. Siddall, *Pigment Compendium: A Dictionary of Historical Pigments*. Oxford, UK: Elsevier Butterworth-Heinemann, 11 2004.
- [84] K. Janssens, G. Van der Snickt, F. Vanmeert, S. Legrand, G. Nuyts, M. Alfeld, L. Monico, W. Anaf, W. De Nolf, M. Vermeulen, J. Verbeeck, and K. De Wael, “Non-invasive and non-destructive examination of artistic pigments, paints, and paintings by means of x-ray methods,” in *Analytical Chemistry for Cultural Heritage*, pp. 77–128, Springer International Publishing, 11 2017.
- [85] R. J. Gettens and G. L. Stout, *Painting materials : a short encyclopaedia*. New Yourk, US: Dover Publications, 1966.
- [86] P. Colomban, “Rocks as blue, green and black pigments/dyes of glazed pottery and enamelled glass artefacts ? a review,” *European Journal of Mineralogy*, vol. 25, pp. 863–879, 01 2014.
- [87] K. Petrie, “Ceramic transfer printing,” 2011.

- [88] M. Twyman, C. Bye, and C. Gibbs, *A History of Chromolithography: Printed Colour for All*. London, UK: British Library, 2013.
- [89] R. Eppler, “Selecting ceramic pigments,” in *Materials and equipment/whitewares: ceramic engineering and science proceedings*, ch. 1, pp. 1139–1149, London, UK: John Wiley and Sons, Ltd, 1987.
- [90] S. Mangani, A. Mazzinghi, P. Mandò, S. Legnaioli, and M. Chiari, “Characterisation of decoration and glazing materials of late 19th-early 20th century french porcelain and fine earthenware enamels: a preliminary non-invasive study,” *The European Physical Journal Plus*, vol. 136, 10 2021.
- [91] S. Wei, X. Fang, X. Cao, and M. Schreiner, “Characterization of the materials used in chinese ink sticks by pyrolysis-gas chromatography–mass spectrometry,” *Journal of Analytical and Applied Pyrolysis - J ANAL APPL PYROL*, vol. 91, pp. 147–153, 05 2011.
- [92] <https://www.newport.com/p/URS150BPP>, Retrieved 09 April 2023.
- [93] <https://www.theobjects.com/dragonfly/index.html>, Retrieved 09 April 2023.

# INFN-CHNet meets CCR La Venaria Reale: first results

L. Sottili<sup>1,2</sup>, L. Guidorzi<sup>1,2</sup>, A. Mazzinghi<sup>3,4</sup>, C. Ruberto<sup>3,4</sup>, L. Castelli<sup>3</sup>, C. Czelusniak<sup>3</sup>,  
L. Giuntini<sup>3,4</sup>, M. Massi<sup>3</sup>, F. Taccetti<sup>3</sup>, M. Nervo<sup>5,2</sup>, A. Re<sup>1,2</sup> and A. Lo Giudice<sup>1,2</sup>

<sup>1</sup> *Dipartimento di Fisica, Università degli Studi di Torino, Via Pietro Giuria 1, 10125 Torino, Italy,  
leandro.sottili@unito.it, alessandro.re@unito.it, laura.guidorzi@unito.it,  
alessandro.logiudice@unito.it*

<sup>2</sup> *INFN, Sezione di Torino, Via Pietro Giuria 1, 10125 Torino, Italy*

<sup>3</sup> *INFN, Sezione di Firenze, Via Giovanni Sansone 1, 50019, Sesto Fiorentino, Firenze, Italy,  
castelli@fi.infn.it, czelusniak@fi.infn.it, massi@fi.infn.it, ruberto@fi.infn.it, taccetti@fi.infn.it*

<sup>4</sup> *Dipartimento di Fisica e Astronomia, Università degli Studi di Firenze, Via Giovanni Sansone 1,  
50019, Sesto Fiorentino, Firenze, Italy, lorenzo.giuntini@unifi.it, anna.mazzinghi@unifi.it*

<sup>5</sup> *Centro Conservazione e Restauro “La Venaria Reale”, Piazza della Repubblica, 10078 Venaria  
Reale, Torino, Italy, marco.nervo@centrorestaurovenaria.it*

Keywords: MA-XRF, INFN CHNet, CCR “La Venaria reale”, Pigment identification.

**Abstract – In the field of Heritage Science, mobile instruments for diagnostic of artworks are more and more in use. INFN-CHNet, the network of INFN devoted to Cultural Heritage, develops instruments and methods to support the research in the field. Among the others, a MA-XRF scanner was built for in-situ analysis, and is now fully operative. The INFN-CHNet MA-XRF scanner was employed at the CCR “La Venaria Reale”, Turin, for the analysis of different artworks under conservation. The versatility of the MA-XRF scanner is highlighted by the diversity among the applications (painting on canvas, panel painting, and wooden cabinet).**

## I. INTRODUCTION

Presently the use of non-destructive non-invasive X-Ray based techniques is well established in Heritage Science for the analysis and the conservation of artworks [1-7]. X-Ray fluorescence (XRF) technique plays a fundamental role since it provides information on the elemental composition, and thus contributes to identify the materials present on the superficial layers of an

artwork.

Whenever XRF is combined with the capability of scanning an area, providing an elemental distribution on a surface, the technique is indicated as Macro X-Ray Fluorescence (MA-XRF).

A number of MA-XRF scanners, commercial [8] as well as built in-house [9], are nowadays available and in use for Cultural Heritage applications. Due to the impossibility, for their preciousness or high weight, to transport some artworks inside a laboratory for the analysis needed, an important class of instruments is made up by portable and transportable scanners.

In the present paper we are going to present the Cultural Heritage Network of the National Institute of Nuclear Physics (INFN-CHNet) MA-XRF scanner, developed in-house within the collaboration, through the analyses carried out at the Centro Conservazione e Restauro (CCR) “La Venaria Reale”, located nearby Turin. Different examples of artworks are presented, and elemental maps are shown to illustrate the capabilities of the instrument.

## II. EXPERIMENTAL SET-UP

The INFN-CHNet MA-XRF scanner, shown in Fig. 1 during its installation at the CCR “La Venaria Reale”, is a compact ( $60 \times 50 \times 50$  cm<sup>3</sup>) and lightweight (around 10 kg) instrument. Its main parts are a measuring head, three



*Fig.1 INFN-CHNet MA-XRF scanner positioned in front of a panel on canvas at the CCR La Venaria Reale.*

motor linear stages and a case containing all the electronics for acquisition and control.

The measuring head is composed by a X-Ray tube (Moxtek©, 40 kV maximum voltage, 0.1 mA maximum anode current, Mo anode) with a collimator (typically 800  $\mu$ m of diameter), a Silicon Drift Detector (Amptek© XR100 SDD, 50 mm<sup>2</sup> effective active surface) and a telemeter (Keyence IA-100). The motor stage (Physik Instrumente©, travel ranges 30 cm in x, 15 cm in y and 5 cm in z directions) holding the measuring head is screwed on the carbon-fibre case. Typical operating voltage is 30 kV. Signals are collected with a digitizer (model CAEN DT5780) and the whole system is controlled by a laptop.

The control-acquisition-analysis software is developed within the collaboration and allows both an on-line and an off-line analysis. For the MA-XRF analysis the output is a file containing the scanning coordinates and for each position the spectrum acquired. For each map, a single element can be selected and shown in the scanned area, or

in a part of it. The relative intensity of each element in a map is shown with a grey scale, in which the maximum intensity is in white and the lower is in black. Scan is carried out on the x axis, and a step size of typically 1 mm is set on the y axis resulting in a pixel size of 1 mm<sup>2</sup>. A complete review on the instrument can be found in [10].

## III. CASE STUDIES

In this paragraph different applications are presented. The first is a painting on canvas, the second is a painting on panel, and the last is a wooden cabinet. One single problematic for each artwork is reported.

### A. Partial loss of the painting layer

“Madonna con Bambino e i Santi Crescentino e Donnino” by Timoteo Viti, early XVI c., is reported as an example of tempera on canvas. This painting was analysed since its condition required to find out the traces of the original pigments, in order to assess its conservation state. A picture of the painting is presented in Fig.2.

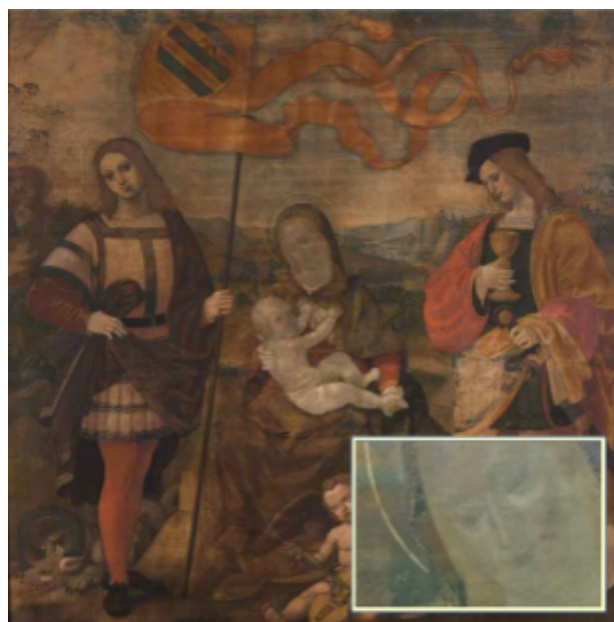


*Fig.2 Madonna con Bambino e i Santi Crescentino e Donnino by Timoteo Viti. On the bottom right, a magnification of the Virgin's face.*

To retrieve the original pigments used in the area of the Virgin's face, the elemental maps of Fe, Hg, Cu, and Au have been extracted and are reported. The scanned area is  $170 \times 110$  mm<sup>2</sup>, acquisition parameters were 40  $\mu$ A beam 82

current and 3 mm/s speed.

The MA-XRF analysis led to the hypothesis of the use of earths-ochres in the shading, due to the presence of Fe, and vermilion-cinnabar (Fig. 3, Hg) in the fleshtones as well as the use of azurite (Fig. 3, Cu) for the Virgin's robe, decorated with gold like the halo (Fig. 3, Au) [11].

For this artwork, the MA-XRF analysis has permitted the detection of the traces of remaining painting layers and the study of the painting technique.

After the conservation carried out at the CCR "La Venaria Reale", the painting owned by La Pinacoteca di Brera was displayed at the exhibition *Raffaello e gli amici di Urbino*.

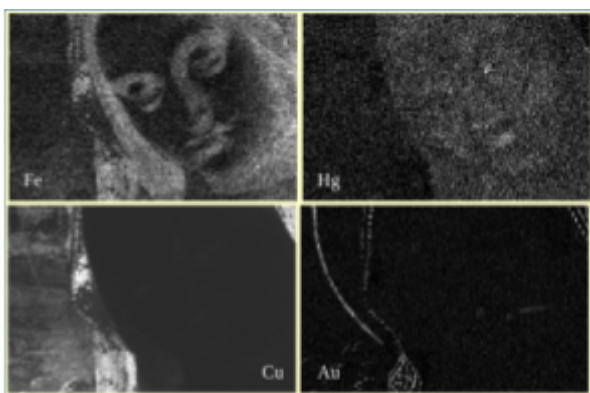


Fig.3 Elemental maps of Fe, Hg, Cu, Au of the area of the Virgin's face.

### B. Characterisation of the blue pigments

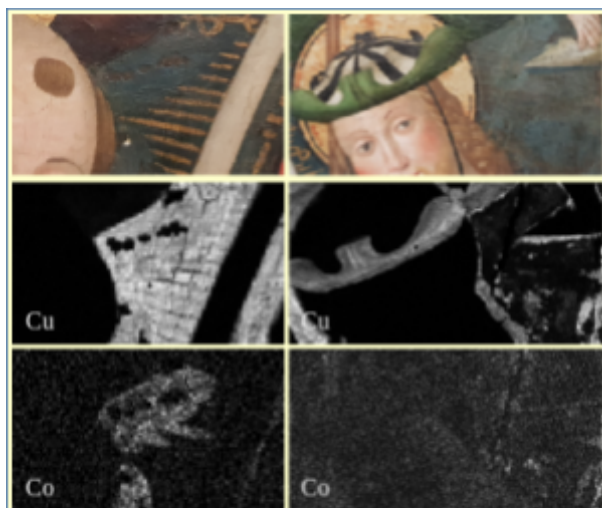


Fig.4 Two areas of the *Madonna con Bambino* by Francesco Sparapane, oil on panel, XVI c. The corresponding maps of Cu and Co are presented. The scanned areas are, respectively, 12.7 cm<sup>2</sup> and 28.7 cm<sup>2</sup>.

Blue pigments may be realized with different compounds (such as ultramarine, azurite, smalt, indigo). To identify the pigments used in the blue areas of "Madonna con Bambino e S. Antonio e S. Rocco" by Sparapane, partially visible in Fig.1, the MA-XRF analysis was carried out and two areas are presented in Fig.4.

The presence of Cu is likely due to the use of azurite, whereas the presence of Co, with traces of Bi and K, likely attests the presence of smalt [11]. In the first area (left), the elemental maps should indicate the presence of a large area of azurite with the presence of smalt in a smaller area (the maps of Bi and K are not reported), that could be explained with a later retouch or an original glaze. On the contrary, the map of Cu in the second area shows only a well-defined region outlining the face, due to a partial loss of the painting layer. The same conclusion is confirmed from the map of Co.

### C. Study of a Chinese wooden cabinet

Together with paintings, the MA-XRF scanner was used on a wooden cabinet from the Castello di Masino, Piedmont, Italy, shown in Fig.5.

For this case study, the query was related to the presence of orpiment (As<sub>2</sub>S<sub>3</sub>) in the yellow areas. The maps of the area with flowers and stems is reported in Fig.6. The beam current was set to 30 μA and the speed to 3 mm/s.



Fig.5 Chinese wooden cabinet. On the bottom right, a magnification of the area studied.

Due to the overlap of their energies, the detection of As and S can not be stated directly with one map. By

comparing the maps of different lines of As, Hg and Pb (not all reported), it was possible to attest the likely presence of orpiment in the stems. Further, the map of Au is reported in Fig.6, showing the gilding in the yellow flowers and leaves.

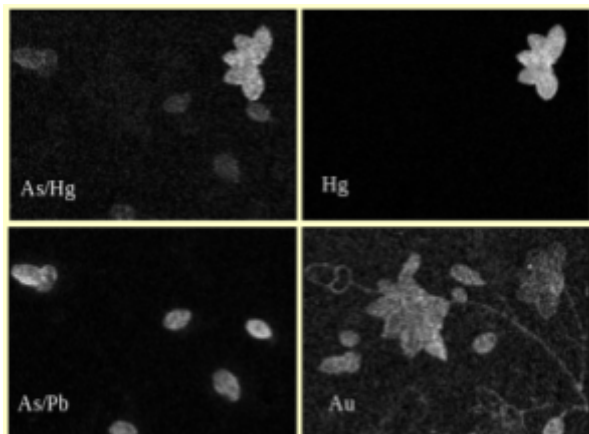


Fig.6 Elemental maps at 11.7 keV (As/Hg), 9.9 keV (Hg), 10.5 keV (As/Pb) 9.6 keV (Au). The scanned is 14,5 10,5 cm<sup>2</sup>.

#### IV. CONCLUSIONS

The INFN-CHNet MA-XRF scanner was employed at the CCR “La Venaria Reale” to support the conservation activity. Its analytical performances and its versatility have demonstrated the usefulness of the instrument in the Cultural Heritage field. Further, thanks to the expertise within the collaboration, an upgrade of the scanner for adapting it to more and more application is continuously on-going.

#### ACKNOWLEDGMENTS

This project has received funding from the European Union’s Horizon 2020 research and innovation programme under the Marie Skłodowska-Curie grant agreement No 754511 (PhD Technologies Driven Sciences: Technologies for Cultural Heritage – T4C).

#### REFERENCES

[1] C. Ruberto, A. Mazzinghi, M. Massi, L. Castelli, C. Czelusniak, L. Palla, N. Gelli, M. Betuzzi, A. Impallaria, R. Brancaccio, E. Peccenini, M. Raffaelli, “Imaging study of Raffaello's “La Muta” by a portable XRF spectrometer”, *Microchemical Journal*, Volume 126, 2016, Pages 63-69.

[2] P. Ricciardi, A. Mazzinghi, S. Legnaioli, C. Ruberto, L. Castelli, “The Choir Books of San Giorgio Maggiore in Venice: Results of in Depth

Non-Invasive Analyses”. *Heritage*, 2019, 2, 1684-1701.

[3] M-P. Morigi, F. Casali, M. Bettuzzi, *et al.* “Application of X-ray Computed Tomography to Cultural Heritage diagnostics.” *Appl. Phys. A* 100, 2010,653–661.

[4] D. Angelici, A. Borghi, F. Chiarelli, R. Cossio, G. Gariani, A. Lo Giudice, A. Re, G. Pratesi, G. Vaggelli “μ-XRF analysis of trace elements in lapis lazuli-forming minerals for a provenance study” *Microscopy and Microanalysis*, 21, 2015, 526-533.

[5] A. Re, A. Lo Giudice, M. Nervo, P. Buscaglia, P. Luciani, M. Borla, C. Greco, “The importance of tomography studying wooden artefacts: a comparison with radiography in the case of a coffin lidn from Ancient Egypt” *International Journal of Conservation Science* 7(SI2), 2016, 935-944.

[6] J. Corsi, A. Lo Giudice, A. Re, A. Agostino, F. Barello, “Potentialities of X-ray fluorescence analysis in numismatics: the case study of pre-Roman coins from Cisalpine Gaul”, *Archaeological and Anthropological Sciences* 10(2), 2018, 431-438.

[7] G. Fiocco *et al.*, “Synchrotron radiation micro-computed tomography for the investigation of finishing treatments in historical bowed string instruments: issues and perspectives” *European Physical Journal Plus*, 2018, 133: 525.

[8] M. Alfeld *et al.*, “A mobile instrument for in situ scanning macro-XRF investigation of historical paintings”, *Journal of Analytical Atomic Spectrometry*, 28, 2013, 760-767.






[9] Romano, F.P., Caliri *et al.*, Real-time elemental imaging of large dimension paintings with a novel mobile macro X-ray fluorescence (MA-XRF) scanning technique, *Journal of Analytical Atomic Spectrometry*, 32 (4), 2017, pp. 773-781.

[10] Taccetti *et al.*, A multi-purpose X-ray fluorescence scanner developed for in situ analysis. *Rendiconti Lincei. Scienze Fisiche e Naturali*, 2019, 30:307-322.

[11] C. Seccaroni, P. Moiola - “Fluorescenza X-Prontuario per l’analisi XRF portatile applicata a superfici policrome” - *Nardini Editore- Firenze*, Ed. 2002.

## Article

# The Importance of Being Versatile: INFN-CHNet MA-XRF Scanner on Furniture at the CCR “La Venaria Reale”

Leandro Sottili <sup>1,2</sup>, Laura Guidorzi <sup>1,2</sup> , Anna Mazzinghi <sup>3,4</sup>, Chiara Ruberto <sup>3,4</sup>, Lisa Castelli <sup>4</sup>, Caroline Czelusniak <sup>4</sup>, Lorenzo Giuntini <sup>3,4</sup> , Mirko Massi <sup>4</sup> , Francesco Taccetti <sup>4</sup>, Marco Nervo <sup>5</sup> , Stefania De Blasi <sup>5</sup>, Rodrigo Torres <sup>6</sup>, Francesco Arneodo <sup>6</sup>, Alessandro Re <sup>1,2,\*</sup>  and Alessandro Lo Giudice <sup>1,2</sup>

- <sup>1</sup> Dipartimento di Fisica, Università degli Studi di Torino, Via Pietro Giuria 1, 10125 Torino, Italy; leandro.sottili@unito.it (L.S.); laura.guidorzi@unito.it (L.G.); alessandro.logiudice@unito.it (A.L.G.)
- <sup>2</sup> Istituto Nazionale di Fisica Nucleare (INFN), Sezione di Torino, Via Pietro Giuria 1, 10125 Torino, Italy
- <sup>3</sup> Dipartimento di Fisica e Astronomia, Università degli Studi di Firenze, Via Giovanni Sansone 1, Sesto Fiorentino, 50019 Firenze, Italy; anna.mazzinghi@unifi.it (A.M.); ruberto@fi.infn.it (C.R.); lorenzo.giuntini@unifi.it (L.G.)
- <sup>4</sup> Istituto Nazionale di Fisica Nucleare (INFN), Sezione di Firenze, Via Giovanni Sansone 1, Sesto Fiorentino, 50019 Firenze, Italy; castelli@fi.infn.it (L.C.); czelusniak@fi.infn.it (C.C.); massi@fi.infn.it (M.M.); taccetti@fi.infn.it (F.T.)
- <sup>5</sup> Centro Conservazione e Restauro “La Venaria Reale”, Piazza della Repubblica, Venaria Reale, 10078 Torino, Italy; marco.nervo@centrorestaurovenaria.it (M.N.); stefania.deblasi@centrorestaurovenaria.it (S.D.B.)
- <sup>6</sup> Division of Science, New York University Abu Dhabi, P.O. Box, Saadiyat Island, Abu Dhabi 129188, United Arab Emirates; rodrigo.torres@nyu.edu (R.T.); francesco.arneodo@nyu.edu (F.A.)
- \* Correspondence: alessandro.re@unito.it



**Citation:** Sottili, L.; Guidorzi, L.; Mazzinghi, A.; Ruberto, C.; Castelli, L.; Czelusniak, C.; Giuntini, L.; Massi, M.; Taccetti, F.; Nervo, M.; et al. The Importance of Being Versatile: INFN-CHNet MA-XRF Scanner on Furniture at the CCR “La Venaria Reale”. *Appl. Sci.* **2021**, *11*, 1197. <https://doi.org/10.3390/app11031197>

Academic Editor: Anna Galli;  
Letizia Bonizzoni  
Received: 31 December 2020  
Accepted: 24 January 2021  
Published: 28 January 2021

**Publisher’s Note:** MDPI stays neutral with regard to jurisdictional claims in published maps and institutional affiliations.



**Copyright:** © 2021 by the authors. Licensee MDPI, Basel, Switzerland. This article is an open access article distributed under the terms and conditions of the Creative Commons Attribution (CC BY) license (<https://creativecommons.org/licenses/by/4.0/>).

**Abstract:** At present, the use of non-destructive, non-invasive X-ray-based techniques is well established in heritage science for the analysis and conservation of works of art. X-ray fluorescence (XRF) plays a fundamental role since it provides information on the elemental composition, contributing to the identification of the materials present on the superficial layers of an artwork. Whenever XRF is combined with the capability of scanning an area to provide the elemental distribution on a surface, the technique is referred to as macro X-ray fluorescence (MA-XRF). The heritage science field, in which the technique is extensively applied, presents a large variety of case studies. Typical examples are paintings, ceramics, metallic objects and manuscripts. This work presents an uncommon application of MA-XRF analysis to furniture. Measurements have been carried out with the MA-XRF scanner of the INFN-CHNet collaboration at the Centro di Conservazione e Restauro “La Venaria Reale”, a leading conservation centre in the field. In particular, a chinoiserie lacquered cabinet of the 18th century and a desk by Pietro Piffetti (1701–1777) have been analysed with a focus on the characterisation of decorative layers and different materials (e.g., gilding in the former and ivory in the latter). The measurements have been carried out using a telemeter for non-planar surfaces, and with collimators of 0.8 mm and 0.4 mm diameter, depending on the spatial resolution needed. The combination of the small measuring head with the use of the telemeter and of a small collimator has guaranteed the ability to scan difficult-to-reach areas with high spatial resolution in a reasonable time (20 × 10 mm<sup>2</sup> with 0.2 mm step in less than 20 min).

**Keywords:** MA-XRF; conservation studies; furniture; Pietro Piffetti; chinoiserie lacquered cabinet

## 1. Introduction

X-ray fluorescence (XRF) is well established in the non-destructive, non-invasive analysis for the conservation, characterisation and prevention of works of art [1–5]. Whenever it is associated with the ability to scan an area, XRF provides the elemental composition related with the spatial distribution of the scanned area, and it is typically referred as macro X-ray fluorescence (MA-XRF) [1,4,6]. The MA-XRF technique is widely in use in the



heritage science field, and a number of research groups have been developing customized instruments to improve the quality of data obtainable with this technique [6–9].

The MA-XRF technique may be provided by portable instruments or by large-scale facilities like synchrotrons [10–12]. Despite their higher performances in terms of output beam parameters (higher intensity, smaller spot size), synchrotron facilities have the limitation of needing the artifacts to be transported to the laboratory, which is not always feasible.

Among others, the Cultural Heritage Network of the National Institute of Nuclear Physics (INFN-CHNet) [13–15] is engaged in the development of instruments, methods and techniques for applications in the heritage science field [16–19]. With this intent, the INFN-CHNet collaboration has developed its own MA-XRF scanner. The main characteristics of this device are its compactness, light weight, user-friendly interface, and versatility as described in the next section. It has already been employed for a number of different applications, including paintings [20–22], illuminated manuscripts [23], coins [24], mosaics [25] and ceramics [24].

The INFN-CHNet MA-XRF scanner has recently been employed on furniture. This further application is particularly interesting since, at the present time, the literature on XRF analysis on furniture is still poor [26–28], and no cases of MA-XRF analysis on furniture have been reported.

In this paper, the application of the INFN-CHNet MA-XRF scanner on two different pieces of furniture of the 18th century is presented. One is a chinoiserie wooden cabinet placed at the *Castello e Parco di Masino*, property of the *Fondo Ambiente Italiano* (FAI) in Piedmont. The other is a writing desk *Scrivania con scansia* by Pietro Piffetti, placed in the *Palazzo Chiabrese* in Turin, Piedmont.

Both works of art have been studied in a specific framework at the Centro di Conservazione e Restauro (CCR) “La Venaria Reale”. The lacquered cabinet was part of the research project “*Un ponte tra l’Oriente e il Piemonte*”, a comparative study between lacquered oriental works of art of the 18th and 19th centuries, and their contemporary Western imitations. The main focus of the study was to determine the manufacturing techniques and materials employed in order to determine the elements required to date the manufactures and to distinguish between “original” oriental works of art and their Western replicas [29]. The study of the writing desk *Scrivania con scansia* by Pietro Piffetti from the *Palazzo Chiabrese* has been realised within the research project on Pietro Piffetti carried out by the CCR [30,31]. This ongoing project is aimed at studying works of art by Pietro Piffetti and the Piedmontese cabinetmakers of the second half of the 18th century.

Thanks to the versatility of the INFN-CHNet MA-XRF scanner, it has been possible to study the decorative layers of the furniture, thus supporting their conservation processes and providing fundamental information to the research projects in which they are involved. The present work demonstrates the potentialities of the systematic use of a customized MA-XRF technique as a first approach to scientific studies on furniture.

## 2. Materials and Methods

The chinoiserie lacquered cabinet of the *Castello di Masino* (Figure 1b) is a typical example of furniture largely diffused throughout Europe in the second half of the 18th century. Historical research made it possible to date the furniture to 1780 and to attest to its production by a French workshop that was specialised in making furniture in imitation of oriental works assembling original Eastern lacquered panels. For this reason, it represents an important case study that permits the analysis of the aspects of both materials used in the Western imitations and those of the original oriental lacquers.

The writing desk *Scrivania con scansia* of *Palazzo Chiabrese* (Figure 1a,  $288 \times 155.5 \times 57.5$  cm<sup>3</sup>) is a particularly significant work since it is the last documented masterpiece by Pietro Piffetti (Turin, 1701–1777), cabinetmaker of the Savoy court, dated to 1767. As part of the research on the Piedmontese cabinet-making, in particular on the furnishings by Pietro Piffetti, over the years, the CCR has been able to establish a database on the techniques

and materials used, which today makes it possible to accurately document the evolution of the history of furniture technology, the basis of these great multi-material masterpieces of international furniture.

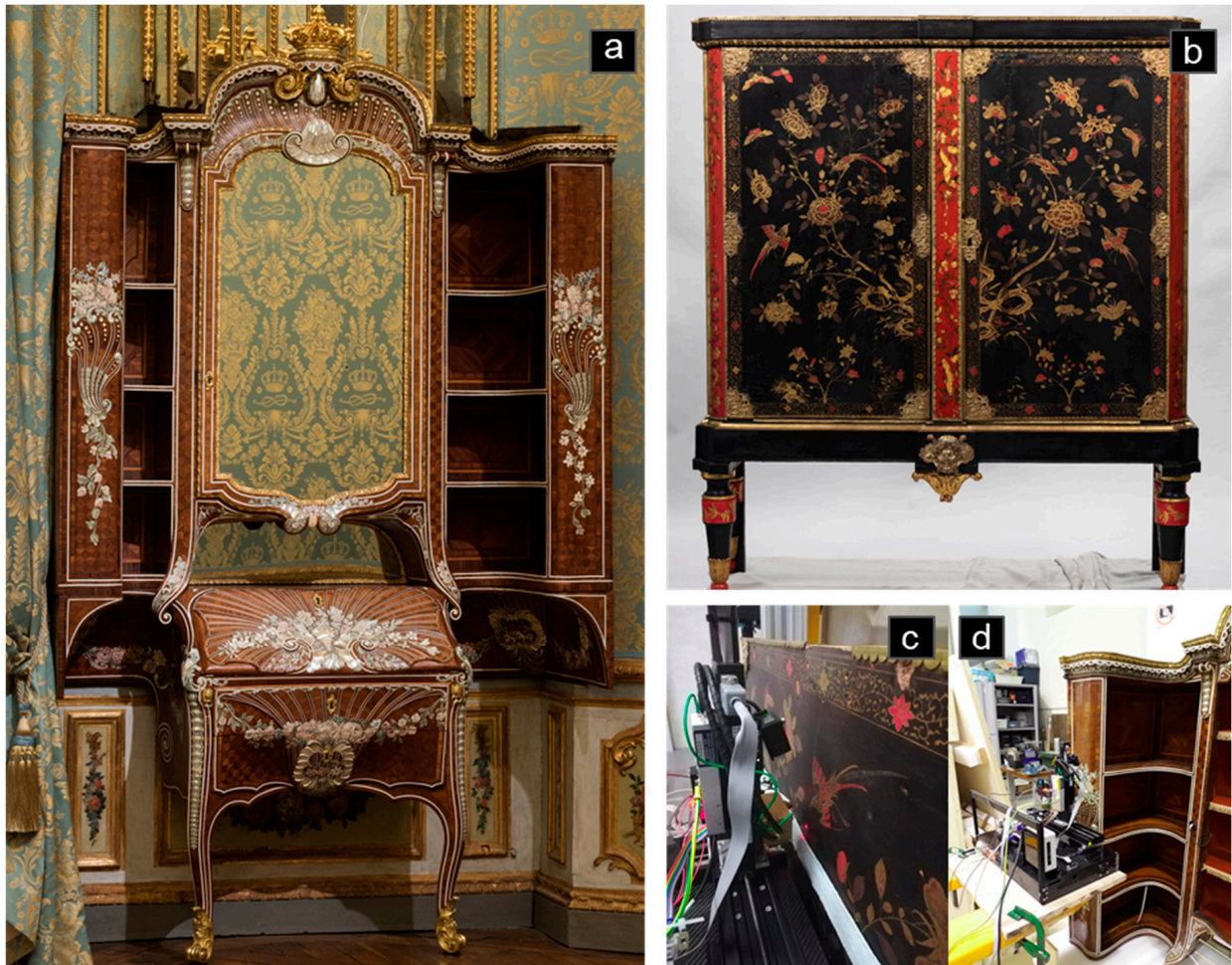


**Figure 1.** Pictures of the furniture and of the Cultural Heritage Network of the National Institute of Nuclear Physics (INFN-CHNet) macro X-ray fluorescence (MA-XRF) scanner during the measurements: (a) Writing desk *Scrivania con scansia* by Pietro Piffetti; (b) Chinoiserie wooden cabinet; (c) Scanner placed in front of the chinoiserie wooden cabinet; and (d) in front of the external side of the *scansia*.

The desk was created as a corner element of a *boiserie* inside the alcove hall of the *Palazzo Chiabrese*. It is entirely inlaid and composed of veneers in violet rosewood and *bois de rose* and of polychrome engraved ivories and mother-of-pearl inlays. The cabinet-making furnishings of this period very rarely show inlays with polychrome engravings. Usually, they are made with black ink; hence, the possibility of mapping the nature of the inks and pigments present on this piece has provided an important element of comparison between the works that have been studied by the CCR in recent years [32,33].

The measurements have been carried out with the INFN-CHNet MA-XRF scanner at the CCR “La Venaria Reale”. It is a compact ( $60 \times 50 \times 50 \text{ cm}^3$ ) and lightweight (around 10 kg) instrument completely assembled within the INFN-CHNet collaboration. Its main parts are the measuring head, composed by an X-ray tube (Moxtek© MAGNUM, 40 kV maximum voltage, 0.1 mA maximum anode current, Mo anode) with a collimator (changeable, typically between 400  $\mu\text{m}$  and 2000  $\mu\text{m}$  diameter), a silicon drift detector (Amptek© XR100 SDD, 50  $\text{mm}^2$  effective active surface, 140 eV FWHM at 5.9 keV), a telemeter (Keyence, model IA-100), three motor linear stages and a case containing all the electronics for acquisition and control. The motor stages (Physik Instrumente©, travel

ranges 30 cm horizontally,  $x$  axis; 15 cm vertically,  $y$  axis; and 5 cm towards the specimen,  $z$  axis) holding the measuring head are screwed onto the carbon-fibre case containing the electronic components and the power supplies. The maximum operating voltage is 40 kV. Signals are collected with a multichannel analyser (model CAEN DT5780, also inside the carbon-fibre case), and the whole system is controlled by a laptop. The control-acquisition-analysis software is developed within the collaboration and allows both on-line and off-line analysis.

The output of the MA-XRF analysis is a file containing the scanning coordinates and, for each position, the spectrum acquired. As a result, the counts are recorded for each position. For each scanned area, or a part of it, a single element can be selected by its energy transition value and shown as an elemental 2D map. For each peak, the energy range is manually selected around the centroid according to its FWHM. The relative intensity of each element in a map is shown in greyscale, in which the maximum intensity is in white and the minimum in black.

Furthermore, multi-elemental maps can be created. In those maps, different elements are displayed in different colours (red, green, blue). This option permits the association of one or more pigments, by means of their chemical elements, to the visible features, allowing an immediate spatial distribution of the pigments (see, for example, Section 3.1).

A scan is carried out on the  $x$  axis, and a step size of 1 mm is typically set on the  $y$  axis, resulting in a pixel size of 1 mm<sup>2</sup>. However, both the measuring speed and the pixel size can be adjusted depending on the need, as reported in the case of the writing desk. This ability, combined with the changeable dimension of the collimator, allows optimisation of the measuring time, and thus the maintenance of an adequate spatial resolution.

During measurements, the distance between the specimen and the measuring head is kept constant by means of the telemeter. The distance is set to the value of 6 mm, allowing the detector to point at the area irradiated by the source and to maximise the covered solid angle. Therefore, the detection efficiency is also improved for non-flat surfaces, especially for low-energy X-rays subjected to higher absorption by the air.

Moreover, for the detection of low-energy X-rays, helium flow may be conveyed between the target and the detector system from a nozzle installed close by the detector.

With the set-up described above, maps of elements with atomic numbers higher than Sodium ( $Z > 11$ ) are efficiently provided by the instrument. A full review on the instrument can be found in [34].

### 3. Results and Discussion

#### 3.1. Chinoiserie Lacquered Cabinet

For the investigation of this furniture, two areas, one for each panel, have been studied: one area corresponding to a flower (Figure 2), the other area to a flying bird (Figure 3).

For the two measurements, helium flow has been used. The scanning parameters are reported in Table 1.

**Table 1.** Scanning parameters of the areas of the chinoiserie lacquered cabinet.

Area	Dimension (mm <sup>2</sup> )	Source Voltage (kV)	Anode Current (μA)	Scanning Speed (mm/s)	Collimator Diameter (μm)	Step Size (mm)
Flowers	145 × 105	28	30	3	800	1
Flying bird	175 × 135	28	30	3	800	1

In the first area, the query was related to the possible presence of arsenic-based compounds in the transparent yellow buds and flowers. Due to the overlap of the As K $\alpha$  transition (10,544 keV) with the Pb L $\alpha$  (10,552 keV), and of the As K $\beta$  (11,726 keV) with the Hg L $\beta$  (11,823 keV), the presence of arsenic can not be ascertained by a single elemental map. Therefore, maps of the major overlapping transitions among arsenic, mercury, and lead have been made and are reported in Figure 2d–f. As can be seen, even though the Hg

$L\beta$ / $As$   $K\beta$  transition shows a high intensity in the red flower and the transparent yellow buds (Figure 2d), the  $L\alpha$  of Hg clearly shows its presence only in the red flower (Figure 2e), indicating that the signals in the area of the transparent yellow buds come from arsenic. The presence of the Pb  $L\beta$  transition has not been detected in the spectrum, confirming this result.

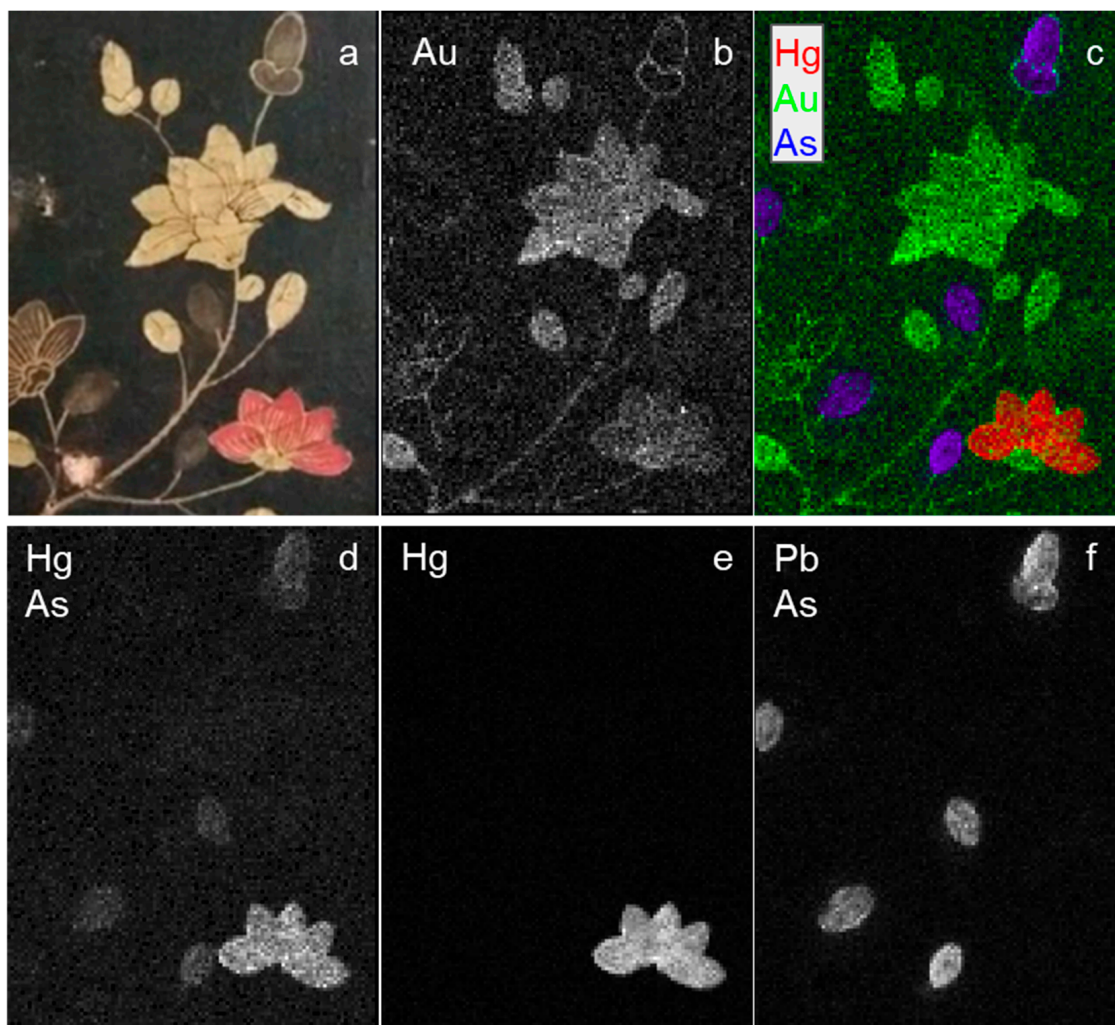


**Figure 2.** Elemental maps of the first area obtained by the INFN-CHNet MA-XRF scanner. (a) Visible. The maps presented are: (b) Au; (c) RGB map of Hg  $L\alpha$  (red), Au  $L\alpha$  (green) and As  $K\alpha$  (blue); (d) Hg  $L\beta$ / $As$   $K\beta$  transitions; (e) Hg  $L\alpha$  transition; (f) Pb  $L\alpha$ / $As$   $K\alpha$  transitions.

The presence of arsenic may be due to orpiment, but the use of realgar, pararealgar, or arsenic sulphide glass may not be excluded [35,36].

In order to clarify the composition of the different parts of the plant, an RGB map of Hg  $L\beta$  (red), Au  $L\alpha$  (green) and As  $K\alpha$ /Pb  $L\alpha$  (blue) transitions has been created and is reported in Figure 2c. As can be seen from Figure 2b, the bright yellow flowers, stems, outlines and highlights over red areas were made with gold. The red flower was likely realised with cinnabar-vermilion, of which the elemental composition is HgS [37].

The other area, even though it shows similarities with the previous, presents some essential differences in the decorative palette. The elemental maps of this area are shown in Figure 3. Compared with the area of the plant, the maps of mercury (Figure 3d) and gold (Figure 3g) attest to the probable use, respectively, of cinnabar-vermilion in the red tones, and of gold in the outline of the body and in one of the tails of the bird. The red tail is highlighted in gold as well.

As can be seen in the map of iron (Figure 3c), ochres-earths seem to have been used for the body of the bird. The eight black-blue feathers are related with a higher intensity of arsenic (Figure 3e), silicon (Figure 3h) and calcium (Figure 3b) compared with the rest of the area. In this case, with this technique it has not been possible to formulate a conclusive hypothesis on the decorative palette used by comparing the information with the present literature [38].

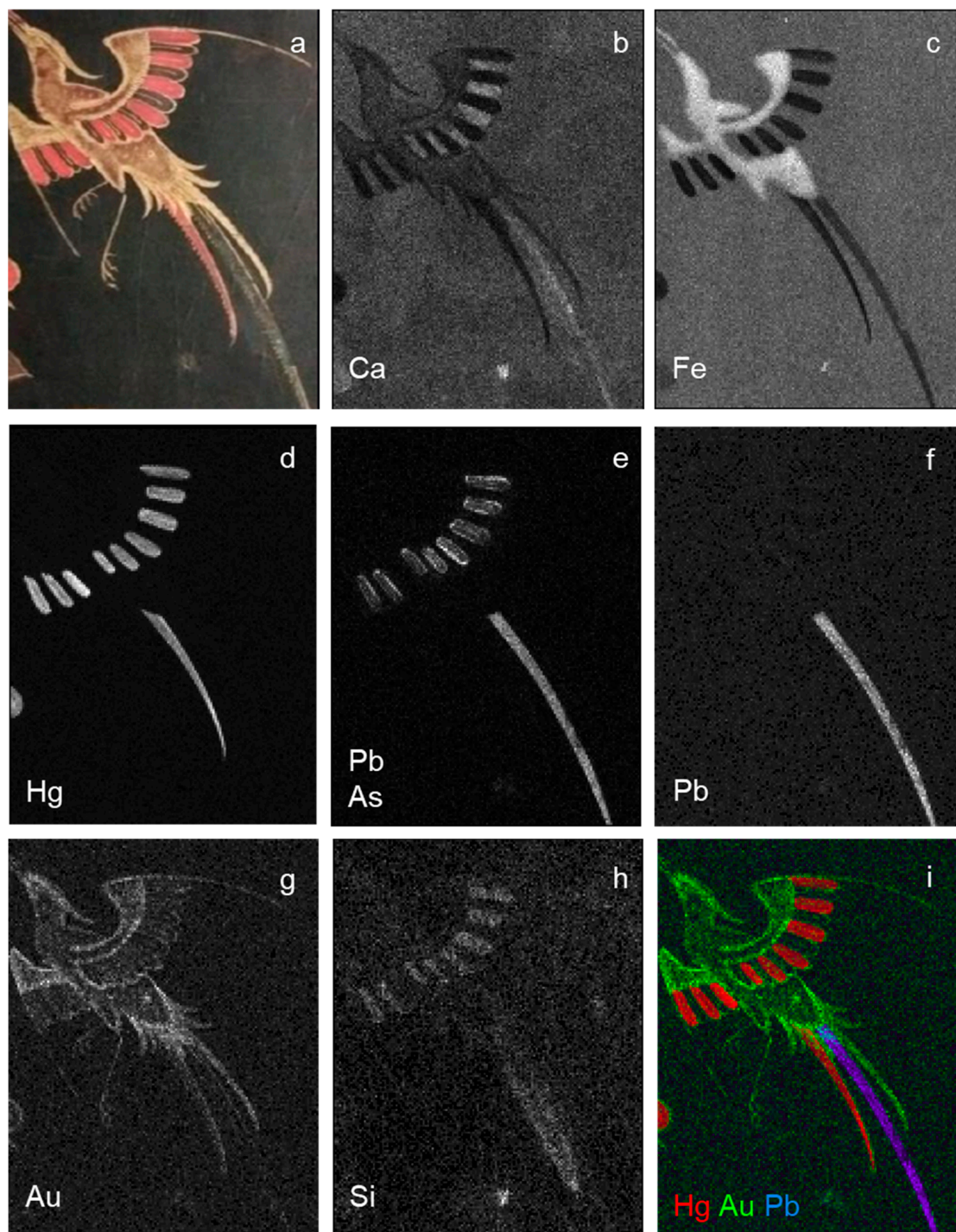


**Figure 3.** Elemental maps of the second area obtained by the INFN-CHNet MA-XRF scanner. (a) Visible. The maps presented are: (b) Ca  $K\alpha$  transition; (c) Fe  $K\alpha$  transition; (d) Hg  $L\alpha$  transition; (e) Pb  $L\alpha$ /As  $K\alpha$  transitions; (f) Pb  $L\beta$  transition; (g) Au  $L\alpha$  transition; (h) Si  $K\alpha$  transition; (i) RGB map of Hg (red), Au (green) and Pb (blue).

A different result has been achieved for the longest black tail, in which the presence of high Pb L $\beta$  transition values reveals the use of Pb (Figure 3f). The literature [39,40] suggests that the presence of lead in black compounds may indicate the use of galena (PbS). The presence of sulphur can only be hypothesised since its transition (2.31 keV) overlaps with the transitions of mercury (M series) and lead (M series). However, with only XRF analysis, the use of another material like plattnerite (PbO<sub>2</sub>) cannot be excluded. In addition, as can be seen from the map of silicon (Figure 3h), this element is present in the area of the tails, which may indicate a possible fourth tail with a similar composition to black-blue feathers. Finally, regarding the white small area below the red tail, the presence of a retouch is clearly visible in the maps of silicon (Figure 3h) and calcium (Figure 3b).

### 3.2. Writing Desk by Pietro Piffetti

The *Scrivania con scansia* by Pietro Piffetti has been analysed to characterise the decorating layers up on the marquetry. Three different areas were selected for this purpose: two areas on a drawer placed inside the writing desk, and one on a side, as shown in Figure 4. The choice was based on the hypotheses of different materials used and two possible conservation states inside and outside the writing desk.

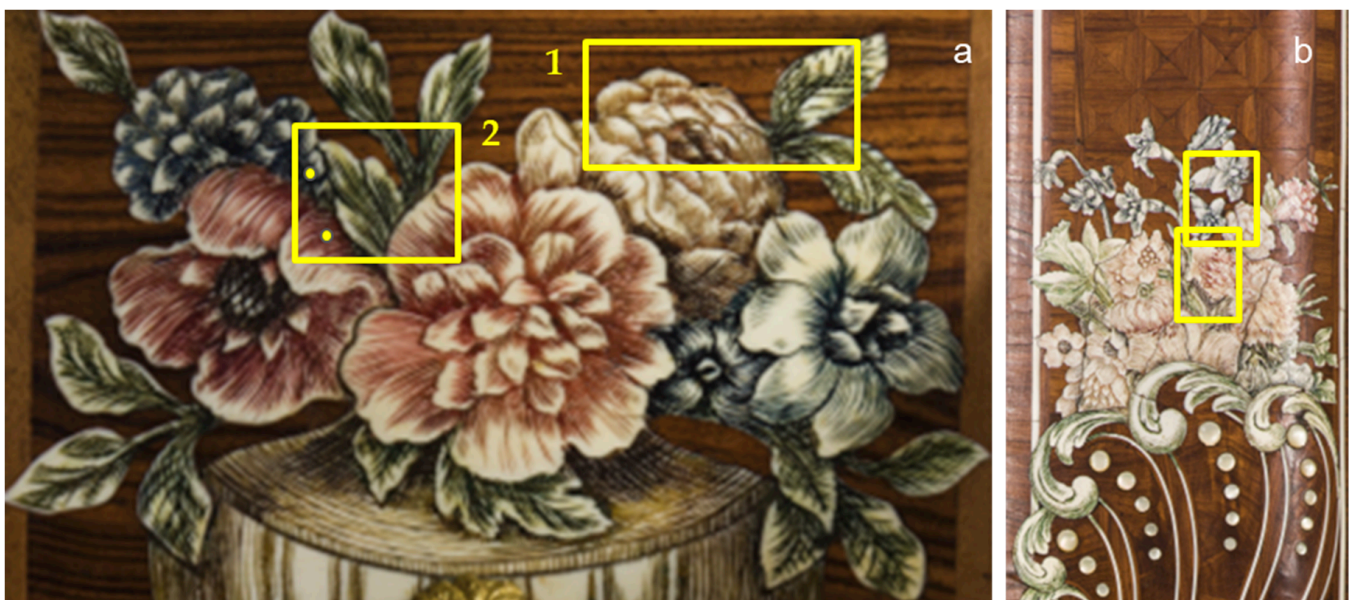


**Figure 4.** Selected areas for the measurements: (a) selected areas outlined in yellow and the two points in the black and red shades on the drawer; (b) particular of the external side. The scanned areas are outlined in yellow.

The scanning parameters are reported in Table 2. Because of the small size of the details of the decoration, a better spatial resolution compared to the lacquered cabinet was required. Since the scanner has an available set of different collimators, for this application the smallest one, with the diameter of 400  $\mu\text{m}$ , has been used. Thanks to this feature, a higher spatial resolution has been achieved in the elemental maps.

**Table 2.** Scanning parameters of the areas analysed on the *Scrivania con scansia* by Pietro Piffetti.

Area	Dimension (mm <sup>2</sup> )	Source Voltage (kV)	Anode Current ( $\mu\text{A}$ )	Scanning Speed (mm/s)	Collimator Diameter ( $\mu\text{m}$ )	Step Size (mm)
Drawer area 1	30 × 13	38	50	1	400	0.2
Drawer area 2	20 × 10	28	50	1	400	0.2
External side	40 × 130	28	70	1	400	0.2

The elemental maps of the first area of the drawer are shown in Figure 5. From the maps of lead (Figure 5c,d) it can be seen that its presence is detected in correspondence of the white highlights of the flower, most likely due to the use of lead white [41].

The shading in the central part of the flower is related to the presence of iron (Figure 5g) and manganese (Figure 5h), which may lead to the hypothesis of the use of ochre-earths [39]. In the green leaves, high signals of copper (Figure 5f) and arsenic (Figure 5d,e) are clearly visible. Even though this can be explained by the presence of a copper-based pigment or dye mixed with an arsenic-based compound, the literature suggests that this combination is an unlikely possibility, whereas the green colour may be related to the use of emerald green or Scheele's green [39,42]. However, it is reported that the latter has only been used since 1814, excluding its use for this piece of furniture; therefore, it is plausible that emerald green was used for the green leaves.

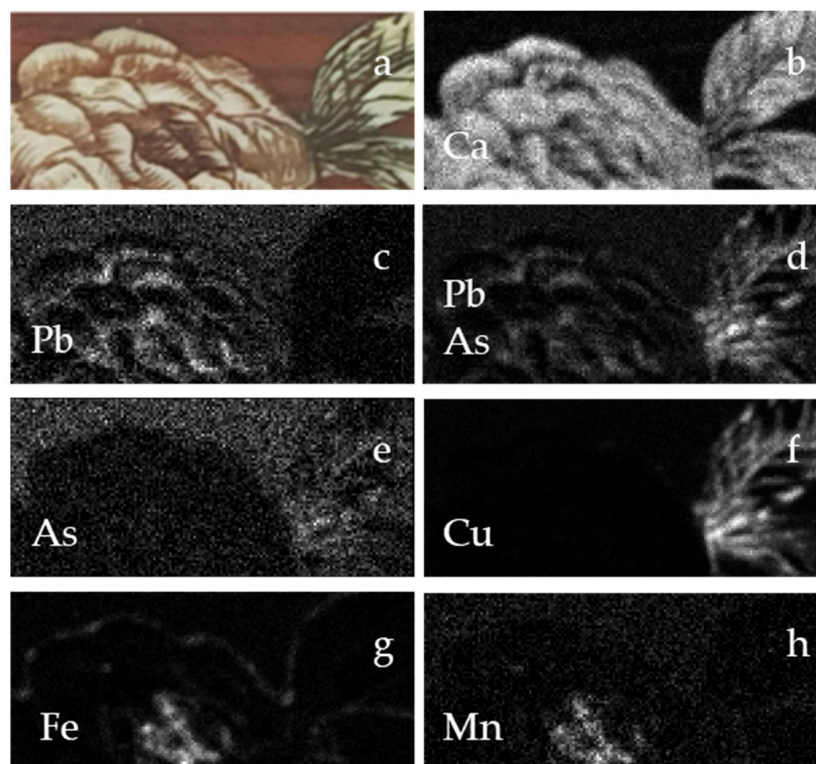


**Figure 5.** Elemental maps of the first area of the drawer obtained by the INFN-CHNet MA-XRF scanner. (a) Visible. The maps presented are: (b) Ca  $K\alpha$  transition; (c) Pb  $L\beta$  transition; (d) Pb  $L\alpha$ /As  $K\alpha$  transitions; (e) As  $K\beta$  transition; (f) Cu  $K\alpha$  transition; (g) Fe  $K\alpha$  transition; (h) Mn  $K\alpha$  transition.

The maps in the second area of the drawer, reported in Figure 6, confirm the same results of the first map, even though the black-blue flower on the top left shows a higher contribution of lead and iron. From the present literature, no single pigment is directly associated with the presence of those two elements [38,39]. Their presence can be explained by the use of Prussian blue combined with lead white, as reported in [43].

In the second area of the drawer shown in Figure 4, two points have been measured: one in the red tone and the other in the black tone. The measuring time was set to 120 s for each one to enhance the statistics of the spectra. As can be seen from Figure 7a, in the red tone the most intense peak is the calcium peak, probably related to the ivory beneath the decorative layer, whereas no other element with an atomic number above sodium was detected with relevant statistics. This result may indicate the use of organic dyes for this colour. The spectrum of the black-blue point (Figure 7b) shows a different elemental composition: the most prominent peaks are related to iron and lead (calcium is also present as a second peak in terms of intensity), confirming the result already discussed above.

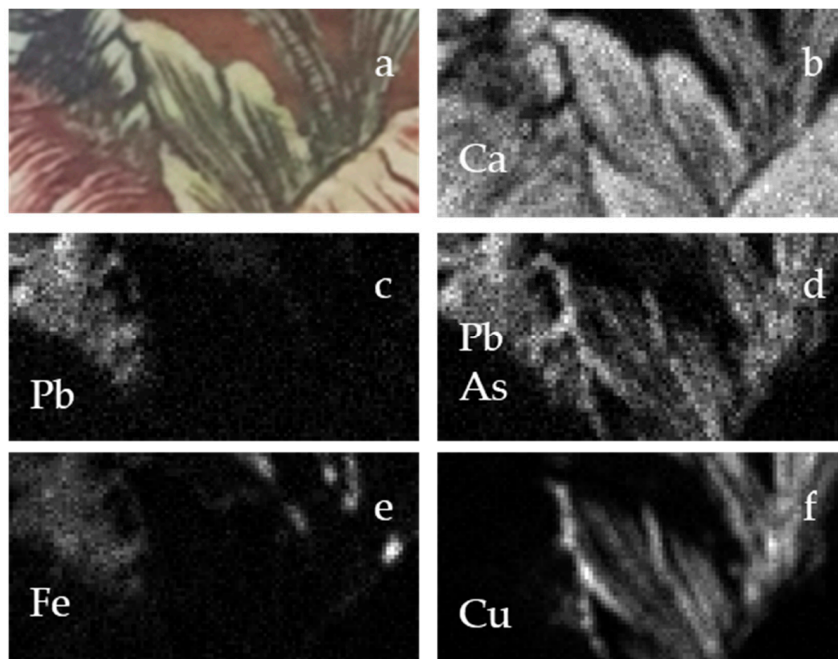


**Figure 6.** Elemental maps of the second area of the drawer. (a) Visible. The maps presented are: (b) Ca K $\alpha$  transition; (c) Pb L $\beta$  transition; (d) Pb L $\alpha$ /As K $\alpha$  transitions; (e) Fe K $\alpha$  transition; (f) Cu K $\alpha$  transition.

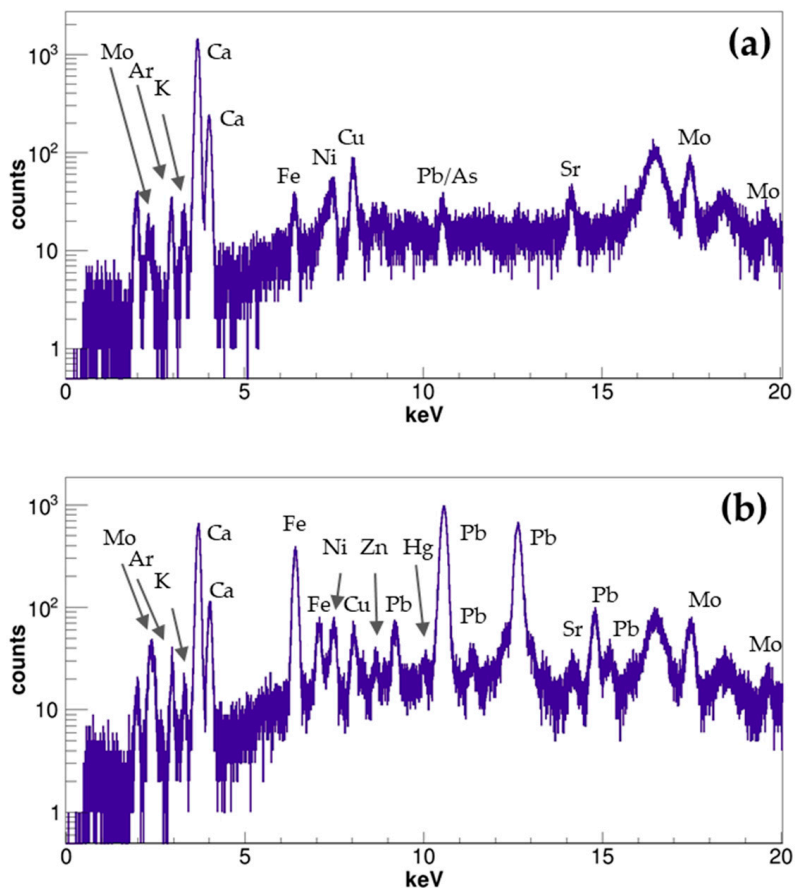


**Figure 7.** Spectra of the two points analysed with XRF: (a) red tone; (b) black tone. The presence of Ca probably due to ivory was detected in both.



On the external side, the two scans have been merged. As a result, elemental maps of the whole area indicated in Figure 4b were realised and are shown in Figure 8. In the area are green leaves, a dark blue-black stem and different flowers of red, black-blue and brown-orange tones. Some similarities with the drawer can be noted.

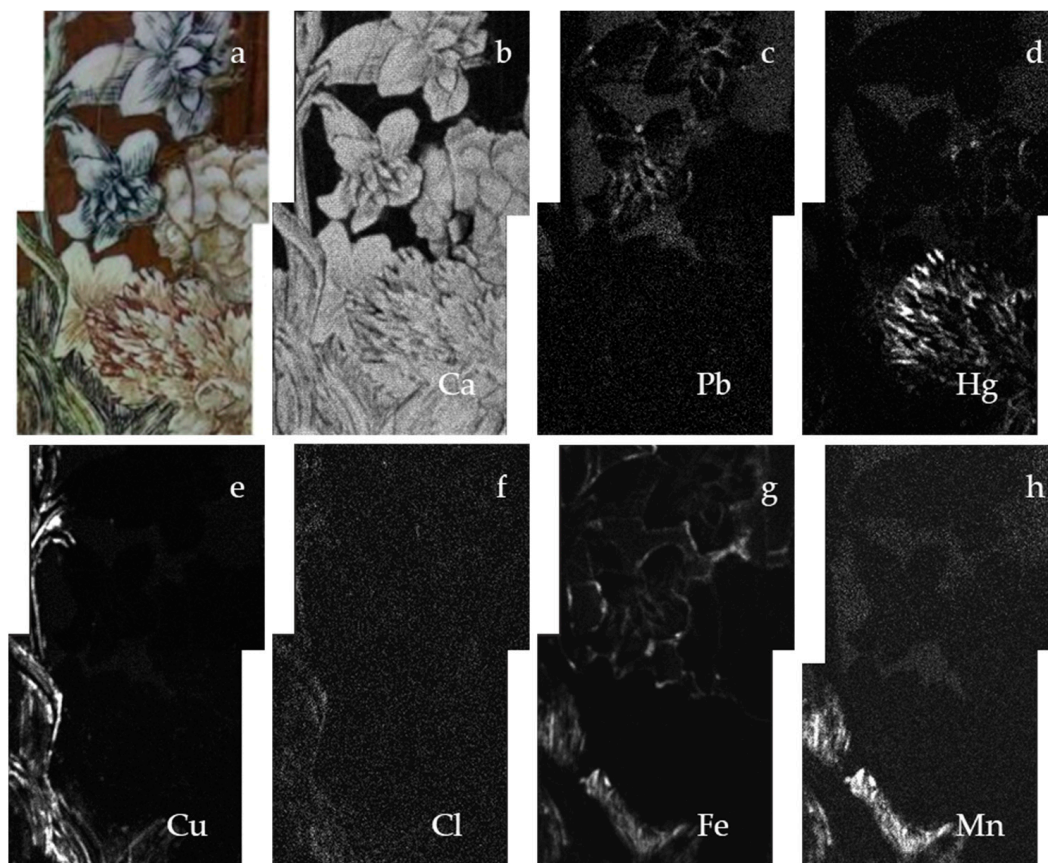


**Figure 8.** Elemental maps of the external area of the *Scrivania con scansia* obtained by the INFN-CHNet MA-XRF scanner. (a) Visible. The maps presented are: (b) Ca K $\alpha$  transition; (c) Pb L $\alpha$  transition; (d) Hg L $\alpha$  transition; (e) Cu K $\alpha$  transition; (f) Cl K $\alpha$  transition; (g) Fe K $\alpha$  transition; (h) Mn K $\alpha$  transition.

In the shading of the red flower, mercury has been detected (Figure 8d), possibly due to the use of cinnabar-vermilion (HgS). Regarding the black-blue flowers, the same elements as in the black-blue flowers of the drawer—iron (Figure 8g) and lead (Figure 8c)—are present. Therefore, the decoration may have been realised with Prussian blue and lead white. In the blue-black stem area, the signals of iron and manganese are present in the elemental maps due to the probable use of iron-oxide-based compounds enriched with manganese oxides or other ochres-earths.

Regarding the dull-yellow flower, no map shows evidence of the presence of a characteristic element; therefore, the use of organic compounds can be hypothesised. Conversely, regarding the green parts in the drawer, a strong signal of copper (Figure 8e) associated with chlorine traces (Figure 8f) is present in the leaves on the side, whereas the presence of arsenic was not detected. This result led to the hypothesis of the use of different pigments in the green areas on the external side compared with the same colour in the drawer. Because the MA-XRF analysis does not allow the identification of compounds, it is not possible to determine which of the copper-based pigments has been used, or even if it was due to degradation effects as reported in [44].

A summary of the pigments hypothesised by the use of MA-XRF analysis is reported in Table 3.

**Table 3.** Summary of the hypothesised materials employed in the different areas.

Area Scanned	Colour	Elements Detected	Materials Hypothesised
Chinoiserie cabinet—flowers	red flower	Hg	cinnabar-vermilion
	bright yellow flowers	Au	gold
	transparent yellow buds	As	arsenic-based compound
Chinoiserie cabinet—flying bird	red tail and feathers	Hg	cinnabar-vermilion
	bright yellow outlines	Au	gold
	buff body	Fe	ochres-earths
	black-blue feathers	As, Si, Ca	?
	black tail	Pb	galena
Writing desk—drawer area 1	green leaves	As, Cu	emerald green
	dark rust tone of the flower	Fe, Mn	ochres-earths
	rust tone of the flower	-	organic compounds
	white highlights	Pb	lead white
Writing desk—drawer area 2	black-blue flower	Pb, Fe	Prussian blue and lead white
	green leaves	As, Cu	emerald green
Writing desk—external side	green leaves	Cu, Cl	copper-based compound
	black-blue flower	Pb, Fe	Prussian blue and lead white
	red flower	Hg	cinnabar-vermilion
	blue-black dark stem	Fe, Mn	ochres-earths
	dull yellow flower	-	organic compounds

#### 4. Conclusions

The use of the MA-XRF technique on furniture has provided information on the elemental spatial distribution of the decorative layers. In particular, the INFN-CHNet MA-XRF scanner, due to its versatility in terms of hardware adaptability (different size of collimators, use of the telemeter) and in terms of software settings (scanning speed and step size during the measurements, data saving for an off-line analysis) has proved to be suitable for studies on this genre of works of art. A number of results have been achieved in identifying materials in the decorative layer. In both cases, the data on the polychromatic surfaces have provided information on the materials used: for instance, the use of arsenic-based compounds in the chinoiserie cabinet and the use of different pigments in the engraved ivories of the writing desk by Pietro Piffetti. However, the detection of only the elemental composition is a strong limitation for this kind of study. Therefore, the use of the technique is suggested as a first approach, while a multi-technical study is advisable for the identification of the compounds, as reported in [28]. For this reason, the INFN-CHNet group is involved in the development of instruments and techniques to support conservation processes, characterisation, and dating techniques in the heritage science field.

**Author Contributions:** Conceptualization, F.T., A.R. and A.L.G.; Data curation, L.S., L.G. (Laura Guidorzi), A.M. and C.R.; Formal analysis, L.S., L.G. (Laura Guidorzi), A.M. and C.R.; Funding acquisition, F.T. and A.L.G.; Investigation, L.G. (Laura Guidorzi), C.R., L.C., M.N., R.T. and A.R.; Methodology, L.G. (Laura Guidorzi), C.R., L.C., C.C., L.G. (Lorenzo Giuntini), M.M., F.T., M.N., R.T., F.A. and A.R.; Resources, M.N. and S.D.B.; Software, L.C., C.C. and F.T.; Supervision, A.R.; Visualization, L.S., L.G. (Laura Guidorzi), A.M. and C.R.; Writing—original draft, L.S.; Writing—review and editing, L.S., L.G. (Laura Guidorzi), A.M., A.R. and A.L.G. All authors have read and agreed to the published version of the manuscript.

**Funding:** The research was funded within the INFN-CHNet project. This project has received funding from the European Union's Horizon 2020 research and innovation programme under the Marie Skłodowska-Curie grant agreement No 754511 (PhD Technologies Driven Sciences: Technologies for Cultural Heritage—T4C).

**Institutional Review Board Statement:** Not applicable.

**Informed Consent Statement:** Not applicable.

**Data Availability Statement:** Not applicable.

**Acknowledgments:** The authors wish to warmly thank Marco Manetti for his suggestions, advice and invaluable technical support.

**Conflicts of Interest:** The authors declare no conflict of interest.

## References

1. Alfeld, M.; Broekaert, J.A.C. Mobile Depth Profiling and Sub-Surface Imaging Techniques for Historical Paintings—A review. *Spectrochim. Acta Part B At. Spectrosc.* **2013**, *88*, 211–230. [[CrossRef](#)]
2. Angelici, D.; Borghi, A.; Chiarelli, F.; Cossio, R.; Gariani, G.; Lo Giudice, A.; Re, A.; Pratesi, G.; Vaggelli, G.  $\mu$ -XRF analysis of trace elements in lapis lazuli-forming minerals for a provenance study. *Microsc. Microanal.* **2015**, *21*, 526–533. [[CrossRef](#)]
3. Corsi, J.; Lo Giudice, A.; Re, A.; Agostino, A.; Barello, F. Potentialities of X-ray fluorescence analysis in numismatics: The case study of pre-Roman coins from Cisalpine Gaul. *Archaeol. Anthropol. Sci.* **2018**, *10*, 431–438. [[CrossRef](#)]
4. Alfeld, M.; Siddons, D.P.; Janssens, K.; Dik, J.; Woll, A.; Kirkham, R.; van de Wetering, E. Visualizing the 17th century underpainting in Portrait of an Old Man by Rembrandt van Rijn using synchrotron-based scanning macro-XRF. *Appl. Phys. A* **2013**, *111*, 157–164. [[CrossRef](#)]
5. Alfeld, M.; Van der Snickt, G.; Vanmeert, F.; Janssens, K.; Dik, J.; Appel, K.; van der Loeff, L.; Chavannes, M.; Meedendorp, T.; Hendriks, E. Scanning XRF investigation of a Flower Still Life and its underlying composition from the collection of the Kröller-Müller Museum. *Appl. Phys. A* **2013**, *111*, 165–175. [[CrossRef](#)]
6. Romano, F.P.; Caliri, C.; Nicotra, P.; di Martino, S.; Pappalardo, L.; Rizzo, F.; Santos, H.C. Real-time elemental imaging of large dimension paintings with a novel mobile macro X-ray fluorescence (MA-XRF) scanning technique. *J. Anal. At. Spectrom.* **2017**, *32*, 773–781. [[CrossRef](#)]
7. Alfeld, M.; Pedrosa, J.V.; van EikemaHommes, M.; Van der Snickt, G.; Tauber, G.; Blaas, J.; Haschke, M.; Erler, K.; Dik, J.; Janssens, K. A mobile instrument for in situ scanning macro-XRF investigation of historical paintings. *J. Anal. At. Spectrom.* **2013**, *28*, 760–767. [[CrossRef](#)]
8. Ravaut, E.; Pichon, L.; Laval, E.; Gonzalez, V.; Eveno, M.; Calligaro, T. Development of a versatile XRF scanner for the elemental imaging of paintworks. *Appl. Physics. A* **2015**, *122*. [[CrossRef](#)]
9. Alberti, R.; Frizzi, T.; Bombelli, L.; Gironde, M.; Aresi, N.; Rosi, F.; Miliani, C.; Tranquilli, G.; Talarico, F.; Cartechini, L. CRONO: A fast and reconfigurable macro X-ray fluorescence scanner for in-situ investigations of polychrome surfaces. *X-ray Spectrom.* **2017**, *46*. [[CrossRef](#)]
10. Bergmann, U.; Bertrand, L.; Edwards, N.P.; Manning, P.L.; Wogelius, R.A. *Chemical Mapping of Ancient Artifacts and Fossils with X-ray Spectroscopy*; Jaeschke, E., Khan, S., Schneider, J., Hastings, J., Eds.; Synchrotron Light Sources and Free-Electron Lasers; Springer: Cham, Switzerland, 2019. [[CrossRef](#)]
11. Debastiani, R.; Simon, R.; Batchelor, D.; Dellagustin, G.; Baumbach, T.; Fiederle, M. Synchrotron-based scanning macro-X-ray fluorescence applied to fragments of Roman mural paintings. *Microchem. J.* **2016**, *126*, 438–445. [[CrossRef](#)]
12. Bergmann, U.; Manning, P.L.; Wogelius, R.A. Chemical mapping of paleontological and archeological artifacts with synchrotron X-Rays. *Annu. Rev. Anal. Chem.* **2012**, *5*, 361–389. [[CrossRef](#)] [[PubMed](#)]
13. Fernandez, J.E.; Taccetti, F.; Kenny, J.M.; Amendola, R. Conclusive editorial on non-destructive techniques for cultural heritage. *Rend. Fis. Acc. Lincei* **2020**, *31*, 819–820. [[CrossRef](#)]
14. Castelli, L.; Felicetti, A.; Proietti, F. Heritage Science and Cultural Heritage: Standards and tools for establishing cross-domain data interoperability. *Int. J. Digit. Libr.* **2019**. [[CrossRef](#)]
15. Sottili, L.; Guidorzi, L.; Mazzinghi, A.; Ruberto, C.; Castelli, L.; Czelusniak, C.; Giuntini, L.; Massi, M.; Taccetti, F.; Nervo, M.; et al. INFN-CHNet meets CCR La Venaria Reale: First results. In Proceedings of the 2020 IMEKO TC-4 International Conference on Metrology for Archaeology and Cultural Heritage 2020, Trento, Italy, 22–24 October 2020; pp. 507–511.
16. Re, A.; Zangirolami, M.; Angelici, D.; Borghi, A.; Costa, E.; Giustetto, R.; Gallo, L.M.; Castelli, L.; Mazzinghi, A.; Ruberto, C.; et al. Towards a portable X-Ray Luminescence instrument for applications in the Cultural Heritage field. *Eur. Phys. J. Plus* **2018**, *133*, 362. [[CrossRef](#)]
17. Czelusniak, C.; Palla, L.; Massi, M.; Carraresi, L.; Giuntini, L.; Re, A.; Lo Giudice, A.; Pratesi, G.; Mazzinghi, A.; Ruberto, C.; et al. Preliminary results on time-resolved ion beam induced luminescence applied to the provenance study of lapis lazuli. *Nucl. Instrum. Methods Phys. Res. B* **2016**, *371*, 336–339. [[CrossRef](#)]
18. Palla, L.; Czelusniak, C.; Taccetti, F.; Carraresi, L.; Castelli, L.; Fedi, M.E.; Giuntini, L.; Maurenzig, P.R.; Sottili, L.; Taccetti, N. Accurate on line measurements of low fluences of charged particles. *Eur. Phys. J. Plus* **2015**, *130*. [[CrossRef](#)]
19. Lo Giudice, A.; Corsi, J.; Cotto, G.; Mila, G.; Re, A.; Ricci, C.; Sacchi, R.; Visca, L.; Zamprota, L.; Pastrone, N. A new digital radiography system for paintings on canvas and on wooden panels of large dimensions. In Proceedings of the 2017 IEEE International Instrumentation and Measurement Technology Conference (I2MTC 2017) Proceedings; IEEE: Piscataway, NJ, USA, 2017; pp. 1834–1839, FP17IMT-ART; ISBN 9781509035960.
20. Ruberto, C.; Mazzinghi, A.; Massi, M.; Castelli, L.; Czelusniak, C.; Palla, L.; Gelli, N.; Bettuzzi, M.; Impallaria, A.; Brancaccio, R.; et al. Imaging study of Raffaello's "La Muta" by a portable XRF spectrometer. *Microchem. J.* **2016**, *126*, 63–69. [[CrossRef](#)]

21. Vadrucci, M.; Mazzinghi, A.; Sorrentino, B.; Falzone, S.; Gioia, C.; Gioia, P.; Loreti, E.M.; Chiari, M. Characterisation of ancient Roman wall-painting fragments using non-destructive IBA and MA-XRF techniques. *X-Ray Spectrom.* **2020**, *49*, 668–678. [[CrossRef](#)]
22. Dal Fovo, A.; Mazzinghi, A.; Omarini, S.; Pampaloni, E.; Ruberto, C.; Striova, J.; Fontana, R. Non-invasive mapping methods for pigments analysis of Roman mural paintings. *J. Cult. Herit.* **2020**, *43*, 311–318. [[CrossRef](#)]
23. Mazzinghi, A.; Ruberto, C.; Castelli, L.; Ricciardi, P.; Czelusniak, C.; Giuntini, L.; Mandò, P.A.; Manetti, M.; Palla, L.; Taccetti, F. The importance of being little: MA-XRF on manuscripts on a Venetian island. *X-ray Spectrom* **2020**, 1–7, in press. [[CrossRef](#)]
24. Lazic, V.; Vadrucci, M.; Fantoni, F.; Chiari, M.; Mazzinghi, A.; Gorghinian, A. Applications of laser-induced breakdown spectroscopy for cultural heritage: A comparison with X-ray Fluorescence and Particle Induced X-ray Emission techniques. *Spectrochim. Acta Part B At. Spectrosc.* **2018**, *149*, 1–14. [[CrossRef](#)]
25. Mazzinghi, A. Sviluppo di Strumentazione XRF a Scansione per Applicazioni ai Beni Culturali. Ph.D. Thesis, University of Florence, Firenze, Italy, 2016.
26. Andersson, E.; Cattersel, V. A Dutch Seventeenth-Century European Lacquer Cabinet. Material-Technical Analysis to Gain Insight into the Deteriorated Surface. In *Material Imitation and Imitation Materials in Furniture and Conservation*; Vasques Dias, M., Ed.; Stichting Ebenist: Amsterdam, The Netherlands, 2017; pp. 190–206.
27. Salvemini, F.; Grazi, F.; Agostino, A.; Iannaccone, R.; Civita, F.; Hertmann, S.; Lehmann, E.; Zoppi, M. Non-invasive characterization through X-ray fluorescence and neutron radiography of an ancient Japanese lacquer. *Archaeol. Anthropol. Sci.* **2013**, *5*, 197–204. [[CrossRef](#)]
28. Felix, V.S.; Mello, U.L.; Pereira, M.O.; Oliveira, A.L.; Ferreira, D.S.; Carvalho, C.S.; Silva, F.L.; Pimenta, A.R.; Diniz, M.G.; Freitas, R.P. Analysis of a European cupboard by XRF, Raman and FT-IR. *Radiat. Phys. Chem.* **2018**, *151*, 198–204. [[CrossRef](#)]
29. Tagliante, S. Problematiche Conservative e Restauro di uno Stipo Settecentesco con Decorazioni in Lacca Orientale e “Alla China”. Master’s Thesis, University of Turin, Torino, Italy, 2018.
30. Spantigati, C.; De Blasi, S. *Il Restauro degli Arredi Lignei. L’ebanisteria Piemontese. Studi e Ricerche*; Nardini Editore: Firenze, Italy, 2011.
31. Re, A.; Albertin, F.; Avataneo, C.; Brancaccio, R.; Corsi, J.; Cotto, G.; De Blasi, S.; Dughera, G.; Durisi, E.; Ferrarese, W.; et al. X-ray tomography of large wooden artworks: The case study of “Doppio corpo” by Pietro Piffetti. *Herit. Sci.* **2014**, *2*. [[CrossRef](#)]
32. De Blasi, S.; Nervo, M.; Ravera, M.; Spantigati, C. Structural characters of Piedmontese eighteenth-century cabinetmaking: Historical documents, restorations and new technologies, in restoring joints, conserving structures. In Proceedings of the Tenth International Symposium on Wood and Furniture Conservation, Amsterdam, The Netherlands, 8–9 October 2010; pp. 98–107.
33. Luciani, P.; De Blasi, S.; Nervo, M.; Piccirillo, A. *Il Restauro del Mobile di Ebanisteria Piemontese del Settecento: Le Opere di Pietro Piffetti e Luigi Prinotto. Alcuni Casi Studio, Conservació-Restauració del Moble i la Fusta. L’ experiència dels Experts*; Costa Galobart, N., Ed.; Associació per a l’Estudi del Moble: Ajuntament de Barcelona, Institut de Cultura, Museu del Disseny de Barcelona: Barcelona, Spain, 2020; pp. 85–98.
34. Taccetti, F.; Castelli, L.; Czelusniak, C.; Gelli, N.; Mazzinghi, A.; Palla, L.; Ruberto, C.; Censori, C.; Lo Giudice, A.; Re, A.; et al. A multipurpose X-ray fluorescence scanner developed for in situ analysis. *Rend. Fis. Acc. Lincei* **2019**, *30*, 307–322. [[CrossRef](#)]
35. Fitzhugh, E. *West, Orpiment and Realgar in Artists Pigments*; West Fitzhugh, E., Ed.; National Gallery of Art: London, UK, 1997; Volume 3, pp. 45–81.
36. Vermeulen, M.; Sanyova, J.; Janssens, K. Identification of artificial orpiment in the interior decorations of the Japanese tower in Laeken. *Bruss. Belg. Herit. Sci.* **2015**, *3*, 9. [[CrossRef](#)]
37. Gettens, R.J.; Robert, L.F.; Chase, W.T. Vermilion and Cinnabar. *Stud. Conserv.* **1972**, *17*, 45–69. [[CrossRef](#)]
38. Marika, S.; Grout, R.; White, R. ‘Black Earths’: A Study of Unusual Black and Dark Grey Pigments Used by Artists in the Sixteenth Century. *Natl. Gallery Tech. Bull.* **2003**, *24*, 96–114.
39. Seccaroni, C.; Moioli, P. *Fluorescenza X-Prontuario per l’ analisi XRF Portatile Applicata a Superfici Policrome*; Nardini Editore: Firenze, Italy, 2002; pp. 60–89.
40. Siddall, R. Mineral Pigments in Archaeology: Their Analysis and the Range of Available Materials. *Minerals* **2018**, *8*, 201. [[CrossRef](#)]
41. Eastaugh, N. *Pigment Compendium: A Dictionary and Optical Microscopy of Historical Pigments*; Butterworth-Heinemann: Amsterdam, The Netherlands, 2008; pp. 239–241.
42. Kriznar, A.; Muñoz, M.; Paz, F.; Respaldiza, M.; Vega, M. Non-destructive XRF analysis of pigments in a 15th century panel painting. In Proceedings of the 9th International Conference on NDT of Art, Jerusalem, Israel, 25–30 May 2008.
43. Kirby, J.; Saunders, D. Fading and colour change of Prussian blue: Methods of manufacture and the influence of extenders. *Natl. Gallery Tech. Bull.* **2004**, *25*, 73–99.
44. Vermeulen, M.; Sanyova, J.; Janssens, K.; Nuyts, G.; De Meyer, S.; De Wael, K. The Darkening of Copper- or Lead-Based Pigments Explained by a Structural Modification of Natural Orpiment: A Spectroscopic and Electrochemical Study. *J. Anal. At. Spectrom.* **2017**, *32*, 1331–1341. [[CrossRef](#)]



# Macro X-ray fluorescence analysis of XVI-XVII century Italian paintings and preliminary test for developing a combined fluorescence apparatus with digital radiography

Leandro Sottili<sup>1,2</sup>, Laura Guidorzi<sup>1,2</sup>, Alessandro Lo Giudice<sup>1,2</sup>, Anna Mazzinghi<sup>3,4</sup>, Chiara Ruberto<sup>3,4</sup>, Lisa Castelli<sup>4</sup>, Caroline Czelusniak<sup>4</sup>, Lorenzo Giuntini<sup>3,4</sup>, Mirko Massi<sup>4</sup>, Francesco Taccetti<sup>4</sup>, Marco Nervo<sup>5</sup>, Rodrigo Torres<sup>6</sup>, Francesco Arneodo<sup>6</sup>, Alessandro Re<sup>1,2</sup>

<sup>1</sup> Dipartimento di Fisica, Università degli Studi di Torino, Via Pietro Giuria 1, 10125 Torino, Italy

<sup>2</sup> Istituto Nazionale di Fisica Nucleare (INFN), Sezione di Torino, Via Pietro Giuria 1, 10125 Torino, Italy

<sup>3</sup> Dipartimento di Fisica e Astronomia, Università degli Studi di Firenze, Via Giovanni Sansone 1, Sesto Fiorentino, 50019 Firenze, Italy

<sup>4</sup> Istituto Nazionale di Fisica Nucleare (INFN), Sezione di Firenze, Via Giovanni Sansone 1, Sesto Fiorentino, 50019 Firenze, Italy

<sup>5</sup> Centro Conservazione e Restauro "La Venaria Reale", Piazza della Repubblica, Venaria Reale, 10078 Torino, Italy

<sup>6</sup> New York University Abu Dhabi, Division of Science, P.O. Box 129188, Saadiyat Island, Abu Dhabi, United Arab Emirates

## ABSTRACT

Using portable instruments for the preservation of artworks in heritage science is more and more common. Among the techniques, Macro X-Ray Fluorescence (MA-XRF) and digital radiography (DR) play a key-role in the field, therefore a number of MA-XRF scanners and radiographic apparatuses have been developed for this scope. Recently, the INFN-CHNet group, the network of the INFN devoted to cultural heritage, has developed a MA-XRF scanner for in-situ analyses. The instrument is fully operative, and it has already been employed in museums, conservation centres and out-door fields. In the present paper, the MA-XRF analysis conducted with the instrument on four Italian artworks undertaking conservation treatments at the conservation centre CCR "La Venaria Reale" are presented. Results on the preliminary test to combine DR with MA-XRF in a single apparatus are also shown.

Section: RESEARCH PAPER

Keywords: MA-XRF; digital radiography; pigments identification; paintings

Citation: Leandro Sottili, Laura Guidorzi, Alessandro Lo Giudice, Anna Mazzinghi, Chiara Ruberto, Lisa Castelli, Caroline Czelusniak, Lorenzo Giuntini, Mirko Massi, Francesco Taccetti, Marco Nervo, Rodrigo Torres, Francesco Arneodo, Alessandro Re, Macro X-ray fluorescence analysis of XVI-XVII century Italian paintings and preliminary test for developing a combined fluorescence apparatus with digital radiography, Acta IMEKO, vol. 11, no. 1, article 6, March 2022, identifier: IMEKO-ACTA-11 (2022)-01-06

Section Editor: Fabio Santaniello, University of Trento, Italy

Received March 7, 2021; In final form December 13, 2021; Published March 2022

Copyright: This is an open-access article distributed under the terms of the Creative Commons Attribution 3.0 License, which permits unrestricted use, distribution, and reproduction in any medium, provided the original author and source are credited.

Funding: This project has received funding from: the European Union's Horizon 2020 research and innovation programme under the Marie Skłodowska-Curie grant agreement No 754511 (PhD Technologies Driven Sciences: Technologies for Cultural Heritage – T4C); INFN-CHNet and Compagnia di San Paolo (NEXTO project, Progetti di Ateneo 2017).

Corresponding author: Alessandro Lo Giudice, e-mail: [alessandro.logiudice@unito.it](mailto:alessandro.logiudice@unito.it)

## 1. INTRODUCTION

Nowadays, the use of non-destructive non-invasive X-Ray based techniques is well established in heritage science for analysis and conservation of artworks [1]-[3]. X-Ray Fluorescence (XRF) technique plays a fundamental role since it provides information on the elemental composition of painted surfaces, contributing to identify the materials employed in artworks. Whenever XRF is combined with scanning capability

on macroscopic surfaces, the technique is indicated as Macro X-Ray Fluorescence (MA-XRF) [4]. Conversely, due to the impossibility to transport most of the artworks inside a laboratory to undertake scientific analyses, e.g., for their preciousness or considerable weight, an important class of instruments is made up of portable and transportable scanners [5]. A number of MA-XRF scanners are nowadays in use in heritage science, both commercial [6] and built in-house [7]-[9]. Despite the high analytical capabilities of the MA-XRF

technique, it is worth underlining the importance of a thorough multi-analytical approach for a better comprehension of the artworks.

Another well-established non-destructive non-invasive and transportable X-ray technique is the digital radiography (DR) whose potentialities are widely known [10] as a tool for conservators and art historians [11]. It is frequently used in combination with MA-XRF by means of a dedicated instrument for a more complete information of artworks, as in the case of painting on canvas and on wooden panels [12], [13]. However, the possibility to employ a single apparatus integrating XRF and DR is not yet well investigated [14]. The advantage would be to have a single X-ray tube for a straightforward combined analysis in the same area.

In this work, the MA-XRF scanner [15] developed in-house by the Cultural Heritage Network of the National Institute of Nuclear Physics (INFN-CHNet) was used to analyse XVI-XVII century paintings under conservation at the Centro Conservazione e Restauro (CCR) “La Venaria Reale” [16], located nearby Torino. To date, the INFN-CHNet network gathers 18 local divisions, 4 Italian partners among which the CCR “La Venaria Reale”, that is a second level node in the network, and international partners as the New York University of Abu Dhabi (UAE) [17].

Moreover, a flat panel detector for DR coupled with a mini-X-ray tube that will be used in a modified version of the INFN-CHNet MA-XRF was tested on a painting on canvas. Information obtained by means of elemental mapping and radiography were combined for a better comprehension of the realisation of the artwork.

## 2. EXPERIMENTAL SET-UP

For the measurements presented in this paper two set-up were used: the MA-XRF scanner developed by the INFN-CHNet group for compositional information and a mini-X-Ray tube combined with a flat panel detector for DR, that will be added in a modified version of the MA-XRF scanner in the near future.

### 2.1. The INFN-CHNet MA-XRF scanner

The INFN-CHNet MA-XRF scanner (Figure 1) is a compact ( $60 \times 50 \times 50 \text{ cm}^3$ ) and lightweight (around 10 kg) instrument. Its main parts are the measuring head, a three axes motor stage and a case containing all the electronics for acquisition and control.

The measuring head is composed by an X-Ray tube (Moxtek©, 40 kV maximum voltage, 0.1 mA maximum anode current, 4 W maximum power, Mo anode) with a brass collimator (typically 800  $\mu\text{m}$  of diameter), a Silicon Drift Detector (Amptek© XR100 SDD, 50  $\text{mm}^2$  effective active surface, 12.5  $\mu\text{m}$  thickness Be window) and a telemeter (Keyence IA-100). The motor stage (Physik Instrumente©, travel ranges 30 cm horizontally (x axis), 15 cm vertically (y axis) and 5 cm in z direction) holding the measuring head is screwed on the carbon-fibre case. Typical operating voltage is around 30 kV. Signals are collected with a multi-channel analyser (model CAEN DT5780) and the whole system is controlled by a laptop.

The control-acquisition-analysis software is developed within the INFN-CHNet network and allows both an on-line and an off-line analysis. The output of the acquisition process is a file containing the scanning coordinates and, for each position, the spectrum acquired. For each map, a single element can be selected and shown in the scanned area, or in a part of it. Using the raw data, for each element the relative intensities are shown

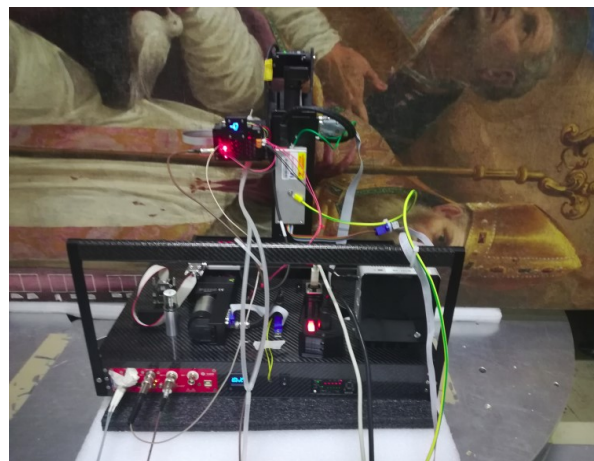


Figure 1. INFN-CHNet MA-XRF scanner placed in front of the panel painting *Madonna e i Santi* by Cristoforo Roncalli, known as il Pomarancio.

in grey scale, in which the maximum intensity is in white and the lower is in black. Scan is carried out on the x axis, and a step size of typically 1 mm is set on the y axis resulting in a pixel size of 1  $\text{mm}^2$ . A complete review on the instrument can be found in [15]. The instrument has already been used for a number of different applications, i.e. paintings [18]-[21], illuminated manuscripts [22], coins [23], ceramics [24], and furniture [25].

### 2.2. The digital radiography set-up

Structural information of artworks can be obtained by a radiographic approach. Although a radiography could be carried out in principle using the same X-ray tube employed in the present INFN-CHNet MA-XRF apparatus, for future applications a modified version with a different source will be considered. Considering the higher distance from the object needed to obtain a radiography than XRF maps, and the thickness of artworks to be passed through, an X-ray tube with a slightly higher voltage and power was used. In particular, the measurements were made with a Moxtek©, 60 kV X-Ray tube (1 mA maximum anode current, 12 W maximum power, 0.4 mm diameter nominal focal spot size, Rh anode). If not collimated, it generates a 20 cm diameter beam at about 25 cm of distance. As the present MA-XRF apparatus only has a 5 cm z travel range, the future version will be capable of a translation in z up to 30 cm to avoid the handling of the artwork between XRF and DR measurements.

About X-ray imaging, a Shad-o-Box HS detector by Teledyne, model 6K was selected. The detector contains a large active area (11,4 cm  $\times$  14,6 cm) that is fully covered by the X-ray beam at 25 cm of distance from the source; the pixel size is 49.5  $\mu\text{m}$  and the maximum integration time 65 s. The video signal is digitised to 14 bits, reassembled within the camera's FPGA, and then transferred to a computer via a high-speed Gigabit Ethernet interface. The CMOS sensor inside the detector contains a direct-contact CsI scintillator, that converts X-ray photons into visible light that is sensed by the CMOS photodiodes. A thin graphite cover protects the sensor from accidental damage as well as from ambient light. The Shad-o-Box HS camera also contains lead and steel shielding to protect its electronics from X-ray radiation. The cameras are sensitive to X-ray energies as low as 15 keV, and may be used with generators up to 225 kV<sub>p</sub>. The detector, that has already been used for X-ray imaging with conventional tubes [26], is part of the NEXTO project that has the aim to integrate MA-XRF, DR and X-Ray Luminescence (XRL) [27] in a single portable instrument.

### 3. APPLICATIONS AT THE CCR “LA VENARIA REALE”

In this section different applications of the instrumentation on paintings are presented. The works of art represent case studies from Italian central regions of different periods (from the beginning of the 16<sup>th</sup> to the beginning of the 17<sup>th</sup> century). They were analysed during conservation processes carried out at the CCR “La Venaria Reale” [28]. For the MA-XRF measurements, a collimator of 800 µm diameter was used. The vertical step was set to 1 mm and a scanning speed of 3 mm/s. Furthermore, the Keyence IA-100 telemeter was switched on to maintain the sample distance during the scanning process.

#### 3.1. *Madonna di San Rocco* by Francesco Sparapane

The first painting presented is the oil on panel *Madonna di San Rocco* depicting the Virgin with the Child, Saint Antonio from Padua and Saint Rocco by Francesco Sparapane (Preci, Umbria region, 1530 ca.). The importance of the work of art is related to the lack of documented paintings by the author, thereby its study represents a key-feature for understanding the painting technique of the artist [29].

The MA-XRF measurements were conducted on two areas as shown in Figure 2, from which a number of maps were created. The source voltage was set to 30 kV and its anode current to 20 µA.

The maps around Saint Rocco (Figure 3) show the use of lead white, most likely due to the imprimatur layer and as proper pigment in the flesh tones. From the map of copper, the green part of the hat was realised with copper-based compounds [30]. The presence of tin is also detected in this same region, although in moderate amounts, and might be due to the use of lead-tin yellow in mixture with the copper-based pigment. A more precise identification of the material cannot be made with XRF



Figure 2. Painting *Madonna con Bambino e S. Antonio e S. Rocco* by Francesco Sparapane. The scanned areas are indicated in the white boxes.

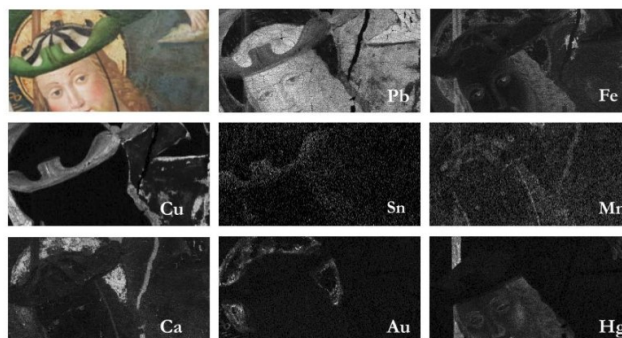


Figure 3. MA-XRF maps of area 1 of the *Madonna di San Rocco* by Francesco Sparapane (size 280 mm × 70 mm).

technique: for instance, it is not possible to distinguish between a mixture of tin-based yellow with malachite rather than with azurite [31].

The shadows of the flesh tones were realised with ochre-earths, as can be inferred from the match between iron and manganese maps [32]. Corresponding to the red tone in the checks, a high signal of mercury is present, most likely due to the use of vermilion-cinnabar (HgS) [33]. Furthermore, calcium is present in the strings of the hat, the dark strips and in the eyes, that may indicate the use of bone black for darkening [34] as well as manganese in the same areas may indicate the use of manganese black [35].

The halo was made with gold (Figure 3), while the corresponding presence of calcium and iron is probably due to a calcium/iron-based preparation, as discussed in [36].

The second area around the upper part of the head of S. Antonio (Figure 4) presents similar results. However, a marked difference is related to the sky, that is made with a copper-based compound (most likely azurite [31]) with a glaze realised with smalt, a material rarely used as a pigment from the 15<sup>th</sup> century and which was widespread from the 17<sup>th</sup> c. onwards. Concisely, smalt is a blue potash glass (thus characterised also by presence of potassium and aluminium) where the chromophore is cobalt and it usually contains impurities, among others, of bismuth when produced after 1520 [37]. Its presence is thus hypothesised by the maps of the corresponding elements. A similar palette was probably used for the sky in the first area; however, due to the bad conservation condition, only traces of the characteristic elements are present in the maps of copper and cobalt.

#### 3.2. *Madonna con bambino e santi* by Pomarancio

The oil on canvas *Madonna con bambino e santi* by Cristoforo Roncalli, known as il Pomarancio, was made in the first decade of the 17<sup>th</sup> century, and it is placed in the Santa Maria Argentea church in Norcia (Umbria region, Italy). The Virgin and the Child are depicted with the Saints Eutizio, Fiorenzo, Santolo, and Spes.

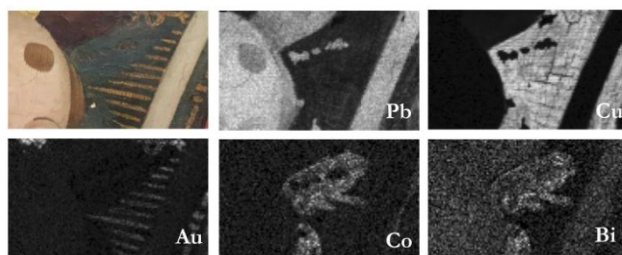


Figure 4. MA-XRF maps of the area 2 of the *Madonna di San Rocco* by Francesco Sparapane (size 120 mm × 70 mm).



Figure 5. Painting *Madonna con bambino e i Santi* by Il Pomarancio. The scanned areas are indicated in white boxes. The saints are, from left, S. Eutizio, S. Fiorenzo, S. Santolo, and S. Spes.

The focus of the analysis was the painting palette used in the flesh tones by the author [38], of which two representative areas were scanned, as shown in Figure 5.

The source voltage was set to 28 kV and its anode current to 20  $\mu$ A.

The maps realised in the first area (Figure 6) show the use of lead white for the flesh tones and the book, while a high signal

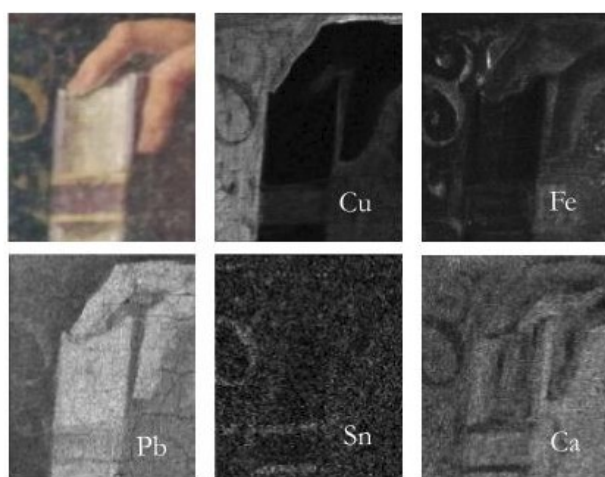


Figure 6. Maps of the area 1 of *Madonna con bambino e i Santi* by Il Pomarancio (size 130 mm  $\times$  110 mm).

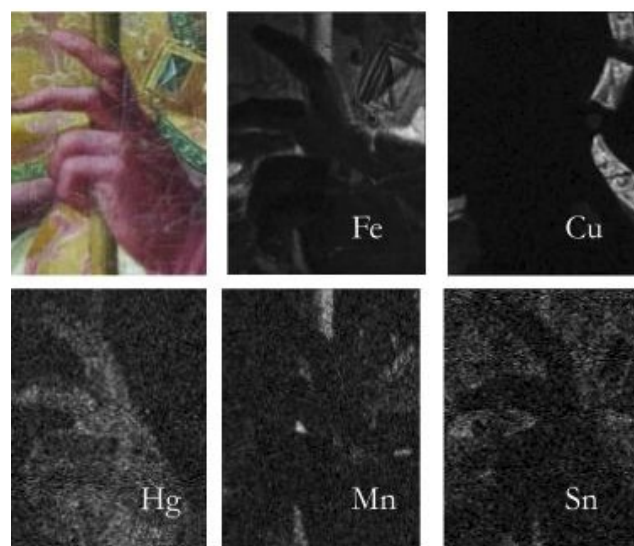


Figure 7. MA-XRF maps of area 2 of *Madonna con bambino e i Santi* by Il Pomarancio (size 150 mm  $\times$  137 mm).

of iron is present corresponding to the shadows. The blue cope of Saint Fiorenzo shows an intense signal of copper, due to a copper-based compound, leading to the hypothesis of azurite [31].

The darkest colour is related to a high signal of calcium, that, by only means of the XRF technique, cannot lead to a precise hypothesis on the material used.

Furthermore, the presence of tin was detected in the squiggles as well as a higher intensity of lead, most likely due to the use of lead-tin yellow [32].

The second area (Figure 7) shows a different composition: the map of mercury matches with the hand, leading to the hypothesis of vermilion-cinnabar for the glove. As opposed to the previous area, the map of iron does not show an intense signal in the hand of Saint Spes. The main signal of iron comes from the stick and the cope in correspondence to the yellow colour. By comparing the maps of iron, manganese, mercury, and tin, it can be noted that all of them are present in the crosier, even if tin and mercury are in the highlights, whereas the manganese and iron are in the shadows. This result can be explained by the use of vermilion-cinnabar mixed with lead-tin yellow [32] in the highlights, and the use of ochre-earths [32] in the shading. Iron, manganese, and tin are also present in the yellow cope. Furthermore, iron and manganese are present in the green medallion, which present a strong signal from copper, related to copper-based pigments.

From the map of copper, it may be seen that all the green colours in the area are related to its presence. However, as in the hat of Saint Rocco seen in the previous section, it is not possible to hypothesise a conclusion on the material used.

### 3.3. Adorazione dei Magi by Sante Peranda

The oil on canvas *Adorazione dei Magi* by Sante Peranda (Figure 8) is dated around the first decade of the 17<sup>th</sup> century. In this case the interest was focused on the blue colours.

The measurements were conducted in three areas: one on the robe of the Virgin, one behind the Magus on the far left wearing the white dress, and the last one behind the kneeling Magus. The composition detected is different for each area. The source voltage was set to 28 kV and its anode current to 30  $\mu$ A.

In the first area, the Virgin's robe (Figure 9), cobalt is present. As in the previous sections, this may suggest the use of smalt as



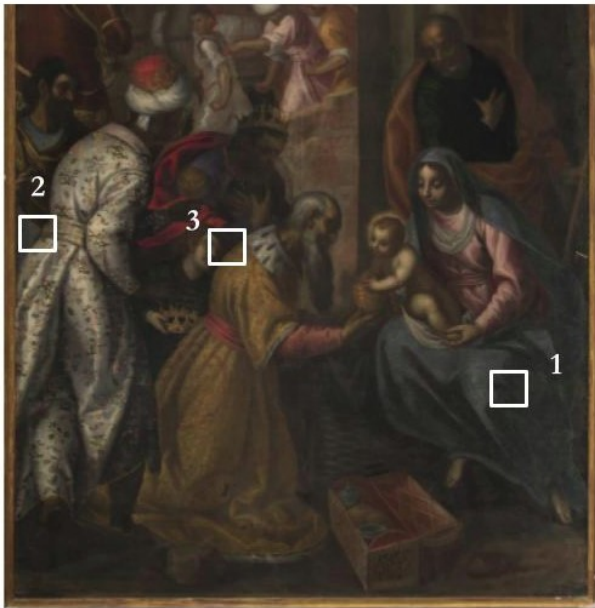


Figure 8. *Adorazione dei Magi* by Sante Peranda. The scanned areas are indicated in white boxes.

blue pigment [37]. The match between the cobalt and the silicon maps most likely indicates the use of such blue glass in this area. Furthermore, the localised lack of these two elements in the area is related with the presence of a conservation intervention with a titanium-based material [32].

In the second area, shown in Figure 10, the composition of the blue is similar to the previous, despite the presence of a significant iron signal, probably due to the use of ochre-earths for the shading [34]. However, with this technique alone a later retouch with Prussian blue cannot be excluded [39]. Beside the map of cobalt, the map of bismuth is also reported to confirm the hypothesis of smalt and, consequently, the dating of the painting [34]. Moreover, it can be seen that the  $L\alpha$ -line of lead (10.55 keV) is detected in the whole area, whereas the M-lines (2.34 keV) are present only in the robe. This is due to the different absorption for different X-Ray energies (the lower is the energy and the higher is the absorption), therefore the comparison of the two maps suggests that lead white was used for the imprimatur, as well as for the white robe of the Magus on the far left.

A different composition is detected in the last blue area (Figure 11). In this case a strong signal of copper is present,

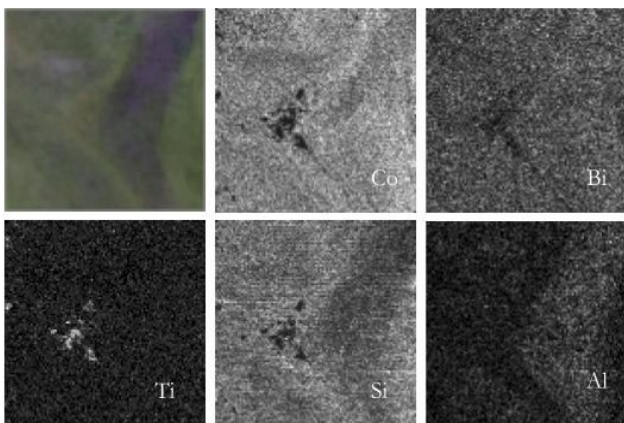


Figure 9. Maps of area 1 in the robe of the Virgin in Figure 8 (size 100 mm × 100 mm).

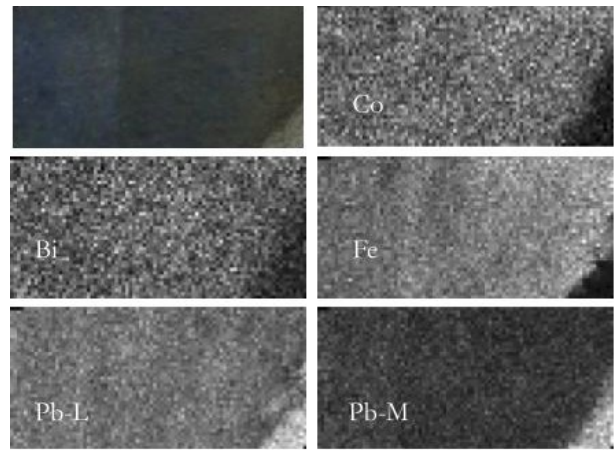


Figure 10. Maps of area 2 in the robe of the Magus wearing the white dress in Figure 8 (size 85 mm × 40 mm).

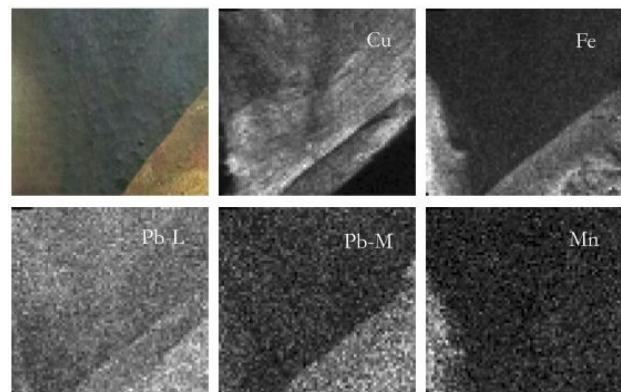


Figure 11. Maps of area 3 in the blue robe behind the kneeling Magus in Figure 8 (size 70 mm × 65 mm).

whereas no presence of cobalt was detected. For this reason, conversely to the previous cases, the use of azurite can be hypothesised for the blue tone in the area. It is also clearly visible from the map of copper its presence beneath the yellow robe, probably due to a pentimento in the back of the kneeling Magus. The last hypothesis can be also supported by the maps of lead, in which its use up on the copper can be hypothesised by the detection of the M-line only in the region of the robe, whereas the rest of the area shows only the L-lines of lead.

The yellow robe shows the presence of iron and lead, which may suggest a combined use of white lead and yellow ochre-earths [31].

The hair of the servant present in the area shows a signal of iron and manganese, probably due to the employment of ochre-earths.

#### 3.4. *Madonna con Bambino ed i Santi Crescentino e Donnino* by Timoteo Viti

The last painting presented is the *Madonna con Bambino ed i Santi Crescentino e Donnino* by Timoteo Viti (Figure 12), dated between 1500 and 1510. The work is a tempera on canvas, its size is 168 cm × 165 cm. The painting presented bad conservation conditions on the areas around the faces of the Virgin and the Child. The painting technique is *tempera magra* [40], in which the binder tends to be absorbed by the preparatory layer. Moreover, the application of a protective varnish was not envisaged, leaving the paint in direct contact with the external environment.

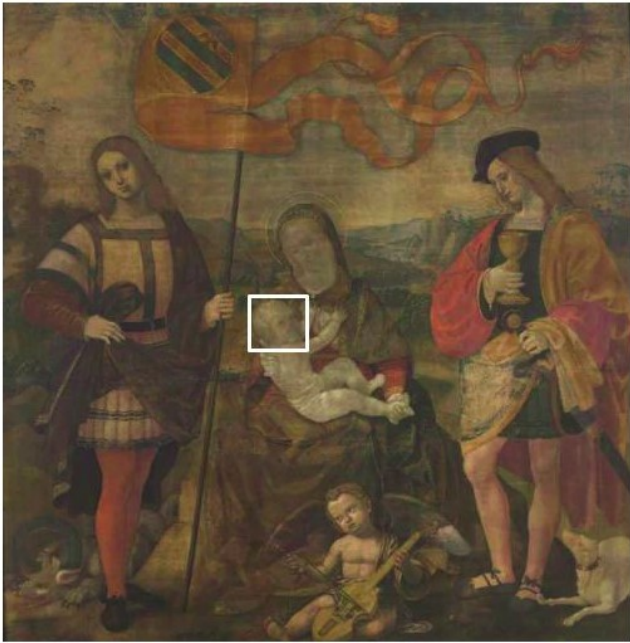


Figure 12. Madonna con Bambino e i santi Crescentino e Donnino by Timoteo Viti. The results presented are from the area in the white box.

The source voltage was set to 28 kV and the anode current to 30  $\mu$ A. The maps of the area around the Child's head are presented in Figure 14.

As can be seen from Figure 13, the flesh tones are characterised by a strong signal of calcium, whereas no evidence of the use of lead was detected. Moreover, the shading was made most likely with ochre-earths, according to the map of iron. In addition, the highlights of the mouth and the cheeks show a signal of mercury, most likely due to the use of cinnabar-vermilion. The high presence of calcium can be explained with the use of white of San Giovanni (white lime) pigment or other calcium-based compounds [41].

Furthermore, by creating a spectrum in the area of the face, and comparing it with a spectrum obtained outside (Figure 13), it can be noted a higher intensity of the 2.0 keV line compared with the  $K\alpha$  of calcium, that can be explained with the presence of phosphorus in the flesh tone. This may be explained with the presence of bone black, a pigment used for shading [34].

The signal of lead is present in the hair of the Child. Furthermore, the match of the spatial distribution of tin with lead

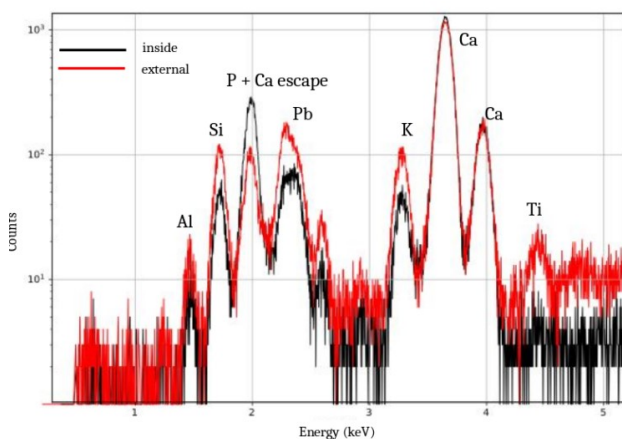


Figure 13. Comparison between two spectra, one obtained selecting an area inside the face (black) and outside (red).

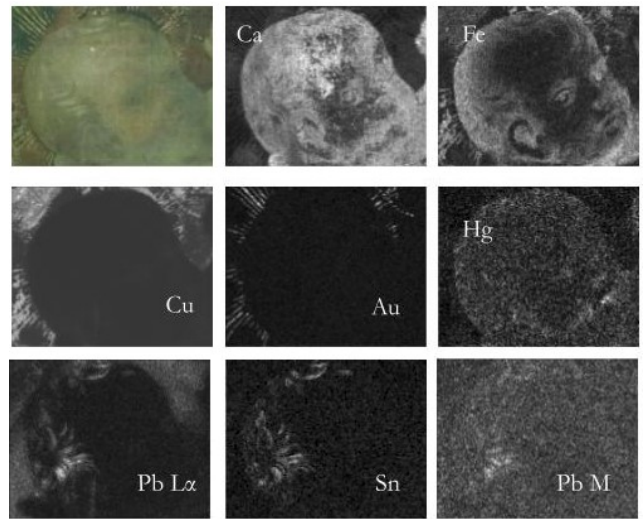


Figure 14. MA-XRF maps of the area around the face of Jesus Christ in *Madonna ed i Santi Crescentini e Donnino* painting (size 140 mm  $\times$  110 mm).



Figure 15. Radiography of the area around Jesus Christ's face.

may indicate the use of lead-tin yellow for it.

The landscape of the background was realised with copper-based compounds mixed with ochre-earths, while the halo was realised with gold.

In addition to the MA-XRF measurements, a radiographic investigation was carried out in the same area using the set-up described in section 2.2. The voltage was set to 20 kV, the anode current to 0.6 mA and the integration time to 2 seconds. As shown in Figure 15, for example in Jesus Christ's hair, the image is more detailed than the MA-XRF map: this allows the visualization of warp and weft threads of the canvas. Moreover, it can be observed to match with the MA-XRF map distributions of the heavy metals (Pb, Sn, Au, Cu), and only partially with the distribution of calcium. This result is due to the very thin thickness of the painting layer, typical of the *tempera magra* painting technique.

#### 4. CONCLUSIONS

The INFN-CHNet MA-XRF scanner was applied on four Italian paintings at the CCR "La Venaria Reale". For each application, different queries were advanced during the conservation processes and the described analysis achieved important information on the painting layers.

In the *Madonna di San Rocco* by Francesco Sparapane, the

composition of the flesh tones of S. Antonio and S. Rocco were identified, even though a definite composition cannot be measured, due to the limitation of the XRF technique to detect elements lighter than sodium. A similar conclusion has been made for other parts of the painting (the sky and S. Rocco's clothes).

In the *Madonna con bambino e i santi* by il Pomarancio, the wide painting palette (lead white, lead-tin yellow, cinnabar-vermilion, copper-based compounds) was measured, confirming the skills of the author.

For the *Adorazione dei Magi* by Sante Peranda, the blue colours in the areas under study have shown different compositions. It is worth noting that a more precise identification of the materials employed in the painting layers is not possible with only XRF technique, but a further investigation with other techniques such as Fiber Optics Reflectance Spectroscopy (FORS) or Raman spectroscopy is needed.

In the last painting, the presence of calcium-based white in the face of the Child was detected. However, no signal of lead is present in that area, whereas it is present in the background. In addition, DR was conducted in the same area using a new set-up that was proven to be suitable to be combined with XRF in a single instrument. The test carried out at the CCR "La Venaria Reale" is the first step for the development of this multi-technique device.

The complete realisation will rely on the expertise of the INFN-CHNet group, which has already allowed to achieve several important technological results in heritage science applications [42]-[46].

#### ACKNOWLEDGEMENT

This project has received funding from Compagnia di San Paolo (NEXTO project, progetto di Ateneo 2017) and the INFN-CHnet project.

This project has received funding from the European Union's Horizon 2020 research and innovation programme under the Marie Skłodowska-Curie grant agreement No 754511 (PhD Technologies Driven Sciences: Technologies for Cultural Heritage – T4C).

The authors wish to warmly thank Marco Manetti of the INFN-Fi for his invaluable technical support, the students Giulia Corrada, Francesca Erbetta, Daniele Dutto, Giulia Dilecce and their supervisors, Prof.ssa Gianna Ferraris di Celle, Prof. Alessandro Gatti, Prof. Bernadette Ventura, Prof. Antonio Iaccarino Idelson and the staff of the CCR "La Venaria Reale" for its support.








#### REFERENCES

- [1] V. Gonzalez, M. Cotte, F. Vanmeert, W. de Nolf, K. Janssens, X-ray Diffraction Mapping for Cultural Heritage Science: a Review of Experimental Configurations and Applications, *Chem. Eur. J.*, 2020, 26, 1703.  
DOI: [10.1002/chem.201903284](https://doi.org/10.1002/chem.201903284)
- [2] M. P. Morigi, F. Casali, Radiography and Computed Tomography for Works of Art, In *Handbook of X-ray Imaging: Physics and Technology*, Editor P. Russo, Boca Raton: CRC Press, 2018, pp. 1185-1210.
- [3] F. P. Romano, C. Caliri, P. Nicotra, S. Di Martino, L. Pappalardo, F. Rizzo, H. C. Santos, Real-time elemental imaging of large dimension paintings with a novel mobile macro X-ray fluorescence (MA-XRF) scanning technique, *J. Anal. Atomic Spectrom.*, 32 (4) (2017), pp. 773-781.  
DOI: [10.1039/c6ja00439c](https://doi.org/10.1039/c6ja00439c)
- [4] P. Ricciardi, S. Legrand, G. Bertolotti, K. Janssens, Macro X-ray fluorescence (MA-XRF) scanning of illuminated manuscript fragments: potentialities and challenges, *Microchemical Journal*, ISSN 0026-265X, Volume 124, 2016, pp. 785-791.  
DOI: [10.1016/j.microc.2015.10.020](https://doi.org/10.1016/j.microc.2015.10.020)
- [5] M. Alfeld, K. Janssens, J. Dik, W. de Nolf, G. van der Snickt, Optimization of mobile scanning macro-XRF systems for the in situ investigation of historical paintings, *J. Anal. At. Spectrom.*, 26 (2011), 899-909.  
DOI: [10.1039/c0ja00257g](https://doi.org/10.1039/c0ja00257g)
- [6] M. Alfeld, J. Vaz Pedroso, M. van Eikema Hommes, G. Van der Snickt, G. Tauber, J. Blass, M. Haschke, K. Erler, J. Dik, K. Janssens, A mobile instrument for in situ scanning macro-XRF investigation of historical paintings, *Journal of Analytical Atomic Spectrometry*, 28, 2013, 760-767.  
DOI: [10.1039/C3JA30341A](https://doi.org/10.1039/C3JA30341A)
- [7] E. Pouyet, N. Barbi, H. Chopp, O. Healy, A. Katsaggelos, S. Moak, R. Mott, M. Vermeulen, M. Walton, Development of a highly mobile and versatile large MA-XRF scanner for in situ analyses of painted work of arts, *X-Ray Spectrom.* 2020; 1–9.  
DOI: [10.1002/xrs.3173](https://doi.org/10.1002/xrs.3173)
- [8] S. A. Lins, E. Di Francia, S. Grassini, G. Gigante, S. Ridolfi, MA-XRF measurement for corrosion assessment on bronze artefacts, 2019 IMEKO TC4 International Conference on Metrology for Archaeology and Cultural Heritage, MetroArchaeo 2019, 2019, pp. 538-542. Online [Accessed 11 March 2022]  
<https://www.imeko.org/publications/tc4-Archaeo-2019/IMEKO-TC4-METROARCHAEO-2019-105.pdf>
- [9] E. Ravaut, L. Pichon, E. Laval, V. Gonzalez, Development of a versatile XRF scanner for the elemental imaging of paintworks, *Appl. Phys. A* 122, 17 (2016).  
DOI: [10.1007/s00339-015-9522-4](https://doi.org/10.1007/s00339-015-9522-4)
- [10] J. Lang, A. Middleton, *Radiography of Cultural Material*, 2nd Edition, Elsevier, Oxford, 2005, ISBN 978-0-08-045560-0
- [11] D. Graham, T. Eddie, *X-ray Techniques in Art Galleries and Museums*, A. Hilger (editor), Bristol, 1985, ISBN 10: 0852747829
- [12] M. Alfeld, J. A. C. Broekaert, Mobile depth profiling and sub-surface imaging techniques for historical paintings-A review, *Spectrochimica Acta Part B* 88, 2013, pp. 211–230.  
DOI: [10.1016/j.sab.2013.07.009](https://doi.org/10.1016/j.sab.2013.07.009)
- [13] M. Alfeld, L. de Viguerie, Recent developments in spectroscopic imaging techniques for historical paintings - A review, *Spectrochimica Acta Part B*, 2017, pp 81-105.  
DOI: [10.1016/j.sab.2017.08.003](https://doi.org/10.1016/j.sab.2017.08.003)
- [14] A. Shugar, J. J. Chen, A. Jehle, X-radiography of cultural heritage using handheld XRF spectrometers, *Xray Spectrom* 21 (2017) pp. 311-318.  
DOI: [10.1002/xrs.2947](https://doi.org/10.1002/xrs.2947)
- [15] F. Taccetti, L. Castelli, C. Czelusniak, N. Gelli, A. Mazzinghi, L. Palla, C. Ruberto, C. Corsori, A. Lo Giudice, A. Re, D. Zafirooulos, F. Arneodo, V. Conicella, A. Di Giovanni, R. Torres, F. Castella, N. Mastrangelo, D. Gallegos, M. Tascon, F. Marte, L. Giuntini, A multi-purpose X-ray fluorescence scanner developed for in situ analysis, *Rendiconti Lincei, Scienze Fisiche e Naturali*, 2019, 30:307-322.  
DOI: [10.1007/s12210-018-0756-x](https://doi.org/10.1007/s12210-018-0756-x)
- [16] Centro Conservazione e Restauro La Venaria Reale, Online [Accessed 11 March 2022]  
[www.centrorestaurovenaria.it/en](http://www.centrorestaurovenaria.it/en)
- [17] Cultural Heritage Network of the Italian National Institute for Nuclear Physics, Online [Accessed 11 March 2022]  
<http://chnet.infn.it/en/who-we-are-2/>
- [18] C. Ruberto, A. Mazzinghi, M. Massi, L. Castelli, C. Czelusniak, L. Palla, N. Gelli, M. Bettuzzi, A. Impallaria, R. Brancaccio, E. Peccenini, M. Raffaelli, Imaging study of Raffaello's "La Muta" by a portable XRF spectrometer, *Microchemical Journal*, 2016, Volume 126, pp. 63-69.  
DOI: [10.1016/j.microc.2015.11.037](https://doi.org/10.1016/j.microc.2015.11.037)
- [19] M. Vadrucchi, A. Mazzinghi, B. Sorrentino, S. Falzone, Characterisation of ancient Roman wall-painting fragments using

- non-destructive IBA and MA-XRF techniques, X-Ray Spectrom. 2020; 49: pp. 668–678.  
DOI: [10.1002/xrs.3178](https://doi.org/10.1002/xrs.3178)
- [20] A. Dal Fovo, A. Mazzinghi, S. Omarini, E. Pampaloni, C. Ruberto, J. Striova, R. Fontana, Non-invasive mapping methods for pigments analysis of Roman mural paintings, *Journal of Cultural Heritage*, Volume 43, 2020, pp. 311-318.  
DOI: [10.1016/j.culher.2019.12.002](https://doi.org/10.1016/j.culher.2019.12.002)
- [21] A. Mazzinghi, C. Ruberto, L. Castelli, C. Czelusniak, L. Giuntini, P. A. Mandò, F. Taccetti, MA-XRF for the Characterisation of the Painting Materials and Technique of the Entombment of Christ by Rogier van der Weyden, *Applied Sciences*, 2021; 11(13):6151.  
DOI: [10.3390/app11136151](https://doi.org/10.3390/app11136151)
- [22] A. Mazzinghi, C. Ruberto, L. Castelli, P. Ricciardi, C. Czelusniak, L. Giuntini, P. A. Mandò, M. Manetti, L. Palla, F. Taccetti, The importance of being little: MA-XRF on manuscripts on a Venetian island, *X-Ray Spectrom*, 2020; pp. 1–7.  
DOI: [10.1002/xrs.3181](https://doi.org/10.1002/xrs.3181)
- [23] V. Lazić, M. Vadrucchi, F. Fantoni, M. Chiari, A. Mazzinghi, A. Gorghinian, Applications of laser-induced breakdown spectroscopy for cultural heritage: A comparison with X-ray Fluorescence and Particle Induced X-ray Emission techniques, *Spectrochimica Acta Part B: Atomic Spectroscopy*, Volume 149, 2018, pp. 1-14.  
DOI: [10.1016/j.sab.2018.07.012](https://doi.org/10.1016/j.sab.2018.07.012)
- [24] S. M. E. Mangani, A. Mazzinghi, P. A. Mandò, S. Legnaioli, M. Chiari, Characterisation of decoration and glazing materials of late 19th-early 20th century French porcelain and fine earthenware enamels: a preliminary non-invasive study, *Eur. Phys. J. Plus*, 2021, 136 (10).  
DOI: [10.1140/epip/s13360-021-02055-x](https://doi.org/10.1140/epip/s13360-021-02055-x)
- [25] L. Sottili, L. Guidorzi, A. Mazzinghi, C. Ruberto, L. Castelli, C. Czelusniak, L. Giuntini, M. Massi, F. Taccetti, M. Nervo, S. De Blasi, R. Torres, F. Arneodo, A. Re, A. Lo Giudice, The Importance of Being Versatile: INFN-CHNet MA-XRF Scanner on Furniture at the CCR “La Venaria Reale”, *Applied Sciences* 2021;11(3):1197.  
DOI: [10.3390/app11031197](https://doi.org/10.3390/app11031197)
- [26] L. Vigorelli; A. Lo Giudice.; T. Cavaleri.; P. Buscaglia; M. Nervo; P. Del Vesco; M. Borla; S. Grassini, A. Re, Upgrade of the x-ray imaging set-up at CCR “La Venaria Reale”: the case study of an Egyptian wooden statuette, *Proceedings of 2020 IMEKO TC4 International Conference on Metrology for Archaeology and Cultural Heritage*, Trento, Italy, October 22-24, 2020. Online [Accessed 11 March 2022]  
<https://www.imeko.org/publications/tc4-Archaeo-2020/IMEKO-TC4-MetroArchaeo2020-118.pdf>
- [27] A. Re, M. Zangirolami, D. Angelici, A. Borghi, E. Costa, R. Giustetto, L.M. Gallo, L. Castelli, A. Mazzinghi, C. Ruberto, F. Taccetti, A. Lo Giudice, Towards a portable X-Ray Luminescence instrument for applications in the Cultural Heritage field, *Eur. Phys. J. Plus*, 2018, pp. 133-362.  
DOI: [10.1140/epip/i2018-12222-8](https://doi.org/10.1140/epip/i2018-12222-8)
- [28] L. Sottili, L. Guidorzi, A. Mazzinghi, C. Ruberto, L. Castelli, C. Czelusniak, L. Giuntini, M. Massi, F. Taccetti, M. Nervo, A. Re, A. Lo Giudice, INFN-CHNet meets CCR La Venaria Reale: first results, 2020 IMEKO TC4 International Conference on Metrology for Archaeology and Cultural Heritage 2020, 2020, pp. 507-511. Online [Accessed 11 March 2022]  
<https://www.imeko.org/publications/tc4-Archaeo-2020/IMEKO-TC4-MetroArchaeo2020-096.pdf>
- [29] D. Dutto, La Madonna di San Rocco di Francesco Sparapane: problemi conservativi e intervento di restauro di un dipinto su tavola del XVI secolo proveniente dalla Valnerina, MSc Thesis, Master's Degree Programme in Conservation and Restoration for cultural heritage, University of Torino, Torino, 2018
- [30] E. Nicholas, *Pigment Compendium: A Dictionary of Historical Pigments*, Amsterdam: Butterworth-Heinemann (editor), 2008.
- [31] *Artists' Pigments: A Handbook of Their History and Characteristics*, Vol. 2, editor Ashok Roy, National Gallery of Art, Washington Archetype Publications, London, 1993
- [32] C. Seccaroni, P. Moiola, *Fluorescenza X- Prontuario per l'analisi XRF portatile applicata a superfici policrome*, Nardini Editore; Firenze, 2002.
- [33] R. J. Gettens, R. L. Feller, W. T. Chase, Vermilion and Cinnabar, *Studies in Conservation* 17, no. 2, 1972, 45-69.  
DOI: [10.2307/1505572](https://doi.org/10.2307/1505572)
- [34] *Artists' Pigments: A Handbook of Their History and Characteristics*, Vol. 4, editor B. H. Berrie, National Gallery of Art, Washington Archetype Publications, London, 2007
- [35] M. Spring, R. Grout, R. White, 'Black Earths': A Study of Unusual Black and Dark Grey Pigments Used by Artists in the Sixteenth Century, *National Gallery Technical Bulletin*, 2003, 24, pp. 96–114. Online [Accessed 11 March 2022]  
<https://www.jstor.org/stable/42616306>
- [36] I. C. A. Sandu, L. U. Afonso, E. Murta, M. H. De Sa, Gilding techniques in religious art between east and west, 14th -18th centuries, *Int. J. of Conserv. Sci.* 1 (2010) pp. 47-62 .
- [37] B. H. Berrie, Mining for Color: New Blues, Yellows, and Translucent Paint, *Early Science and Medicine*, Volume 20: Issue 4-6, 2015, 308–334.  
DOI: [10.1163/15733823-02046p02](https://doi.org/10.1163/15733823-02046p02)
- [38] F. Erbetta, Restaurare dopo il terremoto: il dipinto olio su tela Madonna con bambino e santi del Pomarancio dalla chiesa di Santa Maria Argentea di Norcia, MSc Thesis, Master's Degree Programme in Conservation and Restoration for cultural heritage, University of Torino, Torino, 2018
- [39] J. Kirby, D. Saunders, Fading and colour change of Prussian blue: methods of manufacture and the influence of extenders, *Natl Gallery Tech Bull.* 2004, 25: 73-99.
- [40] G. Corrada, Studio interdisciplinare del dipinto a tempera magra su tela Madonna con bambino e i santi Crescentino e Donnino, Timoteo Viti, MSc Thesis, Master's Degree Programme in Conservation and Restoration for cultural heritage, University of Torino, Torino, 2013
- [41] S. Rinaldi, *La fabbrica dei colori: pigmenti e coloranti nella pittura e nella tintoria*, Roma, Il bagatto, 1986
- [42] L. Guidorzi, F. Fantino, E. Durisi, M. Ferrero, A. Re, L. Vigorelli, L. Visca, M. Gulmini, G. Dughera, G. Giraud, D. Angelici, E. Panero, A. Lo Giudice, Age determination and authentication of ceramics: advancements in the thermoluminescence dating laboratory in Torino (Italy), *Acta IMEKO*, vol 10 (2021), no 1, pp. 32-36.  
DOI: [10.21014/acta\\_imeko.v10i1.813](https://doi.org/10.21014/acta_imeko.v10i1.813)
- [43] E. Di Francia, S. Grassini, G. Ettore Gigante, S. Ridolfi, S. A. Barcellos Lins, Characterisation of corrosion products on copper-based artefacts: potential of MA-XRF measurements of MA-XRF measurement, *Acta IMEKO*, vol 10 (2021), no 1, pp. 136-141.  
DOI: [10.21014/acta\\_imeko.v10i1.859](https://doi.org/10.21014/acta_imeko.v10i1.859)
- [44] A. Impallaria, F. Evangelisti, F. Petrucci, F. Tisato, L. Castelli, F. Taccetti, A new scanner for in situ digital radiography of paintings, *Applied Physics A*, 122, 12, 2016.  
DOI: [10.1007/s00339-016-0579-5](https://doi.org/10.1007/s00339-016-0579-5)
- [45] C. Czelusniak, L. Palla, M. Massi, L. Carraresi, L. Giuntini, A. Re, A. Lo Giudice., G. Pratesi, A. Mazzinghi, C. Ruberto, L. Castelli, M. E. Fedi, L. Liccioli, A. Gueli, P. A. Mandò, F. Taccetti, Preliminary results on time-resolved ion beam induced luminescence applied to the provenance study of lapis lazuli, *Nucl. Instrum. Methods Phys. Res. B* 2016, 371, 336–339.  
DOI: [10.1016/j.nimb.2015.10.053](https://doi.org/10.1016/j.nimb.2015.10.053)
- [46] L. Palla., C. Czelusniak., F. Taccetti, L. Carraresi, L. Castelli, M. E. Fedi, L. Giuntini, P. R. Maurenzig, L. Sottili., N. Taccetti, Accurate on line measurements of low fluences of charged particles, *Eur. Phys. J. Plus* 2015, 130.  
DOI: [10.1140/epip/i2015-15039-y](https://doi.org/10.1140/epip/i2015-15039-y)

Review

# The Role of PIXE and XRF in Heritage Science: The INFN-CHNet LABEC Experience

Leandro Sottili <sup>1,2</sup>, Lorenzo Giuntini <sup>3,4,\*</sup> , Anna Mazzinghi <sup>3,4,\*</sup> , Mirko Massi <sup>4</sup> , Luca Carraresi <sup>3,4</sup>, Lisa Castelli <sup>4</sup>, Caroline Czelusniak <sup>4</sup>, Francesca Giambi <sup>4</sup> , Pier Andrea Mandò <sup>3,4</sup>, Marco Manetti <sup>4</sup>, Chiara Ruberto <sup>3,4</sup>, Laura Guidorzi <sup>2</sup>, Alessandro Re <sup>1,2</sup> , Alessandro Lo Giudice <sup>1,2</sup>, Rodrigo Torres <sup>5</sup>, Francesco Arneodo <sup>5</sup> , Simi Maria Emilia Mangani <sup>6</sup> , Silvia Calusi <sup>7</sup> and Francesco Taccetti <sup>4</sup>

- <sup>1</sup> Dipartimento di Fisica, Università degli Studi di Torino, Via Pietro Giuria 1, 10125 Torino, Italy; leandro.sottili@unito.it (L.S.); alessandro.re@unito.it (A.R.); alessandro.logiudice@unito.it (A.L.G.)
  - <sup>2</sup> Istituto Nazionale di Fisica Nucleare (INFN), Sezione di Torino, Via Pietro Giuria 1, 10125 Torino, Italy; guidorzi@to.infn.it
  - <sup>3</sup> Dipartimento di Fisica e Astronomia, Università degli Studi di Firenze, Via Giovanni Sansone 1, Sesto Fiorentino, 50019 Firenze, Italy; carraresi@fi.infn.it (L.C.); mando@fi.infn.it (P.A.M.); ruberto@fi.infn.it (C.R.)
  - <sup>4</sup> Istituto Nazionale di Fisica Nucleare (INFN), Sezione di Firenze, Via Giovanni Sansone 1, Sesto Fiorentino, 50019 Firenze, Italy; massi@fi.infn.it (M.M.); castelli@fi.infn.it (L.C.); czelusniak@fi.infn.it (C.C.); giambi@fi.infn.it (F.G.); manetti@fi.infn.it (M.M.); taccetti@fi.infn.it (F.T.)
  - <sup>5</sup> Division of Science, New York University Abu Dhabi, Saadiyat Island, Abu Dhabi 129188, United Arab Emirates; rodrigo.torres@nyu.edu (R.T.); francesco.arneodo@nyu.edu (F.A.)
  - <sup>6</sup> Dipartimento di Chimica “Ugo Schiff”, Università degli Studi di Firenze, Via della Lastruccia, 3, Sesto Fiorentino, 50019 Firenze, Italy; simimariaemilia.mangani@unifi.it
  - <sup>7</sup> Dipartimento di Scienze Biomediche Sperimentali e Cliniche “Mario Serio”, Università degli Studi di Firenze, Viale Pieraccini 6, 50139 Firenze, Italy; silvia.calusi@unifi.it
- \* Correspondence: giuntini@fi.infn.it (L.G.); mazzinghi@fi.infn.it (A.M.)



**Citation:** Sottili, L.; Giuntini, L.; Mazzinghi, A.; Massi, M.; Carraresi, L.; Castelli, L.; Czelusniak, C.; Giambi, F.; Mandò, P.A.; Manetti, M.; et al. The Role of PIXE and XRF in Heritage Science: The INFN-CHNet LABEC Experience. *Appl. Sci.* **2022**, *12*, 6585. <https://doi.org/10.3390/app12136585>

Academic Editor: Asterios Bakolas

Received: 29 May 2022

Accepted: 26 June 2022

Published: 29 June 2022

**Publisher's Note:** MDPI stays neutral with regard to jurisdictional claims in published maps and institutional affiliations.



**Copyright:** © 2022 by the authors. Licensee MDPI, Basel, Switzerland. This article is an open access article distributed under the terms and conditions of the Creative Commons Attribution (CC BY) license (<https://creativecommons.org/licenses/by/4.0/>).

**Abstract:** Analytical techniques play a fundamental role in heritage science. Among them, Particle Induced X-ray Emission (PIXE) and X-ray Fluorescence (XRF) techniques are widely used in many laboratories for elemental composition analysis. Although they are well-established, a strong effort is put on their upgrade, making them suitable for more and more applications. Over the years, at the INFN-LABEC (the laboratory of nuclear techniques for the environment and cultural heritage of the Italian National Institute of Nuclear Physics), the INFN-CHNet group, the network devoted to cultural heritage, has carried out many technological improvements to the PIXE and XRF setups for the analysis of works of art and archaeological finds. Among the many, we recall here the scanning external microbeam facility at the TANDEM accelerator and the MA-XRF scanner. The two instruments have shown complementary features: the former permits quantitative analysis of elements heavier than sodium, which is not possible with the latter in most of the case studies. On the contrary, the scanner has the undeniable advantage of portability, allowing it to work in situ. In this framework of technological developments in heritage science, INFN, CERN, and OPD are jointly carrying on the MACHINA (Movable Accelerator for Cultural Heritage In-situ Non-destructive Analysis) project for on-site Ion Beam Analysis (IBA) studies on cultural heritage.

**Keywords:** PIXE; MA-XRF; IBA; material analysis; heritage science

## 1. Introduction

IBA activities related to fundamental physics and other disciplines have been carried out at the INFN-LABEC since its foundation in 2004. Tests of detectors for nuclear and particle physics [1–3], studies of ion-matter interaction for solid state physics [4] and compositional measurements for heritage science (HS) [5], and environmental aerosol science [6] are just some examples of the diverse applications. Those activities have been conducted

thanks to the six beamlines of the TANDETRON accelerator: the external beamline for aerosol measurements [7]; the external microbeam line [8]; the pulsed beamline [9,10]; the ion beam analysis beamline in vacuum [11]; the external beamline for cultural heritage measurements; and the atomic mass spectrometry beamline for  $^{14}\text{C}$  dating [12]. Reviews on past and current activities at the INFN-LABEC are found in [13,14].

On the other side, especially in the field of HS, the possibility of performing measurements on site is more and more required due to the problems of transporting a work of art and the invaluable support of analytical techniques. For this reason, in 2011, a transportable XRF device was developed. Moreover, thanks to the expertise within the INFN-CHNet group, in the last ten years, a constant effort has been put in R&D for cultural heritage applications [15,16]; therefore, several instruments have been developed and others are presently in progress.

In this review, after a brief recall of the PIXE and XRF techniques, salient aspects of the dedicated facilities (XRF device and microbeam facility) at the INFN-LABEC laboratory are presented towards several applications. The INFN-CHNet MA-XRF scanner, a transportable device capable of mapping non-planar surfaces, is then described. The article closes with an introduction of the MACHINA project, for the development of the first transportable accelerator for IBA inside conservation centres and museums.

## 2. Brief Overview of the Particle Induced X-ray Emission and X-ray Fluorescence Techniques

PIXE and XRF techniques have in common the emission of X-rays equal in energy to the difference between atomic shells. In the first, the probes are ions, typically few MeV protons provided by an accelerator, whereas in the latter they are X-rays, indicated as primary X-rays, and are provided by synchrotrons, radioactive sources, or X-ray tubes [17].

Due to the specific energy levels of each atomic species, X-rays emitted from a target are characteristic of the impinged atoms; therefore, different elements can be simultaneously identified, acquiring an X-ray spectrum. It is worth mentioning that elements lighter than sodium cannot be normally detected with those techniques because of the absorption of low energy X-rays between their emission and their detection [18]. Therefore, they are best-suited for detecting pigments made of medium/high Z elements. Some examples can be cinnabar, lead white, lead-tin yellow, and bismuth black. On the contrary, other techniques, such as FORS (Fiber Optics Reflectance Spectroscopy) and RAMAN spectroscopy may also be used for detecting organic pigments or dyes and may be successfully used in combination for a comprehensive analysis of the materials [19].

To overcome this limitation of PIXE, it is used in combination with other IBA techniques that may provide complementary information on lighter elements as Particle Induced Gamma-ray Emission (PIGE) [20] and on stratigraphy such as Rutherford Backscattering (RBS) [21].

Both PIXE and XRF analysis are non-destructive (or not deliberately destructive in the case of PIXE) and non-invasive multi-analytical techniques and are therefore largely in use in HS. An important difference between them is the penetration depths of primary probes. In XRF spectroscopy, in typical conditions, due to the radiation matter interaction, the probed depth is much bigger than in PIXE. Just to give an example, the range of a 3 MeV proton beam in a carbon matrix (somehow simulating light organic medium) is about 74  $\mu\text{m}$ . Conversely, 20 keV X-rays (half of the maximum energy of the typical X-ray beams used at INFN-LABEC, where beam intensity is still quite high, see e.g., [22]), through the same carbon thickness, have a 100% transmission factor, which slowly decreases down to 92% for a 740  $\mu\text{m}$  slab and to 48% for 7.4 mm (from [23], see also [24] for a comparison of PIXE and XRF probed depth in the study of metal samples).

Therefore, roughly, PIXE analysis can be considered a surface technique, or in a way more superficial than XRF, although it depends on the energy of the X-ray considered [25].

Another crucial difference is the quantitative analysis that can be carried out with PIXE technique, and it is not typically possible with XRF analysis in HS [26]. Experimental aspects of the PIXE and XRF techniques are reported in [27].

Both techniques are largely in use in many laboratories [28–31] and, recently, they were combined in a single facility [32].

### 3. PIXE: From Point Analysis to Elemental Maps: An Example

At the INFN-LABEC, the PIXE technique was employed for many works of art. One of the earliest case studies was the study of the inks of Galileo's handwritten letters, for determining their chronological order by studying their elemental composition [33,34].

One of the works of art, presented here, is a parchment, a bifolio originally belonging to an antiphonary. It contains a musical notation composed of a system of six tetragrams on each page, with neumes and the text of the chant. It is decorated with calligraphic initials and a figured illuminated letter. Details of the irradiated areas are presented in Figure 1. Measurements were carried out to characterise the elemental composition of the pigments of the inks.



Figure 1. Areas in which PIXE measurements were performed.

At the time, the X-rays emitted were detected by two Si(Li) detectors, whose absorbers and whose distances from the sample were chosen so that one was primarily sensitive to elements lighter than  $Z = 25$  and the other to heavier elements. Helium flux was continuously flown in front of the measuring set-up for minimising the argon K-lines production from the atmosphere and to reduce the absorption of low energy X-rays.

The proton current was of the order of a few hundred pA and the energy around 3 MeV; typical acquisition time ranged from a few seconds to a few minutes, with no risk of damaging the target. The proton beam intensity was monitored by rotating a stage with a thin nickel surface layer regularly through the beam and measuring the nickel K X-rays.

For what concerns the pigments, blue and red areas were characterised by the presence of copper and mercury, respectively, suggesting the use of azurite [35], and of cinnabar/vermilion [36].

The PIXE spectra of the yellow areas showed the presence of tin, lead, and a significant amount of silicon. After correcting for self-absorption of X-rays within the paint layer, the measured atomic ratio Pb:Sn:Si approximates to 1:0–25:0–65, a result that suggests the presence of lead-tin yellow of type II,  $Pb(Sn, Si)O_3$ . This result allows an indirect dating of the miniature since, from studies of lead-tin yellow samples from Italian paintings of the fourteenth and fifteenth centuries, the transition from the use of type II to type I ( $Pb_2SnO_4$ ) had taken place in Italy around the second quarter of the fifteenth century, as stated in [37].

The atomic ratio of lead-tin yellow detected here is compatible with type II. Therefore, determining which of these was used may indicate, in a non-destructive and non-invasive way, a *terminus ante quem* the miniature was painted.

Green areas showed the presence of copper, lead, tin, and silicon. The Pb:Sn ratio is the same as that in yellow areas. This result led to the hypothesis that green was obtained by mixing lead-tin yellow and a copper-based pigment, such as blue azurite or green malachite [35]. Further information on this study is included in [38].

An improvement for scanning an area of the target was achieved using two motor stages (Micos KR-33) and a home-made software for the acquisition. The system was based on continuous motion of the target in the plane perpendicular to the beam direction designed and developed for the beamline, as presented in Figure 2. Furthermore, a software for the analysis was developed in-home. The spatial distribution of the elements in an area of a few cm<sup>2</sup> was obtained by recording the spectra for each position and selecting the corresponding energy peaks.



**Figure 2.** Scanning system at the end of the PIXE beamline.

The spiral was the scanning mode used since it brings some fundamental advantages. There is no periodical sharp direction change that would impose high acceleration to the sample as in each strip of a raster scan, and the time spent by the beam on each position is rather uniform. The motors complete the first spiral anticlockwise, then stop and retrace the same trajectory clockwise, returning to the initial position. The whole path is inserted in a loop.

Here a blue penwork initial of the same parchment is reported. The aim is to evaluate the spatial resolution of the scan. To do this, the red decoration was analysed with a proton



beam diameter of 0.2 mm. The proton energy was set to 3 MeV and the beam current to few pA. The whole scan lasted about 20 min.

As can be seen in Figure 3, the blue area is realised with a copper-based pigment, most likely azurite [35], whereas the red scrolling pattern is made with an Hg-based compound as cinnabar [36]. The pattern is rather well resolved, despite some local non-homogeneity of the red lines, probably due to the variability of the red ink thickness.

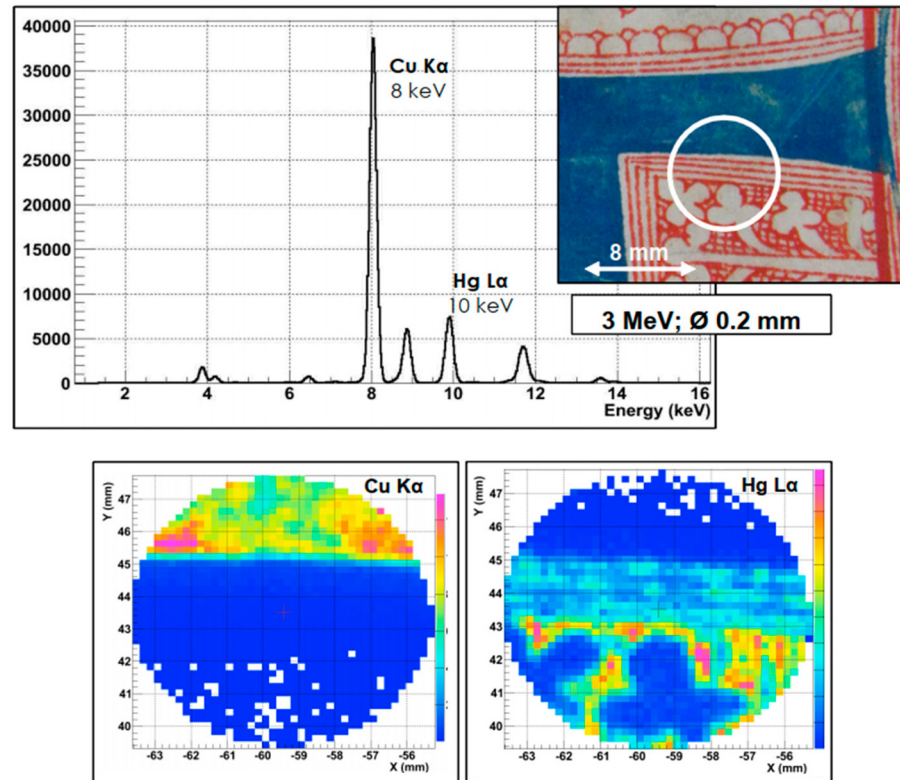


**Figure 3.** PIXE spectrum of the area around a letter and elemental maps of Cu and Hg.

As will be explained in the next section this is, in practice, the lower limit of the spatial resolution achievable by means of mechanical collimation; otherwise, a microbeam facility needs to be used.

It is worth mentioning that in recent years, the Si(Li) detectors have been replaced by Silicon drift detectors [39]. Their higher efficiency due to the higher solid angle they cover in the set-up, together with their higher energy resolution, and the higher sustainable counting rate, lowers the detection limits, even for shorter measurement times [40].

#### 4. Technological Advance: The Micro-PIXE Technique at the INFN-LABEC

The capability to produce ion beams with size lower than 100  $\mu\text{m}$ , known as microbeams, has been a natural development of PIXE technique. This is of great importance for samples with microstructures such as biological tissues, geological materials, micro-electronic devices, or small specimens such as cultured individual cells, microcrystals, and single aerosol particles.

The simplest way of producing a small beam spot is clearly to use a very fine collimator to select a portion of the beam, as in the case of Section 3. However, this method presents several drawbacks, the most evident of which is a strong reduction of beam intensity. A second important problem arises because the X-ray detectors' background increases due the interactions of the stopped beam particles in the collimator bulk. As the collimator aperture is reduced, the stopped beam fraction increases and so the originated background can become unacceptable. In addition, the power dissipated by the stopped beam can noticeably heat the collimator, thus changing its geometrical properties and making the

beam size reduction unreliable (especially for very small aperture). Furthermore, the large number of particles hitting the collimator can rapidly deteriorate the aperture edges compromising the quality of the transmitted beam.

However, as a consequence of particle scattering in the aperture, the beam acquires a divergence passing the collimator, one consequence of which is the formation, at a certain distance from the collimator exit, of a scattered beam halo, the size of which depends on the distance from the collimator. As the aperture radius is reduced, the ratio of halo intensity to transmitted beam intensity increases, so that the final effective beam spot size can be much larger than the aperture dimension. Therefore, it is possible to have a fine beam only very close to the collimator, which implies that the distance between sample and collimator should be very short, and this can result in a serious limitation in setting up the detectors.

An ion beam focusing system typically allows overcoming the above mentioned problems with collimated beams. The idea was proposed in 1972 [41] and it is now at the basis of almost all ion microprobes currently in use. Moreover, the scanning ability, which allows for mapping spatial distribution of the sample elements, was planned to be used. There are two approaches for scanning an area of the sample: sweeping the beam over a static target or moving the target relative to a fixed beam.

Sweeping the beam by electrostatic or magnetic deflection has the advantage that the mechanical design of the target holder is much simplified. In addition, the response time of a swept beam is usually faster than the one of a mechanical stage. When larger areas have to be scanned, the alternative approach is that of sweeping the target under a fixed beam. This also has, in principle, the advantage that the resolution of the beam is not degraded by a worsening of the focusing system; in practice, repeatable mechanical movements are not trivial to achieve to the degree of accuracy implied by the use of a high spatial resolution beam. This method therefore requires careful design and construction, and is much slower than deflecting the beam over the sample using electrostatic or magnetic dipole fields. In addition, the long time required for a mechanical full scan can result in artefacts in elemental maps if long-term beam intensity fluctuations are present and beam charge normalisation is not carried out in every analysed point.

In the scanning system of the microbeam facility at the INFN-LABEC, the beam was swept over the target in horizontal and vertical directions by a magnetic field, perpendicular to the beam direction, generated by ferrite-cored coils positioned immediately before the lens. The magnetic deflector coils allowed, in principle, a maximum scanned area of several mm<sup>2</sup> for 3 MeV protons but was, however, limited by the exit window aperture (2 × 2 mm<sup>2</sup>, typically).

Furthermore, the facility was developed for exploiting and combining the advantages of the two scanning modes, magnetic and mechanical. The magnetic scanning allowed for collecting elemental maps in times faster than the mechanical scanning but within an area limited to ~1 × 1 mm<sup>2</sup> by the beam exit window size, whereas the travel range of the motorised stages permitted the possibility to analyse an area on the sample surface up to 25 × 25 mm<sup>2</sup>. Depending on the case study and on the query, one or both systems could be used.

The number of the beam particles impinging in each point was indirectly measured by counting the number of Si X-rays produced by the beam in the exit window and was used to normalise X-ray yield during measurements. As results from an extensive series of tests, for a given window, the emitted X-rays from the exit window to the collected charge ratio kept constant within 1%, varying the current of two orders of magnitude, from about 10 nA down to about 100 pA.

A summary of the results of the beam profile characteristics, in air or in a helium atmosphere, is shown in Table 1. The effect of the width of the grid bar (10 µm), used for the measurements, on the profiles is already taken into account [42].

**Table 1.** Experimental FWHM of lateral microbeam profiles measured after traversing 2 mm in different atmospheres.

Atmosphere	FWHM X × Y (μm × μm)
Vacuum	~7 × 5
Helium	~9 × 8
Air	~15 × 15

Among the different applications, this beamline was used to analyse lapis lazuli [43,44], a blue semi-precious stone used for more than 7000 years for carved jewels, decorative objects, as well for pigments. This study, besides increasing the knowledge on this blue rock, could shed light on many unresolved questions, especially regarding the trade routes exploited in ancient times.

For those measurements, both μ-PIXE and μ-IBIL (micro-Ion Beam Luminescence) techniques were performed. They allow for analysing single crystals of different mineral phases, a fundamental aspect in a heterogeneous material as lapis lazuli, and they are non-invasive, a necessary feature since it is impossible to take samples from artworks. In this study, different markers were found and proposed to distinguish among the four possible provenances: Afghanistan (Badakhshan), Tajikistan (Pamir Mountains), Siberia (near Lake Baikal), and Chile (Ovalle) [45].

For example, the presence of diopside ( $\text{CaMgSi}_2\text{O}_6$ ) or wollastonite ( $\text{CaSiO}_3$ ) was studied as a potential marker for the Chilean provenance. The presence of wollastonite, due to the double band at 560 and 620 nm, is a clear indication of the Chilean provenance, quickly distinguishable even only by means of luminescence with this set-up. Instead, diopside shows its main IBIL signal band at 585 nm.

As an example of application, six objects of the *Collezione Medicea* carved in lapis lazuli were studied in order to obtain some indications about the provenance of the raw material used for their execution [45]. The absence of wollastonite allowed excluding the Chilean provenance for all the lapis lazuli in these artworks, whereas diopside was detected. Moreover, μ-PIXE results obtained for diopside crystals of these samples show that the titanium, vanadium, and chromium amount are comparable with that in the Afghan rock samples of certain provenance [46].

Further information about the micro-beam line at INFN-LABEC and additional results can be found in [47,48].

## 5. XRF: From Point Analysis to Elemental Maps with Portable Equipment

The main limit of the PIXE and the other IBA techniques is the lack of portability, a feature that is a severe limitation when a work of art cannot be moved to a laboratory. The XRF technique preserves non-invasive, non-destructive, and multi-elemental characteristics; moreover, it exploits portable instrumentation. For this reason, it is one of the most widely used techniques for material analysis in the field of cultural heritage. Its main drawback is a much lower sensitivity than PIXE to light elements [49] and the limited possibility of a quantitative analysis in HS [26].

At INFN-LABEC, a portable XRF spectrometer was designed and assembled, exploiting the experience acquired over the years with X-ray spectroscopy using ion beams. In this device, different tubes (Mo, Ti and W anodes available) were used for maximising the efficiency of the production of X-rays over a wide range of energies, as it depends on the main emission lines of the anode material. In addition, since any source emits its own X-rays, and they can hide X-rays emitted by the sample in spectra, the combination of more tubes with different materials limits this effect. For example, the M-lines of Molybdenum at 2.3 keV overlap with the sulphur, whereas the K-lines of Ti (4.5 keV and 4.9 keV) overlap with the L-lines of Barium; therefore, for detecting sulphur, the Ti anode is preferable to Mo, and vice-versa for detecting titanium.

The detector installed was an SDD by Ketek GmbH with an energy resolution of 139 eV at the Mn  $K\alpha$  line. The electronic chain was also supplied by Ketek GmbH and was

assembled on the top of the detector case. The entrance window (8  $\mu\text{m}$  thick in beryllium) was located at about 20 mm from the measuring point. Despite the collimation and the quite large distance between tubes and target, the X-ray rate on the detector was satisfactory with current values around 0.3 mA, thanks to the limited target-detector distance. Furthermore, a continuous helium flow in front of the tubes and the detector enhanced the production and detection of low-energy X-rays. The angle between the tubes was reduced as much as possible, to minimise the difference of the two irradiated volumes.

During the measurements, the positioning of the measuring head was obtained through the superposition, on the target surface, of the spots of two appropriately aimed lasers. The measuring area was continuously monitored through a camera. The instrument is presented in Figure 4.

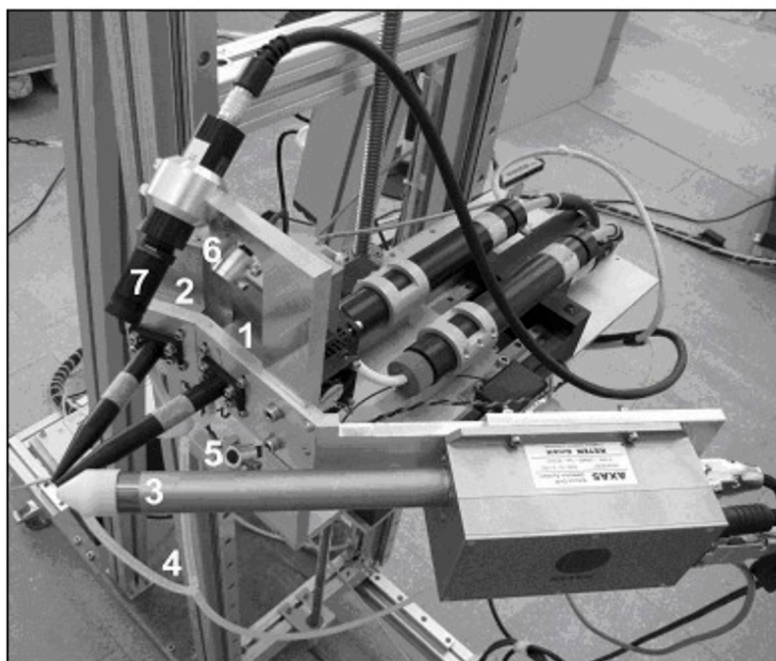


**Figure 4.** Picture of the measuring head: X-ray tubes (1,2); SDD detector (3); pipe for helium flow (4); lasers (5,6); camera (7).

Among the many applications, see for example [50,51]. This instrument was also successfully employed for the discrimination between polishing methods of Japanese swords, or “katanas”.

Katanas have the high features of hardness and elasticity of steel and require a long polishing process traditionally carried out with a layer of clay mixed with charcoal after forging. Polishing of the blade can be repeated for maintenance during their life. A fast method to visually imitate a traditional polishing process is to use an acid bath to mimic the aspect of the undamaged blade but, in spite of a good appearance, the martensitic structure of the sword becomes severely damaged. It is worth noting that on the market their price can vary from a few k€ for a damaged blade to tens of k€ for a well-preserved one. Thus, a doable way to analytically distinguish the two methods is to detect silicon traces left by the stone-based traditional polishing method.

For the study, a set of katanas, both damaged and well-conserved, from the Stibbert Museum of Florence, were analysed, exploiting the XRF spectrometer. The measurements were conducted with Mo anode at 9 kV and 25 kV anode voltages. As can be seen from Figure 5, the silicon peak is present in the blade conserved with traditional methods, whereas the other does not show any evidence of the presence of silicon.

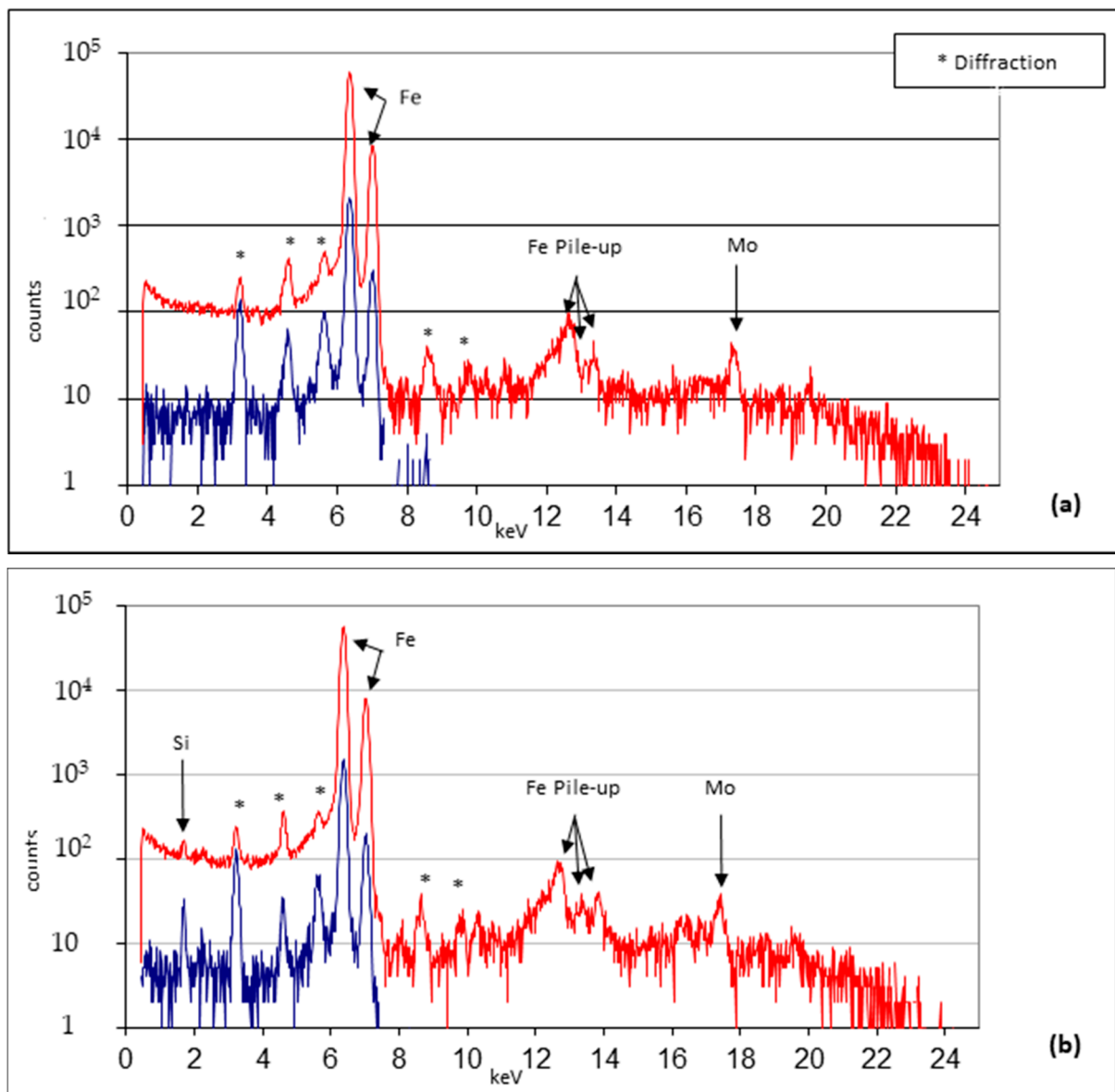


**Figure 5.** Spectra of a katana treated with acid (a) and of a well-polished katana (b). Two anode voltages (9 kV in blue and 25 kV in red) were used for each measuring point.

The measurements were conducted on a set of 13 katanas, confirming the goodness of this method to distinguish between the two groups of katanas. Further information is available in the publication [52].

**6. Comparison between PIXE and XRF Techniques at the INFN-LABEC**

As a practical example, here, the same area of the parchment irradiated at the PIXE beamline described in Section 3 is reported and with the XRF spectrometer presented in Section 5. The scan was conducted with the motor system shown in Figure 2. Experimental parameters are reported in Table 2 and the areas measured are presented in Figure 6.

**Table 2.** Experimental parameters of PIXE and XRF techniques.

Technique	Probe	Energy	Current	Diameter
PIXE	Proton beam	4 MeV	tens of pA	0.5 mm
XRF	X-rays Mo anodes 114	26 keV max.	0.8 mA	0.5 mm

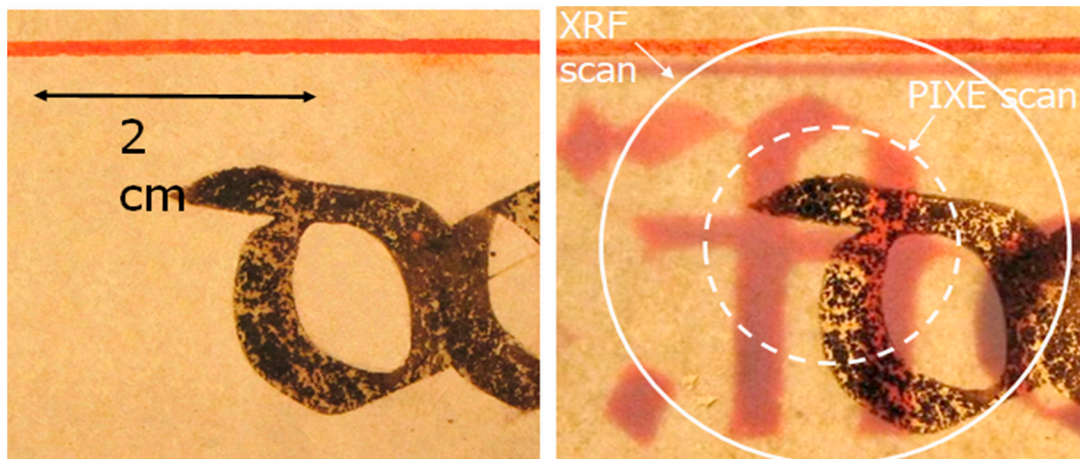


**Figure 6.** The area irradiated by PIXE and XRF. The backlit image shows the presence of the backside.

As can be seen from the backlit picture (Figure 6), lyrics are present on the backside of the bifolio.

Results of the irradiation are presented in Figures 7 and 8. As can be seen from Figure 7, with XRF it is possible to detect the ink from the two sides of the parchment, both iron from the front side (Figure 7, left) and mercury (Figure 7, right).

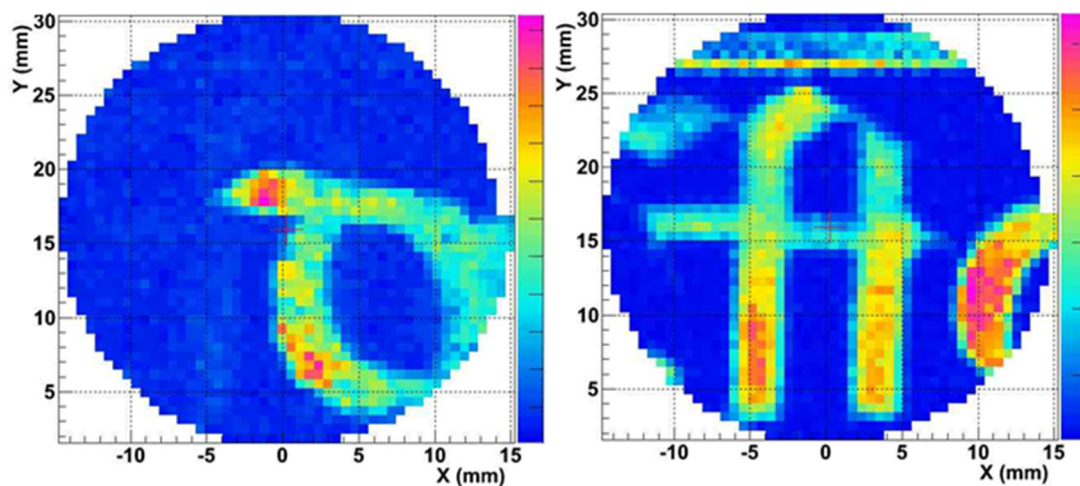


**Figure 7.** Maps of Fe (left) and mercury (right) of the area scanned in Figure 6 by XRF technique.

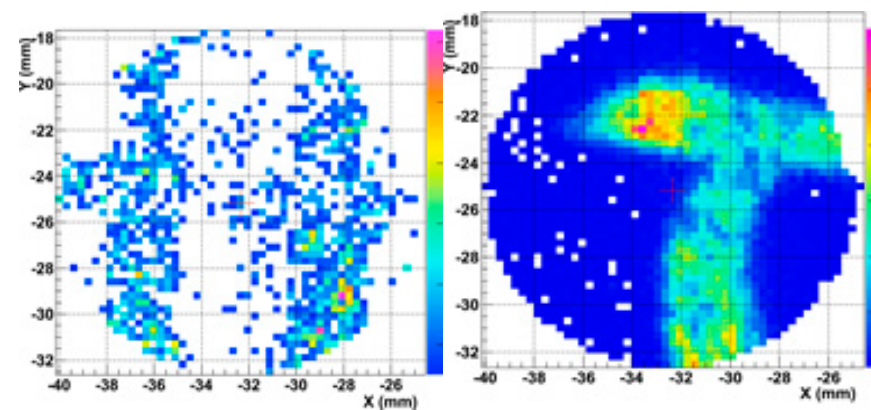


**Figure 8.** Maps of Fe (left) and mercury (right) of the area scanned in Figure 6 by PIXE technique.

On the contrary, with the PIXE technique, only the ink on the front side was clearly detected, whereas the letter on the other side is not clearly visible from the map of mercury.

This result is a consequence of the higher penetration depth of XRF in comparison with PIXE. This can be considered an example of the advantage of matching the two techniques; indeed, the detection of the materials on the verso of the folio together with those on the recto may complicate the reading. On the other hand, two materials can be detected with only one measurement (easily distinguishable thanks to the mapping methods) and, moreover, the eventual interaction with these materials may be observed.

## 7. Technological Advances: INFN-CHNet MA-XRF Scanner

As for the PIXE technique, a natural development of the XRF technique is to allow scanning without disclaiming the portability of the device. With this aim, within the INFN-CHNet group, a MA-XRF scanner was designed with a special focus on portability and lightness. The technical characteristics and analytical capabilities (detection efficiency, spatial resolution, etc.) of this equipment are thoroughly described in [53], and only the main characteristics are reported here. The measuring head of the instrument is composed of an X-ray tube by Moxtek (40 kV maximum voltage, 0.1 mA maximum anode current) and an SDD detector by Amptek (XR100 SDD, 25 mm<sup>2</sup> effective active surface, 500 µm thickness). A telemeter by Keyence (model IA-100) is also placed on the measuring head for the on-line control and adjustment of the sample-instrument distance. This measuring head is mounted on three linear motor stages by Physik Instrumente, with a 200 mm travel range in the x and y directions for this version, plus a 50 mm stage along the z perpendicular direction. The whole system is placed on a carbon-fibre box containing motor controllers, a multi-channel analyser (model CAEN DT-5780), and other electrical components. The software controlling acquisition and data analysis is entirely developed by researchers of the INFN-CHNet group. The instrument has been successfully employed in several HS applications over the years and, thanks to its versatility, it is a matter of continuous upgrade.

With the use of the scanner, the painting techniques of the Old Masters, such as Raffaello [54] and Van der Weyden [55] were conducted. In the painting *La Muta* by Raffaello, the painting palette was characterised and a *pentimento*—the presence or emergence of earlier images, forms, or strokes that have been changed and painted over by the author—was found. In the work *Entombment of Christ* by Van der Weyden, the painting technique—in particular the use of powdered glass in mixture with the pigments—was studied.

Further type of works of art analysed with this instrument are Venetian illuminated manuscripts [56], furniture of the XVIII century [57], and French ceramics [58].

Here are presented elemental maps of two areas around the initial of the same parchment presented in Section 3. During the measurements, a preliminary version of the scanner was used with a chromium anode. The operating conditions of the X-ray tube for all measurements were: 30 kV anode voltage, 0.1 mA current, and an 800 µm diameter collimator was used. The scanning velocity was set to 1 mm/s.

Comparing the maps with the measurements conducted in Sections 3 and 5, the advantage of a scanning system is evident: it is straightforward to match the visible pattern with the elemental distribution and therefore to identify the material that was probably used for the painting layer.

The elemental maps are shown in Figure 9. The blue colour—the background and the body of the peacock—is painted with a copper-based pigment, most likely azurite [35]. The tail of the peacock is characterised by the presence of tin, in this case probably indicating the presence of mosaic gold [59]. Blue eyespots of the feathers are likely painted with azurite as the body of the peacock. Lead and tin are detected in the yellow outline of the initial, suggesting the use of lead-tin yellow [59]. The light grey wings and decorative leaves are characterised by the presence of lead and of copper traces, most likely due to the use of lead white and little amount of azurite. It is worth noting that the use of other organic compounds cannot be conclusively identified with this technique, but the fact that

the pink initial is characterised only by the presence of lead (usually lead white or red lead) is a strong hint of the use of a red organic dye.

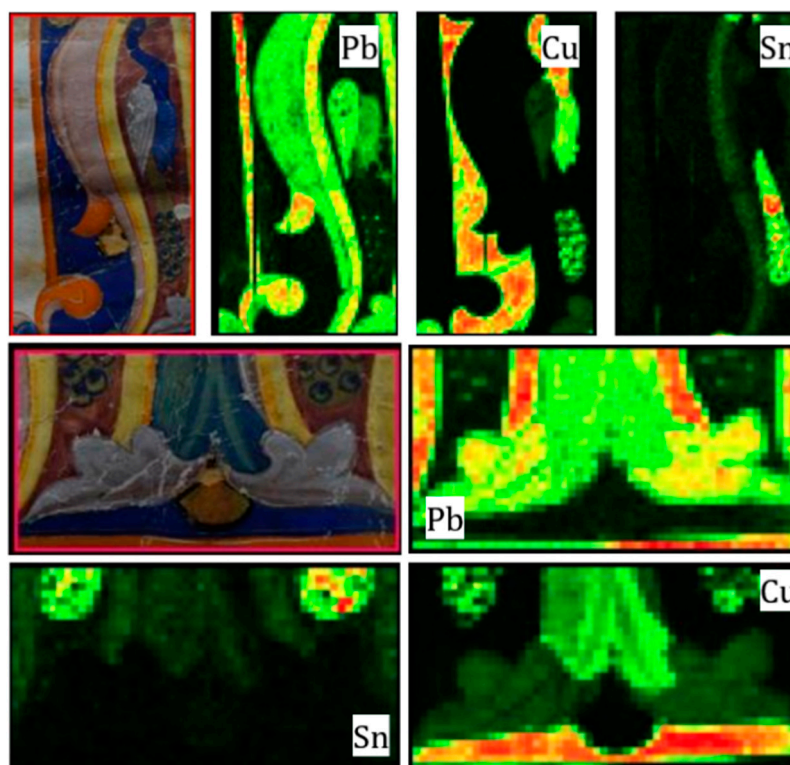


**Figure 9.** Visible and elemental maps of the two areas of the parchment scanned.

Thanks to the versatility of the scanner, further developments of it are under study. As an example, the likely combination of different techniques using the same X-ray source is under study. Results of the combination of the XRF with digital radiography is presented in [60].

The limit of this technique is of course related to the fact that it allows only elemental analysis. This is of course a limit for the analysis of a number of materials, such as glasses, for which it is important to determine the polymerisation degree of enamels successfully evaluated with Raman spectroscopy [61].

## 8. The MACHINA Project

The strong demand of scientific analysis for conservation and preservation of works of art led to the project of an instrument with the same performance as the standard IBA techniques (effectiveness and sensitivity, non-invasiveness and non-destructiveness), with the additional features of transportability, lightness, and low power consumption. To answer the query, the INFN-CHNet group, in collaboration with the Conseil Européen pour la Recherche Nucléaire (CERN) and the Opificio delle Pietre Dure (OPD) in Florence, a world-renowned conservation institution, has started the MACHINA project [62], an accelerator of about 600 kg weight, with a footprint of about 2.5 m × 1.6 m, services included, and a power consumption of a few kW. It will produce 2 MeV proton beams thanks to a RadioFrequency source and an high-frequency RFQ accelerating part. The RF source produces 20 keV protons that will be delivered into the Low Energy Beam Transport (LEBT) line, which consists of a focusing stage and a diagnostic station. The beam will then be injected in the HF-RFQ, where it is focused and accelerated to the final energy of 2 MeV. A permanent magnet quadrupole doublet focusing system and a second diagnostic station will be installed downstream before the beam extraction in air. Moreover, it will be possible to insert two beam energy degraders to lower the proton beam energy.



The detection system of MACHINA has been designed to hold two SDD detectors for PIXE analysis, each optimised for the acquisition of different X-ray ranges, and one CdTe detector for Particle Induced Gamma-ray emission (PIGE) analysis. Another SDD detector will monitor the beam current detecting the X-rays emitted by the exit window. As underlined in the article [27], with the expertise of the INFN-CHNet group with detector systems, other techniques can be added to the ones already planned.

## 9. Conclusions

In this review, the facilities dedicated to PIXE and XRF techniques in air developed at the INFN-LABEC laboratory have been described. Starting from the first PIXE beamline, thanks to the expertise of the group, the equipment for the irradiation of micrometric areas (the microbeam line) and for in situ analysis (XRF spectrometer) were developed.

Currently, within the INFN-CHNet collaboration, a MA-XRF scanner is fully operative for mapping works of art. Furthermore, a device for in-situ PIXE analysis is in progress. It will be the first transportable accelerator based on the RFQ technique and will make available IBA techniques in museums and conservation centres.

**Author Contributions:** Conceptualization, P.A.M., F.T., L.G. (Lorenzo Giuntini) and A.L.G.; methodology, P.A.M., F.T. and L.G. (Lorenzo Giuntini); software, F.T., C.C. and R.T.; formal analysis, L.C. (Lisa Castelli), S.M.E.M., A.M., C.R., S.C. and A.R.; investigation, L.C. (Luca Carraresi) and M.M. (Marco Manetti); data curation, F.G. and L.C. (Lisa Castelli); writing—original draft preparation, L.S., A.M., M.M. (Mirko Massi) and L.G. (Lorenzo Giuntini); writing—review and editing, A.R., L.G. (Laura Guidorzi), L.G. (Lorenzo Giuntini), M.M. (Mirko Massi), L.S. and A.M.; visualization, L.C. (Luca Carraresi), L.S. and S.M.E.M.; supervision, F.A., P.A.M. and L.G. (Lorenzo Giuntini); project administration, P.A.M., L.G. (Lorenzo Giuntini), F.T. and A.L.G. All authors have read and agreed to the published version of the manuscript.

**Funding:** The research was funded within the INFN-CHNet project. This project has received funding from the European Union's Horizon 2020 research and innovation programme under the Marie Skłodowska-Curie grant agreement No 754511 (PhD Technologies Driven Sciences: Technologies for Cultural Heritage—T4C).

**Institutional Review Board Statement:** Not applicable.

**Informed Consent Statement:** Not applicable.

**Acknowledgments:** The authors wish to warmly thank Paulene Linda Healey and Hilary Peebles from the University Language Centre at the University of Florence for their invaluable linguistic support.

**Conflicts of Interest:** The authors declare no conflict of interest.

## References

1. Castoldi, A.; Guazzoni, C.; Mezza, D.; Montemurro, G.V.; Carraresi, L.; Taccetti, F. Upgrade of the DEFEL proton beam line for detector response mapping. In Proceedings of the 2013 IEEE Nuclear Science Symposium and Medical Imaging Conference (2013 NSS/MIC), Seoul, Korea, 27 October–2 November 2013; pp. 1–5. [\[CrossRef\]](#)
2. Bardelli, L.; Bini, M.; Bizzeti, P.G.; Carraresi, L.; Danevich, F.A.; Fazzini, T.F.; Grinyov, B.V.; Ivannikova, N.V.; Kobychyev, V.V.; Kropivnyansky, B.N.; et al. Further study of CdWO<sub>4</sub> crystal scintillators as detectors for high sensitivity 2 $\beta$  experiments: Scintillation properties and pulse-shape discrimination. *Nucl. Instrum. Methods Phys. Res. Sect. A Accel. Spectrometers Detect. Assoc. Equip.* **2006**, *569*, 743–753. [\[CrossRef\]](#)
3. Rocchini, M.; Hadyńska-Kłęk, K.; Nannini, A.; Valiente-Dobón, J.J.; Goasduff, A.; Testov, D.; Mengoni, D.; John, P.R.; Siciliano, M.; Melon, B. SPIDER: A Silicon Pie DEtectoR for low-energy Coulomb-excitation measurements. *Nucl. Instrum. Methods Phys. Res. Sect. A Accel. Spectrometers Detect. Assoc. Equip.* **2020**, *971*, 164030. [\[CrossRef\]](#)
4. Lagomarsino, S.; Flatae, A.M.; Kambalathmana, H.; Sledz, F.; Hunold, L.; Soltani, N.-; Reuschel, P.; Sciortino, S.; Gelli, N.; Massi, M.; et al. Creation of Silicon-Vacancy Color Centers in Diamond by Ion Implantation. *Front. Phys.* **2021**, *8*, 601362. [\[CrossRef\]](#)
5. Petrucci, F.; Caforio, L.; Fedi, M.; Mandò, P.; Peccenini, E.; Pellicori, V.; Rylands, P.; Schwartzbaum, P.; Taccetti, F. Radiocarbon dating of twentieth century works of art. *Appl. Phys. A* **2016**, *122*, 983. [\[CrossRef\]](#)
6. Nava, S.; Calzolari, G.; Chiari, M.; Giannoni, M.; Giardi, F.; Becagli, S.; Severi, M.; Traversi, R.; Lucarelli, F. Source Apportionment of PM<sub>2.5</sub> in Florence (Italy) by PMF Analysis of Aerosol Composition Records. *Atmosphere* **2020**, *11*, 484. [\[CrossRef\]](#)

7. Lucarelli, F. How a small accelerator can be useful for interdisciplinary applications: The study of air pollution. *Eur. Phys. J. Plus* **2020**, *135*, 538. [[CrossRef](#)]
8. Calusi, S. The External Ion Microbeam of the LABEC Laboratory in Florence: Some Applications to Cultural Heritage. *Microsc. Microanal.* **2011**, *17*, 661–666. [[CrossRef](#)]
9. Taccetti, N.; Giuntini, L.; Casini, G.; Stefanini, A.A.; Chiari, M.; Fedi, M.E.; Mandò, P.A. The pulsed beam facility at the 3 MV Van de Graaff accelerator in Florence: Overview and examples of applications. *Nucl. Instrum. Methods Phys. Res. Sect. B Beam Interact. Mater. Atoms* **2002**, *188*, 255–260.
10. Lagomarsino, S.; Sciortino, S.; Gelli, N.; Flatae, A.M.; Gorelli, F.; Santoro, M.; Chiari, M.; Celusniak, C.; Giuntini, L. The center for production of single-photon emitters at the electrostatic-deflector line of the Tandem accelerator of LABEC (Florence). *Nucl. Instruments Methods Phys. Res. Sect. B Beam Interactions Mater. Atoms* **2018**, *422*, 31–40. [[CrossRef](#)]
11. Chiari, M.; Melon, B.; Salvestrini, L.; Fonseca, M.; Alves, E.; Jesus, A.P. Measurement of proton induced  $\gamma$ -ray emission cross-sections on Al from 2.5 to 4.1 MeV. *Nucl. Instrum. Methods Phys. Res. Sect. B* **2014**, *332*, 355–358. [[CrossRef](#)]
12. Palla, L.; Castelli, L.; Czelusniak, C.; Fedi, M.; Giuntini, L.; Liccioli, L.; Mandò, P.; Martini, M.; Mazzinghi, A.; Ruberto, C.; et al. Preliminary measurements on the new TOF system installed at the AMS beamline of INFN-LABEC. *Nucl. Instrum. Methods Phys. Res. Sect. B Beam Interact. Mater. Atoms* **2015**, *361*, 222–228. [[CrossRef](#)]
13. Mandò, P. The Florence accelerator laboratory for Ion Beam Analysis and AMS radiocarbon dating. *Il Nuovo Cim. C* **2007**, *30*, 85–92. [[CrossRef](#)]
14. Chiari, M.; Barone, S.; Bombini, A.; Calzolari, G.; Carraresi, L.; Castelli, L.; Czelusniak, C.; Fedi, M.E.; Gelli, N.; Giambi, F.; et al. LABEC, the INFN ion beam laboratory of nuclear techniques for environment and cultural heritage. *Eur. Phys. J. Plus* **2021**, *136*, 472. [[CrossRef](#)] [[PubMed](#)]
15. Czelusniak, C.; Palla, L.; Massi, M.; Carraresi, L.; Giuntini, L.; Re, A.; Lo Giudice, A.; Pratesi, G.; Mazzinghi, A.; Ruberto, C.; et al. Preliminary results on time-resolved ion beam induced luminescence applied to the provenance study of lapis lazuli. *Nucl. Instrum. Methods Phys. Res. B* **2016**, *371*, 336–339.
16. Palla, L.; Czelusniak, C.; Taccetti, F.; Carraresi, L.; Castelli, L.; Fedi, M.E.; Giuntini, L.; Maurenzig, P.R.; Sottili, L.; Taccetti, N. Accurate on line measurements of low fluences of charged particles. *Eur. Phys. J. Plus* **2015**, *130*, 39. [[CrossRef](#)]
17. Janssens, K.; Vincze, L.; Rubio, J.; Adams, F.; Bernasconi, G. Microscopic X-ray fluorescence analysis. Invited lecture. *J. Anal. At. Spectrom.* **1994**, *9*, 151–157. [[CrossRef](#)]
18. Ishii, K. PIXE and Its Applications to Elemental Analysis. *Quantum Beam Sci.* **2019**, *3*, 12. [[CrossRef](#)]
19. Ricciardi, P.; Mazzinghi, A.; Legnaioli, S.; Ruberto, C.; Castelli, L. The Choir Books of San Giorgio Maggiore in Venice: Results of in Depth Non-Invasive Analyses. *Heritage* **2019**, *2*, 1684–1701. [[CrossRef](#)]
20. Vadrucci, M.; Mazzinghi, A.; Sorrentino, B.; Falzone, S.; Gioia, C.; Gioia, P.; Loreti, E.M.; Chiari, M. Characterisation of ancient Roman wall-painting fragments using non-destructive IBA and MA-XRF techniques. *X-ray Spectrom.* **2020**, *49*, 668–678. [[CrossRef](#)]
21. Calligaro, T.; Banas, A.; Banas, K.; Radović, I.B.; Brajković, M.; Chiari, M.; Forss, A.-M.; Hajdas, I.; Krmpotić, M.; Mazzinghi, A.; et al. Emerging nuclear methods for historical painting authentication: AMS-14C dating, MeV-SIMS and O-PTIR imaging, global IBA, differential-PIXE and full-field PIXE mapping. *Forensic Sci. Int.* **2022**, *336*, 111327. [[CrossRef](#)]
22. Available online: <https://www.amptek.com/products/mini-x2-x-ray-tube> (accessed on 28 May 2022).
23. Available online: <https://calc.weingos.com/> (accessed on 28 May 2022).
24. Lekki, J.; Matosz, M.; Paluszkiwicz, C.; Pięta, E.; Pieprzycza, T.; Szklarz, Z.; Meléndez, J.M.D.H. Comparison of PIXE and XRF in the analysis of silver denarii of the early Piast. *J. Radioanal. Nucl. Chem.* **2017**, *314*, 2309–2316. [[CrossRef](#)] [[PubMed](#)]
25. Mandò, P.A.; Przybyłowicz, W.J. Particle-Induced X-ray Emission (PIXE). In *Encyclopedia of Analytical Chemistry*; Meyers, R.A., Ed.; John Wiley & Sons: New York, NY, USA, 2009. [[CrossRef](#)]
26. Bonizzoni, L. ED-XRF analysis for Cultural Heritage: Is quantitative evaluation always essential? *J. Phys. Conf. Ser.* **2015**, *630*, 12001. [[CrossRef](#)]
27. Giuntini, L.; Castelli, L.; Massi, M.; Fedi, M.; Czelusniak, C.; Gelli, N.; Liccioli, L.; Giambi, F.; Ruberto, C.; Mazzinghi, A.; et al. Detectors and Cultural Heritage: The INFN-CHNet Experience. *Appl. Sci.* **2021**, *11*, 3462. [[CrossRef](#)]
28. Käyhkö, M.; Laitinen, M.; Arstila, K.; Maasilta, I.; Sajavaara, T. A new beamline for energy-dispersive high-resolution PIXE analysis using polycapillary optics. *Nucl. Instrum. Methods Phys. Res. Sect. B Beam Interact. Mater. Atoms* **2019**, *447*, 59–67. [[CrossRef](#)]
29. Hanf, D.; Buchriegler, J.; Renno, A.D.; Merchel, S.; Munnik, F.; Ziegenrucker, R.; Scharf, O.; Nowak, S.H.; von Borany, J. A new Particle-Induced X-ray Emission set-up for laterally resolved analysis over wide areas. *Nucl. Instr. Methods Phys. Res. B* **2016**, *377*, 17–24. [[CrossRef](#)]
30. Romano, F.P.; Caliri, C.; Nicotra, P.; di Martino, S.; Pappalardo, L.; Rizzo, F.; Santos, H.C. Real-time elemental imaging of large dimension paintings with a novel mobile macro X-ray fluorescence (MA-XRF) scanning technique. *J. Anal. At. Spectrom.* **2017**, *32*, 773–781. [[CrossRef](#)]
31. Alfeld, M.; Pedroso, J.V.; van EikemaHommes, M.; Van der Snickt, G.; Tauber, G.; Blaas, J.; Haschke, M.; Erler, K.; Dik, J.; Janssens, K. A mobile instrument for in situ scanning macro-XRF investigation of historical paintings. *J. Anal. At. Spectrom.* **2013**, *28*, 760–767. [[CrossRef](#)]
32. Mihalic, I.B.; Fazinic, S.; Barac, M.; Karydas, A.G.; Migliori, A.; Doracic, D.; Desnica, V.; Mudronja, D.; Krstic, D. Multivariate analysis of PIXE plus XRF and PIXE spectral images. *J. Anal. At. Spectrom.* **2021**, *36*, 654–667. [[CrossRef](#)]

33. Giuntini, L.; Lucarelli, F.; Mandò, P.; Hooper, W.; Barker, P. Galileo's writings: Chronology by PIXE. *Nucl. Instrum. Methods Phys. B* **1995**, *95*, 389–392. [[CrossRef](#)]
34. Carmine, P.; Giuntini, L.; Hooper, W.; Lucarelli, F.; Mandò, P. Further results from PIXE analysis of inks in Galileo's notes. *Nucl. Instrum. Methods Phys. Res. Sect. B Beam Interact. Mater. Atoms* **1996**, *113*, 354–358. [[CrossRef](#)]
35. Roy, A. (Ed.) *Artists' Pigments: A Handbook of Their History and Characteristics*; National Gallery of Art, Washington Archetype Publications: London, UK, 1993; Volume 2.
36. Gettens, R.J.; Robert, L.F.; Chase, W.T. Vermilion and Cinnabar. *Stud. Conserv.* **1972**, *17*, 45–69.
37. KUHN, H. 'Lead-tin yellow'. *Stud. Conserv.* **1968**, *13*, 7–33.
38. Bussotti, L.; Giuntini, L.; Carboncini, M.P.; Mandò, P.A.; Castellucci, E. Identification of Pigments in a Fourteenth-Century Miniature by Combined Micro-Raman and Pixe Spectroscopic Techniques. *Stud. Conserv.* **1997**, *42*, 83–92. [[CrossRef](#)]
39. Gatti, E.; Rehak, P.; Walton, J.T. Silicon drift chambers—First results and optimum processing of signals. *Nucl. Instrum. Methods Phys. Res. Sect. A Accel. Spectrom. Detect. Assoc. Equip.* **1984**, *226*, 129–141. [[CrossRef](#)]
40. Lucarelli, F.; Calzolari, G.; Chiari, M.; Giannoni, M.; Mochi, D.; Nava, S.; Carraresi, L. The upgraded external-beam PIXE/PIGE set-up at LABEC for very fast measurements on aerosol samples. *Nucl. Instrum. Methods Phys. Res. Sect. B Beam Interact. Mater. Atoms* **2014**, *318*, 55–59. [[CrossRef](#)]
41. Cookson, J.A.; Ferguson, A.T.G.; Pilling, F.D. Proton microbeams, their production and use. *J. Radioanal. Chem.* **1972**, *12*, 39–52. [[CrossRef](#)]
42. Massi, M. The ion microbeam facility of Florence: A versatile instrument for the analysis and modification of materials. *Il Nuovo Cim. C* **2011**, *34*, 91–102.
43. Re, A.; Lo Giudice, A.; Angelici, D.; Calusi, S.; Giuntini, L.; Massi, M.; Pratesi, G. Lapis lazuli provenance study by means of micro-PIXE. *Nucl. Instrum. Methods Phys. Res. B* **2011**, *269*, 2373–2377. [[CrossRef](#)]
44. Re, A.; Angelici, D.; Lo Giudice, A.; Maupas, E.; Giuntini, L.; Calusi, S.; Gelli, N.; Massi, M.; Borghi, A.; Gallo, L.M.; et al. New markers to identify the provenance of lapis lazuli: Trace elements in pyrite by means of micro-PIXE. *Appl. Phys. A* **2013**, *111*, 69–74. [[CrossRef](#)]
45. Lo Giudice, A.; Angelici, D.; Re, A.; Gariani, G.; Borghi, A.; Calusi, S.; Giuntini, L.; Massi, M.; Castelli, L.; Taccetti, F.; et al. Protocol for lapis lazuli provenance determination: Evidence for an Afghan origin of the stones used for ancient carved artefacts kept at the Egyptian Museum of Florence (Italy). *Archaeol. Anthropol. Sci.* **2017**, *9*, 637–651. [[CrossRef](#)]
46. Re, A.; Angelici, D.; Giudice, A.L.; Corsi, J.; Allegretti, S.; Biondi, A.F.; Gariani, G.; Calusi, S.; Gelli, N.; Giuntini, L.; et al. Ion Beam Analysis for the provenance attribution of lapis lazuli used in glyptic art: The case of the "Collezione Medicea". *Nucl. Instrum. Methods Phys. Res. B* **2015**, *348*, 278–284. [[CrossRef](#)]
47. Grassi, N.; Giuntini, L.; Mandò, P.; Massi, M. Advantages of scanning-mode ion beam analysis for the study of Cultural Heritage. *Nucl. Instrum. Methods Phys. Res. Sect. B Beam Interact. Mater. Atoms* **2007**, *256*, 712–718. [[CrossRef](#)]
48. Giuntini, L.; Massi, M.; Calusi, S. The external scanning proton microprobe of Firenze: A comprehensive description. *Nucl. Instrum. Methods Phys. Res. Sect. A Accel. Spectrom. Detect. Assoc. Equip.* **2007**, *576*, 266–273. [[CrossRef](#)]
49. Malmqvist, K.G. Comparison between PIXE and XRF for applications in art and archaeology. *Nucl. Instrum. Methods Phys. Res. Sect. B Beam Interact. Mater. Atoms* **1986**, *14*, 86–92. [[CrossRef](#)]
50. Mazzinghi, A.; Giuntini, L.; Gelli, N.; Ruberto, C. XRF study on the gilding technique of the fresco 'Crocifissione con Santi' by Beato Angelico in the San Marco monastery in Florence. *X-ray Spectrom.* **2016**, *45*, 28–33. [[CrossRef](#)]
51. Mazzinghi, A. XRF analyses for the study of painting technique and degradation on frescoes by Beato Angelico: First results. *Nuovo Cim. Soc. Ital. Fis. C* **2014**, *37*, 253–262. [[CrossRef](#)]
52. Castelli, L.; Giuntini, L.; Taccetti, F.; Barzagli, E.; Civita, F.; Czelusniak, C.; Fedi, M.; Gelli, N.; Grazzi, F.; Mazzinghi, A. Traditionally maintained and artificially restored Japanese swords (katanas) by XRF spectroscopy. *X-ray Spectrom.* **2013**, *42*, 537–540. [[CrossRef](#)]
53. Taccetti, F.; Castelli, L.; Czelusniak, C.; Gelli, N.; Mazzinghi, A.; Palla, L.; Ruberto, C.; Corsi, C.; Lo Giudice, A.; Re, A.; et al. A multipurpose X-ray fluorescence scanner developed for in situ analysis. *Rend. Fis. Acc. Lincei* **2019**, *30*, 307–322. [[CrossRef](#)]
54. Ruberto, C.; Mazzinghi, A.; Massi, M.; Castelli, L.; Czelusniak, C.; Palla, L.; Gelli, N.; Bettuzzi, M.; Impallaria, A.; Brancaccio, R.; et al. Imaging study of Raffaello's "La Muta" by a portable XRF spectrometer. *Microchem. J.* **2016**, *126*, 63–69. [[CrossRef](#)]
55. Mazzinghi, A.; Ruberto, C.; Castelli, L.; Czelusniak, C.; Giuntini, L.; Mandò, P.A.; Taccetti, F. MA-XRF for the Characterisation of the Painting Materials and Technique of the *Entombment of Christ* by Rogier van der Weyden. *Appl. Sci.* **2021**, *11*, 6151. [[CrossRef](#)]
56. Mazzinghi, A.; Ruberto, C.; Castelli, L.; Ricciardi, P.; Czelusniak, C.; Giuntini, L.; Mandò, P.A.; Manetti, M.; Palla, L.; Taccetti, F. The importance of being little: MA-XRF on manuscripts on a Venetian island. *X-ray Spectrom.* **2020**, *50*, 272–278. [[CrossRef](#)]
57. Sottili, L.; Guidorzi, L.; Mazzinghi, A.; Ruberto, C.; Castelli, L.; Czelusniak, C.; Giuntini, L.; Massi, M.; Taccetti, F.; Nervo, M.; et al. The Importance of Being Versatile: INFN-CHNet MA-XRF Scanner on Furniture at the CCR "La Venaria Reale". *Appl. Sci.* **2021**, *11*, 1197. [[CrossRef](#)]
58. Mangani, S.M.E.; Mazzinghi, A.; Mandò, P.A.; Legnaioli, S.; Chiari, M. Characterisation of decoration and glazing materials of late 19th-early 20th century French porcelain and fine earthenware enamels: A preliminary non-invasive study. *Eur. Phys. J. Plus* **2021**, *136*, 1079. [[CrossRef](#)]
59. Seccaroni, C.; Moiola, P. *Fluorescenza X-Prontuario per l'analisi XRF Portatile Applicata a Superfici Policrome*; Nardini Editore: Firenze, Italy, 2002; pp. 60–89.

60. Sottili, L.; Guidorzi, L.; Lo Giudice, A.; Mazzinghi, A.; Ruberto, C.; Castelli, L.; Czelusniak, C.; Giuntini, L.; Massi, M.; Taccetti, F.; et al. Macro X-ray fluorescence analysis of XVI-XVII century Italian paintings and preliminary test for developing a combined fluorescence apparatus with digital radiography. *Acta Imeko* **2022**, *11*, 8. [[CrossRef](#)]
61. Philippe Colomban, Polymerization degree and Raman identification of ancient glasses used for jewelry, ceramic enamels and mosaics. *J. Non-Cryst. Solids* **2003**, *323*, 180–187. [[CrossRef](#)]
62. Mathot, S.; Anelli, G.; Atieh, S.; Bilton, A.; Bulat, B.; Callamand, T.; Calvo, S.; Favre, G.; Geisser, J.-M.; Gerardin, A.; et al. The CERN PIXE-RFQ, a transportable proton accelerator for the machina project. *Nucl. Instrum. Methods Phys. Res. Sect. B Beam Interact. Mater. Atoms* **2019**, *459*, 153–157. [[CrossRef](#)]

## INFN-CHNet at work: X-ray fluorescence analyses on works of art at the CCR “La Venaria Reale”

L. SOTTILI<sup>(1)(2)</sup>, L. GUIDORZI<sup>(1)(2)</sup>, A. MAZZINGHI<sup>(3)(4)</sup>, C. RUBERTO<sup>(3)(4)</sup>,  
L. CASTELLI<sup>(4)</sup>, C. CZELUSNIAK<sup>(4)</sup>, L. GIUNTINI<sup>(3)(4)</sup>, M. MASSI<sup>(4)</sup>, F. TACCETTI<sup>(4)</sup>,  
M. NERVO<sup>(5)</sup>, M. FERRERO<sup>(5)</sup>, R. TORRES<sup>(6)</sup>, F. ARNEODO<sup>(6)</sup>, A. RE<sup>(1)(2)</sup>  
and A. LO GIUDICE<sup>(1)(2)</sup>

<sup>(1)</sup> *Dipartimento di Fisica, Università di Torino - Torino, Italy*

<sup>(2)</sup> *INFN, Sezione di Torino - Torino, Italy*

<sup>(3)</sup> *Dipartimento di Fisica e Astronomia, Università di Firenze - Firenze, Italy*

<sup>(4)</sup> *INFN, Sezione di Firenze - Firenze, Italy*

<sup>(5)</sup> *Centro Conservazione e Restauro “La Venaria Reale” - Venaria Reale, Italy*

<sup>(6)</sup> *Division of Science, New York University Abu Dhabi - Abu Dhabi, United Arab Emirates*

received 31 January 2022

**Summary.** — INFN-CHNet, the network of the Italian National Institute for Nuclear Physics (INFN) devoted to Cultural Heritage, has the mission to develop instruments and methods for heritage science. Within this network, a Macro X-Ray Fluorescence (MA-XRF) scanner was realised for both elemental imaging and spectroscopy. It has been used for a number of applications, such as paintings, ceramics, mosaics and manuscripts. As an example, some measurements conducted at the Centro di Conservazione e Restauro “La Venaria Reale” will be presented. Furthermore, general aspects of the analysis with the INFN-CHNet MA-XRF scanner will be discussed.

### 1. – The INFN-CHNet Collaboration

The National Institute for Nuclear Physics (INFN) is the Italian research agency dedicated to the study of the fundamental constituents of matter and the laws that govern them. The main fields of research are nuclear, particle, theoretical and astroparticle physics. However, it conducts technological research and promotes the use of fundamental physics instruments, methods and technologies in other sectors. One of the fields of application of nuclear techniques is heritage science and, in 2017, the network of the INFN for cultural heritage, INFN-CHNet [1,2], was founded, with the mission to harmonise and to enhance the expertise of the Institute in the field towards its structures spread over the Italian territory. Several results have already been achieved by developing facilities for heritage science applications as reported in [3,4].

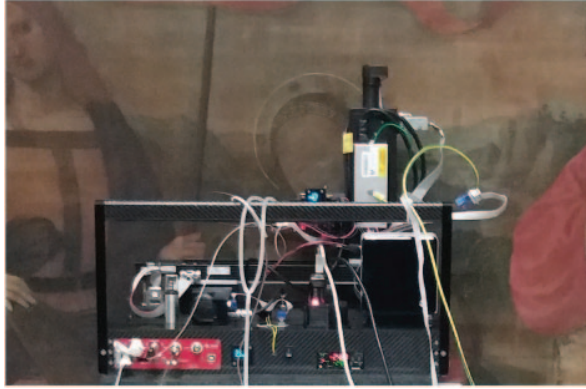


Fig. 1. – INFN-CHNet MA-XRF scanner placed in front of a painting at the CCR “La Venaria Reale”.

## 2. – The INFN-CHNet MA-XRF scanner

The INFN-CHNet MA-XRF scanner (fig. 1) is a compact ( $60 \times 50 \times 50 \text{ cm}^3$ ) and lightweight (around 10 kg) instrument developed within the collaboration. Its main parts are the measuring head, three motor linear stages and a case containing all the electronics for acquisition and control.

The measuring head is composed of an X-Ray tube (Moxtek, 40 kV maximum voltage, 0.1 mA maximum anode current, Mo anode) with a removable collimator, a Silicon Drift Detector (Amptek XR100 SDD,  $50 \text{ mm}^2$  effective active area) and a telemeter (Keyence IA-100). The motor stages (Physik Instrumente, travel ranges 30 cm in  $x$ , 15 cm in  $y$  and 5 cm in  $z$  directions) holding the measuring head are screwed to the carbon-fibre case. Signals are collected with a multi-channel analyser (model CAEN DT5780) and the whole system is controlled by a laptop. The control-acquisition-analysis software is developed within the network and allows both on-line and off-line analysis.

The output of the acquisition process is a file containing the scanning coordinates and, for each position, the spectrum acquired. For each map, or in a part of it, a single element can be selected and represented. The relative intensity of each element is shown with a grey scale, in which the maximum intensity is in white and the lowest is in black. Scanning is carried out on the  $x$  axis, and a step size of typically 1 mm is set on the  $y$  axis resulting in a pixel size of  $1 \text{ mm}^2$ . A complete review on the instrument can be found in [5]. The instrument has already been successfully used for a number of different applications, *e.g.*, paintings [6, 7], manuscripts [8], ceramics [9], and furniture [10].

## 3. – Applications at the CCR “La Venaria Reale”

The work of art presented, the *Madonna con Bambino ed i Santi Crescentino e Donatino* by Timoteo Viti, is a painting on canvas ( $168 \times 165 \text{ cm}^2$ , Milano, Pinacoteca di Brera, inv. 576), dated between 1500 and 1510 [11]. The painting presented bad conservation conditions on the areas around the faces of the Virgin and the Child. The match of the elemental maps with the painted areas allowed the identification of pigments in a non-invasive and non-destructive way. Here the area of the Virgin’s face is presented

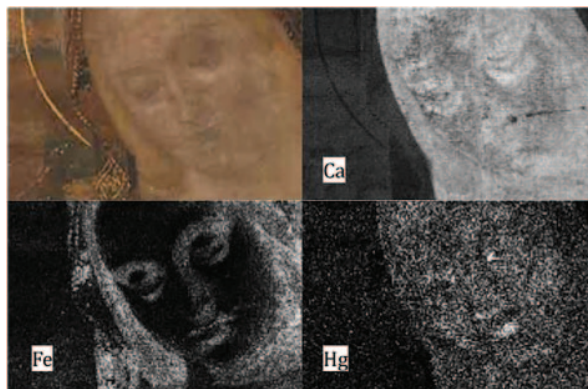


Fig. 2. – Image of the scanned area (top left) and XRF maps of Ca, Fe, Hg.

and discussed. The scanned area is  $170 \times 110 \text{ mm}^2$ , the parameters of the source were 28 kV,  $40 \mu\text{A}$ , and a  $800 \mu\text{m}$  collimator was used.

As can be seen from fig. 2, the visage area is characterised by calcium, which can be explained with a calcium-based compound such as gypsum for the preparatory layer [11], and low intensity lead peaks, which suggest the use of a proper white pigment (*biacca*). This result is confirmed by infrared spectroscopy in the painted area [12]. Moreover, from the lead distribution map (fig. 3, Pb), it is possible to notice that the counts related to this element increase in the background. In addition, the match of the spatial distributions of tin with lead may indicate the use of lead-tin yellow for the *aura* of the Virgin.

The blue mantle was painted with a copper-based pigment, most likely azurite, and iron-based compounds, such as earths and ochres, were employed for shading. The embroidery as well as the outline of the halo were realised with the use of gold. Mercury was detected in the flesh tone, highlighting the presence of vermilion. Mercury and iron-based pigments were also employed to paint the hair of the Virgin.

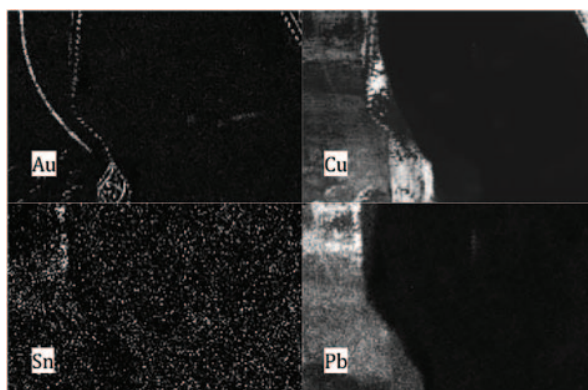


Fig. 3. – XRF maps of Au, Cu, Sn, Pb of the same area presented in fig. 2.

#### 4. – Conclusion

The INFN-CHNet MA-XRF scanner was successfully employed during the conservation process at the CCR “La Venaria Reale”. Most of the painting palette was identified, even though the impossibility to detect elements lighter than sodium limits its knowledge. Thanks to the versatility of the device and the expertise within the INFN-CHNet group, further improvements of the scanner are planned in the near future.

\* \* \*

This project has received funding from the European Union’s Horizon 2020 research and innovation programme under the Marie Skłodowska-Curie grant agreement No 754511 (PhD Technologies Driven Sciences: Technologies for Cultural Heritage - T4C). This project has received funding from Compagnia di San Paolo (NEXTO project, progetto di Ateneo 2017) and the INFN-CHnet project. The authors wish to warmly thank Marco Manetti of the INFN-Fi and the staff of the CCR “La Venaria Reale” for their support.

#### REFERENCES

- [1] GIUNTINI L., CASTELLI L. and MASSI M., *Appl. Sci.*, **11** (2021) 3462.
- [2] <https://chnet.infn.it/en/home-3/> (accessed 05 June 2022).
- [3] PALLA L. *et al.*, *Eur. Phys. J. Plus*, **130** (2015) 39.
- [4] CZELUSNIAK C., PALLA L. and MASSI M., *Nucl. Instrum. Methods Phys. Res. B*, **371** (2016) 336.
- [5] TACCETTI F., CASTELLI L., CZELUSNIAK C. *et al.*, *Rend. Lincei*, **30** (2019) 307.
- [6] RUBERTO C., MAZZINGHI A., MASSI M. *et al.*, *Microchem. J.*, **126** (2016) 63.
- [7] MAZZINGHI A., RUBERTO C. and CASTELLI L., *Appl. Sci.*, **11** (2021) 6151.
- [8] MAZZINGHI A., RUBERTO C., CASTELLI L. *et al.*, *X-Ray Spectrom.*, **50** (2021) 272.
- [9] MANGANI S. M. E. *et al.*, *Eur. Phys. J. Plus*, **136** (2021) 1079.
- [10] SOTTILI L., GUIDORZI L. and MAZZINGHI A., *Appl. Sci.*, **11** (2021) 1197.
- [11] CORRADA G. *et al.*, *Atti del XII Congresso Nazionale IGIIC, Milano* (2014) pp. 663–671.
- [12] CORRADA G., *Studio interdisciplinare del dipinto a tempera magra su tela Madonna con bambino e i santi Crescentino e Donnino, Timoteo Viti*, Master’s Degree Programme in Conservation and Restoration for Cultural Heritage (University of Turin) 2013, pp. 42–46.